

Responsive Pipe Networks

Report to the
WATER RESEARCH COMMISSION

by

SW JACOBSZ

Department of Civil Engineering
University of Pretoria

WRC Report No. 2726/1/19

ISBN 978-0-6392-0094-1

October 2019



Obtainable from

Water Research Commission

Private Bag X03

GEZINA, 0031

orders@wrc.org.za or download from www.wrc.org.za

DISCLAIMER

This report has been reviewed by the Water Research Commission (WRC) and approved for publication. Approval does not signify that the contents necessarily reflect the views and policies of the WRC, nor does mention of trade names or commercial products constitute endorsement or recommendation for use

EXECUTIVE SUMMARY

BACKGROUND

The work presented in this report is aimed at investigating the performance of a potential leakage detection system detecting leaks in newly installed piped water distribution networks. The envisaged system will comprise of a fibre optic cable either fixed to the pipe or buried in the pipe bedding near the pipeline during pipe installation. By measuring back scatter of laser light emitted through the fibre using a commercially available interrogator, temperature and strain changes along the length of the cable can be measured to high resolution. It is hypothesised that a water leak will result in a temperature and/or strain changes in the ground below the pipe. Observing such a temperature/strain change using the abovementioned technology may be indicative of a leak, allowing early remedial measures to be taken. Such a system can be monitored periodically or continuously depending on the application to measure temperature and strain profiles along the pipeline.

RATIONALE

It is estimated that approximately 26% of the potable water distributed by the City of Tshwane is lost due to leakages from the aging distribution system. Just in the City of Tshwane this amounts to approximately 75 million cubic metres per annum. In towns like Grahamstown with older infrastructure the percentage losses is substantially larger and it is often mentioned in the media that up to a third of potable water distributed in South Africa is lost from the system. In a water scarce country like South Africa with a growing population and growing urbanisation, this can barely be afforded.

Not only does this non-revenue water (NRW) result in large financial losses to local authorities and water distribution agencies, but in the province of Gauteng, of which approximately 20% is underlain by dolomite bedrock, leaking water services may trigger the development of sinkholes and subsidence. This poses a serious threat to all types of infrastructure and even human safety. It has, in fact, been reported by Buttrick and Van Schalkwyk (1998) that 98.9% of all new sinkholes in the Tshwane area are triggered by leaking water services, either from the distribution network or from the wastewater system. Before the leak is detected and as the sinkhole develops due to leakage, the leak is likely to be made worse by the ground movement associated with the development of the sinkhole, resulting in a large volume of water being lost.

Perhaps the most significant problem with water lost from the distribution system is that the presence and location of leaks are not easily detected before a very large volume of water had been lost so that remedial action is normally only taken very late.

In the last approximately 20 years, fibre optic instrumentation has been developed to measure temperature and strain with an unprecedented resolution exceeding that of conventional instrumentation. It is possible to take continuous strain readings along the length of a fibre optic cable extending several kilometres or, by creating imperfections referred to as Bragg gratings at known locations along the length of a fibre optic cable, strain can be measured at discrete locations at a high sampling rate. This also applies to temperature. A major advantage is that fibre optic cables are cheap and completely inert in that it is not affected by the electrical disturbances that electric monitoring systems typically suffer from.

A major initiative by the Division of Civil Engineering at the Department of Engineering at the University of Cambridge has seen the formation of a group known as the Cambridge Centre for Smart Infrastructure and Construction (CSIC) who, over the last 10 years, have demonstrated that by applying fibre optic technology, an unprecedented amount of data can be obtained at very reasonable cost, thus allowing engineers to monitor the performance of numerous types of infrastructure. Collaboration to monitor strains in integral bridges (bridges constructed without expansion joints) has already been established between the Department of Civil Engineering at the University of Pretoria and CSIC in Cambridge.

During this project the application of fibre optic technology to monitor the performance of newly installed pipelines was investigated. Identifying and timeously fixing leaks will save large volumes of potable water currently being wasted, potentially realising large cost savings. In dolomitic areas this will also assist in the prevention of sinkhole formation which impacts on human safety and integrity of infrastructure.

OBJECTIVES AND AIMS

The following objectives and aims were set at the conceptual stage of the project.

AIM 1

Understand temperature changes around a leaking pipe

AIM 2

Understand strains in pipes undergoing leakage-induced ground movement

AIM 3

Assessing the severity of a leak from rate of change in the measured temperature and strains

METHODOLOGY

The work described in this report was carried out in the Civil Engineering laboratories and the Hillcrest Campus (experimental farm) of the University of Pretoria. The project duration was two years. The work was led by Prof SW Jacobsz, assisted by Prof Elsabe Kearsley, two Masters degree students and two fourth year Civil Engineering students.

Literature review

The project commenced with a literature study on water leaks, conventional and new techniques employed to monitor the integrity and performance of pipelines and the application of fibre optic monitoring to observe the behaviour/performance of structures. The literature review was subsequently expanded to cover strain response of pipes affected by ground movement to obtain an understanding of how ground movements caused by pipe leaks could affect pipelines of various stiffness.

A study of temperature changes resulting from water leaks

This aspect of the work is reported in Chapter 3 of this report and Progress Reports 1 and 2 submitted to the WRC and are briefly summarised here.

Due to water circulating under pressure in water mains it was expected that the temperature of water in a pipeline would differ somewhat from the temperature of the ground surrounding the pipe. It was hypothesised that leakage of water from a pipe will result in a temperature change near the pipe, especially underneath it, as leaking water should be carried downwards by gravity. A series of experiments was therefore carried out in the laboratory where water was allowed to leak into a soil mass instrumented with an array of thermistors. Various rates of leakage were imposed to assess the impact of the leakage rate on the measured temperature change.

A series of thermistors were installed at depth increments of 250 mm in a testpit down to a depth of 3 m to provide information on the normal daily and seasonal temperature variation in the ground. The installation was carried out on the University of Pretoria's experimental farm. This information is necessary so that temperature changes due to leakage can be distinguished from the normal ambient changes. The installation had been monitored for two years at the time of drafting this report as originally proposed in the research proposal.

An installation comprising a short length (12 m) of pipeline, laid at the University of Pretoria's Hillcrest Campus (experimental farm), instrumented with an array of conventional and fibre optic thermistors and strain sensors, was tested in 2017 and 2018 to verify whether the proposed leak detection system would work in the field. The field investigation was necessary because the ambient temperature changes occurring in the field are likely to differ from that in the laboratory and it is necessary to observe whether temperature changes from leakage can be distinguished from the ambient.

The temperature measurement phase of the investigation is described in Chapter 3 of this report and in the second progress report to the WRC submitted on 1 November 2017. It was originally proposed that the next part of the work following completion of the temperature measurement phase would comprise solely of an investigation into the effects of strains undergone by leaking pipes. However, due to the fact that temperature changes also result in strain changes, there was some inter-dependency between the two phenomena so that the second progress report also contained some comment on strain effects on leaking pipes. It was clear that leaks induced strain changes in the affected pipe and surrounding soil soon after leak initiation to an extent that we not expected at the outset of the project. This had imported implication for the project as it meant that the detection of leakage-induced strains is also an important parameter that could indicate a leak.

Model study into leakage-induced pipe strain changes

At the time of drafting the research proposal it was expected that temperature changes near a pipeline will provide the first indication of a leak occurring. It was hypothesised that, over time, leakage is likely to result in softening of the ground near the leak and this is likely to impose some strain on the pipe due to changes in the support conditions underneath the pipe. It was hypothesised that these strains can be detected using fibre optic strain measurement. It was originally also hypothesised that, how soon after detection of a temperature change a change in pipe strain becomes detectable, may possibly provide an indication of the severity of the leak. The detection of strain will be especially important in dolomitic ground because it may provide an indication that a sinkhole is forming which would be a trigger for urgent remedial action.

In addition to the temperature measurement referred to for the field installation above, the pipe installed in the field was also instrumented for strain. It was found that pipe leaks resulted in very significant pipe strain changes, much more so than expected at the outset of the project. Pipes are subjected to strain changes due to leaking water causing softening of ground supporting this pipe, changing the support conditions around the pipe. Saturation of the soil

surrounding the pipe also result in an increase in the load on the pipe. Importantly, the advance of a wetting front through a soil mass, caused by a water leak, is accompanied by the generation of negative pore pressure (soil suction) during passage of the wetting front. Depending on the grain size distribution of the soil these suction values can be large. They result in large changes in the stress in the soil and hence stress on the pipe, which result in changes in bending moments in the pipe giving rise to strains which are easily detected using fibre optic instrumentation. However, pipelines are also subjected to strains due to normal pressure fluctuations occurring in water distribution networks. These strain changes occur on a continuous basis and result in substantial background noise in terms of pipe strains, which could result in difficulty in detecting leakage-induced strains from strain occurring during the normal operation of a pipe network. Testing was carried out to investigate leak-induced strain changes in pipes under controlled conditions by means of a model study in the geotechnical centrifuge at the University of Pretoria and using the field installation on the university's Hillcrest Campus. The test installation was monitored over the entire course of 2018 to observe natural fluctuations in temperature and pipe strains as these parameters need to be understood to assess the potential performance of the proposed a leakage detection system.

RESULTS AND DISCUSSION

The following work, as set out in the research proposal, have been completed leading to the results and conclusions presented below:

- Measurement of in situ ground temperature variation with depth down to 3 m using an array of thermistors. The temperature monitoring has been done from January 2017 to December 2018.
- Temperature monitoring in an operational water main from May to Sept 2017.
- Temperature-based leakage experiments in the laboratory.
- Field installation and temperature testing of a short length of pipeline (12 m, 100 mm ID), equipped with three leakage points that could be controlled from the surface, instrumented with several arrays of conventional thermistors and fibre optic strain and temperature sensors.

- A series of centrifuge tests, complimented by selected field testing using the field installation on the University's experimental farm, have been completed to investigate leakage-induced strain changes on leaking pipes.
- The fibre optic strain measurement system monitoring the pipe installation in the field at the university's Hillcrest campus has been monitored from January 2018 to mid-December 2018 to provide a baseline against which to interpret seasonal variation in pipe and ground strains.
- A leak test was carried out in September 2018 after 9 months of baseline temperature and strain measurements had been obtained against which the results of the test could be evaluated.

Aim 1

Understand temperature changes around a leaking pipe

Natural daily temperature variation rapidly reduces with depth to amount to generally less than 2° below 0.75 m, a depth at which most water distribution pipes are generally installed. Water temperatures measured to date in a distribution main is more than 3° lower than the minimum temperature recorded in the ground, implying that temperature changes associated with water leaks should be readily detectable. Laboratory leakage tests investigating temperature measurement as a means of leak detection under controlled conditions were successful. Work carried out on the mentioned field installation has indicated that temperature changes due to water leaks are readily detectable, thereby providing warning of a leak. Fibre Bragg gratings (FBGs) (analogous to fibre optic strain or temperature sensors) have proved to be even more sensitive to register leakage-induced temperature changes than conventional thermistors.

AIM 2

Understand strains in pipes undergoing leakage-induced ground movement

Strain development in a pipe in the vicinity of a leak was studied using the field installation referred to above, complimented by model tests in the geotechnical centrifuge at the University of Pretoria. The models showed that, even in the absence of a pipe, water leaked into dry or unsaturated ground results in significant ground strain changes and hence deformation due to changes in the effective stress in the ground. This causes a change in the support conditions around a pipe and additional loading, inducing bending moments and strains in the pipe. These strains are easily detected using FBGs attached to the pipe so that pipe strain monitoring provides an even more sensitive means of leakage detection than temperature monitoring. However, a complication could arise in that pressure fluctuations

normally occurring in operational pipe networks also result in pipe strains. It might therefore be difficult to distinguish leakage-induced strain changes from strain changes resulting from pressure fluctuations, but results from the in situ pipe test showed that leakage-induced strain changes significantly exceeded changes from in-pipe pressure fluctuation. This problem can also be avoided by measuring strain in the ground using an optic fibre buried some distance from the pipe, so that it does not react to in-pipe pressure fluctuations. Physical model tests and tests using the field installation showed that for a leakage detection system based on strain measurement, the actual strain values are not of concern, but rather sudden strain changes. The actual strain values are influenced by many factors which are difficult to account for or predict.

AIM 3

Assessing the severity of a leak from rate of change in the measured temperature and strain
At the onset of the project it was hypothesised that the correlation between pipe strain and ground temperature will enable pipe owners to judge the urgency by which remedial action is required. For example: If a sudden temperature change is detected and no measureable strain, it would imply that the pipe is leaking but had not suffered significant structural damage yet. However, should significant strains be detected in addition to a temperature change, the pipe has probably suffered some damage or deformation and more urgent remedial action is required. This hypothesis was found to be flawed because it was found that the advance of a wetting front through the soil immediately result in large strains due to pore water suctions which cause substantial stress and hence strain changes in the soils. The use of temperature and strain to assess the degree of damage as hypothesised above is therefore not feasible. However, the measurement of leakage-induced ground strain does provide a highly sensitive means of leak detection, up to five time more sensitive than temperature detection, an aspect not anticipated at conception of the project.

CONCLUSIONS

The following conclusions are presented from the study:

A water pipe leak results in significant ground strains in **unsaturated ground** and hence soil movement which can be measured using sensitive fibre optic strain measurement. This is due to pore water suctions which are generated when wetting an unsaturated soils, causing substantial stress and hence measurable strain in the soil. In unsaturated soils the strain effects were found to far exceed the temperature effects and therefore potentially provide a

highly sensitive parameter for leak detection. A literature and patent search was conducted but reports making use of ground strain as a means of leak detection was not found.

A water leak induces significant strains in the leaking pipe due to changes in ground deformation. This exerts additional load on the leaking pipe and changes the pipe support conditions. These strains are easily detected using strain sensors attached to the pipe. However, internal pressure fluctuations also result in significant strain changes so that it may be difficult to distinguish leakage-induced strains. It was however found that leakage-induced strain significantly exceeded those from internal pressure fluctuation in this study.

A water leak induces significant strain and hence deformation in **unsaturated ground** during wetting. These strains can be detected using a fibre optic strain sensing cable buried in close proximity to the pipe. A fibre optic sensing cable detached from the pipe also has the advantage of not being prone to pressure fluctuation in the pipe and should therefore not give false alarms. It is therefore proposed that the leakage detection system on newly installed pipes should comprise of a fibre optic cable buried near the pipe in the same pipe trench.

Field and model testing described in this report showed that the relative rigidity of the combined soil-pipe system, which was initially thought to be important to consider as it would affect the spacing of strain sensors on the leaking pipe, is not relevant to a practical leak detection system. The main reason is that the envisaged leakage detection system will rely on distributed strain measurement and not measurements at discrete locations. Only short lengths of pipe can be monitoring with discrete sensors.

Due to variation in the relative rigidity (stiffness) of the soil-pipe system along its length due to variation in material properties, pipe bedding support, compaction of backfill and other factors, it is difficult to predict the strain change that is likely to occur in the ground or in the pipe itself due to a leak. This is however not a concern as the indicator of a potential leak is a sudden change in strain rather than actual magnitude of the strain measurement.

A fibre optic cable buried in close proximity above a pipe may react to leakage-induced ground strains as some ground movement is likely to occur due to a leak. This may enable a leakage detection system to be retrofitted to existing pipes by burying a cable in close proximity to the pipe. It is recommended that such an installation be field-tested using distributed strain measurement technology.

The behaviour of the proposed leakage detection system over the course of a year has been evaluated by continuously recording strain measurements on the field installation at the University of Pretoria's Hillcrest Campus to study seasonal changes in pipe and ground strains. This is important as leakage-induced strain changes will have to be distinguishable from seasonal change. It was found that major rainfall events (more than 40 mm in a single event) which result in deep wetting of the soil also affect the strain measurement and may therefore provide false pipe leak alarms. It is therefore important to interpret the results from the leakage detection system in the context of the rainfall record. In addition, a major rainfall event will have an effect over the entire length of pipeline passing through the area affected by the event which will allow the false alarm to be easily distinguished from a leak. The effect of the latter should be much more localised to the leak location only.

RECOMMENDATIONS FOR FUTURE RESEARCH

Indications from the laboratory and field installation trials are that the proposed leakage detection system will be successful to detect pipe line leaks. Arrangements should be made to carry out a trial installation of the proposed detection system on a working pipeline to allow the system to be tested under the realistic operating conditions.

The current work is based on fibre optic strain and temperature measurement at discrete locations. The study should proceed to investigate distributed strain and temperature fibre optic sensing and the necessary hardware should be sourced.

Optic fibres are of the order of 10 μm in diameter and therefore have to be protected by several protective layers/reinforcement elements when buried in the ground. A wide range of fibre optic cables, ranging in rigidity depending on their robustness, is available on the market. The performance of a range of cables of various degrees of robustness to act as leakage sensors should therefore be investigated. Cables which are too rigid may possibly not respond sensitively enough to indicate a leak.

Fibre optic cable manufacturers advise against the use of metal-armoured cables due to their tendency to conduct lightning, resulting in damage to readout units.

Seasonal variations in ground temperature and strain changes on buried fibre optic cables should continue to be studied as leakage-induced temperature and strain changes need to be identifiable despite naturally occurring variation.

The detection of leakage-induced ground and pipe strains are the principles on which the proposed leakage detection system is based. However, attaching a fibre optic cable to a pipe is problematic on a construction site. Manufacturing of a pipe with a pre-formed slot to accommodate the fibre optic sensing cable could be pursued, creating a so called “Smart pipe”.

ACKNOWLEDGEMENTS

The author would like to thank the Reference Group of the WRC Project K5/2726//3 for the assistance and the constructive discussions over the duration of the project.

TABLE OF CONTENTS

EXECUTIVE SUMMARY	III
ACKNOWLEDGEMENTS	XII
TABLE OF CONTENTS	XIII
LIST OF FIGURES	XVI
LIST OF TABLES	XXII
LIST OF ABBREVIATIONS	XXIII
LIST OF SYMBOLS	XXIV
1 INTRODUCTION AND OBJECTIVES	1
1.1 Background	1
1.2 Objective	2
1.3 Methodology	2
2 LITERATURE STUDY	5
2.1 Introduction to literature review	5
2.2 Potable water pipe leaks	5
2.2.1 Soil hydraulics	11
2.2.2 Additional impacts of water leaks	12
2.3 Leak detection and management methods	13
2.3.1 Effect of pressure in pipeline on leak	18
2.4 Pipeline construction material, pipe support and construction specifications	18
2.4.1 Pipe materials	18
2.4.2 Pipe-soil support	20
2.4.3 Pipeline construction specifications	21
2.5 Fibre optic sensors (FOS)	22
2.5.1 Type of sensors	24
2.5.2 Fibre Optic Bragg Sensors (FBGS)	25
2.5.3 Distributed strain and temperature sensors (DSTS)	28
2.5.4 Examples of fibre optic leak detection	30
2.5.5 Calibrating fibre optic strain and temperature sensors	36
2.6 Relevant thermal properties of soils	37
2.6.1 Thermal conductivity of soil and rock	37
2.6.2 Thermal conductivity of buried pipes	38
2.7 Temperature measurement	40

2.7.1	Negative thermal coefficient thermistors.....	40
2.8	Pipe-soil interaction	42
2.8.1	Pipe bending behaviour	42
2.8.2	Pipe response to ground settlement.....	48
2.9	Sinkhole formation due to leaking pipes.....	56
2.10	Summary of literature review and the way forward	59
3	LEAKAGE-INDUCED TEMPERATURE AND STRAIN CHANGES	61
3.1	Investigating natural temperature variation in the ground	61
3.2	Temperature variation in water mains	63
3.3	Investigating temperature changes caused by water leaks (laboratory phase)	64
3.4	Investigating temperature changes caused by water leaks (field phase)	66
3.5	Observed natural temperature changes in the ground	77
3.6	Temperature variation in water mains	82
3.7	Temperature changes caused by water leaks (laboratory phase).....	83
3.8	Investigating temperature changes caused by water leaks (field phase)	86
3.8.1	Thermistor data.....	89
3.8.2	Fibre Optic Bragg data.....	104
4	PHYSICAL MODEL STUDY INTO LEAKAGE-INDUCED STRAIN CHANGES	113
4.1	Introduction.....	113
4.2	Soil properties	114
4.2.1	Particle size distribution	114
4.2.2	Soil stiffness	115
4.3	Physical model description	116
4.3.1	Geotechnical centrifuge facility	117
4.3.2	Model setup	118
4.3.3	Simulation and additional measuring equipment.....	119
4.3.4	Pipeline instrumentation and properties	120
4.3.5	Strain gauged brass strip.....	122
4.3.6	Imposing water leaks	123
4.3.7	Scaling laws	123
4.3.8	Model set-up and testing procedure	124
4.3.9	Surface and trapdoor settlement	127

4.3.10	Monitoring soil displacement fields	128
4.3.11	Test sequence	129
4.4	Leakage-induced ground strains	129
4.4.1	Greenfield conditions	129
4.4.2	Ground strains in the presence of a pipe.....	134
4.5	Leakage-induced pipe strains	136
4.5.1	Pipe-soil interaction – Silica sand	137
4.5.2	Pipe-soil interaction – chert gravel.....	140
4.6	Pipe strains from in-pipe pressure fluctuation	143
4.6.1	Centrifuge study.....	143
4.6.2	Field study	145
4.7	The effect of pipe stiffness on strain response.....	147
4.7.1	Relative rigidity of pipe-soil system.....	147
4.8	Discussion	150
5	LONG TERM FIBRE OPTIC STRAIN MEASUREMENT AND LEAK DETECTION	152
5.1	Introduction.....	152
5.2	Strain calculation using Bragg gratings	152
5.3	Pipe and ground strain variation.....	153
5.4	September 2018 leak test	154
5.5	Strain changes during significant rainfall events	158
5.6	Comparison between thermal and mechanical leakage-induced ground strains.....	160
6	CONCLUSIONS	163
7	RECOMMENDATIONS FOR FURTHER RESEARCH AND DEVELOPMENT.....	165
7.1	Smart pipes	165
7.2	Distributed strain measurement	166
7.3	Selection of the most suitable fibre optic cable	166
8	LIST OF REFERENCES	167
APPENDIX A	Temperature fluctuation with depth over study period	173

LIST OF FIGURES

Figure 2-1: NRW international statistics (McKenzie et al., 2012).....	6
Figure 2-2: AWWA M36 leak classification and intervention methods (AWWA, 2009).....	8
Figure 2-3: Life cycle for a buried pipe (Rajani and Tesfamariam, 2004)	9
Figure 2-4: Factor of safety decrease over time (Rajani and Tesfamariam, 2004).....	10
Figure 2-5: Leaking service pipe causing sinkhole (Oosthuizen and Richardson, 2011).....	12
Figure 2-6: Damage to houses in Laudium in Pretoria due to a sinkhole (Oosthuizen and Richardson, 2011).....	12
Figure 2-7: Leaking water pipe caused a sinkhole to form in Waterkloof, Pretoria (Oosthuizen and Richardson, 2011).....	13
Figure 2-8: SANS 1529 water meter accuracy (du Plessis and Hoffmann, 2015)	14
Figure 2-9: Pipe materials – pressure vs. diameter (Van Dijk, 2016).....	19
Figure 2-10: Rigid PIPE trench specification	22
Figure 2-11: Flexible pipe trench specification.....	22
Figure 2-12: Optical Fibre Schematic (National Instruments, 2011)	23
Figure 2-13: FBGS operating principal (National Instruments, 2011)	26
Figure 2-14: Distributed fibre optic methods (Soga, 2017)	29
Figure 2-15: Typical Brillouin DSTS readout unit (Soga, 2017)	30
Figure 2-16: Fibre optic placement for different media and parameters (Frings , 2011).....	31
Figure 2-17: Fibre optic cable location to measure strain (Glisic and Yao, 2012).....	32
Figure 2-18: DiTeSt readout unit and fibre optic sensor cable (Inaudi and Glisic, 2010).....	33
Figure 2-19: Steady state temperature distribution around a crude oil pipe (Frings, 2011) ..	40
Figure 2-20: Normalised bending moment for a pipe (Vorster et al., 2005).....	43
Figure 2-21: Vertical settlement profiles for a rigid and flexible pipe (Marshall et al., 2010).	44
Figure 2-22: The influence of shear strain and shear degradation on the determination of the relative rigidity of a pipeline (Marshall et al., 2010).....	46
Figure 2-23: Relationship between normalised hogging and sagging moments and pipe-soil rigidity (Marshall et al., 2010).....	47
Figure 2-24: Schematic of tunnel excavated underneath a pipeline (Vorster et al., 2005) ..	49
Figure 2-25: The effect of pipe-soil rigidity on pipe bending moments (Vorster et al., 2005)	51
Figure 2-26: Schematic of mechanisms that may impact pipe behaviour (Vorster et al., 2006)	53
.....	
Figure 2-27: Relative pipe-soil settlement (Vorster et al., 2006).....	54
Figure 2-28: Change in pipe-soil contact pressures due to gap formation (Vorster et al., 2006).....	55

Figure 2-29: Solution sinkholes (Nel et al., 2011)	58
Figure 2-30: Cover subsidence sinkholes (Nel et al., 2011)	58
Figure 2-31: Cover collapse sinkholes (Nel et al., 2011)	59
Figure 3-1: In situ soil temperature distribution	61
Figure 3-2: Thermistor placement on the experimental farm	62
Figure 3-3: DataTaker DT615 with 10 channels	62
Figure 3-4: Pierre van Ryneveld reservoir location	63
Figure 3-5: RTD 4 – 20 mA corresponding to >0-100°C output.....	64
Figure 3-6: RTD installed at Pierre van Ryneveld reservoir.....	64
Figure 3-7: Experimental arrangement for laboratory leakage experiment.....	65
Figure 3-8: Photograph of the experimental arrangement for laboratory leakage experiment.	65
Figure 3-9: Location of in situ pipe leakage experiment	67
Figure 3-10: View of the location of pipe leakage experiment	67
Figure 3-11: Layout of experimental arrangement installed on the experimental farm of the University of Pretoria.....	72
Figure 3-12: Excavation of trench	73
Figure 3-13: Sensor layout and levelling bottom of trench in preparation for pipe and instrumentation installation	74
Figure 3-14: Installing sensors on the trench bottom.....	74
Figure 3-15: Epoxying FBGS to pipe base	75
Figure 3-16: Instrumented pipe in trench	75
Figure 3-17: Backfilling pipe and sensors	76
Figure 3-18: Finishing off installation	77
Figure 3-19: Box and Whisker plot January 2017	78
Figure 3-20: Box and Whisker plot February 2017	78
Figure 3-21: Box and Whisker plot March 2017	79
Figure 3-22: Box and Whisker plot April 2017	79
Figure 3-23: Box and Whisker plot May 2017	79
Figure 3-24: Box and Whisker plot June 2017	79
Figure 3-25: Box and Whisker plot July 2017	80
Figure 3-26: Box and Whisker plot August 2017	80
Figure 3-27: Box and Whisker plot September 2017	80
Figure 3-28: Box and Whisker plot October 2017	80
Figure 3-29: Soil temperature with depth and rainfall variation over the course of the study period.....	81

Figure 3-30: First and third quartile temperature variation with depth for summer and winter months (2017).....	81
Figure 3-31: Air and water temperatures recorded at Pierre van Ryneveld reservoir (Tshwane) May to October 2017.	82
Figure 3-32: First and third quartile soil and water temperature variation with depth for July 2017.....	83
Figure 3-33: Advancing wetting front in laboratory test.....	84
Figure 3-34: Temperature record from laboratory wetting test.....	84
Figure 3-35: Wetting tests on red-brown silty sand and light brown silica sand to investigate initial rise in temperature during passage of wetting front.....	85
Figure 3-36: Temperature record from wetting test.	85
Figure 3-37: Elevation of experimental installation showing location of Leakage test 1	90
Figure 3-38: Water temperature during the first leak test	90
Figure 3-39: Thermistor layout for each thermistor string	91
Figure 3-40: Temperature changes at leak location LL3 (TS8)	92
Figure 3-41: Temperature changes 0.15 m upstream of leak location LL3 (TS7).....	92
Figure 3-42: Temperature changes 0.15 m downstream of leak location LL3 (TS9).....	92
Figure 3-43: Temperature changes at reference string LL3 (TS1) away from the leak location	92
Figure 3-44: Temperature profile around LL3 before (left) and during (right) the leak.....	94
Figure 3-45: Temperature change profile around LL3 before (left) and during (right) the leak	95
Figure 3-46: Elevation of experimental setup showing location of Leakage test 2	96
Figure 3-47: Water temperature during the second leak test at LL2.....	96
Figure 3-48: Temperature change at leak location LL2 (TS5)	97
Figure 3-49: Temperature change 0.15 m upstream of leak location LL2 (TS4)	97
Figure 3-50: Temperature change 0.15 m downstream of leak location LL2 (TS6).....	97
Figure 3-51: Temperature change at reference string LL2 (TS1)	98
Figure 3-52: Temperature profile around LL2 before (left) and during (right) the leak.....	99
Figure 3-53: Temperature change profile around LL2 before (left) and during (right) the leak	99
Figure 3-54: Experimental elevation schematic of test 3 at LL1	100
Figure 3-55: Water temperature during the second leak test at LL1.....	100
Figure 3-56: Temperature change at leak location LL1 (TS2)	101
Figure 3-57: Temperature change 0.15 m upstream of leak location LL2 (TS1)	101
Figure 3-58: Temperature change 0.15 m downstream of leak location LL1 (TS3).....	102
Figure 3-59: Temperature change at reference string LL1 (TS4)	102

Figure 3-60: Temperature profile around LL1 before (left) and during (right) the leak.....	103
Figure 3-61: Temperature change profile around LL1 before (left) and during (right) the leak	103
Figure 3-62: Elevation of experimental setup	104
Figure 3-63: Cross section through the leak location showing the FBGS layout relative to the pipe	105
Figure 3-64: Elevation of experimental setup for LL3	105
Figure 3-65: Strain changes over time for Leak test 1 from epoxied FBGS.....	106
Figure 3-66: Strain changes over time for Leak test 1 from free FBGS	106
Figure 3-67: Comparison of temperature compensated vs non-compensated strains for epoxied FBGS 6.....	107
Figure 3-68: Comparison of temperature compensated vs non-compensated strains for free FBGS 11	107
Figure 3-69: Elevation of experimental setup for Leak test 2 LL2.....	108
Figure 3-70: Strain changes over time for leak 2 from epoxied FBGS.....	108
Figure 3-71: Strain changes over time for Leak test 2 from free FBGS	109
Figure 3-72: Comparison of temperature compensated vs non-compensated strains for epoxied FBGS 4.....	109
Figure 3-73: Comparison of temperature compensated vs non-compensated strains for free FBGS 13	109
Figure 3-74: Elevation of experimental setup for Leak test 3 LL1.....	110
Figure 3-75: Strain changes over time for Leak test 3 from free FBGS	111
Figure 3-76: Strain changes over time for Leak test 3 from free FBGS	111
Figure 3-77: Comparison of temperature compensated vs non-compensated strains for epoxied FBGS 2.....	111
Figure 3-78: Comparison of temperature compensated vs non-compensated strains for free FBGS 15	112
Figure 4-1: Particle size distribution of soils to be used in model studies	115
Figure 4-2: Oedometer test result – Silica sand.....	116
Figure 4-3: Oedometer test result – Chert gravel	116
Figure 4-4: Geotechnical centrifuge of the University of Pretoria	117
Figure 4-5: Centrifuge strong box	118
Figure 4-6: Schematic few of the centrifuge model frame	119
Figure 4-7: Stepper motor and trapdoor	120
Figure 4-8: The instrumented model pipes	122
Figure 4-9: Brass strip instrumented with strain gauges to measure leakage-induced ground strains.	123

Figure 4-10: Leak mechanism	123
Figure 4-11: Sand hopper used for placing silica sand in models	125
Figure 4-12: Complete model set-up with silica sand	126
Figure 4-13: Experimental model set-up with chert gravel and provision to leak simulation.	127
Figure 4-14: PIV representation of patches on initial images	128
Figure 4-15: Leakage-induced greenfield surface settlement curves	130
Figure 4-16: Leak progression and associated surface settlement under greenfield conditions.....	132
Figure 4-17: Row of patched tracked using PIV to study shape of leakage-induced surface settlement trough	133
Figure 4-18: Greenfield leakage-induced surface settlement troughs tracked using PIV during leak propagation.	133
Figure 4-19: Variation in distance to inflection point (i) as a function of the amount of moisture leaked into soil.	134
Figure 4-20: Comparison of spreading of leakage-induced wetted zones under greenfield conditions (left) and with a pipe in the ground (right).	135
Figure 4-21: Comparison of settlements from greenfield test and with pipe present.....	136
Figure 4-22: Invert level soil deflection – centrifuge sand.....	138
Figure 4-23: Pipe and invert level soil deflection – centrifuge sand.....	139
Figure 4-24: Relative pipe-soil settlement – silica sand.....	140
Figure 4-25: Invert level soil deflection – chert gravel.....	141
Figure 4-26: Pipe and invert level soil deflection – chert gravel.....	142
Figure 4-27: Relative pipe-soil settlement – chert gravel.....	143
Figure 4-28: Pipe hoop strain during internal pressure fluctuation during a leak test studied in the centrifuge	144
Figure 4-29: Longitudinal and hoop pipe strain during internal pressure fluctuation during a leak test studied in the centrifuge.	144
Figure 4-30: Strain changes measured by the epoxied FBGSs during internal pressure fluctuations.....	145
Figure 4-31: Strain changes measured by the free FBGSs in the ground during internal pressure fluctuations in the pipe in (a) unsaturated soil and (b) saturated soil.....	146
Figure 4-32: Relative flexibility classification of uPVC and steel pipe of different radius and leakage-induced trough width parameter (i)	149
Figure 5-1: Variation in pipe strain during 2018	153
Figure 5-2: Variation in ground strain during 2018.....	153
Figure 5-3: FBG location in experimental pipe installation.....	154

Figure 5-4: Flow rate during the September 2018 leak test.....	156
Figure 5-5: Strain readings from FBGs fixed to pipe during the September 2018 leak test	156
Figure 5-6: Strain readings from free-floating FBGs during the September 2018 leak test	156
Figure 5-7: Zeroed strain readings from FBGs fixed to pipe during the September 2018 leak test	157
Figure 5-8: Zeroed strain readings from free-floating FBGs during the September 2018 leak test	157
Figure 5-9: Zeroed strain readings from free-floating FBGs during the September 2018 leak test (enlarged scale)	157
Figure 5-10: Spatial distribution of leakage-induced strain along pipeline.	158
Figure 5-11: Zeroed strain readings from FBGs fixed to pipe during the March 2018 rainfall event	159
Figure 5-12: Zeroed strain readings from free-floating FBGs during the March 2018 rainfall event	159
Figure 5-13: Spatial distribution of rainfall induced strain along pipeline.	160
Figure 5-14: Variation in mechanical and thermal leakage-induced strains during the Sept 2018 leak test at FGB 13.	161
Figure 5-15: Variation in mechanical and thermal leakage-induced strains during the Sept 2018 leak test at FGB 15.	162
Figure 7-1: Modified pipe design to accommodate a fibre optic cable for pipe strain measurement.	165

LIST OF TABLES

Table 2-1: Comparison of different fibre optic sensors (National Instruments, 2011).....	24
Table 3-1: Tests carried out.....	89
Table 4-1: Particle size ranges	114
Table 4-2: Specifications of the geotechnical centrifuge (Jacobsz et al., 2014)	117
Table 4-3: Pipe dimensions	121
Table 4-4: Strain gauge specifications.....	122
Table 4-5: Scaling laws applicable to centrifuge testing (Taylor, 1995).....	124
Table 4-6: Relative rigidity of pipe-soil system in model test	148

LIST OF ABBREVIATIONS

ASSHTO	American Association of State Highway and Transportation Officials
AWWA	American Water Works Association
BFW	Basic Free Water
CARL	Current Annual Real Losses
DSTS	Distributed Strain and Temperature Sensor
EPA	Environmental Protection Agency
FBGS	Fibre Bragg Grating Sensor
FOS	Fibre Optic Sensors or Factor of Safety (look at context)
GIS	Geographical Information System
IAM	Integrated Asset Management
ILI	International Leakage Index
IWA	International Water Association
KPI	Key performance indicator
NRW	Non-Revenue Water
OMC	Optimum Moisture Content
RTD	Resistance Temperature Detector
SABS	South African Bureau of Standards
SANS	South African National Standards
SCADA	Supervisory Control and Data Acquisition
TMH	Technical Methods for Highways
UARL	Unavoidable Annual Real Losses
WDM	Water Demand Management
WSDP	Water Services Development Planning
ZMA	Zone Meter Areas

LIST OF SYMBOLS

σ	Stress in the pipeline [$M.L^{-1}.T^{-2}$]
ε	Axial strain [-]
ε_b	Bending strain [-]
M	Bending moment [$M.L^2.T^{-2}$]
E_p	Stiffness of pipeline material [$M.L^{-1}.T^{-2}$]
E_s	Stiffness of soil at pipeline level [$M.L^{-1}.T^{-2}$]
I_p	Moment of inertia of the pipeline [L^4]
D_p	Outside diameter of the pipeline [L]
r_0	Outside radius of the pipeline [L]
i	Distance between the trapdoor centreline and the soil settlement trough inflection point [L]
A_p	Cross-sectional area of the pipeline [L^2]
R	Relative pipe-soil rigidity [-]
S_{max}	Maximum soil deflection [L]
S_v	Greenfield subsoil settlement at pipe invert level [L]
S_s	Soil deflection at the surface [L]
S_p	Pipe deflection at pipe invert level [L]

1 INTRODUCTION AND OBJECTIVES

1.1 Background

It is estimated that approximately 26% of the potable water distributed by the City of Tshwane is lost due to leakages from the aging distribution system. Just in the City of Tshwane this amounts to approximately 75 million m³ metres per annum. In towns like Grahamstown with older infrastructure the percentage losses is substantially larger and it is often mentioned in the media that up to a third of potable water distributed in South Africa is lost from the system. In a water scarce country like South Africa with a growing population and growing urbanisation, this can barely be afforded. A similar situation is prevalent in practically all arid countries around the world.

Not only does this non-revenue water (NRW) result in large financial losses to local authorities and water distribution agencies, but in the province of Gauteng, of which approximately 20% is underlain by dolomite bedrock, leaking water services may trigger the development of sinkholes and subsidence. This poses a serious threat to all types of infrastructure and even human safety. It has, in fact, been reported by Buttrick and Van Schalkwyk (1998) that 98.9% of all new sinkholes in the Tshwane area are triggered by leaking water services, either from the distribution network or from the wastewater system. Before the leak is detected and as the sinkhole develops due to leakage, the leak is likely to be made worse by the ground movement associated with the development of the sinkhole, resulting in a large volume of water being lost.

Perhaps the most significant problem with water lost from the distribution system is that the presence and location of leaks are not easily detected before a very large volume of water had been lost so that remedial action is normally only taken very late. Many water leaks do not surface, resulting in detection difficulties.

In the last approximately 20 years fibre optic instrumentation has been developed to measure temperature and strain with an unprecedented resolution exceeding that of conventional instrumentation. It is possible to take continuous strain readings along the length of a fibre optic cable extending up to 50 kilometres or, by creating imperfections referred to as Bragg gratings at know locations along the length of a fibre optic cable, strain can be measured at up to 20 discrete locations at a high sampling rate. This also applies to temperature. A major advantage is that fibre optic cables are cheap and completely inert in that it is not affected by the electrical disturbances that electric monitoring systems typically suffer from.

A major initiative by the Division of Civil Engineering at the Department of Engineering at the University of Cambridge has seen the formation of a group known as the Cambridge Centre for Smart Infrastructure and Construction (CSIC) who, over the last 10 years, have demonstrated that by applying fibre optic technology an unprecedented amount of data can be obtained at very reasonable cost, thus allowing engineers to monitor the performance of numerous types of infrastructure. Collaboration to monitor strains in integral bridges (bridges constructed without expansion joints) has already been established between the Department of Civil Engineering at the University of Pretoria and CSIC in Cambridge.

This project investigated the application of fibre optic technology to monitor newly installed pipelines for leakage. Identifying and timeously fixing leaks will save large volumes of potable water currently being wasted, potentially realising large cost savings. This will also assist in the prevention of sinkhole formation and other related damage which impacts on human safety and the integrity of infrastructure.

1.2 Objective

It was hypothesised that by measuring strain and temperature profiles along the length of a pipeline, say, annually and comparing the readings to the record of the previous year, changes, possibly indicative of leaks, can be detected and appropriate and timeous remedial action taken. If this system proves successful, it is envisaged that because of the low cost, new water distribution pipes can in future be fitted with fibre optic instrumentation which can be monitored periodically to detect leaks.

1.3 Methodology

The methodology applied in carrying out the project is briefly summarised.

Literature review

The project commenced with a literature study on conventional and new techniques employed to monitor the integrity and performance of pipelines and the application of fibre optic monitoring to observe the behaviour/performance of structures. The literature review was subsequently expanded to cover strain response of pipes affected by ground movement to obtain an understanding of how ground movements caused by pipe leaks could affect pipelines of various stiffness.

Investigating natural temperature changes in the ground

It was originally hypothesised that the success of the leakage detection system under investigation hinges on the ability to distinguish leakage-induced temperature changes from natural temperature changes in the field. Natural temperature cycles (both day and seasonal) therefore needed to be studied. A set of thermistors were installed at depth increments of 250 mm in a testpit on the University of Pretoria's Hillcrest Campus down to a depth of 3 m and were monitored over the two year project duration to study natural ground temperature variation with depth.

Investigating temperature changes caused by water leaks (laboratory phase)

A number of tests were carried out in the laboratory in which water was allowed to leak under controlled conditions from a pipe instrumented with a number of thermistors to observe temperature changes in the ground around a pipe.

Investigating temperature changes caused by water leaks (field phase)

A short length (12 m) of 100 mm diameter (uPVC) pipeline was installed on the University of Pretoria's Hillcrest Campus to verify whether the proposed system would work in the field. It was instrumented with an array of fibre optic and conventional thermistors. A field experiment was carried out as the ambient temperature changes occurring in the field are different from that in the laboratory and it was necessary to assess whether leakage-induced temperature changes can be distinguished from those occurring naturally.

Pipe strain changes from water leaks

Over time, leakage is likely to result in stress and hence strain changes in the ground near the leak and these are likely to impose strain on the pipe due to changes in the support conditions underneath and loading on the pipe. In addition to the temperature measurement referred to above, the pipe installed in the field was also instrumented for strain. The field testing showed that monitoring strain changes provides a much more sensitive means of leak detection than using temperature measurement on its own. Leakage-induced strain changes in the ground (separate from the pipe) and on pipes themselves were investigated further by means of physical model tests and further field testing as described in this report.

Reporting

This report contains a description of the entire study, presenting the following:

- Chapter 1 Introduction
- Chapter 2 Literature review
- Chapter 3 Leakage-induced temperature and strain changes
- Chapter 4 Physical model study into leakage-induced strain changes

Chapter 5	Long term fibre optic strain measurement and leak detection
Chapter 6	Conclusions
Chapter 7	Recommendations for further research and development
Chapter 8	List of references

2 LITERATURE STUDY

2.1 Introduction to literature review

The project commenced with a literature study on conventional and new techniques employed to monitor the integrity and performance of pipelines and the application of fibre optic monitoring to observe the behaviour/performance of structures. This literature study contains an overview of buried water pipeline installation requirements for different pipe materials, current leak detection techniques and statistics regarding water leaks. Literature that supports the theory that rapid changes in soil temperature can be used as a method to detect potable water leaks is presented. Various options in terms of existing leak detection methods, their advantages and disadvantages are investigated, as well as the use of uncommon fibre optic techniques. South African soil conditions and buried water pipe installation details are examined to determine the applicability and the prospects for success of using measured temperature changes as a leak detection method. Temperature measuring devices are discussed and terminology is clarified

Due to leaking water pipes being one of the leading causes of man-made sinkholes, consideration should be given to the mechanisms that govern sinkhole formation and aspects affecting its occurrence. Thus, the main aim of the literature review is to examine these mechanisms and consider the various behavioural properties of pipelines subjected to ground movement, i.e. sinkholes. The definition and types of sinkholes that may exist, also considering factors influencing it, are discussed. Pipe-soil interaction is the key focus of this review, examining experiments that was conducted in the past, which may be applicable, and in some way similar, to sinkhole formation. Various mechanisms explaining the interaction between a pipe and its surrounding soil were considered, followed by the behavioural (rigidity) characteristics of various buried pipelines – which is a function of the stiffness of the soil and pipeline. The chapter concludes with a section that describes the bending behaviour of a pipeline subjected to ground movement.

2.2 Potable water pipe leaks

Potable water pipe leaks in distribution networks is a major concern to water authorities and suppliers due to incurred financial losses, environmental implications and loss of supply potential. Financial losses are incurred when treated water cannot be sold against a possible income. Raw water abstraction, treatment and distribution forms part of the economic cycle

involved in supplying water and for which municipalities pay suppliers. Waste and storm water systems are generally designed to be gravity driven, whereas potable water is pumped from water treatment works to reservoirs or high points acting as distribution points and then gravity driven to consumers. Therefore the pumping of treated water to high points can be specified as a key cost component of potable water after the treatment process, depending on the conveyance distance between treatment works and consumer (McKenzie, 2001a).

In South Africa it is estimated that NRW amounts to 36% which falls between developed countries such as Australia, with as little as 7% NRW and developing countries such as Armenia, with up to 83%, and Albania with 70% (McKenzie et al., 2012) (see Figure 2-1 below). It should however be noted that data quality concerns with regard to current NRW statistics have been raised as some of the data is estimated from historic trends due to equipment malfunction and limited maintenance. The size and extent of water distribution networks and bulk supply schemes is a major hurdle to overcome. The complexity further intensifies as to decide on a maintenance regime that takes into account the age, materials and operating regimes of the various network zones and the subsequent intervention periods to conduct leak surveys and condition assessments (Henrie et al., 2016).

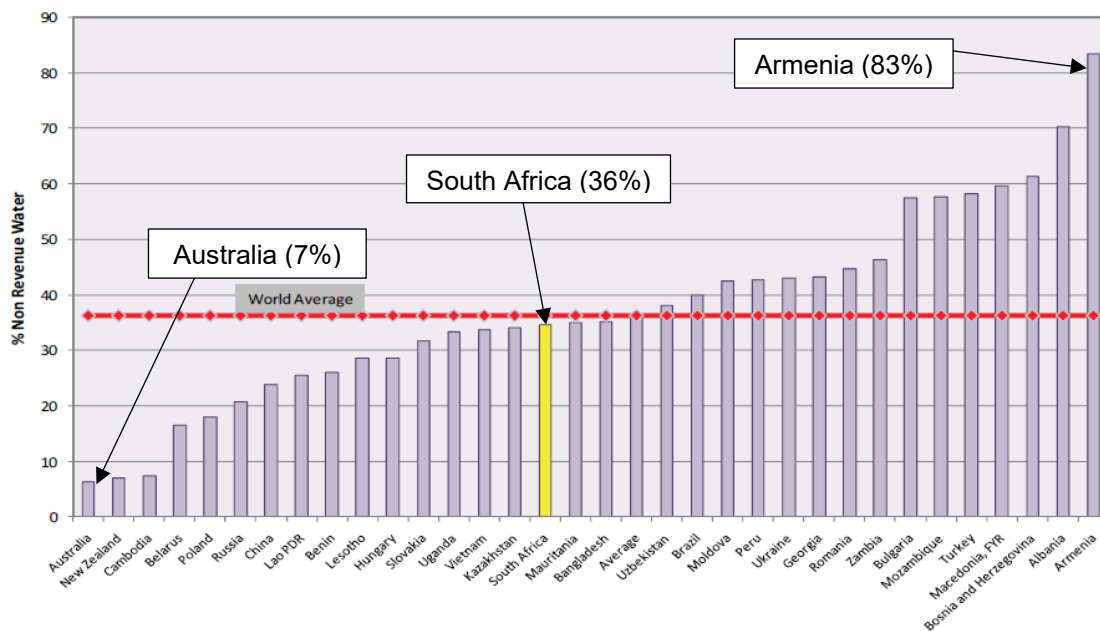


Figure 2-1: NRW international statistics (McKenzie et al., 2012)

A metric known as the Infrastructure Leakage Index (ILI) is commonly used to indicate the amount of water leaked from a system due to actual leaks. It is calculated by taking the ratio of the Current Annual Real Losses (CARL) to the Unavoidable Annual Real Losses (UARL). CARL is defined as the total sum of water losses from a system, even those resulting from

operator errors such as when reservoir overflows. This metric is found by compiling a water balance, considering water input minus water output from the system. UARL is defined as being the minimum technically possible amount of water lost due to leaks, which is a function of network pipeline length, number of household connections, length of service connection (through private property) and the average pressure value in the system, see Equation 2-1 for details (McKenzie et al., 2012).

$$\text{UARL} = (18 \times L_m + 0.8 N_C + 25 \times L_p) \times P \dots\dots\dots \text{Equation 2-1}$$

- UARL = Unavoidable Annual Real Losses (litres/day)
- L_m = pipeline network length (km)
- N_C = total no. of connections in system
- L_p = total length of service connection pipes passing through private property
- P = average pressure value in the system

To establish a technically correct ILI, a water balance has to be obtained from the investigated water network. A water balance is essentially the difference between the water entering an isolated network (one inflow or isolated zone) and water being consumed. The difference between the supply and demand can then be specified as NRW with a small percentage subtracted as UARL (McKenzie et al., 2002).

Studies have been conducted in major municipalities in South Africa to determine the amount of NRW, most major municipalities within South Africa compile their NRW statistics periodically. The NRW then serves as key performance indicator (KPI). These studies were used to create and calibrate leakage models such as BENCHLEAK, ECONOLEAK, PRESMAC and SANFLOW. All of the models mentioned above deal with certain aspects of potable water leaks, such as pressure management, creating working knowledge of water balance and economic implications of leaks and standardizing procedure to classify bursts and background losses (McKenzie et al., 2002).

A number of documents listed below discuss the historic and current potable water loss situation in South Africa and summaries of case studies conducted:

- Metropolitan Municipality Non-Revenue/Water Loss Assessment (Wegelin and McKenzie, 2013)

- Benchmarking of Leakage from Water Reticulation Systems in South Africa (McKenzie et al., 2002)
- LEAKAGE MANAGEMENT – Introduction to WRC Tools to Manage Non-Revenue Water (McKenzie and Bhagwan, 2003)
- The State of Non-Revenue Water in South Africa (2012) (McKenzie et al., 2012)

Buried pipeline leaks are categorised in three main groups, being background, unreported and reported leakage, as shown in Figure 2-2 below. Background and unreported leaks are the biggest concern as they are undetected for many years or decades, depending on the amount of pipeline surveys conducted and the available maintenance budget.

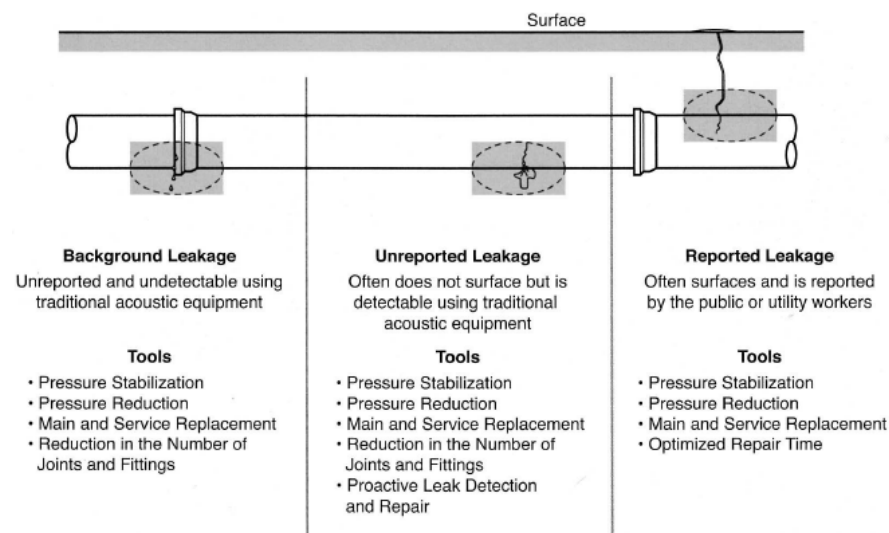


Figure 2-2: AWWA M36 leak classification and intervention methods (AWWA, 2009)

Background leaks commonly occur at joints or couplings they are very minute leaks and therefore not easily detectable by traditional acoustic equipment. Unreported leaks are categorised as leaks occurring throughout a pipeline due to lacking support conditions, excessive bending or other mechanical failures, these leaks commonly have higher flow rates compared to background leaks. Reported leaks tend to have excessive flow rates which surface, are therefore reported and subsequently can be repaired (AWWA, 2009).

Lost water has many other implications besides supply reduction. There is a major financial aspect related to cost recovery, which has to be added to the revenue water portion. The amount of electricity used to abstract, treat and distribute water also has to be taken into

account. Large amounts of electricity are used to transfer water from rural areas to high density areas, where it is treated and stored to meet consumer demands (AWWA, 2009).

In South Africa externally visible leaks are referred to as bursts, while small leaks, which are more difficult to detect are referred to as background leaks. The threshold between background leaks and bursts is 250 l/hr. If the leak exceeds 250 l/hr it is classified as a burst and if it is less than 250 l/hr is classified as a background leak (McKenzie et al., 2006). To put the threshold flow rate into perspective, a flow rate of 250 l/hr is 0.0694 l/s or 4.2 l/min which is a third of the maximum flow rate typically to be expected at a household connection.

The life cycle of a typical buried water distribution pipeline can be described with the life cycle “bathtub” curve as shown in Figure 2-3 below. Three phases can be used to describe the life cycle, the first being the “burn-in phase”, which is used to describe the time just after installation, where leaks or failures are mainly caused due to installation defects or pipe defects. The second phase is the “in-use phase”, where very limited numbers of failures should occur after the pipe had settled. Failure typically occurs due to external interference such as overloading. The third and final phase is the wear out phase, where the pipeline reaches its design life and the pipe corrodes extensively, both internally and externally. The life cycle principle is applicable for all pipeline materials, environments and other important factors. However, the slope of the curve will change accordingly (Rajani and Tesfamariam, 2004).

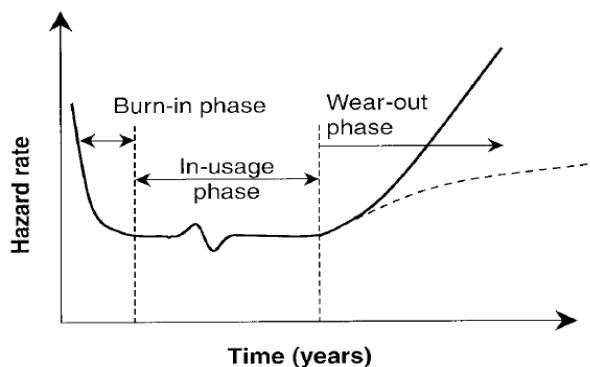


Figure 2-3: Life cycle for a buried pipe (Rajani and Tesfamariam, 2004)

Figure 2-4 indicates the Factor of safety (FOS) of the pipeline over time. If the pipe is defect free and is installed according to good practice, avoiding damage to the pipe, the FOS will initially be far above 1. After a certain period in the ground the pipe starts to deteriorate and corrode, due to a corrosive environment, poor water quality or natural deterioration. Once the initial break has occurred the pipe can start to leak and scour the supporting soil structure, which will eventually lead to failure with the FOS being just over or under 1. Over 1 would

mean very close to failure and under 1 would indicate a failure has occurred (Rajani and Tesfamariam, 2004).

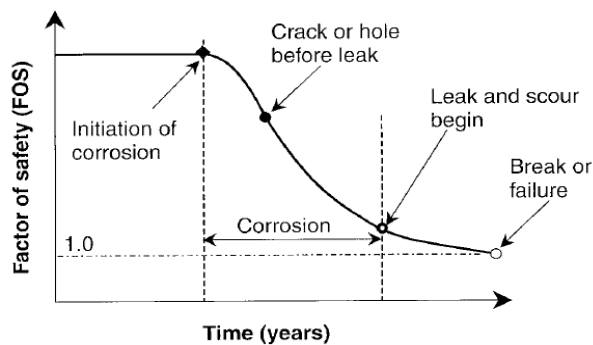


Figure 2-4: Factor of safety decrease over time (Rajani and Tesfamariam, 2004)

Pipe leaks are governed by the following factors: leak hydraulics, pipe material behaviour, soil hydraulics and water demand (Van Zyl, 2014b). Leakage hydraulics are described by the orifice equation below and the orifice or leakage coefficient is defined as 0.5 for turbulent flow, where the Reynolds number is greater than 4000-5000. For laminar flow, where the Reynolds number is less than 10, the orifice coefficient changes dramatically and can become very large. It was however shown that a laminar flow condition is very rare due to the prescribed pressure and flow requirements in pipelines. Equation 2-2 indicates the typical leakage/orifice equation (Van Zyl, 2014b).

$$Q = C_d A \sqrt{2gh} \dots \dots \dots \text{Equation 2-2}$$

- Q = Flow rate (m³/s)
- C_d = Orifice or leakage coefficient (dimensionless)
- A = Leakage area (m²)
- g = gravitational acceleration (9.81 m/s²)
- h = Available pressure head (m)

Pipe material behaviour is commonly based on the FAVAD model, which differentiates between rigid and elastic leaks (van Zyl, 2014b). Elastic pipe leak cross section areas vary linearly with pressure, whereas rigid pipe leaks are fairly independent of pressure. This behaviour has been modelled with finite element software for different pipe materials. For elastic leaks a head-area slope term is defined, which incorporates the shape of the leak, pipe materials and section properties. Equation 2-3 below indicates the change in area due to change in pressure for elastic leaks. The value of coefficient m is very small for round holes,

while for other types of openings the value of m have been approximated using Computational Fluid Dynamics (CFD) (van Zyl, 2014b).

$$A = A_0 + m h \dots\dots\dots \text{Equation 2-3}$$

- A = Area at specific pressure (m²)
- A₀ = Initial area (m²)
- m = head-area slope term
- h = head term

The two equations above are combined and shown in Equation 2-4 below (van Zyl, 2014).

$$Q = C_d (A_0 + m h) \sqrt{2gh} \dots\dots\dots \text{Equation 2-4}$$

2.2.1 Soil hydraulics

Soil hydraulics are often described in terms of the Darcy flow equation, however high flows present at a leak location invalidate the use of the Darcy equation. The flow mechanism should rather be described as piping or hydraulic fracturing (van Zyl, 2014b). The soil in close proximity to the pipe has been observed to act as an energy dissipation zone, but the high water pressures present in a reticulation network indicate that the soil surrounding a pipe does not have a major effect on pressure response of a leak. The area in close proximity to the leak can act as a fluid, therefore being described as soil fluidisation (van Zyl, 2014b).

Soil fluidisation occurs in granular material when soil particles are free to move with pore fluid and the inter-particle forces become negligible (Van Zyl et al., 2013). This phenomenon can also occur under confined conditions, for example in a pipe trench, depending on the support conditions. A two-dimensional fluidisation experiment was carried out with various homogenous glass beads sizes (small balls or beads), depths and orifice sizes to replicate the fluidisation mechanism. It was found that each flow rate reached a specific stable fluidisation area and that the smallest hole produced the biggest pressure loss, between the internal pipe pressure and the external soil interface. The homogeneity of the experimental material does however not replicate in situ backfill material and the variability thereof (Van Zyl et al., 2013).

2.2.2 Additional impacts of water leaks

In addition to a loss of potable water and the associated expense, distribution pipeline leaks in dolomitic areas can cause catastrophic surface failures known as sinkholes (see Figure 2-5 for details), which can also be formed naturally due to surface water ingress. Weathering of dolomitic rock occurs when rain water absorbs carbon dioxide, forming a weak carbonic acid. The slightly acidic groundwater enters tension fractures, faults and joints within dolomitic rock formations, which causes leaching of carbonate known as a dissolution process. The weathered dolomitic rock is usually overlain by much younger rock and soil cover which is highly variable, but typically less than 10 metres thick. These mechanisms cause the soil cover to erode or slump, losing support and exposing a cavity which leads to the formation of a hole as shown in Figure 2-6 and Figure 2-7. The process of dolomitic dissolution is very slow and takes place over geological time (Oosthuizen and Richardson, 2011).

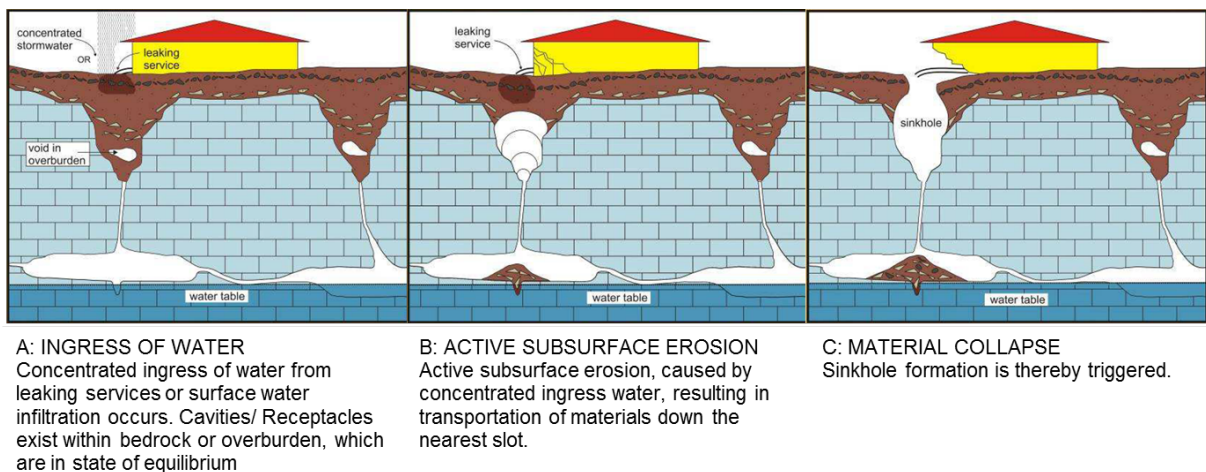


Figure 2-5: Leaking service pipe causing sinkhole (Oosthuizen and Richardson, 2011)



Figure 2-6: Damage to houses in Laudium in Pretoria due to a sinkhole (Oosthuizen and Richardson, 2011)



Figure 2-7: Leaking water pipe caused a sinkhole to form in Waterkloof, Pretoria (Oosthuizen and Richardson, 2011)

Being able to detect small settlements around a service pipe caused by subsurface failure can indicate a leaking service pipe and possibly lead to saving lives and limiting excessive damage to infrastructure caused by sinkholes.

Construction on dolomitic areas is governed by the South African Bureau of Standards (SABS) national standard SANS 1936 (2012). The document covers the following aspects of development on areas underlain by dolomitic areas:

- General Principles and Requirements
- Geotechnical Investigation and Determinations
- Design and Construction of Buildings and Structures
- Risk Management

2.3 Leak detection and management methods

Different methods can be used to detect potable water leaks, being either at a localised scale, looking at small portions of pipelines or at a network scale. So called “water audits” are typically done by municipalities to determine inflows (supply) and outflows (demand) of a subdivided section of a water distribution network. A major water distribution network is split into smaller constituencies, which are evaluated individually by isolating the system with valves or by using flow meters at strategic positions (du Plessis and Hoffmann, 2015).

The demand (consumption) and supply of water is determined according to flow meter readings taken each month by municipal workers, home owners or from estimation, depending

on the location of the flow meter and the availability of staff to conduct water meter readings. Municipal and domestic water meter accuracy is a controversial topic as it is specified by a supplier for a certain inlet and outlet pipe diameter, operating regime (pressure and flow rate), water quality and environmental condition. Water meters are not commonly recalibrated in South Africa or installed according to international best practice with regard to placement of bends and other pipeline components. Depending on the size of installation, the water meter should be installed with a straight upstream and downstream connection pipe to eliminate the effects of eddy currents or turbulence on the water meter (du Plessis and Hoffmann, 2015).

Domestic water meter performance testing is governed by South African National Standards SANS 1529 (2006) guidelines, which allows for very clear set target flow rate deviations, depending on the class of meter tested. There are class A to D meters where a class D meter is supposed to be the most accurate. A lower permissible relative error of 5% and an upper zone of 2% is prescribed in the standard. Pressure tests are performed on new domestic water meters with a test pressure which is 3 times greater than “normal” working pressure (1,600 kPa or 16 bar) and between 4,000 to 6,000 kPa. Figure 2-8 below indicates the lower and upper accuracy specification zones for specified flow rates of water meters (q_{min} , q_t , q_p and q_s) and different flow meter classes (a, b, c and d). The values are given within the SANS 1529 specifications and are not further discussed in this literature study.

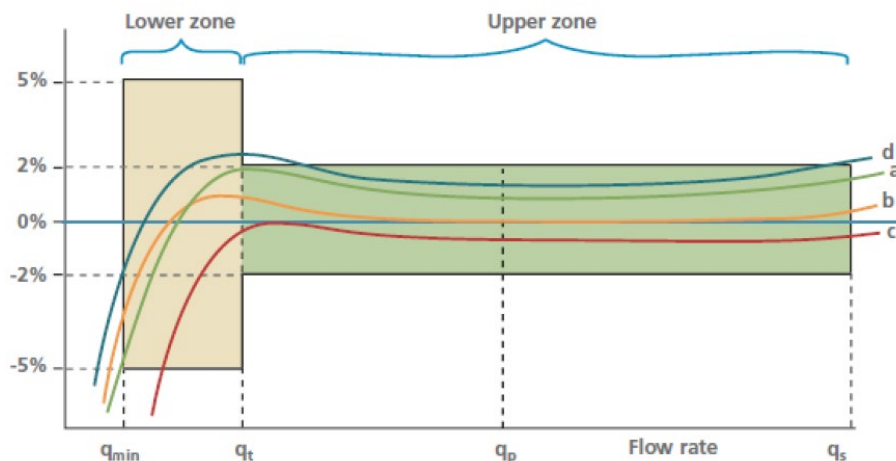


Figure 2-8: SANS 1529 water meter accuracy (du Plessis and Hoffmann, 2015)

A water meter audit was conducted on a minor water network portion in Cape Town to determine the accuracy of domestic water meters. The age of the water meters were in excess of 20 years and the cost of replacement had to be compared to the amount of water not billed to the consumer by possible meter reading errors. The study concluded that the water meter

accuracy is acceptable after the long operational life of the water meters. However, it is very difficult to obtain an absolute accuracy as certain flow meters might be more applicable to specific operating flow regimes and installation detail. It was indicated that extremely low and extremely high flows are either being over or underestimated (du Plessis and Hoffmann, 2015).

Night flow principles (assumption of no or limited flow) and typically high pressure can be used to determine leaks in a pipeline network, as the assumption is made that water is typically not used throughout the night in residential areas. If high flows occur in an isolated network, a leak might be present. This method is very labour intensive and has to be performed in a small time frame, not to affect consumers. Isolating valves in reticulation networks are often in a poor state, as they have not been exercised for a long time period or have been operated incorrectly (McKenzie and Bhagwan, 2003).

Other leak detection methods are listed below and might be used in combination with the above methods, where a mass balance or a water audit is the most common starting point:

- *Acoustic techniques* make use of a sensitive electronic or mechanical listening devices, which can detect vibrations caused by leaks. The success of these methods rely heavily on the experience of the operator, pipe material, diameter, soil type, natural surrounding water table depth, interference signals, type of leak, size of leak and pressure. It was found that pipes having an internal pressure of less than 1 bar absolute pressure, acoustic methods are not effective, as background noise might exceed leakage noise (Van Zyl, 2014a). An increase in internal pressure will lead to an increase in leak detection effectiveness due to greater vibration. More sophisticated leak noise correlators with advances micro-processing can be used to accurately determine the location and size of a leak (EPA, 2010).
- *Tracer gas technique* introduces gases such as helium or hydrogen into an isolated section of a pipeline. The gas is lighter than water and will therefore eventually permeate to the surface where it can be detected. The pipeline route is scanned directly above the surface with a sensitive gas detector, which will indicate the location of a leak (EPA, 2010).
- *Thermography* uses the principle of infrared imaging which detects long range infrared radiation with a range of up to 14,000 nm. A change in temperature will then indicate a leak. Infrared cameras can subsequently be used to locate these thermal radiation anomalies (EPA, 2010).

- *Ground penetrating radar (GPR)* can be used to detect voids caused by leaks or an increase in saturation levels. An increase in saturation levels increases the dielectric properties of soil, creating a discontinuity on the readout. The lag time from the transmitted to the reflected radar waves indicate the depth of a discontinuity, therefore indicating a possible leak or other buried services (EPA, 2010).
- *Remote water network sensing* is defined as small wired or wireless sensors embedded in a water distribution network which can measure flow, pressure and vibration. They are connected to a central control unit to monitor and indicate operational issues and leaks. These sensors are currently expensive and their lifespan might not be sufficiently long. However, they are improving rapidly and might become a good alternative to conventional measuring devices (EPA, 2010).
- *Satellite based radar technology* which uses spectral satellite imaging to detect the spectral signature of potable water in soil. The satellite imagery is superimposed onto the GIS water network to approximate leaks. Algorithms and filters are used to isolate background noise such as open water bodies, irrigation and other interferences. The leaks are then verified with alternative leak detection techniques and site visits (Utilis Israel Ltd., 2017).

South African models to quantify and mitigate leaks have been developed and the following guideline documents have been set up:

- **PRESMAC – Pressure Management Program (McKenzie, 2001)**
Pressure management incorporates the use of pressure management tools to minimise leaks as an increase in pressure will result in an increase in leaks. During high flow periods (high demand) the frictional losses will be very high, resulting in lower pressures throughout a water network the inverse principle applies to low flow scenarios causing a high pressure. To avoid such spikes in a system, certain methods can be used to alleviate high pressures.
- **ECONOLEAK – Economic Model for Leakage Management for Water Suppliers in South Africa (McKenzie and Lambert, 2002)**

Evaluating the most appropriate time for addressing possible leaks is covered by the ECONOLEAK guidelines. The method should however be used in conjunction with SANFLOW, PRESMAC and BENCHLEAK.

- SANFLOW- Development of a standardised approach to evaluate burst and background losses in water distribution systems in South Africa (McKenzie, 1999)

The leak and burst evaluation guidelines are set out to determine the actual losses in zone meter areas (ZMA) and to further priorities areas with unacceptable high losses.

- BENCHLEAK – Benchmarking of Leakage for Water Suppliers in South Africa (McKenzie et al., 2002)

The tools were developed to standardise definitions and to simplify water balances for municipalities and water authorities. The model consist of three main inputs being, the Length of Mains, Number of Service Connections and Average Operating Pressure.

It is clearly stated in the above guidelines that they have to be used in combination with each other to obtain a comprehensive leakage assessment and mitigation framework for a water network. Leaks might also be more pronounced during certain seasons, where the soil moisture content might change or consumption patterns. Disturbance caused by repair actions can introduce new leaks or support failures in a water network.

Most major municipalities in South Africa and internationally make use of integrated asset management software. The use of such software enables decision makers not only to predict infrastructure demand and expansion, but to make informed decisions about existing infrastructure. IMQS for example is a South African company that provides integrated asset management (IAM) solutions for various infrastructure components. The addition of Geographical Information Systems (GIS) into asset management provides a spatial overview for network infrastructure such as water pipelines, electricity grids, roads and many more. Supervisory Control and Data Acquisition (SCADA) systems are used to obtain data from various network components and relay the data to central control centres. Commonly point sensors are used to collect data, compared to a distributed approach, which is a possibility with distributed fibre optic sensors (Gumbo et al., 2003).

Two key words are often used in conjunction with water infrastructure planning, namely water demand management (WDM) and water services development planning (WSDP). A number of aspects cumulatively form these terms, which are, pipeline and water meter replacement, pressure management and zoning, leak detection and repair, stepped water tariffs according to demand, public awareness campaigns and the continuous update of information management tools (Van Zyl, 2014a).

2.3.1 Effect of pressure in pipeline on leak

Leakage management is a universal term used to describe actions taken to reduce losses in a potable water pipeline. It is generally understood that leakage rates and system pressures are directly related. St Venant's principle is often used to describe the shortening of a pipe due to an increase in diameter caused by internal pressure. The shortening effect can cause couplings or joints to leak due to a small pull out effect (AWWA, 2009).

The international leakage index parameter identifies system pressure as one of the main contributors to high leakage rates. It is therefore very important to design and operate a system with various pressure divisions to limit excessive pressure in certain areas of a network. Water supply networks are designed to supply a minimum allowable pressure at the furthest, highest or a combination of both in a system during high flow periods. These low pressure scenarios however only occur at high flow periods in the day such as in the early mornings or late afternoon/evenings. Other times of the day very high pressures can occur which can lead to elevated leakage rates (McKenzie, 1999).

2.4 Pipeline construction material, pipe support and construction specifications

2.4.1 Pipe materials

Various pipe materials are available and their selection depends on environmental aspects, pressure, diameter, stiffness and corrosive resistance requirements. Pipe materials range from thermoplastics such as polyvinylchloride (PVC) and polyethylene (PE), to metals such as ductile cast iron (DCI) and steel. Metal pipes are typically used for high pressure application, whereas plastic pipes are used in reticulation networks or harsh environments. There are different types of PVC pipes on the market such as un-plasticised or uPVC and modified or mPVC pipes (Van Zyl, 2014a). Composite pipes such as glass reinforced plastic (GRP) pipes are available, which are plastic fibres sandwiched between resin layers and cured to produce a solid pipe. Figure 2-9 below indicates different pipe materials with respect to the available diameters and pressure classes (Van Dijk, 2016).

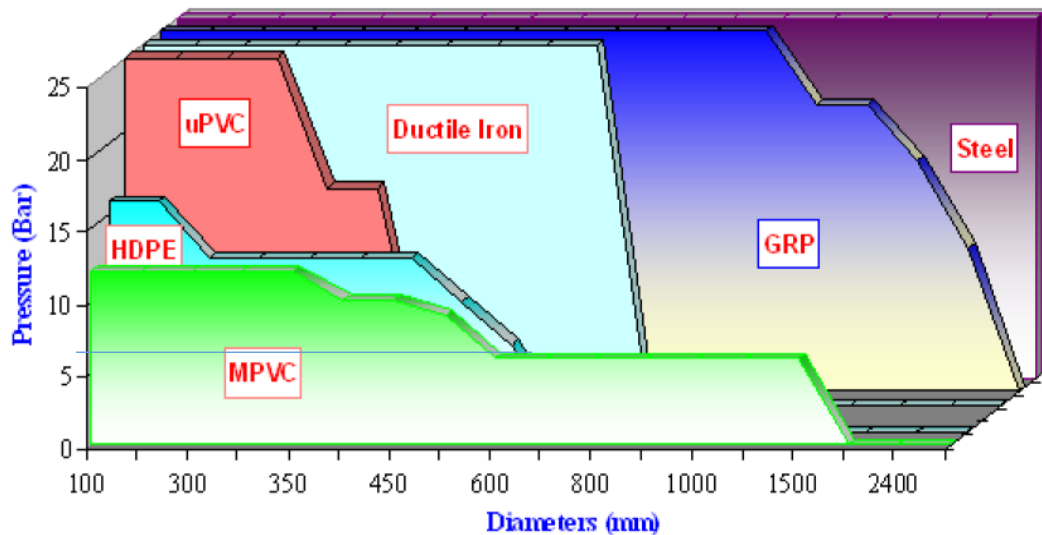


Figure 2-9: Pipe materials – pressure vs. diameter (Van Dijk, 2016)

Summary of pipe materials available:

- Thermoplastics
 - HDPE (high density polyethylene)
 - LDPE (low density polyethylene)
 - mPVC (modified polyvinylchloride)
 - oPVC (oriented polyvinylchloride)
 - uPVC (un-plasticised polyvinylchloride)
- Metal
 - DCI (ductile cast iron)
 - Copper (small diameter)
 - Stainless steel pipes (corrosive processes in industrial plants)
 - Steel (spiral or longitudinal weld)
- Composite
 - Asbestos cement (AC)
 - Fibre cement (FC)
 - GRP (glass reinforced plastic)
 - Pre-stressed concrete pipes

Thermoplastic pipes are commonly used in municipal reticulation networks as they are durable, lightweight and repair collars are inexpensive. Metal pipes such as steel and DCI are used for bulk water transfer schemes, where large diameter pipelines are required, which are able to cope with greater pressures. Composite pipes such as GRP have to be handled with

care to avoid stress fractures, delamination and extensive ultraviolet exposure (Van Zyl, 2014a).

2.4.2 Pipe-soil support

The first phase of this study entails an investigation into the use of temperature measurement as a means of leak detection on pipelines. After prolonged leakage it is likely that pipe support offered by the bedding will deteriorate, possibly resulting in deformation and hence strains on the pipe. The detection of such strains can hypothetically serve as a secondary indicator of leaks, reflecting the degree of structural distress on the pipeline and will be the focus of the second part of the study. Pipe-soil interaction is therefore briefly discussed.

Pipe-soil interaction is a complex topic especially with regard to the support function offered by the surrounding soil to a pipe. It is often difficult to compact around the base of a pipe, as this region cannot easily be accessed. Therefore the contractor has to ensure that the bedding cradle is adequately compacted before placing the pipe (SABS, 2008).

The soil-pipe stiffness interaction can either be classified as rigid or flexible depending on the pipe material, pipe dimensions and soil properties. A number of studies have been conducted on the effect of tunnelling on pipe deflection, characterising pipe and soil stiffness parameters. Similar behaviour experienced by tunnelling underneath pipelines should be expected for sinkhole formation and other type of support failures in buried pipelines (Vorster et al., 2005).

Pipes used in water distribution networks typically have spigot and socket connection with lengths of 6 m. In dolomitic areas continuously welded (fused) HDPE pipes are used to eliminate potential leakage at joint. The spigot and socket connections are allowed to rotate between 3° to 4° to allow for movement of the soil bedding and to follow the natural profile. However, over time this amount of rotation might not be possible due to aging of the rubber seal between two pipes. The design of pipelines to date also does not necessarily take into account aging of the pipe due to physical deterioration. However, the roughness factors are increased to allow for end of life hydraulic supply performance. The design also takes into account the resistance against circumferential stresses, such as overburden loads, live loads (traffic) and internal pressure. Loss of support from soil bedding and temperature dependant loads are not typically analysed in design. This could, however, be important in certain conditions where ground frost or very high temperatures are experienced. It was shown that excessive temperature differentials between water and soil can also lead premature pipeline failure (Rajani and Tesfamariam, 2004).

2.4.3 Pipeline construction specifications

South African Bureau of Standards (SABS) 1200 series is used to specify design details for medium pressure buried pipelines in South Africa. Pipe trenches are designed, constructed and payment is made in accordance with SABS 1200 DB (1989), which provide details pertaining the dimensions of the trenches, backfilling material specifications and compaction details. The pipe trench should be excavated as vertical as possible for at least the height of the bedding to limit excessive excavation. If the in situ trench bottom has been disturbed below the specified invert level, the backfill material has to be compacted to 90% of Modified American Association of State Highway and Transportation Officials (AASHTO) density at specified moisture content (SABS, 1989).

According to Technical Methods for Highways (TMH) 1 method A7, the maximum dry density and optimum moisture content (OMC) determination procedure is defined in terms of establishing a moisture – density relationship when compacted according to Modified AASHTO compaction efforts. The maximum density is defined as the highest density that can be obtainable at various moisture contents. The OMC is defined as the moisture content at which the maximum density can be obtained according to TMH 1 method A7 (CSIR, 1986).

Pipe bedding is specified in SABS 1200 LB, for both rigid (Figure 2-10) and flexible pipes (Figure 2-11) with and without joints and couplings. Bedding types and trench dimensions are categorised in various classes, depending on the pipe material and in situ soil type (SABS, 1983). Requirements for backfill materials are given.

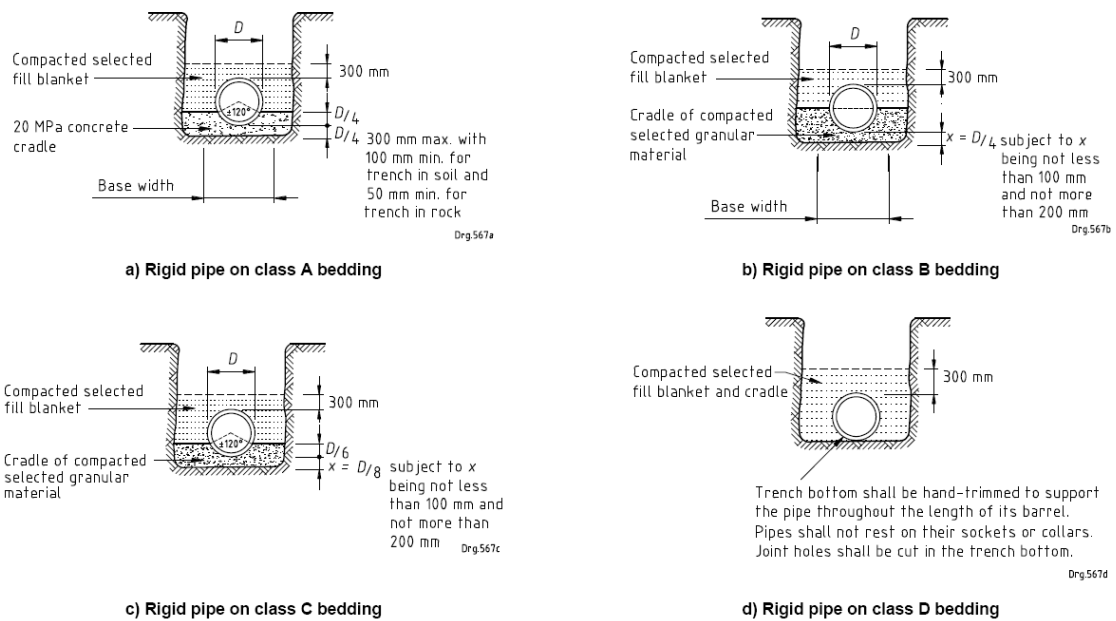


Figure 2-10: Rigid PIPE trench specification

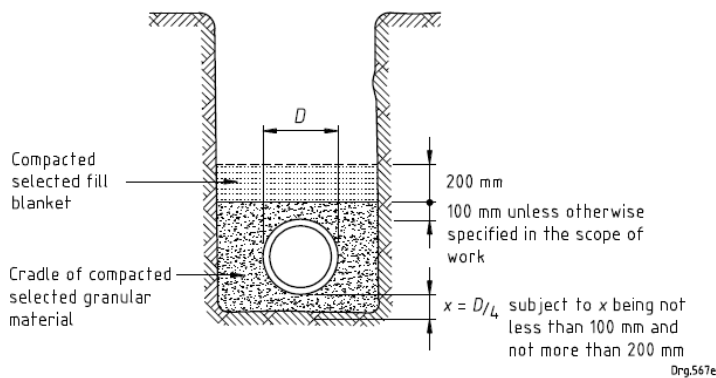


Figure 2-11: Flexible pipe trench specification

2.5 Fibre optic sensors (FOS)

Fibre optics technology was developed as a telecommunication transmitting medium since the 1960s. The development and deployment of the technology over long distances decreased the component cost and improved the cable quality, reducing overall transmission losses or attenuation. The principle of fibre optic transmission makes use of propagating light wave properties such as the intensity, phase, polarisation and frequency. The most simple fibre optical sensor comprises of a light source (pump), fibre optic cable, sensing element and interrogator or readout equipment (National Instruments, 2011).

The use of fibre optic cable as measurement sensors for strain, temperature and vibration evolved as research interest grew in the field of fibre optic technology. Over the past two decades the quality, sensitivity and resolution of FOS and interrogators improved significantly. There are various types of FOS available, depending on the intended application. Interrogators are optical instruments that emit a light pulse into the fibre optic sensor cable and analyse the return signal for changes in backscatter light amplitude and shifts in frequency (Kreuzer, 2013).

Fibre optic sensors (FOS) have many advantages over conventional sensor methods as they are not affected by electromagnetic interference, are nonconductive, electrically passive, low cost compared to alternatives and lightweight. Initially fibre optic cables contained too many impurities causing a high degree of damping (losses), up to 100 dB/km, which has since been reduced to less than 0.2 dB/km due to improved manufacturing processes. Only recently have fibre optic sensors been incorporated as structural health monitoring devices for infrastructure assets such as, bridges, buildings and pipelines (Kreuzer, 2013).

Fibre optic cables comprise of a number of layers, such as the core, cladding, buffer coating and jacket as shown in Figure 2-12 below. The core consist of a fine strand of glass which transmits light (n_1), the cladding (n_2) surrounds the core and reflects stray light into the core. This is achieved by having a core with a higher refractive index compared to the cladding, therefore reflecting the light within the cable. The buffer coating protects the cladding and the core from external influences and damage. The jacket further ruggedises the cable adding more protection to the cable and limiting the bend radius (National Instruments, 2011). More complex variations are available, depending on the intended application.

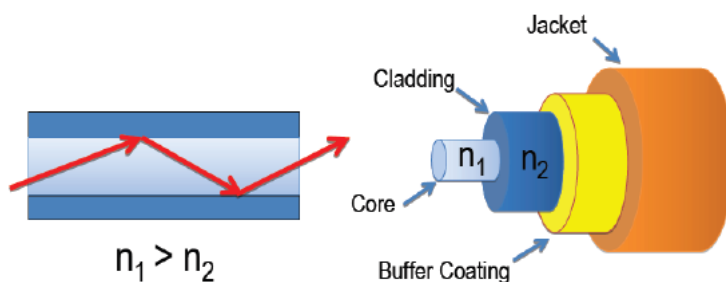


Figure 2-12: Optical Fibre Schematic (National Instruments, 2011)

A summary of the basic structure of a fibre optic cable is listed below:

- Core: Consists of very pure silicon dioxide (SiO₂ or glass).
- Cladding: Fused from SiO₂, has different level of impurities than core to adjust refractive index.
- Buffer coating: protective layer of ultraviolet cured acrylate or polyamide.
- Jacket: Mechanical protection consisting of polyethylene or other thermoplastic. Kevlar layer typically wedged between cladding and jacket.

2.5.1 Type of sensors

There are various fibre optic sensors (FOS) available on the market, which are classified as single-point, multi-point and distributed. A single-point sensor is typically located at the tip of the fibre optic cable, while a multi-point sensor has many discrete measuring points along the length of the fibre optic cable with virtually unlimited spacing options to match user requirements. Distributed sensors makes use of the entire cable length to measure changes in strain, temperature or vibration (National Instruments, 2011).

The focus of this literature study is to investigate Fibre Bragg Grating Sensors (FBGS) and Distributed Strain and Temperature Sensors (DSTS) shown in Table 2-1. Both sensors types are discussed below. There are however other sensor types such as intensity, interferometric, resonant and polarimetric type sensors which are not discussed in this literature study.

Table 2-1: Comparison of different fibre optic sensors (National Instruments, 2011)

Technology	Topology	Range (km)	Parameter			
			Temperature	Strain	Pressure	Vibration
FBGS	Multi- or Single-point	< 50	Yes	Yes	Yes	Yes
DSTS – Rayleigh	Distributed	< 0.07	Yes	Yes	No	No
DSTS – Raman	Distributed	< 20	Yes	No	No	No
DSTS – Brillouin	Distributed	< 50	Yes	Yes	No	No

FBGS are sensitive to temperature, strain, pressure and vibration. However it is difficult to disseminate between temperature and mechanically induced strain components. A temperature compensation technique has to be used, where a Bragg grating is isolated from mechanical strain and used to back calculate only temperature effects from the total strain. The distributed sensors can either measure strain and temperature or, when making use of Raman scattering, only temperature is measured (National Instruments, 2011).

2.5.2 Fibre Optic Bragg Sensors (FBGS)

Bragg gratings are created in single-mode glass fibre strands which consist of a core of between 4-9 μm in diameter and an outer cladding of 125 μm diameter (National Instruments, 2011). The outer core has a lower refractive index compared to the inner core caused by doping the inner core with Germanium or other photosensitive materials. The glass fibre core is coated with acrylate, polyimide or organic modulated ceramic (ORMOCER) to increase mechanical stability and limit attack of hydrogen and water. The fibre Bragg grating are written onto the core by dismantling the coating and using either a phase mask process or a superimposing laser light source to imprint imperfections (reflective fringes) at a desired wavelength (see Figure 2-13). The coating is later reapplied after the fibre grating has been written onto the core. This process has to be completed to a high standard of workmanship to preserve the mechanical stability and resistance of the cable. Three parameters govern FBGS properties, i.e. the grating mechanical strength, grating length and grating wave length (Rao,1997).

There are six different grating structure available, i.e. uniform positive-only index change, Gaussian apodised, raised cosine apodised, chirped, discrete phase shift and superstructure (Rao,1997). These terms define the shape of the grating structure and is defined as the optical filtering technique to improve the optical peak shape. There are five different types of gratings available being, type 1 grating, type 1A grating, type 2A grating, regenerated gratings and type 2 gratings. The type of grating relates to the processed used to produce the fibre. This summary is intended to indicate the variety of Bragg gratings available but details are outside the scope of this research topic. Braggs are typically created (“written”) with a grating wavelength of between 1500 nm and 1600 nm, which is the range in which most optical Bragg interrogators can capture reflected light signals (Kreuzer, 2013).

The FBGS or strain sensors are typically fixed to an object such as a bridge or a pipe by gluing or embedding the sensor in, for example, concrete. If a FBGS is stretched, a change in the wavelength of the reflected ultraviolet (UV) light can be detected. Each fringe will reflect a small amount of the incoming wavelength (Figure 2-13), depending on the amount of energy used to write the Bragg grating and the amount of Germanium used to dope the cable. The reflective factor per fringe varies between 0.001% and 0.1% of the total incoming light (Kreuzer, 2013). By writing Bragg gratings with incrementally different wavelengths (say 5 nm) onto a single fibre optic strand, a multi-point sensor can be created that can be interrogated with a single readout unit.

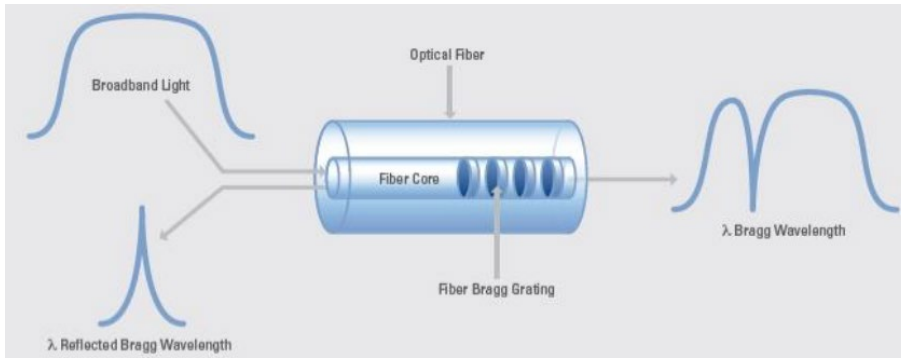


Figure 2-13: FBGS operating principal (National Instruments, 2011)

The wavelength of an FBGS changes with strain and temperature as shown in (Equation 2-5). Mechanical strain can be calculated with Equation 2-6 and temperature can be calculated with Equation 2-7.

$$\frac{\Delta l}{l_0} = k \times \epsilon + \alpha_{\delta} \times \Delta T \dots \dots \dots \text{Equation 2-5}$$

- Δl = change in wavelength (nm)
- l_0 = base wavelength at test start (nm)
- k = gage factor (0.78)
- ϵ = strain
- α_{δ} = change of the refractive index ($5 - 8 \times 10^{-6}/K$)
- ΔT = change in temperature (K)

$$\epsilon_m = \frac{1}{k} \times \frac{l_0}{\Delta l} - \left(\alpha_{sp} + \frac{\alpha_{\delta}}{k} \right) \times \Delta T \dots \dots \dots \text{Equation 2-6}$$

- Δl = change in wavelength (nm)
- l_0 = base wavelength at test start (nm)
- k = gage factor (0.78)
- ϵ_m = mechanical strain
- α_{δ} = change of the refractive index ($5 - 8 \times 10^{-6}/K$)
- α_{sp} = refractive index of specimen
- ΔT = change in temperature (K)

$$\Delta T = \frac{\Delta \lambda}{\lambda_0} \times \frac{1}{k \times \alpha_{glass} + \alpha_{\delta}} \dots \dots \dots \text{Equation 2-7}$$

- $\Delta\lambda$ = change in wavelength (nm)
- λ_0 = base wavelength at test start (nm)
- k = gauge factor (0.78)
- α_{δ} = change of the refractive index ($5 - 8 * 10^{-6}$ per Kelvin)
- α_{glass} = refractive index of glass ($0.55 * 10^{-6}$ per Kelvin)
- ΔT = change in temperature (Kelvin)

Draw Tower Gratings (DTG) FBGS have developed their own approximation formula as shown in Equation 2- below. The coefficient of thermal expansion given by DTG for the SWM-01 strain sensor is 0.5 micro strain per degree Celsius change in temperature.

$$\ln \frac{\lambda}{\lambda_0} = S_1 \times (T_1 - T_0) + S_2 \times (T_1 - T_0)^2 + k \times \varepsilon \dots\dots\dots \text{Equation 2-8}$$

- l = wavelength (nm)
- λ_0 = base wavelength at test start (nm)
- k = gauge factor (0.772 for DTG FBGS SWM-01 sensors)
- T_0 = base temperature at time t0 in Kelvin
- T_1 = temperature at time t1 in Kelvin
- S_1 = temperature coefficient 1 6.37×10^{-6}
- S_1 = temperature coefficient 2 7.46×10^{-9}
- ε = Strain

A summary of FBGS advantages is presented below:

- Very high strains can be measured ($>10\ 000\ \mu\varepsilon$), depending on the elasticity of the fibre optic cable.
- Sensors are small and lightweight
- Passive sensors, can be placed in high voltage, explosive environments and do not need an external power source
- Signal is not distance dependant, can be used for distances exceeding 50 km
- Many FBG sensors can be used in series, creating multi-point sensor
- Long term stable, corrosion resistant and very high temperature applications
- Low magnetic field interaction

A summary of FBGS disadvantages is presented below:

- Bragg gratings are very temperature sensitive. Therefore a temperature compensation techniques must be used if measuring only mechanical strain

- High sensitivity to lateral forces or pressure causing birefringence. Optical material property causing a refractive index depending on the polarisation and light propagation direction.
- FBGS have a much greater stiffness compared to other types of strain gauges
- Interrogator equipment is costly
- The installation of FBGS can require more surface area compared to conventional foil type strain gauges, due to minimum fibre bend radius of 10 mm

Fibre Bragg grating sensors have many advantages over traditional electro-mechanical sensors as shown above. Unfortunately no FBGS are manufactured locally in South Africa for industry use, which makes it currently an expensive alternative to consider. The University of Pretoria has used Bragg gratings manufacture by HBM and Draw Tower Grating (DTG) FBGS.

2.5.3 Distributed strain and temperature sensors (DSTS)

Distributed fibre optic sensors can detect temperature changes with a resolutions up to 0.05°C and spatial resolution of 1 m over 10 km if a specific fibre optic cable is used (Mishra, 2011). The quality of fibre optic cables is commonly tested using optical time-domain reflectometer (OTDR), which sends out a pulse of light and measuring the resulting backscatter. The amount of backscatter and absorption will indicate the quality of the cable and the total losses due to impurities. Exactly the same backscattering principle can be used for optical sensing techniques. DSTS makes use of the full length of cable as sensor to measure various parameters, such as strain, temperature, vibration and pressure. Three main categories of scattering are described, i.e. Rayleigh, Brillouin and Raman scatter (Inaudi and Glisic, 2010).

Figure 2-14 indicates the physical changes which are observed for the different types of backscatter mechanisms. As shown in the figure, Raman scatter is used to measure changes in temperature as the peak intensity of back-scattered light changes, while Brillouin scatter can be used for both temperature and mechanical strain as the wavelength of reflected light shifts in response to strain. Rayleigh backscatter can be used to determine strains for short measurement distances.

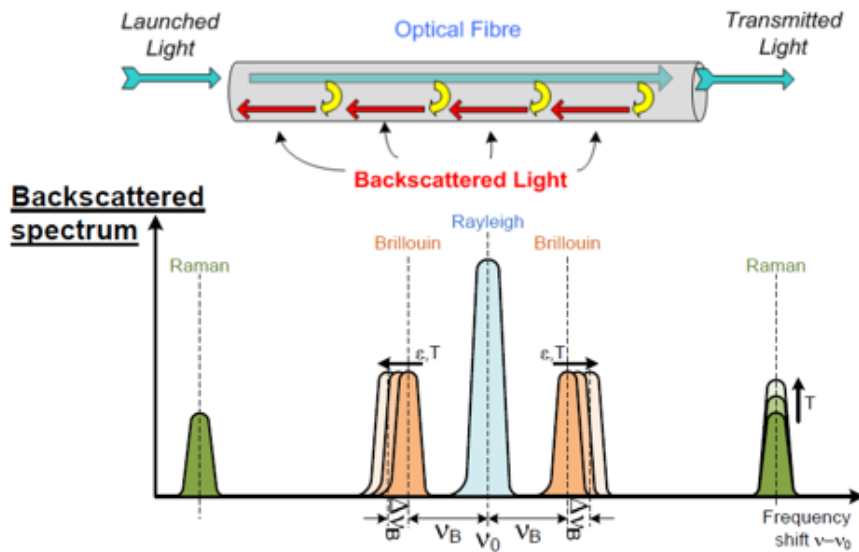


Figure 2-14: Distributed fibre optic methods (Soga, 2017)

The fundamental principle of DSTS is summarised briefly in the list below:

- Light pulse is sent through fibre optic cable
- Back scatter detected by optical interrogator
- Location of back scattering deduced by travel time interval, as speed of light is known
- The shift in frequency of back scatter light corresponds to change in strain
- The frequency shift can be converted to strain
- By repeating this process for all back scatter points a strain profile can be created for whole length of cable

These three different types of scatter principals and analysis methods available are described in detail below (Inaudi and Glisic, 2010):

Rayleigh method is the most dominant scattering and analysis method, and depends on the density and composition fluctuation resulting from the manufacturing process. A narrow wave length light pulse is shone into the cable and impurities or variations cause back-scatter which are used to determine the locations. This backscattering technique is insensitive to temperature changes and is not recommended for distances greater than 70 metres (Inaudi and Glisic, 2010).

Raman scattering makes use of molecular vibrations of glass fibre which is stimulated by incident light. The final scatter has two components, which are on both sides of the wavelength of the incident light. They are referred to as Stokes and anti-Stokes. The ratio between the Stoke and anti-Stoke represents the temperature sensitive component and is independent of

strain influences. This type of scattering application is commonly used for oil and gas applications to monitor temperature (Inaudi and Glisic, 2010).

Brillouin scattering can also be used to detect acoustic vibration. Conservation of energy principles are used to determine the frequency shift between the Brillouin scattering and the incident light. The frequency shift is sensitive to both temperature and strain. It allows for the profiling of temperature and strain throughout the fibre optic cable. There is however some degree of difficulty involved in separating pressure and temperature components. Therefore Brillouin is often used in combination with other sensors to disseminate the various components (Zou and Landolsi, 2014).

DSTS interrogator equipment is currently very expensive and therefore not yet widely used in water network management. Current applications are more common in the field of oil and gas pipelines. As the technology becomes more affordable, it is highly likely that it will find application in the field of water pipeline leak detection and monitoring. A typical interrogator is shown in Figure 2-15 below.

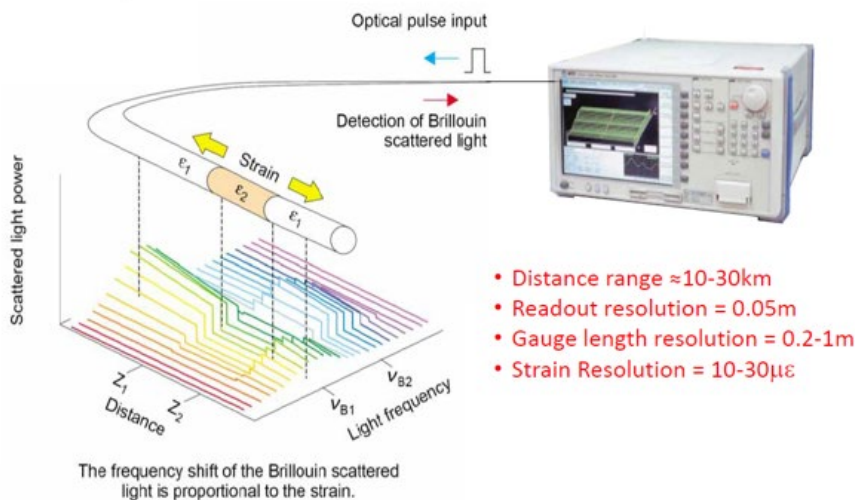


Figure 2-15: Typical Brillouin DSTS readout unit (Soga, 2017)

2.5.4 Examples of fibre optic leak detection

A variety of fibre optic leak detection technologies are available for external and internal applications and different conveyance media, such as gas, crude oil, water and other fluids. Many research papers have been published detailing leak detection with various parameters being investigated such as sensor placement configurations around or inside a pipeline. There

are two different types of fibre optic sensors available for pipeline monitoring, i.e. distributed or multi-point, which measure depending on their configuration either strain, temperature or vibration.

Multi-point sensors or FBGS can be compared to mechanical foil strain gauges which are typically glued to the surface of the monitored specimen accompanied by a temperature compensating FBGS which is mechanically strain relieved and embedded in close proximity to the main FBGS to measure only temperature effects. FBGS can however also be used to measure local temperature changes.

For buried gas pipelines the fibre optic cable is typically embedded above the pipeline and for liquid pipelines below the pipelines, as shown in Figure 2-16 below. This configuration has been chosen based on the physical properties of the transported media and the parameter to be observed. Gas such as liquified petroleum gas typically rises as it expands out of the leak hole from its liquid form, because it is lighter than air. Third party interference such as nearby construction should can also be detected by placing a fibre optic cable above the pipe, immediately informing the authorites of possible damage to the pipeline. Pipeline strain is very difficult to monitor as it is not know to which direction the pipe is moving as only the cahnge in length over the total length can be deducted, therefore 3 cables are attached at equal spaces around the pipe to obtain a strain profile around a pipe. Some liquid leaks such as oil are very easily detected as they are typically transmitted at a much higher temperature compared to the surrounding soil. Water for example might be more difficult to detect as the temperature is not altered for transfer purposes, but authorites try to limit water temperature to less than 20°C. The type of leak will als determine the effectiveness of the method as bigger leaks or bursts facing towards the surface will cause immediate upward piping with downward inundation only occuring as a secondary mechanism (Frings, 2011).

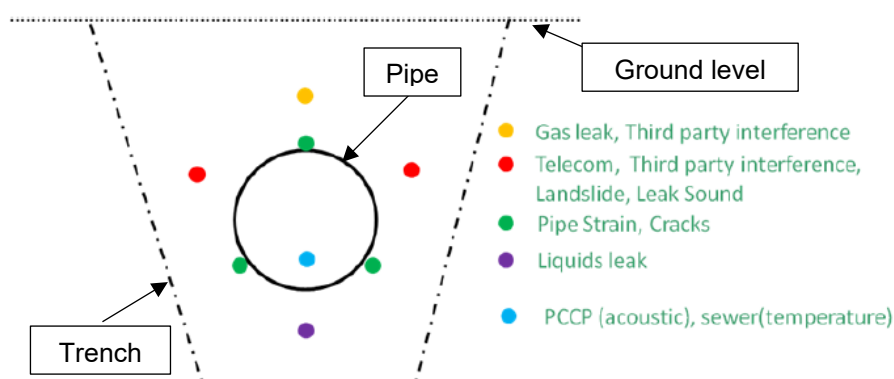


Figure 2-16: Fibre optic placement for different media and parameters (Frings , 2011)

Distributed fibre optic technology is the preferred technology used for monitoring pipelines in terms of strains, surrounding soil temperature and vibration. Using the full length of cable as measurement device compared to a multipoint sensor does create a better mechanistic understanding of pipeline behaviour.

They have been evaluated as a structural health monitoring tool for pipelines with regard to strains induced by earthquakes. An artificial shear fault was simulated in a shear-box setup with various strain sensor locations as shown in Figure 2-17 to validate the use of distributed sensors to detect damage to pipelines caused by ground movements. The study successfully indicated that fibre optic sensing can be a very effective tool to determine possible pipeline failures by earthquakes and landslides (Glisic and Yao, 2012).

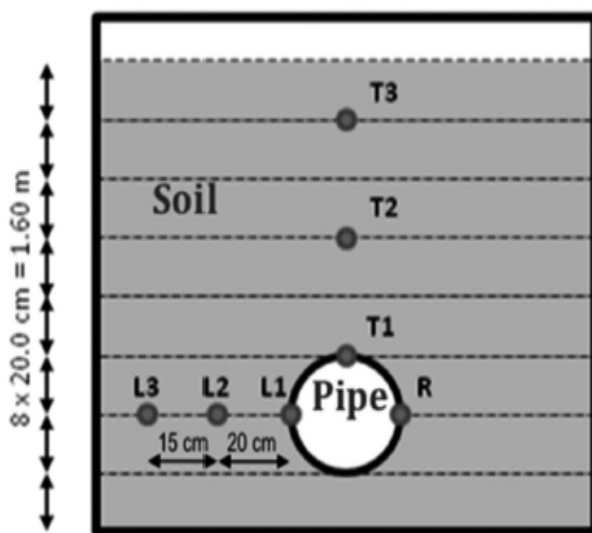


Figure 2-17: Fibre optic cable location to measure strain (Glisic and Yao, 2012)

Henrie et al. (2016) indicates that distributed fibre optic has been researched extensively as a method to detect leaks in water distribution systems. When using temperature as a means of leak detection it is essential that the temperature differential between the water and soil has to be sufficiently large for the method to function successfully.

Various companies have developed long range pipeline monitoring instruments with DSTS as their basis. An example of such a product is the distributed temperature and strain monitoring system or DiTeSt by SMARTEC (see Figure 2-18), which is based on the Brillouin scattering principal. Normal fibre optic telecommunication cable can be used for a temperature range between 20°C to 60°. This limitation is especially prevalent for Brillouin scattering as the mechanical strain component has to be isolated from thermal strain. This is typically done by

having at least one cable bonded to allow for full or partial strain transfer and at least one cable in close proximity unbonded allowing for thermal expansion and contraction irrespective of mechanical strain. A number of sensing cables were developed to measure both temperature and strain either in close proximity to the pipeline or on the pipeline surface. The so called SMARTape is made up of a fused glass fibre reinforced thermoplastic, which can be glued onto a pipeline to measure strains. SMARTprofile is sensor cable which can be used to measure both strain and temperature due to a bonded and unbonded approach as discussed earlier. A number of case studies were conducted by Inaudi and Glisic (2010) to showcase the efficiency of their products, which are briefly summarised below.

The measurement range for the DiTeSt device is 30 km, which can be extended to 150 km and 60 channels with intermediate optical amplifier modules. The spatial resolution is dependent on the length of the fibre optic sensing cable, number of splices and type of cable. A spatial resolution of 1 m over 5 km and 2 m over 25 km is given with a temperature resolution of 0.1°C, the temperature range is dependent on the type of sensing cable used. The strain resolution is given as 0.002 mm/m. The strain and temperature requisition time for the analyser is typically 2 minutes, depending on all of the parameters mentioned above.

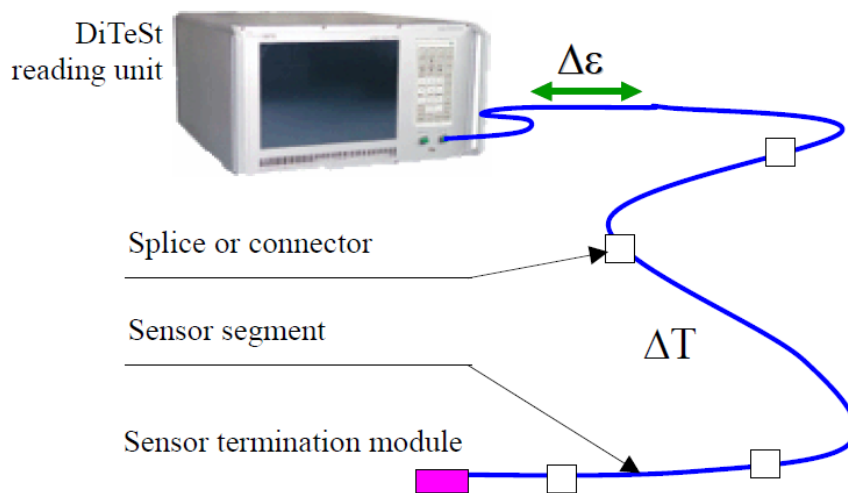


Figure 2-18: DiTeSt readout unit and fibre optic sensor cable (Inaudi and Glisic, 2010)

Brine pipeline leakage detection:

A 55 km long brine pipeline in Berlin (Germany) was instrumented with a distributed fibre optic cable and DiTeSt analyser. Two analysers were used because high losses were experienced at splice points. The whole system is autonomous and obtains a temperature profile of the

whole pipeline every 30 minutes, which is compared to previous temperature profiles. If anomalies are detected during the analyses period an alarm is raised, which alerts authorities to the location of a possible leak (Inaudi and Glisic, 2010).

Monitoring gas pipeline:

A 500 m long and 35 year old gas pipeline situated in an unstable area in Italy was retrofitted with SMARTape and distributed temperature sensing cable in combination with a DiTeSt analyser. The distributed temperature measurement was placed on top of the pipeline crown used primarily as a temperature compensating device. The SMARTape strain sensors are placed on each side with a 120° offset from the vertical top axis position. This sensor layout allows for long term deflection monitoring and an instantaneous warning of excessive strains due to support failure and ground movement. A leak was simulated using a CO₂ fire extinguisher, cooling the soil around the pipe and therefore simulating a gas leak. The study indicated promising results (Inaudi and Glisic, 2010).

SMARTPipe:

This is a reinforced thermoplastic pipe, which incorporates the use of distributed fibre optic sensing. The pipe is designed to be used in a trenchless rehabilitation option or a standalone option. The pipe is customisable to suit the application needs. The fibre optic sensor cable is interwoven with reinforced plastic strings over a thermoplastic pipe, allowing for greater strength and robustness (Inaudi and Glisic, 2010).

Further case studies:

Temperature monitoring of water pipes are very rare. Pipeline subsidence monitoring is available.

“Other systems suffer from cross talk between temperature and strain and require separate fibres to monitor strain and temperature. The Sensornet system provides true independent temperature and strain – removing ambiguity and maximizing the integrity of measurement.”

Monitor Raman and Brillouin scattering independently.

Range – 24 km

Strain resolution – 10 $\mu\epsilon$

Temperature resolution – 1°C

An early pipeline leak detection method based on distributed differential temperature sensors (DdTS) was investigated by Wang et al. (2016). A number of issues and limitations were found with existing fibre optic leak detection methods, such as the ability to detect small leaks and act as an early warning system. It is accepted internationally that leaks being less than 1% of total daily volumetric throughput are defined as small and that these leaks are especially difficult to detect with conventional leak detection methods. The proposed DdTS method not only use differential temperature as a leakage indicator but also an acoustic signature. This is especially useful if the background temperature of the soil surrounding the pipe is very similar to that of the transported media. The technology used for the proposed DdTS method uses coherent optical domain reflectometry (C-OTDR) and is not only limited to a quasi-static measuring regime for strain and temperature but can also be used on dynamic acoustic signature. C-OTDR makes use of the phase shift principal of the backscatter light caused by strain changes which can be replicated by the shift in wavelength of the interrogator light signal. The temperature sensitivity is several orders of magnitude greater than similar Brillouin and Raman based sensors, it is claimed that “temperature differential sensitivity” is 0.0005°C . A test setup with a cable length of 20 km was used, 100 m of the total length was installed inside of a temperature controlled oven. The temperature within the oven was increased in increments of 1°C , in addition point sensors were placed in close proximity to the cable, having an accuracy of 0.01°C . Various orifice leakage opening sizes were investigated to determine their acoustic signature. The spatial resolution of the sensor is however not yet optimised as a localised incident might not be recognised by the readout unit. The results from the study indicated that the proposed sensor is promising (Wang et al., 2016).

A number of case studies have been conducted on oil and gas pipelines due to the significant temperature differential present between the soil surrounding a pipe and the media transported within the pipe in those applications. Oil is typically heated, decreasing its viscosity and subsequently allowing easier transport due to lower friction in a pipeline. Gas expands rapidly at the outside of a pipe at the leak location allowing for an instantaneous cooling effect commonly referred to as Joule-Thompson effect. Water temperature in a distribution network is dependent on the flow rate, water source and soil characteristics, to name a few influencing factors.

Another key difference between water pipelines and oil/gas pipelines is that oil/gas leaking into the surrounding soil has detrimental environmental impacts, leading to contamination. Potable water as such has no apparent adverse environmental impacts, however could lead to erosion and sinkhole formation, as discussed in previous chapters. Potable water within the pipeline could also be contaminated from external pollutants entering the pipeline during

certain operating regimes. The difference in cost of transported product is another driver for oil/gas pipelines to be more accepting and accommodating of new technology such as fibre optic monitoring.

2.5.5 Calibrating fibre optic strain and temperature sensors

Fibre optic sensor properties are described by their manufacturers. For distributed fibre sensing the amount of impurities present in the cable is very important, more impurities would mean a greater measurement sensitivity, but less measuring distance can be covered. This is due to a greater attenuation or more light being backscattered therefore the signal strength is decreasing faster with distance. For FBGS the distance, length and intensity of the individual Bragg are very important, as well as intrinsic cable properties such as strain specific properties and thermal expansion coefficients (Kreuzer, 2013).

FBGS and DSTS are typically temperature calibrated by inserting the sensors into a temperature controlled calibration device which is set to simulate specific temperature changes at specific time intervals. Mechanical strain is measured in a temperature controlled environment where the sensors are stretched a known distance which is back-calculated to a change in wavelength. These methods are typically used to verify the manufacturer specifications (Kreuzer, 2013).

The gauge factor for FBGS is defined as the wavelength-normalisation wavelength change per mechanical strain (ϵ) according to Jülich . (2013) and it is said to be the most important FBGS parameter. A gauge factor value of 0.78 is typically given for an FBGS with a strain sensitivity of $1.2\text{pm}/\mu\epsilon$ at a wavelength of approximately 1535 nm. There are two main components that influence the gauge factor, which are the strain transfer ratio and effective strain-optic coefficient. The strain transfer ratio indicates how efficiently strains are transferred from a structure through an adhesive and the protective layers to the fibre optic cable. It is technically seen as ratio of the strain along the fibre optic cable axis and the strain parallel to fibre optic cable along the structure. The second factor is defined as change in refractive index due to change in strain. If an acceptable adhesive technique is used for surface bonding it can be assumed that the strain transfer ratio is greater than 0.99, which means that there is nearly full strain transfer (1). The physical properties of the cable such as the core radii, Young's moduli, doping materials and concentration have a greater effect on the gauge factor which is attributed to the effective stain-optic coefficient. It is very important that the manufacturer provides a gauge factor for surface mounted FBGS to be used as standardised calibration factor (Jülich et al., 2013).

2.6 Relevant thermal properties of soils

As the proposed research involves the measurement of soil temperatures, an overview of factors relevant to the thermal behaviour of soil is briefly presented.

2.6.1 Thermal conductivity of soil and rock

Thermal conductivity of soil is a function of the soil moisture content, mineralogical composition, density and particle size distribution (Barry-Macaulay et al., 2013). In general, coarse grained soils are said to have a higher thermal conductivity at low saturation levels compared to fine grained soil. Thermal conductivity also increase with an increase in moisture content and dry density. Depending on the mineralogical composition the thermal conductivity differs, for example where moisture content might not change the thermal conductivity. Increasing moisture content increases the contact between particles. Similarly, an increase in dry density, causing a repacking of particles, allows for greater inter-particle contact, leading to an increase in thermal conductivity (Barry-Macaulay et al., 2013).

There are a number of methods available to measure thermal conductivity of soils, one method being a thermal needle probe and another being a divided bar apparatus. The thermal needle probe is based on the infinite line heat source theory, which uses heat dissipation calculations to determine a soil-specific thermal conductivity. A divided bar apparatus is used to test thermal conductivity of rock samples. However, the contact area between the needle probe and a drilled hole in the rock does not provide sufficient heat transfer capability. Thermal conductive grease is used in the cavity between the rock and the thermal needle probe (Barry-Macaulay et al., 2013).

To summarise the parameters that effect thermal conductivity of soil and rocks the following list is presented (Barry-Macaulay et al., 2013):

- Saturation: Fine and coarse soils are distinguished. For fine soils the thermal conductivity increases with an increase in saturation levels, whereas coarse soils show a great initial increase in thermal conductivity with low saturation levels with very little increase at higher saturation levels. The mechanisms is driven by inter-particle contact points, coarse soils have much less contact point compared to finer soils.

- **Mineralogy:** Different minerals have different thermal conductivities, quartz typically has the highest thermal conductivity of 7.7W/mK compared to other soil minerals which have a far lower thermal conductivity of between 1.8 to 2.8W/mK. Fine grained soils typically have a much lower quartz content, therefore having a lower thermal conductivity compared to coarse grained soils at low saturation levels.
- **Density:** A higher soil density indicates a greater thermal conductivity due to greater inter-particle contact points. The same trend can be observed when compacting soils increasing the density and the packing structure.
- **Anisotropy:** In some rock formations the direction of the stratification being either inclined, horizontal or vertical influences the thermal conductivity in various directions.

There are a number of parameters that influence the thermal conductivity of soils. A given pipeline often passes through varying soil types and densities which makes it difficult to predict the effectiveness of the heat transfer mechanisms with great accuracy (AWWA, 2009). Daily and seasonal soil temperature variation decreases with depth as the upper soil layers act as an insulating buffer zone compared to lower soil layers. From a certain depth below the natural ground level, very little temperature variation can be observed, depending on the parameters mentioned above (Florides and Kalogirou, 2007). Given the mentioned factors a study to evaluate the use of temperature measurement as a means of leak detection is best carried out by means of a physical study rather than numerically.

2.6.2 Thermal conductivity of buried pipes

Heat transfer between the soil and a buried pipe occurs naturally as the transported media is introduced from an external source such as a reservoir into the underground pipeline. Depending on the temperature differential between the surrounding soil and the water transported in the pipe, heat transfer occurs between the soil and the fluid in the pipe or vice versa. This heat transfer is affected by the ambient atmospheric temperature, the flow rate in the pipe, the hydraulic conductivity in the soil and other factors (Conway, 2010).

In a study involving numerical modelling of heat transfer in a buried pipe, Conway (2010) describes the mechanisms and the mathematics needed to describe thermal heat exchange in underground pipes.

Heat flow in the ground is described by Fourier's law of heat conduction (Equation 2-9).

$$\vec{q} = -k \nabla T \dots\dots\dots \text{Equation 2-9}$$

\vec{q} = Heat flux (heat flow per unit area)

K = Thermal conductivity of the material

∇T = Temperature gradient

Water temperature in distribution networks should not exceed 20°C as it will reduce the effectiveness of disinfectants (WHO, 2014). Even though there is little scientific evidence that an increase in water temperature is directly related to an increase in corrosion rates, secondary factors such as lower residual chlorine and chloramine are linked to elevated water distribution temperatures which indicate higher corrosion rates. Elevated water temperatures in distribution networks also indicate an increase in biological activity and growth, leading to higher corrosion rates of pipeline walls, referred to as micro-erosion or bio-corrosion (WHO, 2014).

Pipe-soil interaction in terms of heat transfer from the transported media to the surrounding soil (or vice versa) is often investigated with numerical models. Finite element models are commonly used to determine the interaction of ambient air/soil temperature and transported media temperature as shown in an example in Figure 2-19. The air temperature in this example is -10°C and the transported crude oil temperature is 33°C, the heat transfer surrounding the pipeline is significant compared to the surrounding soil temperature. The effects of seasonality, as well as daily temperature fluctuation on both the transported media and the surrounding soil have to be investigated to determine if possible blind periods can occur. Blind periods are referred to as time periods when the transported medium temperature and the surrounding soil temperature is very similar, therefore it becomes very difficult to detect a leak on the basis of temperature changes (Frings, 2011).

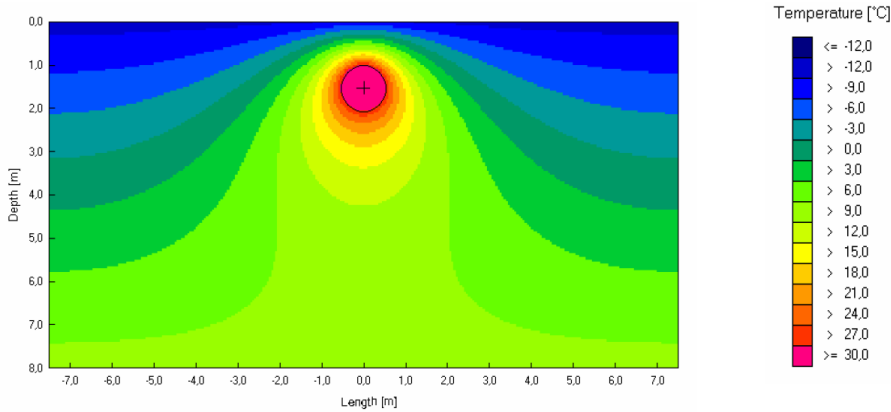


Figure 2-19: Steady state temperature distribution around a crude oil pipe (Frings, 2011)

Buried water pipes in a reticulation network can be described as thermal heat sinks or sources (depending of the relative soil-water temperature) affecting the temperature of the ground around them (Florides and Kalogirou, 2007). The detection of leaks by measuring temperature changes in the ground near a pipeline is dependent on the extent to which the presence of the pipe has affected the temperature of the surrounding ground.

2.7 Temperature measurement

2.7.1 Negative thermal coefficient thermistors

Negative thermal coefficient (NTC) thermistors are resistors that decrease in resistance as the surrounding temperature increases. They are made of different mixtures of metals, such as manganese, nickel, copper, cobalt and iron oxides depending on the desired properties (AVX, 2017). A carefully controlled mixing, pressing and metallisation¹ process ensures very good quality, accuracy and precision. The size and the composition of the thermistor will determine the temperature coefficient and range. The nominal resistance of a thermistor is typically given at 25 degrees Celsius at very low power, making the heating effect of the NTC resistor negligible. The resistance behaviour compared to temperature changes is expressed as temperature – resistance characteristics, where a temperature coefficient (α , Equation 2-10) and a sensitivity index (B, Equation 2--11) are given (AVX, 2017).

$$\alpha = \frac{100}{R} \times \frac{dR}{dT} \dots \dots \dots \text{Equation 2-10}$$

¹ Is the process of coating a metal surface with ceramic or other metal

- α = temperature coefficient % per °C
- $\frac{dR}{dT}$ = Change in resistance over change in temperature (slope of resistance/temperature curve)
- R = resistance value (Ω)

$$B(K) = \frac{1}{\left(\frac{1}{T_1} - \frac{1}{T_2}\right)} \times \ln\left(\frac{R_1}{R_2}\right) \dots \dots \dots \text{Equation 2-11}$$

- B (K) = Sensitivity index
- T_1 = Temperature value 1 (typically 25°C)
- T_2 = Temperature value 2 (controlled °C)
- R_1 = Resistance value 1 (typically 5 000 Ω)
- R_2 = Resistance value 2 (output Ω)

The α and B parameters specific to the thermistor or NTC resistor can then be used to create a resistance/temperature approximation relationship. For the thermistor from AVX with a material Code MA 3960, the following formula was developed at 25 degrees Celsius the resistance is 5 kilo Ohm (Equation 2--12) (AVX, 2017).

$$T = \frac{1}{(2.5374 \times 10^{-4}) \times \ln(R) + (1.1958 \times 10^{-4})} - 273.15 \dots \dots \dots \text{Equation 2-12}$$

- T = Temperature value (°C)
- R = Resistance value (Ω)

The response time to temperature change is dependent on the substance that the thermistor is embedded in or surrounded with. If the thermal conductivity of the media surrounding the thermistor is low, the thermistor will react slowly compared to a fast change in resistance for a material with high thermal conductivity (AVX, 2017).

Alternatively a thermocouple could also be used to measure temperature, which are made by joining two different metals at one end. The voltage output from the thermocouple can be back calculated to a pre-calibrated temperature. Thermocouples are less sensitive, non-linear, have very low output voltage, unstable and measurements are difficult to repeat. Therefore thermistors were preferred for temperature measurement in the work presented here.

Thermistors from AVX and Vishay were used for experiments, both with their respective calibration curves and conversion formulae.

2.8 Pipe-soil interaction

2.8.1 Pipe bending behaviour

An important aspect that requires attention is the reaction of a buried pipeline to its surrounding soil, exposed to soil movement. This forms a major part of this research, as buried pipelines develop additional strains and bending moments upon soil settlement. As mentioned above, the principle that Vorster et al. (2005) investigated, based on the effects tunnelling has on existing pipeline infrastructure, can be applied to sinkhole formation, as both involves subsurface soil movement. Vorster et al. (2005) compared the behaviour of a pipeline (at deep and shallow pipe depths) to that of an infinitely flexible pipe response. Figure 2-20 depicts this behaviour, by normalising the various bending moments corresponding to a specific % face loss (% volume loss), and plotting it against a normalised offset. M_p^* is the measured pipe response, and is the ratio between $M_{norm}/(M_{norm})_{s,max}$. M_s^* , on the other hand, is the ratio between $(M_{norm})_s/(M_{norm})_{s,max}$, which is the infinitely flexible response of a pipeline. M_{norm} is the normalised bending moment and $(M_{norm})_s$ is the normalised bending moment that would occur in a pipeline, if the pipe would have been forced to follow the soil settlement profile exactly.

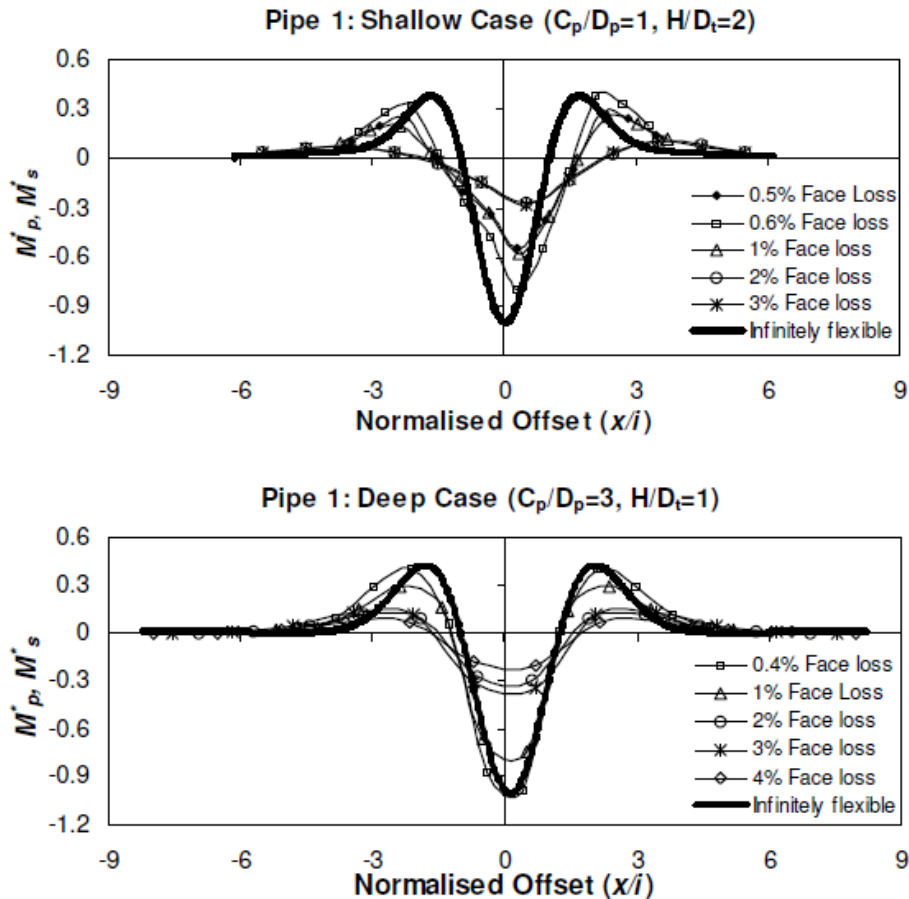


Figure 2-20: Normalised bending moment for a pipe (Vorster et al., 2005)

Vorster et al. (2005) observed the behaviour of these buried pipelines under various % face losses and concluded that all the M_p^* values were less than that of the M_s^* values, indicating that the pipe was not behaving entirely flexible. This contradicts the assumption that pipelines follow the greenfield settlement profile, as mentioned above. Pipelines behaved more flexible at deeper pipe depths than at shallower depths. Pipelines usually respond flexible at low face losses (small amounts of strain in the surrounding soil), but as face loss increases, strain in soil become larger and soil stiffness decreases, resulting in the pipe to become more rigid and M_p^* starts to differ significantly from M_s^* . This phenomenon was described by Marshall et al. (2010), having a similar model set-up as that used by Vorster et al. (2005).

Marshall et al. (2010), like Vorster et al. (2005), indicated that the presence of a pipeline within a soil structure will result in a different soil settlement profile than the profile obtained from greenfield displacement, without a pipeline. An infinitely flexible pipe will follow the greenfield soil settlement profile exactly, displacing by the same amount as the soil. On the other hand, an infinitely rigid pipe will not follow the soil settlement profile, and displacement of the pipe will be significantly less than that of the greenfield measured deflection. They postulated that

the behaviour of real pipelines lies somewhere between these extremes. This behaviour is controlled by the response of the pipeline to the soil displacement. Figure 2-21 shows the settlement of a rigid ($EI_{\text{model}} = 809.6 \text{ N.m}^2$) and flexible ($EI_{\text{model}} = 6.44 \text{ N.m}^2$) pipeline exposed to a percentage volume loss, and compares it to the soil settlement profiles obtained from the greenfield test at that point. The soil deflection just below the pipe invert level was also plotted against the deflections obtained from the greenfield test.

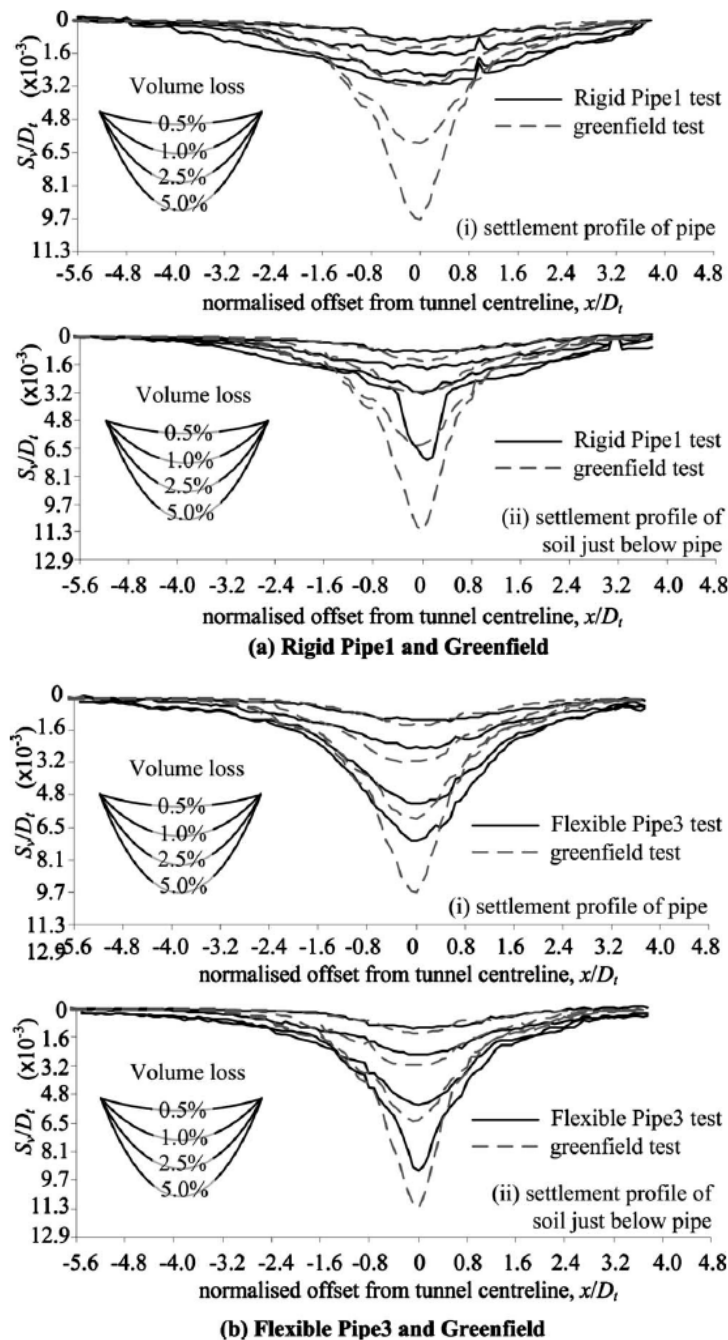


Figure 2-21: Vertical settlement profiles for a rigid and flexible pipe (Marshall et al., 2010)

The data indicates that, with the existence of a pipe, the settlement trough width becomes wider in comparison to that seen during the greenfield test. A flexible pipe aims to follow the greenfield soil profile, whereby a rigid pipe deviates significantly from this behaviour. This phenomenon can be depicted from the graphs above, as the difference between the pipe settlement and soil settlement becomes larger with rigid pipelines. As a result of this difference between the measure pipe deflection and soil deflection, Marshall et al. (2010) postulated that a gap would form underneath the pipeline. They indicated that the existence of this gap can be of concern, as the pipe is no longer supported continuously along the invert level. Even though the gap formation will not have a significant effect on bending moment in the pipeline, it should still be considered important, as it may affect the cross-sectional loading on the pipe, alternating the bending and longitudinal behaviour under future imposed loading.

Marshall et al. (2010) mentioned that the bending moment reactions of the pipeline, to a change in volume loss, is directly correlated to the change in stiffness of the soil, which is a function of the shear strain that exists underneath a pipeline. Marshall et al. (2010) plotted a series of graphs depicting the relationship between shear strain, relative rigidity factor, R , and shear stiffness, to that of % volume loss, as can be seen in Figure 2-22.

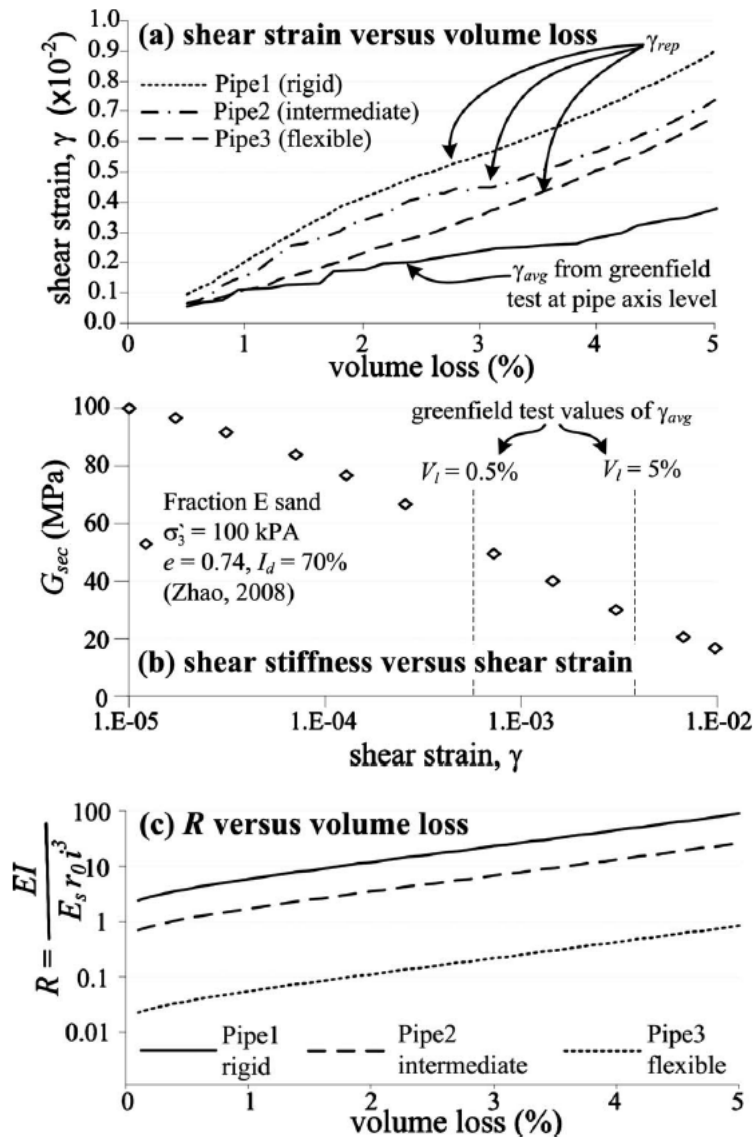


Figure 2-22: The influence of shear strain and shear degradation on the determination of the relative rigidity of a pipeline (Marshall et al., 2010)

It can be noted from the first graph, in Figure 2-22, that the shear strain in the soil increases approximately linear with an increase in % volume loss for a rigid, intermediate and flexible pipeline. Marshall et al. (2010) used this calculated shear strains and determined the effects of these strains on the change in shear stiffness of soil. It can be seen in the second graph that an increase in shear strain, because of an increase in % volume loss, results in a decrease in the shear stiffness of a soil. This has a direct correlation to the relative pipe-soil rigidity factor, R , due to the soil stiffness that decreases with an increase in shear strain. The third graph demonstrated this behaviour. Based on the abovementioned knowledge and data, Marshall et al. (2010) concluded that, due to an increase in shear strains and relative pipe-soil rigidity, from a change in tunnel volume loss, the pipe-soil system becomes more rigid,

resulting in the bending moments sharply decreasing. As mentioned above, this behaviour can be applied to predict the behaviour of a pipeline exposed to sinkhole formation. The fact that the pipe-soil system rarely act flexible, but rather rigid, results in bending moments being significantly smaller, raising the question if bending moments and strain in the pipe can still be of significant magnitude to detect sinkholes. Figure 2-23 indicates the relationship between the maximum normalised bending moments, for hogging and sagging, against the pipe-soil rigidity factor, based on the findings of Marshall et al. (2010).

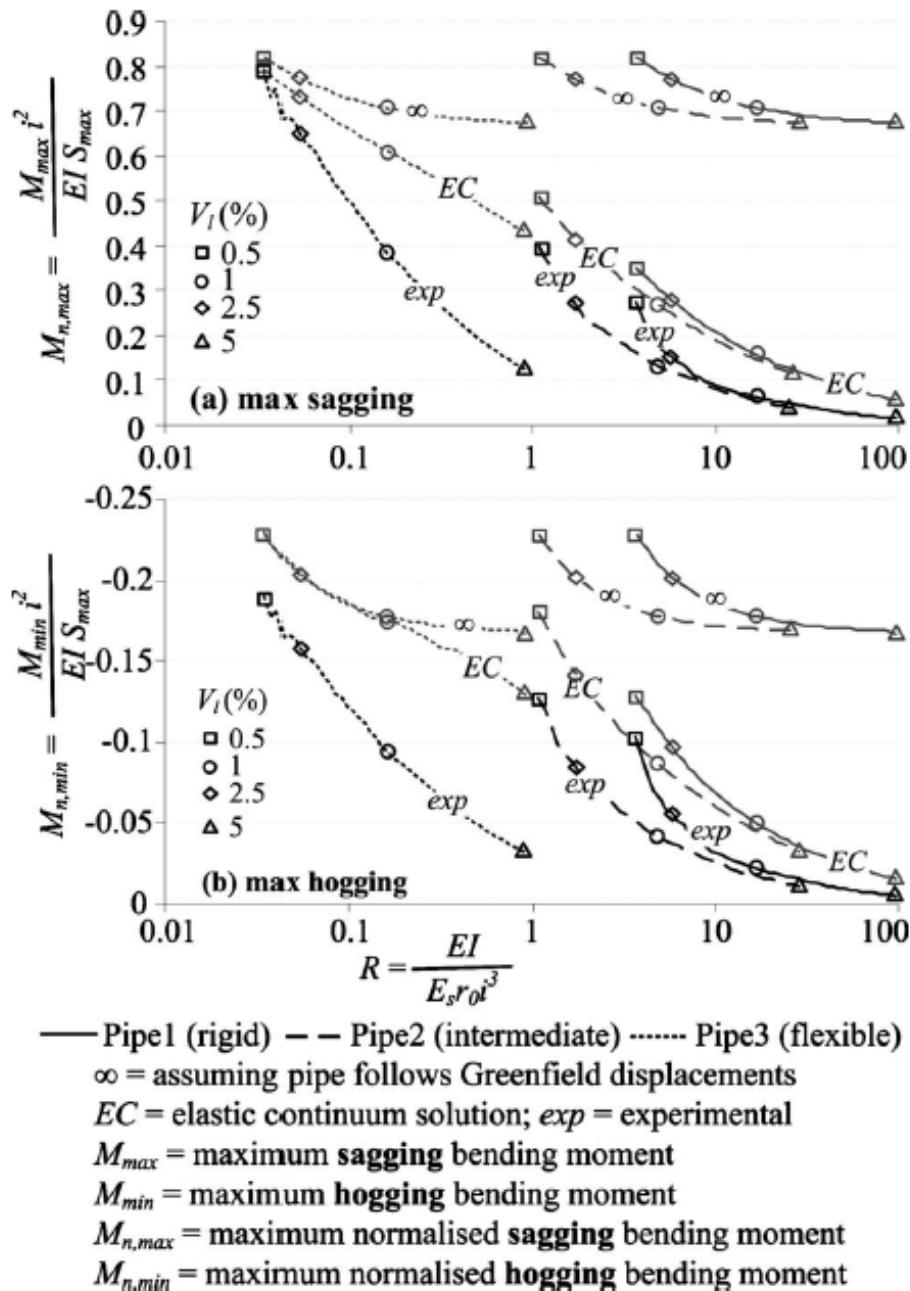


Figure 2-23: Relationship between normalised hogging and sagging moments and pipe-soil rigidity (Marshall et al., 2010)

This observed phenomenon is very important for the design of buried pipelines, as it gives a better prediction of the actual bending behaviour that is experienced by the pipeline. This also contradicts the assumption that a pipeline will behave in a flexible manner, with higher bending moments, as mentioned above.

2.8.2 Pipe response to ground settlement

Sinkholes usually occur due to small settlements of soil that occurs over time, deep underneath the soil surface, accumulating up to a point where it forms a large cavity, prior to collapse. It is thus possible to compare the behaviour of a pipeline exposed to sinkhole formation, to what Vorster et al. (2005) and Marshall et al. (2010) examined when they tested the effects of tunnelling on existing pipelines. Both sinkholes and tunnelling may have a similar effect on the behavioural properties of buried pipelines, since in both cases the soil structure underneath the pipeline is disturbed by the formation of a discontinuity (cavity) and movement of the soil.

The relation between a buried pipeline and its surrounding soil is an important aspect to consider during design. Vorster et al. (2005) focussed their study on the effect tunnelling has on existing buried pipelines. They indicated that current methods of assessment of the behaviour of these pipelines, subjected to activities, such as tunnelling, are largely based on the assumption that soil and pipelines behave in an elastic manner. Even though this is an important aspect for preliminary assessment of the problem, the behaviour of pipelines may contradict the initial assumption, due to soil nonlinearity and the presence of shear strains. Figure 2-24 indicates a schematic of a tunnel excavated underneath an existing pipeline. The presence of the tunnel, within the soil profile, results in the displacement and settlement of soil around the pipeline, causing it to deform and take up additional strain in the form of bending moments. The magnitude of this soil deformation depends on the relative stiffness between the pipeline and the existing soil, and the soil settlement distribution underneath the pipeline. The maximum bending moment in the pipeline is a sagging moment that usually occurs above the centreline of the tunnel. Vorster et al. (2005) and Marshall et al. (2010) simulated ground movement by using a retractable tunnel, controlled by a motor driven actuator. They measured the effects of tunnel volume loss on the behaviour of a buried pipeline, i.e. strains, by reducing the volume taken up by the tunnel, underneath the soil surface. Similarly, this approach can be used to predict the behaviour of a pipeline exposed to sinkhole formation. A cavity is induced within a soil structure, not only creating strains in the soil underneath the pipeline through ground movement, but also affecting the amount of strain development within the pipeline.

Both Vorster et al. (2005) and Marshall et al. (2010) initially conducted a control test, referred to as the greenfield test, on their representative soil models. This test examined and measured the behaviour and deflection of the soil, above the tunnel, due to tunnel volume loss, without the presence of a pipeline. They largely considered the deflection profile of the soil at pipe invert level (known as the greenfield displacement profile) and used it during their analysis of the other tests. Thereafter, tests were conducted, in a similar manner as the greenfield test, but with the presence of a pipeline above the tunnel, examining soil and pipeline behaviour exposed to tunnel volume loss.

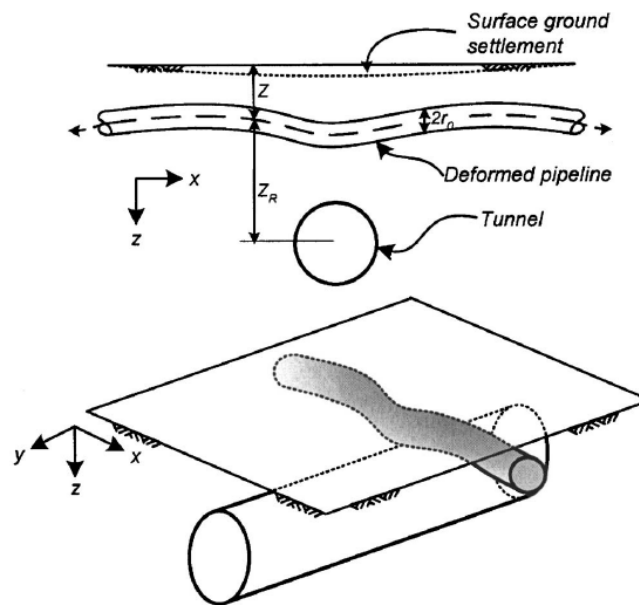


Figure 2-24: Schematic of tunnel excavated underneath a pipeline (Vorster et al., 2005)

Vorster et al. (2005) mentioned that a pipeline, subjected to bending moments, can tend to behave in either one of two ways:

1. The pipeline may act flexible and perfectly follow the greenfield displacement profile, or
2. The pipeline acts rigid and experience the greenfield displacement as a local interference.

More often, pipelines are assumed to follow Case 1, not considering the properties of the pipeline, such as its stiffness.

Significant research has been done on establishing the response and behaviour of a buried pipeline to its supporting soil, referred to as a pipe-soil system. Vorster et al. (2005) discussed this concept in an article based on modelling the effects of tunnelling on buried pipelines in a centrifuge. They postulated that a buried pipeline may behave in two distinct ways, assuming no fracturing of the pipeline. It either interacts with the surrounding soil, or has no interaction

with the soil and takes on the exact shape of the ground movement. This behaviour can be predicted and depends on the relative rigidity, R , of the pipe-soil system.

The relative rigidity, R , for a pipe-soil system can be defined as the relationship between the pipe bending stiffness, $E_p I_p$, the pipe axial stiffness, $E_p A_p$, and the soil stiffness, E_s . Klar et al. (2005) defined the relative rigidity factor of a pipe-soil system, based on elasticity models, only considering the effects of bending, as indicated in Equation 2-13:

$$R = \frac{E_p I_p}{E_s \cdot r_0 \cdot i^3} \quad \text{Equation 2-13}$$

where $E_p I_p$ and E_s is defined, as mentioned above, r_0 being the outer radius of the pipeline and i , the distance from the centreline of the buried tunnel to the inflection point of the greenfield soil settlement curve at pipe invert level. It is quite clear that the stiffness of the soil, E_s , and the inflection point, i , also known as the settlement trough width, are important factors in determining the rigidity behaviour of a pipe-soil system under bending, assuming that the characteristics of the pipeline remains the same.

Attewell et al. (1986) considered the effects of axial loads on the rigidity of a pipe-soil system. They proposed that the relative pipe-soil longitudinal stiffness factor, K^* , can be defined, only considering the effects of axial loads, by using Equation 2:

$$K^* = \frac{E_p A_p}{E_s A_s} \quad \text{Equation 2-14}$$

where E_p is the pipe stiffness and A_p the cross-sectional area of the pipeline. E_s denotes the stiffness of the soil, as mentioned above, and A_s the full cross-sectional area displaced by the pipe. Axial effects are usually very small in comparison to bending, and is usually neglected. Vorster et al. (2005) indicated that, E_s and i , are important factors contributing to the rigidity of a pipe-soil system. However, by only considering the problem from an elastic point of view, important aspects affecting true behaviour of the pipeline cannot be predicted, as soil is highly non-linear (varying E_s) and will not act elastically. If, on the other hand, the relative rigidity factor is adopted as a method of predicting the initial behaviour of soil, careful identification of factors affecting E_s and i should be considered.

To overcome this problem, Vorster et al. (2005) developed a normalised bending moment, M_{norm} , based on the response of the model pipeline in the centrifuge. They defined the normalised bending moment using Equation 2-15:

$$M_{norm} = \frac{Mi^2}{E_p I_p S_m} \quad \text{Equation 2-15}$$

where M is, the pipe bending moment, and S_m the maximum greenfield settlement at the pipe invert level.

They plotted a graph (Figure 2-25), indicating the effect of the relative rigidity factor on the sagging and hogging normalised bending moments for various pipe invert levels.

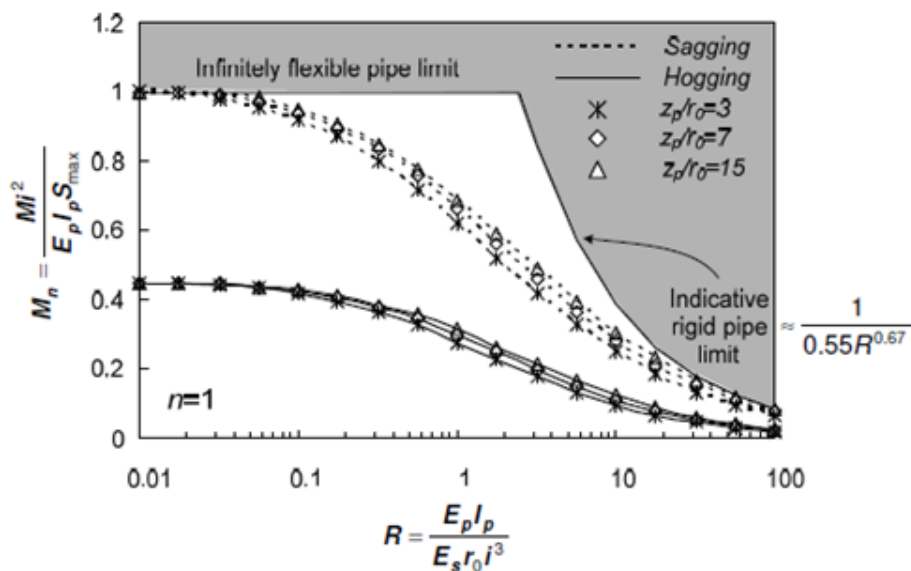


Figure 2-25: The effect of pipe-soil rigidity on pipe bending moments (Vorster et al., 2005)

Figure 2-25 indicates the normalised sagging and hogging bending moments in relation to the rigidity factor (R) of the pipe-soil system for various Z/r_0 ratios. The embedment ratio, Z/r_0 , is the ratio between the embedment depth and the outer radius of the pipeline. Although the embedment depth (Z) largely affects the magnitude of bending moments in pipelines, due to its correlation with i and S_{max} , it does not have a significant effect on the normalised bending moment, for a given value of R .

Vorster et al. (2005) observed various trends that can aid designers in distinguishing between interaction analysis and greenfield measurement requirements. They indicated that a pipeline, with a relative rigidity $R \leq 0.1$ behaved in a flexible manner, approximately coinciding

with a $R = 0$. Thus, the bending moments observed is a function of the curvature of the soil and the pipeline follows the soil deflection profile (greenfield soil displacement). They then showed that if the relative rigidity $R \geq 5$ the pipe-soil system tends to behave in a rigid manner. The curvature of the soil settlement no longer plays an important role in the development of bending moments in the pipe, resulting in a decrease in bending moments.

Furthermore, they concluded that the parameters, i and E_s , used in the calculation of the rigidity factor, changes due to soil nonlinearity and the geometrical configuration of the problem. For example, the pipeline may act in a flexible manner on the sides, following the soil profile, where little soil movement has taken place, and rigid in the centre, where more significant soil movement has occurred.

Vorster et al. (2006) later summarised and explained that there are various mechanisms governing the behaviour of a buried pipeline, and these are classified into five different categories. Primarily, these mechanisms are based on the knowledge of pipe-soil interaction and the relative rigidity factor of the pipe-soil system. These mechanisms indicate the possible reasons for pipeline bending moments and soil stress measurements, and is a combination of local and global effects. They defined global effects to be the effects not only confined to the pipe vicinity (larger soil structure), whereby local effects, on the other hand, were regarded as the effects caused by pipe-soil interaction. It is important to note that these mechanisms were based on the effect of tunnelling on buried pipelines and can thus aid in explaining the effect of sinkholes on pipelines. These mechanisms included the following:

1. Mechanism 1 (M1) – Global Effects
2. Mechanism 2 (M2) – Gap Formation
3. Mechanism 3 (M3) – Decreased Stability
4. Mechanism 4 (M4) – Negative Down Drag Failure
5. Mechanism 5 (M5) – Longitudinal Interaction

Figure 2-26 indicates the location and representation of these mechanisms within the soil structure.

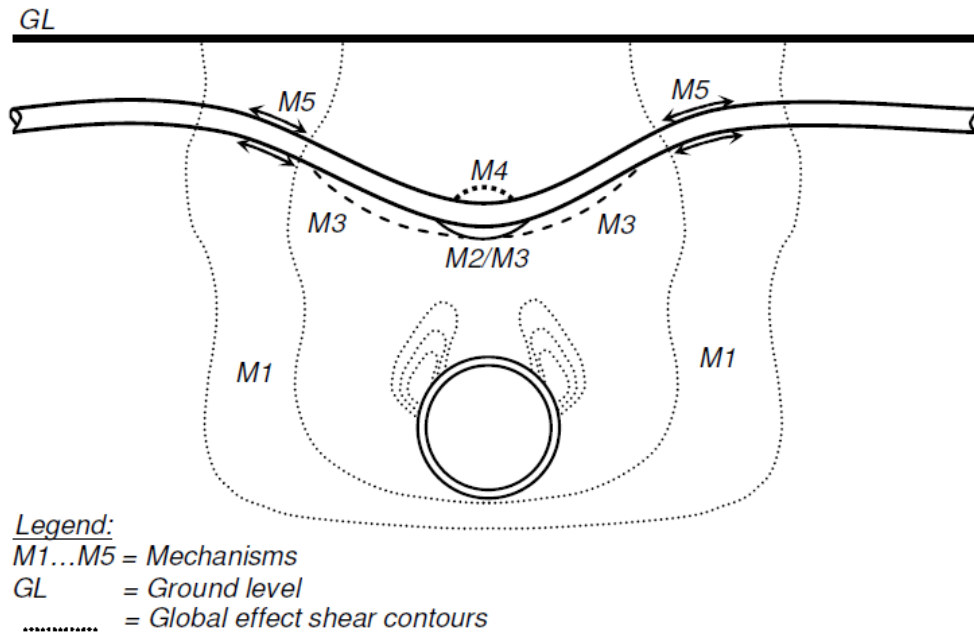


Figure 2-26: Schematic of mechanisms that may impact pipe behaviour (Vorster et al., 2006)

Vorster et al. (2006) described global effects (M1) to be the existence of shear within a soil structure, caused by contraction of the tunnel cavity. This effect only considered the greenfield scenario, not taking into account the properties and existence of the pipeline within the soil structure. This shows the minimum ground shear strain that needs to be considered when looking into the effects of tunnelling on pipelines.

During a greenfield scenario, shear strains increases with distance below the soil surface level and decreases with distance from the tunnel cavity. These effects are reflected by changes in the parameter, i , which is defined as the settlement trough width. This parameter forms part of the pipe-soil rigidity factor, as mentioned above, and is fitted for this application, as it is widely used to describe the settlement profile of soil as a Gaussian curve (Equation 2-16 below).

$$S(x) = S_{max} \exp\left[-\frac{1}{2}\left(\frac{x}{i}\right)^2\right] \quad \text{Equation 2-16}$$

Where S_{max} is the maximum settlement, i the distance to the settlement trough inflection point from the settlement trough centreline and x distance measured relative to the settlement trough centreline.

Vorster et al. (2006) found that the greenfield calculated, i , was not only affected by the depth of pipe invert, but also because of an increase in ground movement. This, in turn, suggested that an increase in localization of ground movement, would have an impact on the relative pipe-soil rigidity factor. Due to a change in this factor, the probability that local mechanisms would develop has increased.

They postulated that the density of the surrounding soil plays a key role in the behavioural characteristics of a buried pipeline. It was found that the shear zone and strains in loose sands and soft clays were higher than that experienced by sands and clays of higher densities.

Local effects include the increase in local shear strains above those caused by global effects. Gap formation (M2), as can be seen above, is the decrease in the vertical contact pressure between the pipe and underlying soil. This can be described in Figure 2-27, based on Vorster et al. (2006), where the relative pipe-soil settlement is plotted against the offset from the centre of the soil model and tunnel cavity. The relative pipe-soil settlement (S_{rel}) is defined as the numerical difference between the greenfield subsoil settlement (S_v), at pipe invert level, and pipe crown settlement (S_p) at that same level.

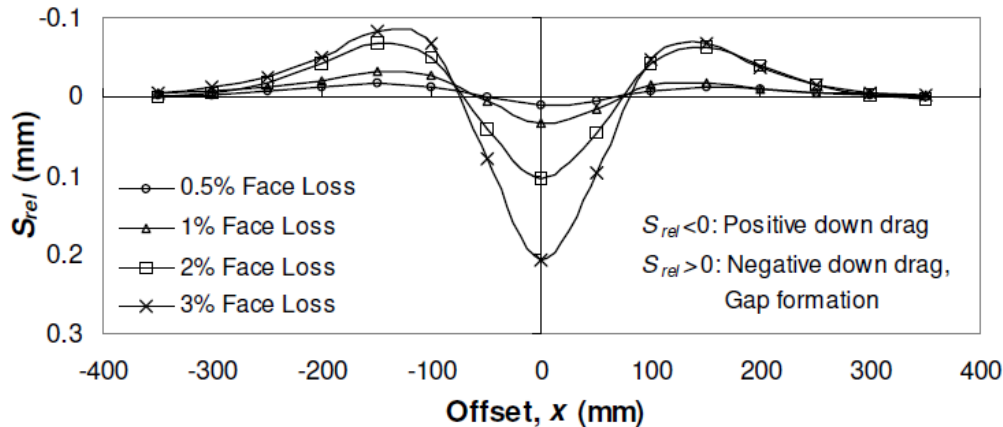


Figure 2-27: Relative pipe-soil settlement (Vorster et al., 2006)

It can be seen in Figure 2-27 that an increase in face loss, results in an increase in the relative pipe-soil settlement. Vorster et al. (2006) mentioned that the magnitude of ground movement directly affects the amount of relative pipe-soil settlement. They furthermore confirmed their theory about gap formation, as can be seen in Figure 2-28, indicating that pipe-soil contact pressures decrease with an increase in face loss up to a specific point, where after contact pressures increases again.

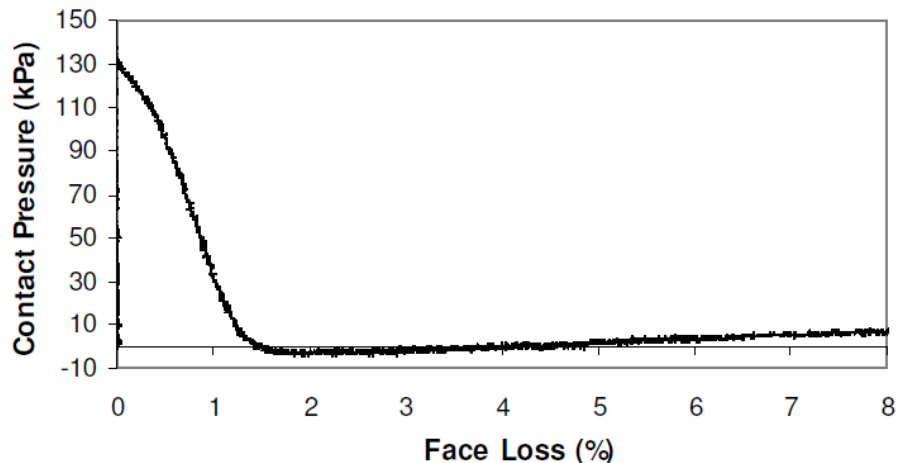


Figure 2-28: Change in pipe-soil contact pressures due to gap formation (Vorster et al., 2006)

A decrease in stability (M3) of soil results from a change in ground movement underneath the pipeline. Due to this movement, the stability and stiffness of soil around the gap region decreases, partly due to the changes in soil stresses in this region. Vorster et al. (2006) explained this phenomenon through various experiments with tunnelling in dense sands. It is common for sands at high densities to arch, resulting in a decrease in effective vertical stresses (σ_v') and increase in the effective horizontal stresses (σ_H'). The amount of stability reduction is correlated to the ability of the soil to support itself under tunnel contraction or any ground movement. They mentioned that the body of soil between the pipe, under the gap formation, and the tunnel has less ability to form the same amount of arching, than that observed by the greenfield experiment. Due to the presence of the pipeline in the soil structure, the soil has a decreased ability to support itself and a slope-like failure (local failure) may occur adjacent to the gap in a plane parallel to that of the pipeline. Vorster et al. (2006) considered this failure as an explanation for the increase in contact pressure when a certain face loss is reached. The gap partially closes, due to this failure, increasing the contact pressures between the pipe and the underlying soil. The process of gap formation is repeated with a further increase in face loss.

Vorster et al. (2006) explain that negative down drag failure (M4) may occur, if the relative pipe-soil rigidity is of significant magnitude. It can be seen in Figure 2-27, that the negative downward drag becomes evident when S_{rel} increases.

Longitudinal pipe-soil interaction (M5) has been pointed out by Attewell et al. (1986) and later by Bracegirdle et al. (1996), to have a larger effect on hogging than on sagging moments, due to its contribution to tensile strain. Strain development in pipelines is the product of many

factors, including, amongst others, the pipe sectional properties, soil properties and pipe-soil interaction. Vorster et al. (2006) postulated that, due to the existence of local and global effects, the tensile strain development in hogging areas of the pipeline becomes less critical and almost negligible. Vorster et al. (2006) tested this hypothesis by applying Attewell et al. (1986) method for estimating the longitudinal strain effects on the pipelines. The main conclusions were as follows:

- Relative pipe-soil bending rigidity determines the criticality of the longitudinal effects, rather than using the relative longitudinal stiffness.
- The higher the flexibility of the pipe-soil system, not only the pipe itself, the more prominent the longitudinal component becomes.
- Global and local mechanisms, along with relative rigidity calculations should be considered when deciding on the severity of longitudinal strains on the pipeline.

Thus, as described above, the behavioural patterns of a buried pipeline may be as a result of a combination of global and local effects. Global effects, primarily include shearing within the soil structure, due to ground movement, and local mechanisms, which is effected by the pipe-soil rigidity and interaction.

2.9 Sinkhole formation due to leaking pipes

Nel et al. (2011) defined that sinkholes, also known as sinks, exist from the hollowing out or formation of a void below the earth's surface. It is the vertical downwards movement of land surface that is formed either naturally, or as a result of man-made activities, owing much of its occurrence to the presence of water. Natural sinkholes usually occur due to erosion or the movement of underground water. Water seeps through soil, rock and minerals to the ground water reservoirs, slowly eroding these materials to ultimately form a sinkhole. The formation of sinkholes can however, also be due to man-made activities. Schöning (1990) described that the formation of anthropogenic (man-made) sinkholes requires three conditions. The first condition being the correct geotechnical conditions, followed secondly by inappropriate development relative to geotechnical conditions and thirdly, adequate rainfall. He mentioned that these activities include construction of roads, groundwater extraction and recharge, and the forming of drainage ditches. Other activities may also include drilling, mining, poorly compacted soil after excavation and the most critical, broken water pipelines. Water from broken or leaking pipes infiltrate the soil structure, eroding soil and bedrock as it moves downwards, resulting in the formation of a sinkhole. Unlike naturally occurring sinkholes, man-made sinkholes can be prevented in time, making maintenance and management of water

distribution and reticulation systems of upmost importance, as leaking water pipes are one of the main contributing factors to sinkhole formation.

Buttrick (1992) mentioned the various factors that may have an effect on sinkhole formation and the size of the sinkhole. These factors included the following:

- The presence of a receptacle (cavity/discontinuity) in the overburden or bedrock that can potentially receive the mobilised sinkhole material.
- Throat size of the conduit that feeds the mobilised soil material into the receptacle.
- Type of blanketing layer material that overlies the bedrock.
- Mobilising agent that will help to induce mobilisation of the material in the blanketing layer through the throat and into the receptacle, i.e. usually water.
- The internal angle of friction of the soil.
- Position of the water table.

The type of bedrock underlying the overburden soil (layer of soil on top of bedrock) determines whether a sinkhole will form or not. Nel et al. (2011) described that sinkholes usually occur in areas where bedrock comprises out of soft minerals and rocks. Primarily, these rocks are made up of limestone, salt deposits, gypsum, dolomite or carbonate classes of rock.

Nel et al. (2011) mentioned that there are three different types of sinkholes that can occur. They can be classified as follow:

1. Solution sinkhole
2. Cover subsidence sinkhole
3. Cover collapse sinkhole

A solution sinkhole, Figure 2-29 exists when underlying bedrock, with a very thin layer of soil on top or even none, is exposed to the land surface, resulting in weathering of this rock by dissolution. Water percolates through the bedrock, carrying small particles of rock away. Particles reposition themselves into these open spaces created by erosion. Over a period, small depressions start to form in the ground (small sinkholes). Surface water are captured in these depressions, causing a sinkhole to enlarge through further dissolving of bedrock.

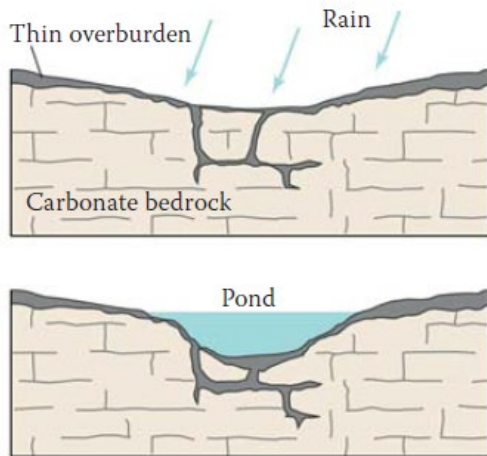


Figure 2-29: Solution sinkholes (Nel et al., 2011)

Nel et al. (2011) described a cover subsidence sinkhole, Figure 2-30, as a sinkhole that is similar to a solution sinkhole, except that the bedrock is covered by a layer of soil or sediment. Infiltration of ground water takes place, eroding bedrock as it moves downwards, forming cavities where bedrock is severely fractured. Over time, overburden soil settles into these cavities, resulting in subsidence of the soil surface and ultimately forming a sinkhole. These sinkholes usually occur in areas where bedrock is covered by a layer of soil that is not knitted together, i.e. cohesionless soil, such as sand.

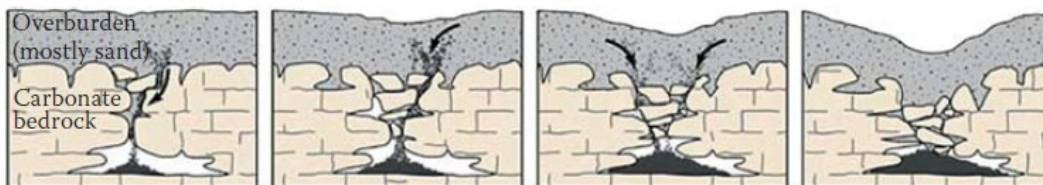


Figure 2-30: Cover subsidence sinkholes (Nel et al., 2011)

A cover collapse sinkhole, Figure 2-31, is a sinkhole that occurs from overburden material and soil that collapses into a subsurface cavity. The cavity is formed by the movement of groundwater through fractures in soluble bedrock, enlarging it through dissolution. Nel et al. (2011) described that the collapse can occur in either one of two ways. The first way is that the cavity becomes relatively large, causing the roof of the cavity to become thin. The thinning of the cavity roof results in it not being able to carry the overlying rock, soil or imposed loads, creating a sinkhole on collapse into the cavity. This failure mechanism is usually aided by the presence of water that seeps through the soil from the ground surface. Secondly, cavities are sometimes filled with groundwater. The presence of the groundwater usually aids in supporting the overlying loads, but if groundwater level lowers, overlying soil and sediments will start to

erode downwards into the dewatered cavity, resulting in a sinkhole. These sinkholes usually occur in areas where bedrock is covered by a layer of soil that has higher cohesive properties, such as clay.

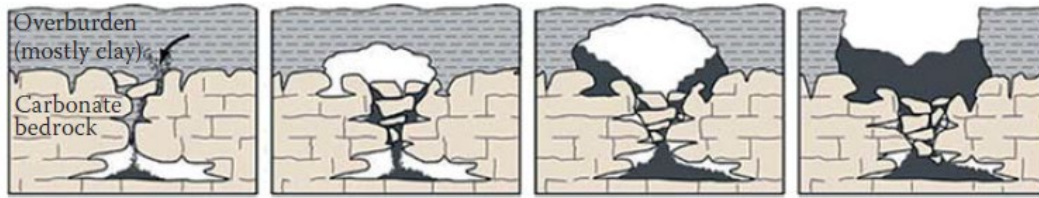


Figure 2-31: Cover collapse sinkholes (Nel et al., 2011)

These holes open without any warning or indication of its occurrence, making it very dangerous. Proper management of underground water networks is therefore of utmost importance to prevent the occurrence of this phenomenon. By detecting small soil settlements deep underneath pipe infrastructure, upon the occurrence of a leak, authorities will be able to take remedial action to prevent it from becoming too severe and be able to stop further potential propagation.

2.10 Summary of literature review and the way forward

Background information on the problem of water loss from leaking pipes was presented, as well as an overview of existing leak detection technologies. At the conception of this project it was hypothesised that, by monitoring temperature changes in the ground along the length of a pipeline, it would be possible to detect water leaks. It is proposed to accomplish this by means of fibre optic instrumentation. This instrumentation also has the capacity to detect strains. Background was therefore also presented on the mechanical aspects of pipe-soil interaction, focusing on how pipes are likely to deform in response to ground movement. Such ground movements can be caused by leaking pipes, with the most extreme case, the formation of sinkholes of which an overview was also presented.

An investigation into the application of fibre optic instrumentation based on temperature and strain measurement for the detection of leaks and pipelines are presented in the remaining chapters, starting with a description of laboratory and field work to first study thermal effects of pipe leaks. This is followed by a description of the strain response of pipes (and the surrounding ground) to water leaks. It was found that the propagation of a wetting through an unsaturated soil mass is accompanied substantial ground strains. A model study is subsequently described which allowed this mechanism to be investigated in greater detail.

The last phase of the study comprise the long term monitoring of a short length of pipe instrumented with fibre optic instrumentation, as well as the observed response to an induced pipe leak.

3 LEAKAGE-INDUCED TEMPERATURE AND STRAIN CHANGES

The experimental work described in this chapter was aimed at understanding the temperature variation in natural ground and potable water in distribution networks. The effect of a buried pipeline leak on the surrounding ground temperature and support conditions was investigated. The above parameters indicated whether temperature and strain observations can be used as a reliable source to determine the location of a leak in a buried pipelines. This chapter contains a description of the experimental work carried out.

3.1 Investigating natural temperature variation in the ground

The success of the monitoring system under investigation is based on the ability to distinguish leakage-induced temperature changes from natural temperature changes in the field. In January 2017 a series of thermistors were installed at depth increments of 250 mm in a test pit on the University of Pretoria's experimental farm to a depth of 3 m as illustrated in Figure 3-1 to provide information on the normal daily and seasonal temperature variation in the ground. This information is necessary so that temperature changes due to leakage can be distinguished from the normal ambient changes. AVX M3950 NTC thermistors were used which indicate 5 kilo ohm at 25 degrees Celsius and their parameter conversion from resistance to temperature is given by the manufacturer.

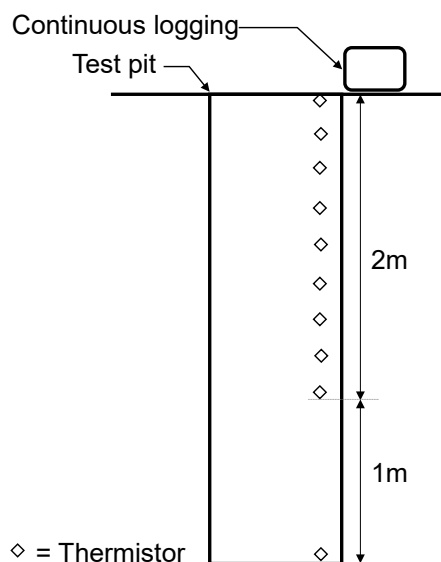


Figure 3-1: In situ soil temperature distribution

A photograph of the test pit with the series of thermistors is presented in Figure 3-2.

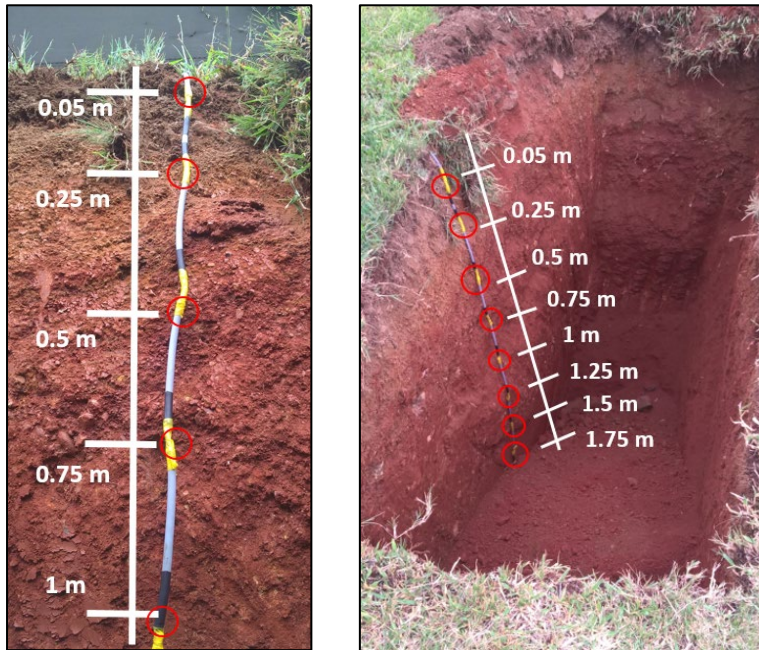


Figure 3-2: Thermistor placement on the experimental farm

Figure 3-3 shows a photograph of the data logger used to continuously record the resistance of the series of thermistors.

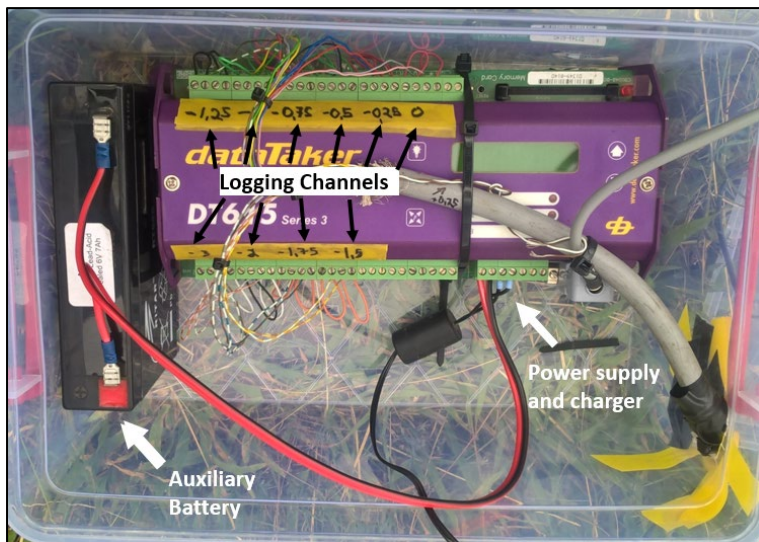


Figure 3-3: DataTaker DT615 with 10 channels

3.2 Temperature variation in water mains

As mentioned above, it is important that temperature deviation induced by water leaking from a pipeline can be distinguished from natural temperature variation in the ground. This aspect is further complicated by the fact that the temperature of water in a distribution network also varies over time. A resistance temperature device (RTD) is used to continuously monitor water temperature upstream of the Pierre van Ryneveld Reservoir in a valve chamber (for location see Figure 3-4). The water supply to the reservoir originates from a large diameter distribution pipe, nearby Rietvlei Dam water treatment works and from the Vaal Dam water supply scheme through Rand Water. This data is used to indicate daily and seasonal temperature trends in a typical water distribution network.

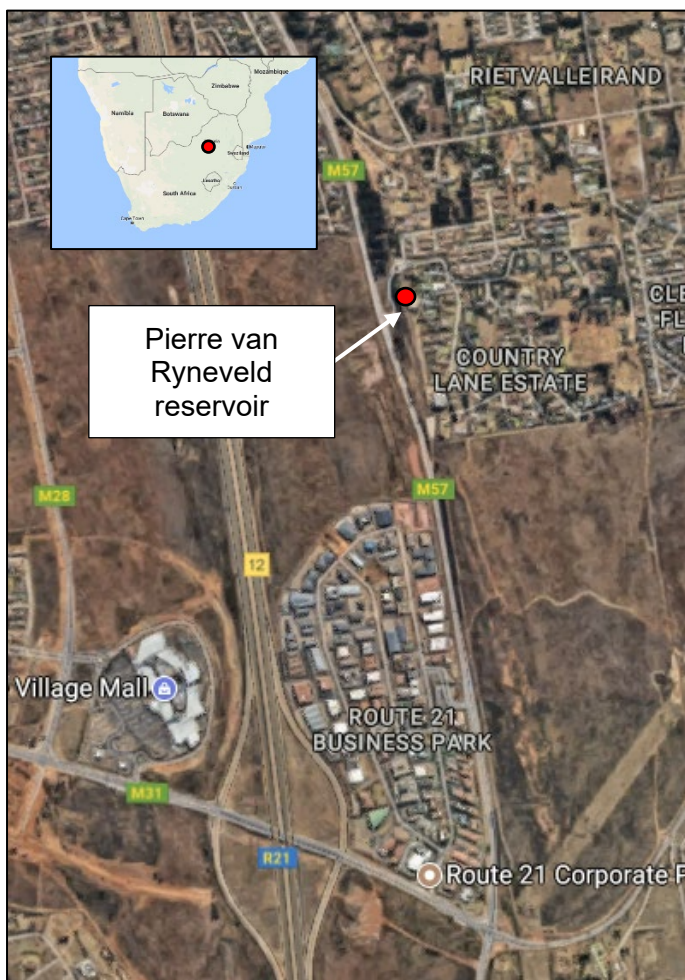


Figure 3-4: Pierre van Ryneveld reservoir location

The specific RTD used for the experiment is shown in Figure 3-5, a current output of 4mA – 20mA corresponds to a temperature of 0-100°C. See Figure 3-6 for the installed RTD in the valve chamber. A data logger is used to capture the temperature data every hour.



Figure 3-5: RTD 4 - 20 mA corresponding to >0-100°C output



Figure 3-6: RTD installed at Pierre van Ryneveld reservoir

3.3 Investigating temperature changes caused by water leaks (laboratory phase)

Experiments were conducted in the laboratory in which water was allowed to leak under controlled conditions into a soil mass into which a number of thermistors were installed to investigate to what extent an advancing wetting front from a leaking pipeline results in a change in temperature in the ground. The tests were carried out in semi-transparent plastic containers measuring 790 mm x 400 mm x 590 mm high to allow the advancing wetting front to be visually observed. Advancing wetting fronts resulting from a number of flow rates were investigated as slow flow rates might result in the water temperature equalising with the soil temperature, resulting in difficulty to detect a temperature variation associated with the arrival of a wetting front. The experiments were carried out in a temperature isolated enclosure where temperature was kept at a constant 25°C to eliminate environmental temperature fluctuation.

Figure 3-7 presents an elevation of the experimental setup, showing the model container, water introduction point and thermistor locations, with a photograph in Figure 3-8.

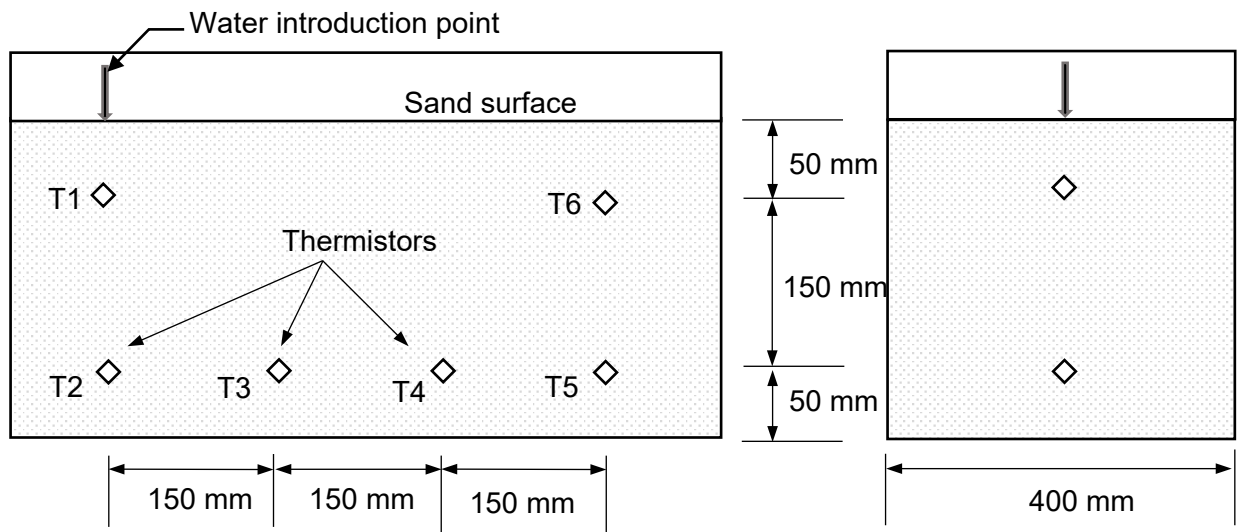


Figure 3-7: Experimental arrangement for laboratory leakage experiment.

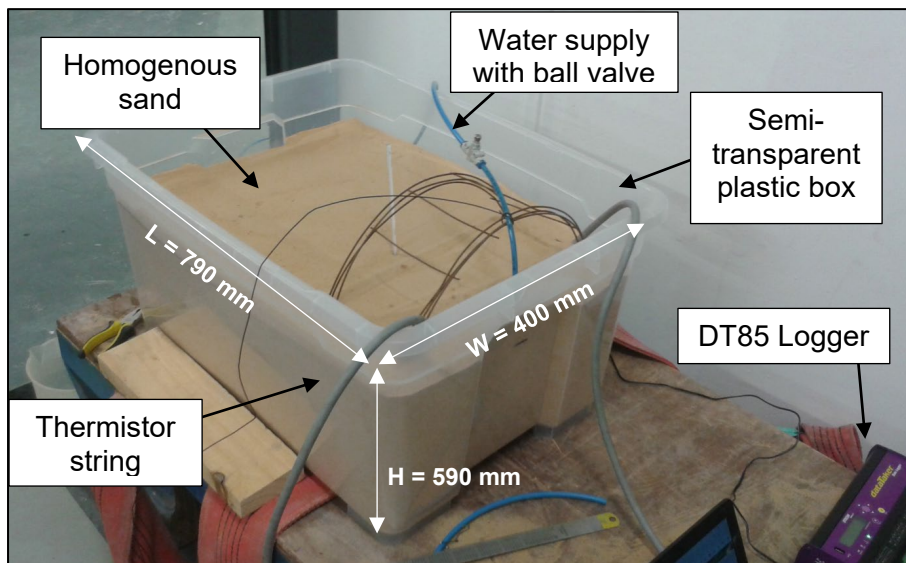


Figure 3-8: Photograph of the experimental arrangement for laboratory leakage experiment.

3.4 Investigating temperature changes caused by water leaks (field phase)

It is expected that temperature changes underneath a pipeline will provide the first indication of a leak occurring. Over time, leakage is likely to result in softening of the ground near the leak and this is likely to impose some strain on the pipe due to changes in the support conditions underneath the pipe. It is hypothesised that these strains can be detected using fibre optic strain measurement. How soon after detection of a temperature change a change in pipe strain becomes detectable may possibly also provide an indication of the severity of the leak. The detection of strain will be especially important in dolomitic ground because it may provide an indication that a sinkhole is forming which would be a trigger for urgent remedial action. A short length of pipeline was therefore installed at the experimental farm of the University of Pretoria which instrumented for both temperature and strain measurement to allow the abovementioned aspects to be investigated under controlled conditions.

It is believed that the correlation between pipe strain and ground movement will enable pipe owners to judge the urgency by which remedial action is required. For example: If a sudden temperature change is detected and no measureable strain, it would imply that the pipe is leaking but has not suffered significant structural damage yet. However, should significant strains be detected in addition to a temperature change, the pipe has probably suffered some damage and more urgent remedial action is required. The knowledge gained in term of this behaviour could assist in refining water distribution network maintenance plans.

A short pipeline section installed on the University of Pretoria's experimental farm is illustrated in Figure 3-9 (see Figure 3-10 for locality). It was instrumented with an array of fibre optic Bragg strain sensors and conventional thermistors. This is done to verify whether the proposed leakage detection system would be able to detect leakage from a pipeline in the field. This is necessary because the ambient temperature changes occurring in the field are different from those in the laboratory and it is necessary to observe whether temperature changes from leakage can be distinguished from the ambient. Furthermore the effect of soil wetting in trench on the support condition has to be investigated.

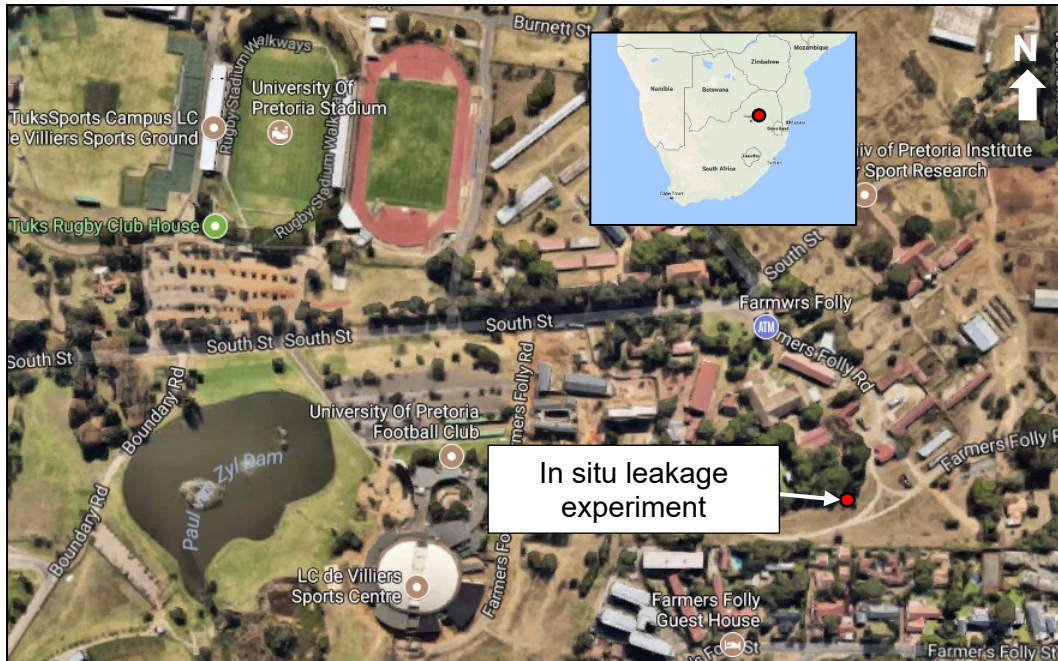


Figure 3-9: Location of in situ pipe leakage experiment



Figure 3-10: View of the location of pipe leakage experiment

The installation comprises of a 12 m long 110 mm diameter uPVC Class 6 pipe buried under backfill of 600 mm to the pipe crown. Provision is being made to allow water to be circulated through the pipe during testing. It is not desirable to leave stagnant water in the pipe during testing as this water will soon take on the temperature of the surrounding soil, significantly reducing the temperature gradient. This scenario will however be investigated in the test-set up.

The pipe is equipped with three leak points installed at 2 m intervals along the pipe length, with one point at the pipe invert, one at the pipe crown and one at the side of the pipe to allow leaks originating from different parts of the pipe to be studied. The leak points will be operated via valves located on the ground surface and are fitted with flow restrictors to impose leakage at the desired rate.

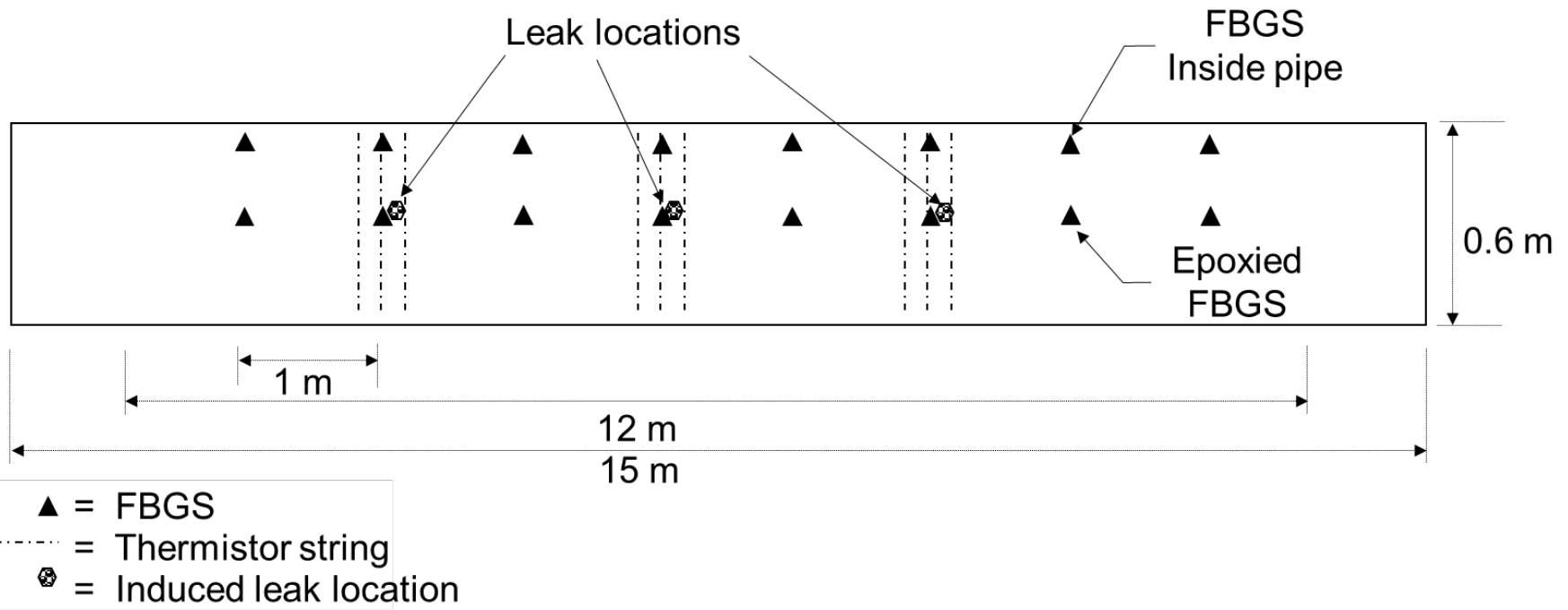
A number of thermistors were installed in the ground and on the pipe around each leak point to allow the temperature changes associated with a leak to be observed in great detail. Vishay NTCLE305E4 thermistors were used which indicate 5 k Ω resistance at 25°C. In addition, fibre optic cable with 16 discrete fibre optic Bragg strain sensors were included in the installation. FBGS DTG SWM-01 strain sensors Braggs were used, they have excellent corrosive properties with an operational temperature range from -40°C to 120°C, an elastic modulus in excess of 48GPa, maximum tensile strain of 25 m ϵ and a maximum longitudinal load of 0.95 kN (FBGS, 2017). Eight of the 16 strain sensors were rigidly fixed (epoxied) to the external pipe base to allow for strain measurement on the pipe. The remaining Bragg sensors were placed within a 4 mm polyurethane (PU) tube filled with low viscosity oil in the (south, see Figure 3-11c) left trench corner looking downstream. The purpose was to ensure that the fibre optic cable was mechanically isolated from any pipe strain. Two locations for the positioning of the fibre optic cables are being investigated to determine the position for optimal leakage detection, i.e. fixed to the pipe and free-floating in the pipe trench.

The installation was completed at the end of July 2017 and testing commenced in August. A number of different tests were carried out to determine the sensitivity of the fibre optic sensors within the PU tube and the epoxied fibre optic sensors. The effects of external influences such as vehicular and human movement in close proximity to the pipeline on the buried sensors were also investigated.

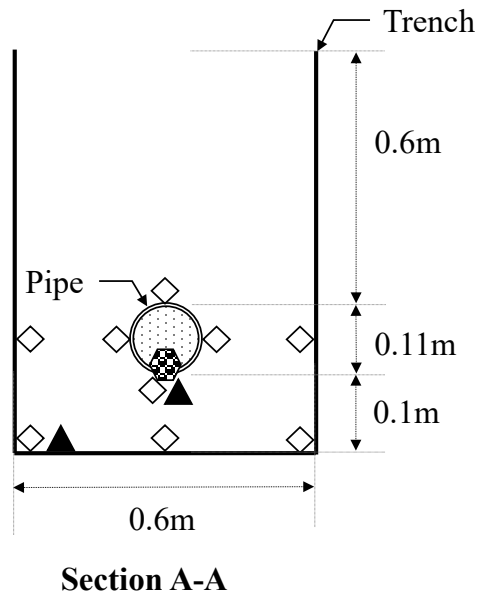
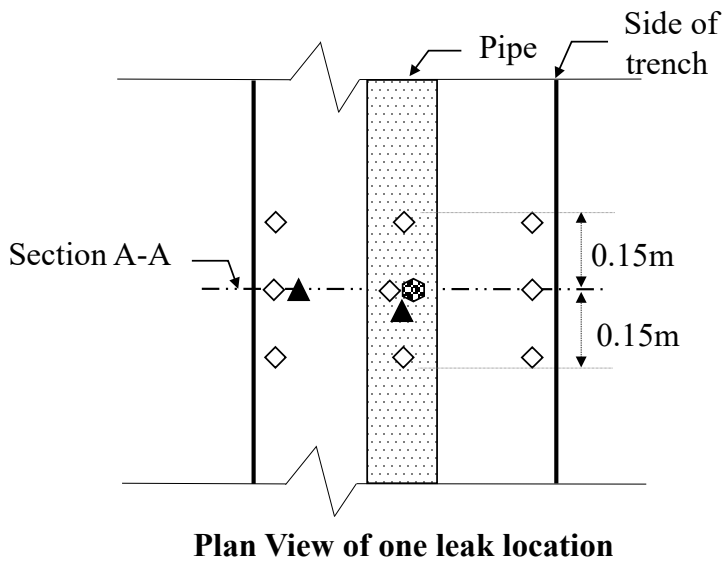
The following phenomena and questions were investigated:

- The daily temperature fluctuation at the installation site in both the soil and water.
- Can the daily temperature fluctuation be distinguished from that caused by a water leak?
- What is the effect of normal operational pressure changes in the water network on longitudinal strain development in a pipe? (Results to follow in report on strain measurement)
- What are the changes in support conditions to the pipe due to wetting for short and long term testing? (Results to follow in report on strain measurement)

A long section schematic of the pipeline is shown in Figure 3-11 (a) with a plan view shown Figure 3-11 (b), the instrument location is indicated in these schematics. A detailed plan and section view of one leak location are indicated in Figure 3-11 (c). Each leak location has a thermistor string located 0.15 m upstream, 0.15 m downstream and at the leak location to allow temperature migration around a leak location to be studied. Each thermistor string consists of 9 individual thermistors, giving a total of 27 thermistors per leak location. Their arrangement around the leak locations are indicated in Figure 3-11(c).



(b) Plan of field installation showing temperature and strain Bragg gratings and thermistor strings.



- ▲ = FBGS
- ◇ = Thermistor
- ⊠ = Induced leak location

(c) Cross section view of field installation.

Figure 3-11: Layout of experimental arrangement installed on the experimental farm of the University of Pretoria

The installation process started with the trench excavation measuring 15 m x 0.6 m x 0.8 m deep, see Figure 3-12 below. Before commencing trenching, test pits were excavated to ensure that no existing services will be damaged during the installation.



Figure 3-12: Excavation of trench

Proceeding trenching, the sensors were laid out according to their planned installation location to the side of the trench. The base of the trench was levelled with reference to the undisturbed ground and the design invert depth of 800 mm. A slope of 1.5° was allowed for, to aid the drainage process in the flow direction from the upstream municipal connection to the downstream drainage tanks used to hold the water circulated through the system. The slope amounts to a level drop of 400 mm over the 15 m long trench (see Figure 3-13).



Figure 3-13: Sensor layout and levelling bottom of trench in preparation for pipe and instrumentation installation

The thermistor strings were placed at the leak locations as well as 150 mm upstream and downstream of the leak location and the leak locations were spaced at 2 m intervals, indicated in Figure 3-14. A 20 mm sleeve was installed in the right hand corner of the trench, looking downstream, to allow for future addition of distributed fibre optics or other sensors. In the left corner of the trench 8 FBGS were placed enclosed within a 4 mm PU tube to allow for mechanically strain-isolated thermal movement. The remaining 8 FBGS were epoxied to the pipe to measure possible changes in strain due to the occurrence of the simulated leak and changes in network pressure (see Figure 3-15).

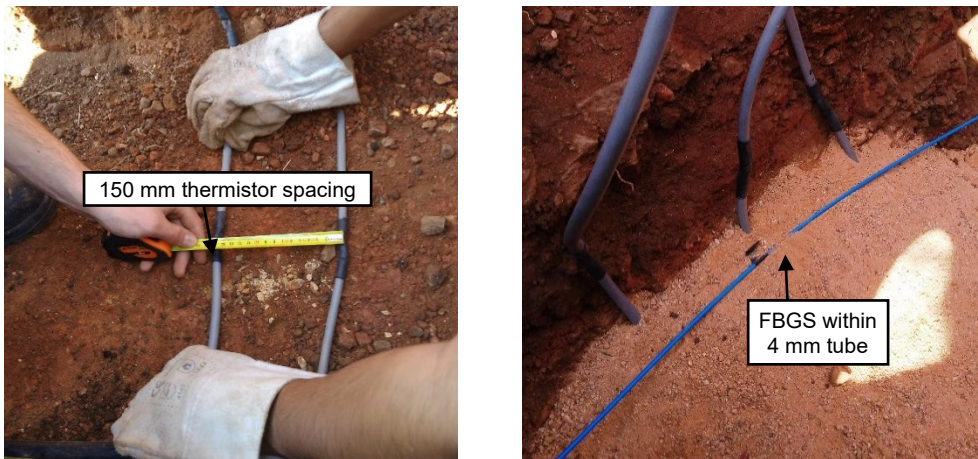
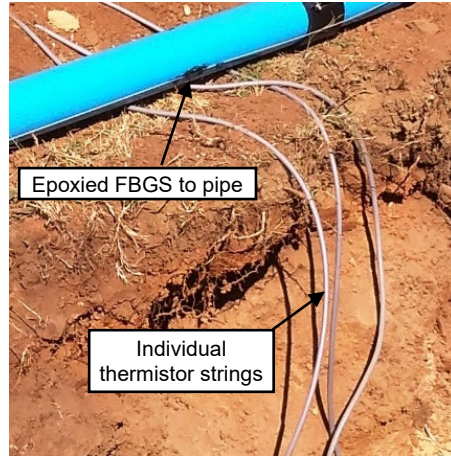


Figure 3-14: Installing sensors on the trench bottom

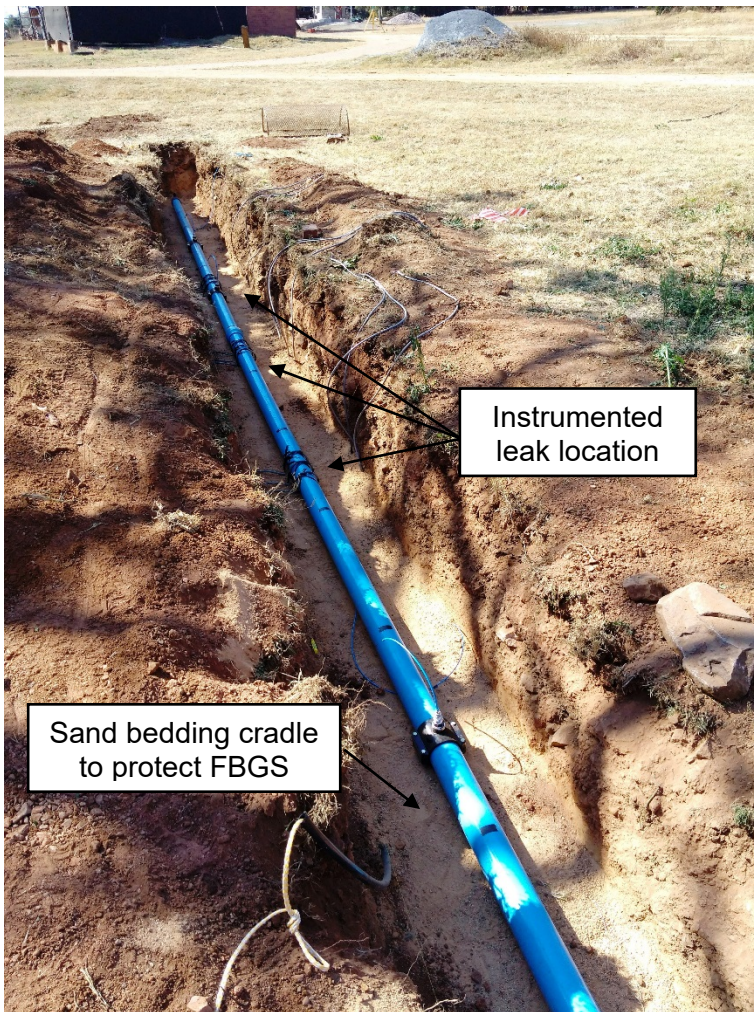


Epoxyed FBGS to pipe

Individual thermistor strings

Figure 3-15: Epoxying FBGS to pipe base

After the epoxyed Bragg bonded to the pipe base, the pipe was laid onto the sand cradle in the trench (see Figure 3-16). The sensor layout was realigned during pipe laying to ensure that the sensor locations were correct and that the strain and temperature sensors are aligned.



Instrumented leak location

Sand bedding cradle to protect FBGS

Figure 3-16: Instrumented pipe in trench

The pipe bedding consist of a 100 mm clean building sand (bedding) layer, covered by a 400 mm sieved in situ material fill blanket, compacted in 100 mm layers with hand stampers and finally un-sieved in situ material for backfilling the remaining 200 mm. A lightweight compactor (“wacker”) was available on site, which was not used for the bedding blanket because it was suspected that it might damage the FBGS. The final layers of the backfill was compacted with the “wacker” and hand stampers. Each individual 100 mm layer was wetted to achieve OMC (see Figure 3-17).



Figure 3-17: Backfilling pipe and sensors

The field installation was completed by ensuring that the trench is sufficiently compacted throughout and that there are no sharp edges or possible erosion gullies on the surface that can form in close proximity to the trench during rain storms (see Figure 3-18). Care was taken to ensure that the pipe ends are sufficiently compacted, acting as thrust blocks. The internal pipe pressure can be limited during testing at the upstream valve, to prevent unnecessary and

unintended leaks forming at connections, joints and couplings. A downstream valve can be used to relieve the internal pipe pressure if necessary.



Figure 3-18: Finishing off installation

The pipe installation was allowed to settle and reach equilibrium for two weeks prior to testing commenced. Undergraduate civil engineering students assisted with the installation of the pipeline and sensors.

3.5 Observed natural temperature changes in the ground

The monitoring of ground temperatures over the top 3 m of the soil profile entered its ninth month in October 2017. Figure 3-19 to Figure 3-27 presents box & whisker plots of temperature variation with depth recorded for the first nine months of 2017. Minimum, maximum and average temperatures are presented, as well as the 25th and 75th percentile values. The measurement array was commissioned towards the end of January which is the reason for the relatively narrow temperature variation shown for that month.

It is evident that temperature variation rapidly reduces with depth. It is interesting to note that at a depth of 0.5 m, the monthly temperature variation is of the order of 3°C, but that the

maximum temperature variation appear to occur during the autumnal months of April and May, during which temperature reduce from the higher summer values. The smallest temperature variation was measuring during August at the end of winter, with a noticeable increase in temperature variation occurring in September as the ground began to warm as spring arrived.

From 0.75 m, the depth below which water distribution pipelines would normally be buried, the monthly temperature variation is generally less than 2°C. The fact that the temperature variation with depth is small is encouraging as it implies that temperature variations caused by water leaks should be readily discernible should such leak-induced temperature variation exceed 2°C.

Monitoring of the thermistor array has continue until the end of the project to allow data to be recorded to study seasonal temperature fluctuation. The complete set of results is presented in Appendix A.

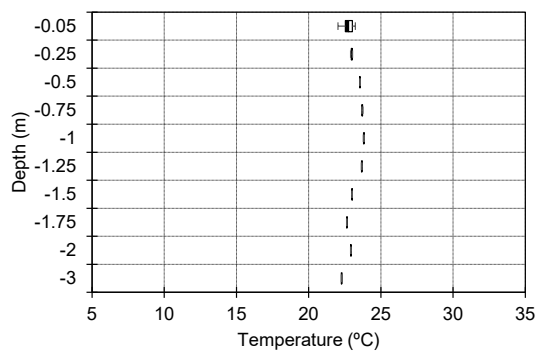


Figure 3-19: Box and Whisker plot January 2017

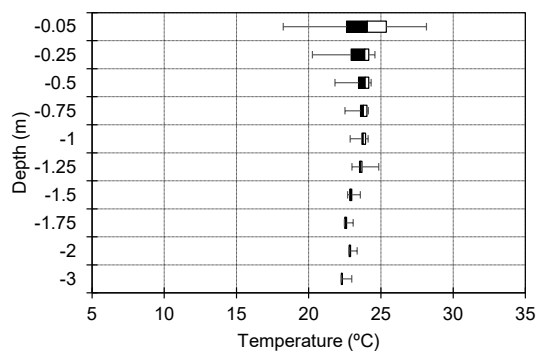


Figure 3-20: Box and Whisker plot February 2017

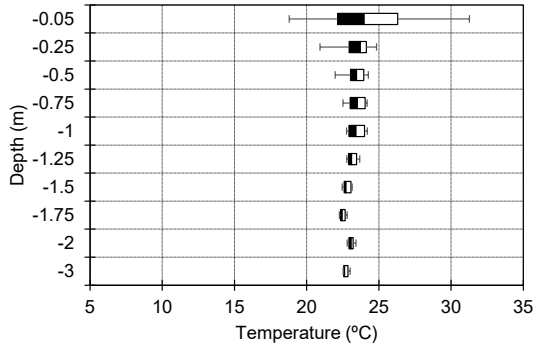


Figure 3-21: Box and Whisker plot March 2017

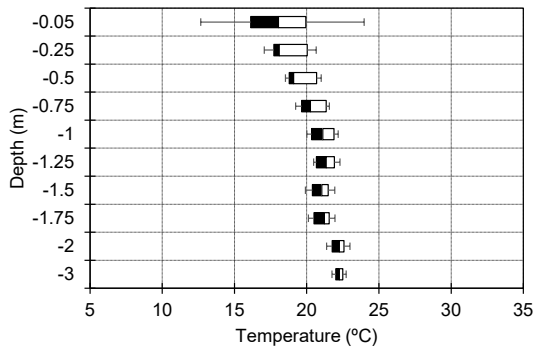


Figure 3-22: Box and Whisker plot April 2017

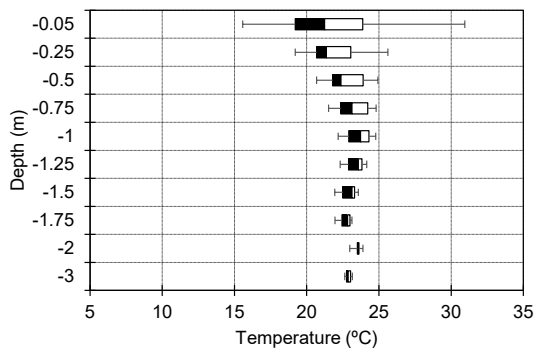


Figure 3-23: Box and Whisker plot May 2017

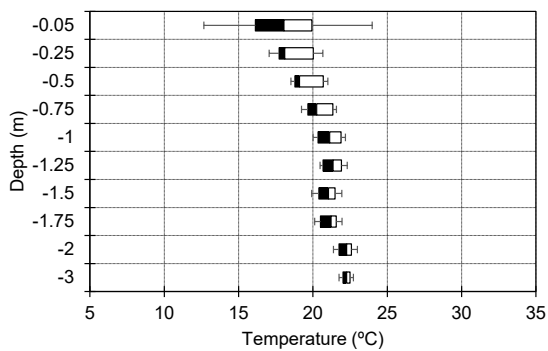


Figure 3-24: Box and Whisker plot June 2017

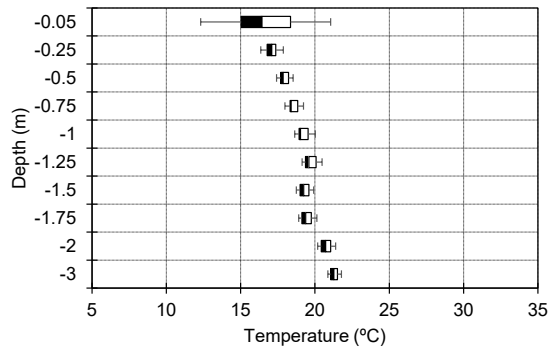


Figure 3-25: Box and Whisker plot July 2017

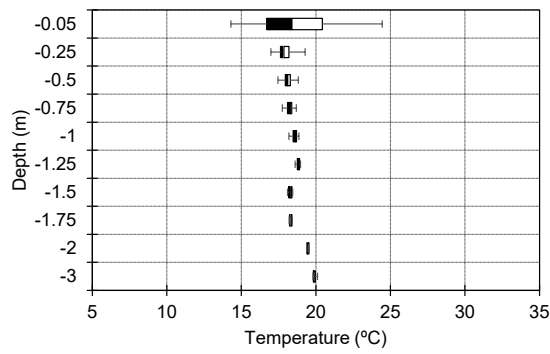


Figure 3-26: Box and Whisker plot August 2017

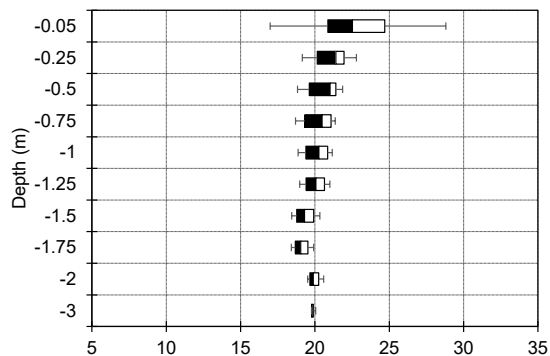


Figure 3-27: Box and Whisker plot September 2017

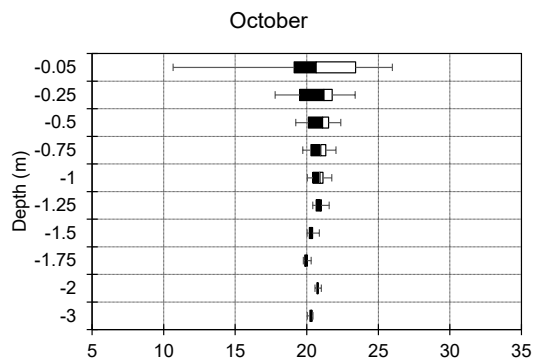


Figure 3-28: Box and Whisker plot October 2017

In Figure 3-29 a strong correlation between depth and seasonal temperature variation can be seen as well as major rainfall events influencing the top soil layers up to 1 metre depth. The lag in ground temperature response to seasonal temperature variation increases with depth with minimum ground temperature at 0.25 m occurring in July, while the minimum ground temperature at 3 m depth was only reached in the beginning of September.

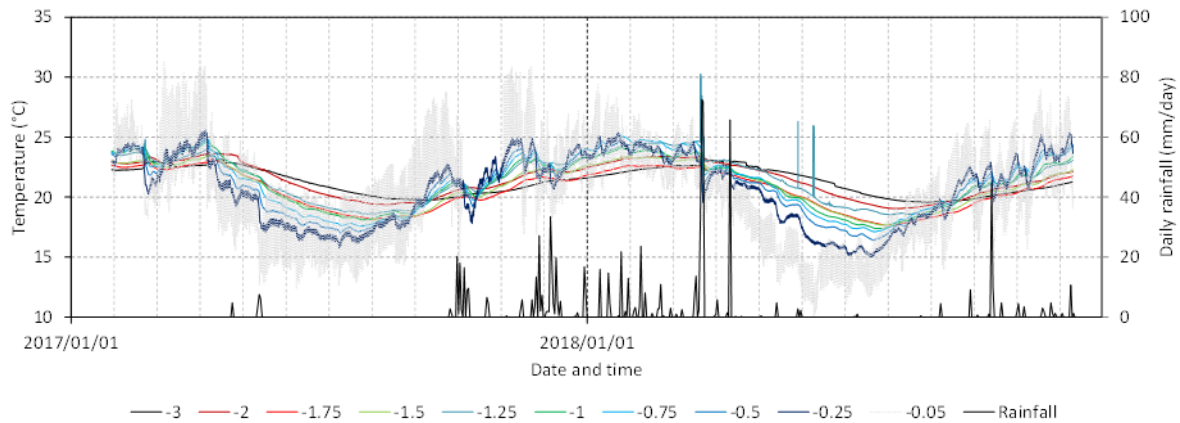


Figure 3-29: Soil temperature with depth and rainfall variation over the course of the study period.

The temperature variation with depth is shown in Figure 3-30 below for the months of February, May and July. These months represent a typical summer, transitional and winter seasonal period. It can be deduced that during summer and winter months the temperature fluctuations taper off rapidly with depth as compared to the seasonal transition period, May.

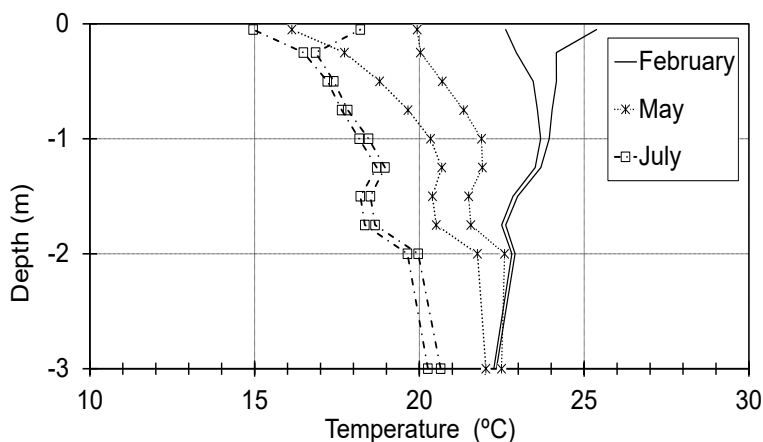


Figure 3-30: First and third quartile temperature variation with depth for summer and winter months (2017)

3.6 Temperature variation in water mains

Figure 3-31 presents air and water temperatures recorded at the Pierre van Ryneveld reservoir in Tshwane during the course of May to October 2017. A clear daily fluctuation in water temperature is evident. However, it can be seen that the fluctuation in the water temperature is considerably smaller than the fluctuation in air temperature, being approximately only 2 to 3°C compared to air temperature variation of typically 15°C over the course of the monitoring period. It is interesting to note that the water temperature seemed to fluctuate around a relatively constant mean of approximately 15° with comparatively little variation. This represents a relatively large temperature differential of 3 to 5°C compared to the May and June soil temperature at depth presented in Figure 4-11 which is encouraging in terms of the potential performance of the monitoring system under investigation in this study.

This temperature monitoring arrangement will continue as long as access is possible to allow data to be recorded to study seasonal temperature fluctuation.

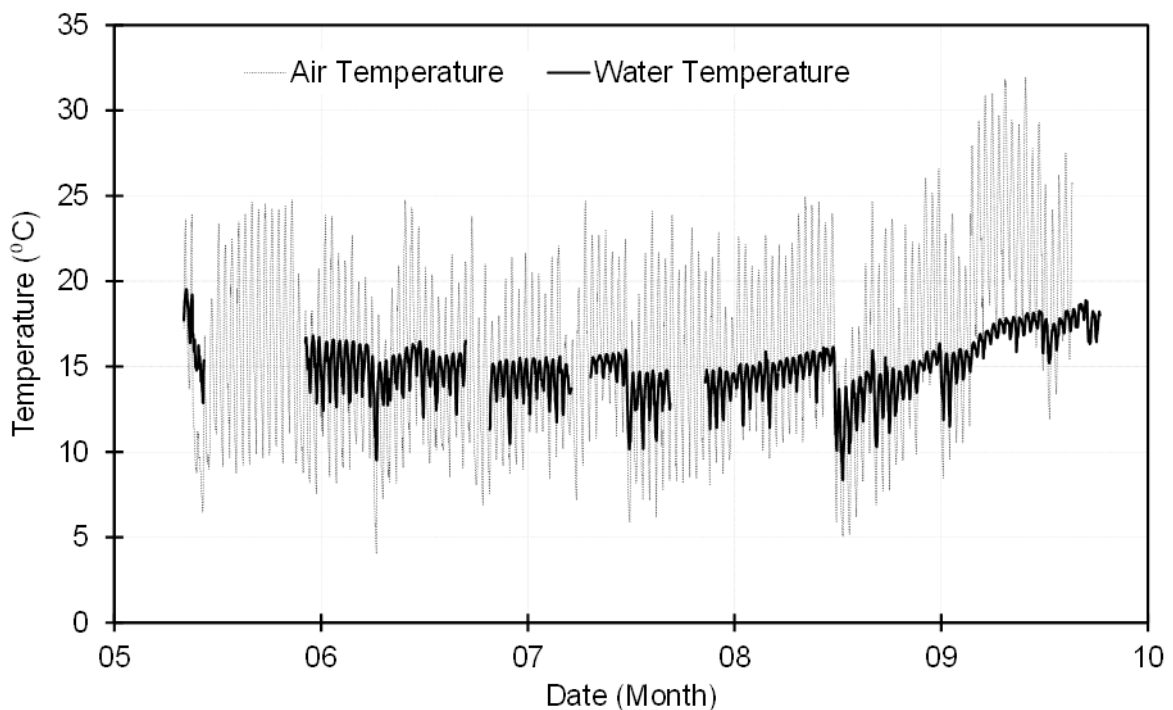


Figure 3-31: Air and water temperatures recorded at Pierre van Ryneveld reservoir (Tshwane) May to October 2017.

Figure 3-32 below indicates the water mains temperature and the natural ground temperature variation with depth for the month of July. It is shown that the water temperature is different to the soil temperature at typical depth at which water mains are typically installed.

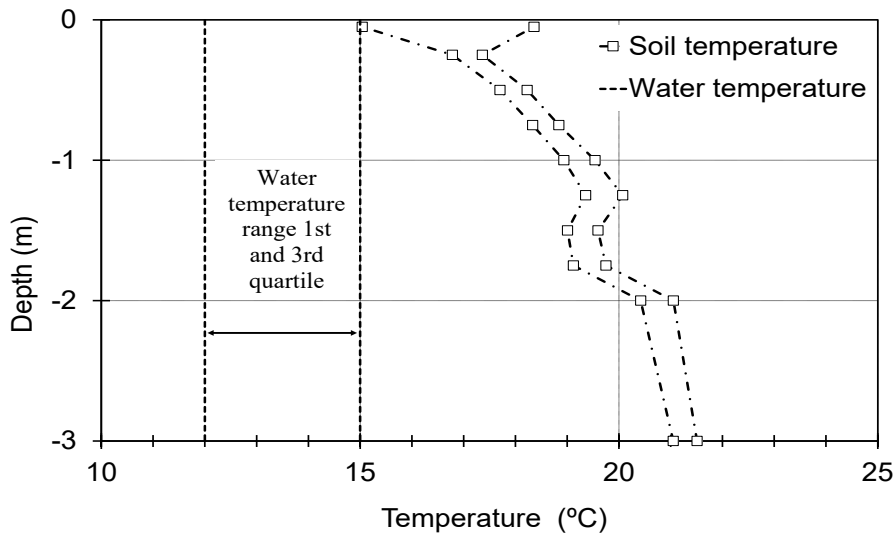


Figure 3-32: First and third quartile soil and water temperature variation with depth for July 2017

Monitoring of the thermistor array has continued until the end of 2018 to allow for a two year dataset to be obtained and to study seasonal soil depth temperature fluctuation. Results can be found in Appendix A.

3.7 Temperature changes caused by water leaks (laboratory phase)

The advance of the wetting front observed during the experiment is illustrated in Figure 3-33. Figure 3-34 presents temperature variation recorded during the laboratory phase of the experiment. The leakage rate was 140 ml per minute and the water temperature measured at 21°C. It is evident from the temperature records that temperatures in the soil reduced markedly in response to the wetting front moving through the soil, which is promising in terms of the performance of the proposed leakage detection system.

Examining the temperature data more closely reveals an interested phenomenon. The passing wetting front do seem to result in a temperature reduction after passing a specific measurement location. However, it is evident from all temperature records that a small temperature increase (0.2-0.5°C) was observed before the temperature reduction followed. This was an unexpected observation, but was consistently observed in all tests.



Figure 3-33: Advancing wetting front in laboratory test.

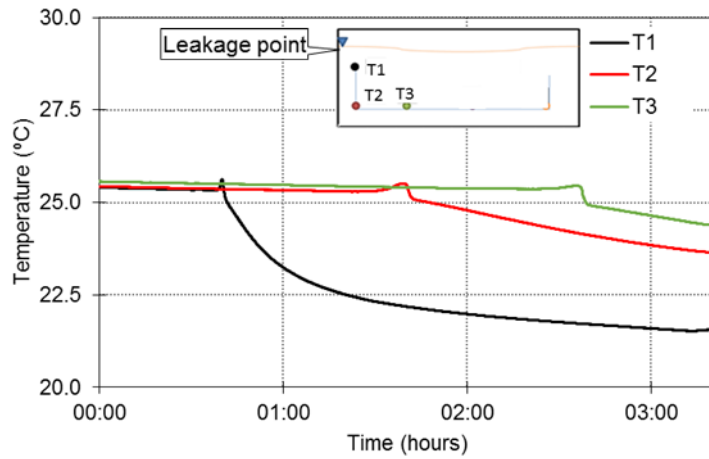


Figure 3-34: Temperature record from laboratory wetting test.

The phenomenon was further investigated by carrying out wetting tests in another material, a red-brown silty slightly clayey sand collected from the University of Pretoria's experimental farm. Figure 3-35 presents an illustration of the simple experimental setup. The tests on the

original material was repeated as control. The temperatures recorded during wetting of the soils are presented in Figure 3-36. It can be seen that the same phenomenon was observed, but that the temperature increased in the case of the red-brown sand was smaller.

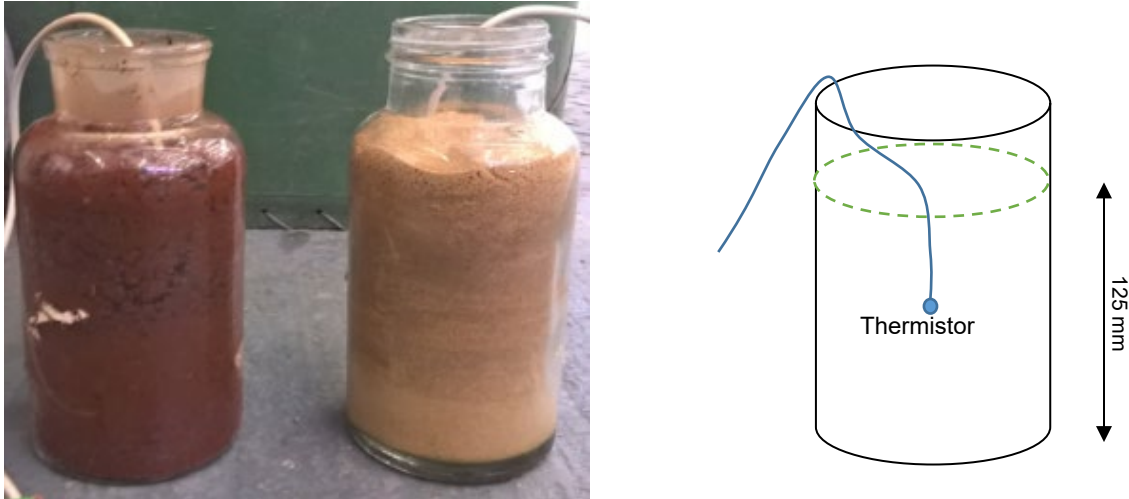


Figure 3-35: Wetting tests on red-brown silty sand and light brown silica sand to investigate initial rise in temperature during passage of wetting front.

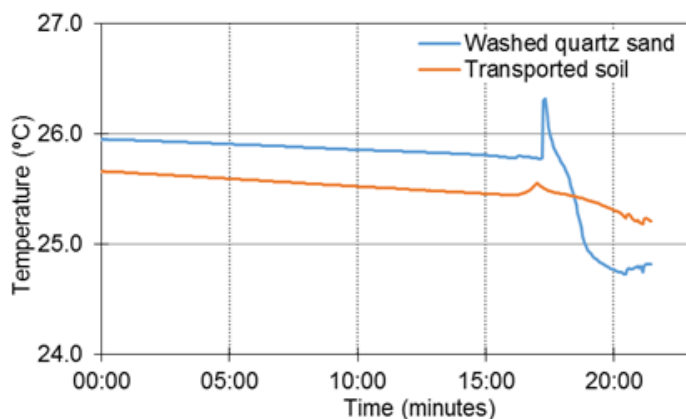


Figure 3-36: Temperature record from wetting test.

A literature search revealed that the phenomenon can be attributed to the release of surface energy from the surfaces of the soil grains upon wetting with water. The process of wetting of a solid surface with a liquid involves interaction between three interface types, i.e. solid-liquid, solid-air and liquid-air. Wetting results in an area of solid-air interface to be replaced by an area of solid-liquid interface. Each solid surface has its own specific surface energy which is associated with the way in which atoms are bonded into that solid (e.g. co-valent, ionic or hydrogen bonding) (Parks, 1984). A certain amount of energy, referred to as surface energy, needs to be added to a surface to allow atoms to be removed from the lattice structure. Wetting can result in a net increase or a net decrease in total surface energy. When energy

is released upon wetting, wetting occurs spontaneously. Should energy be required to be added for wetting to occur, the surface will not wet naturally and will be hydrophobic (Wenzel, 1936).

Wetting of quartz by water results in a reduction in the specific surface energy of quartz by about 72 mJ/m² (Parks, 1984). Due to the fine grained particulate nature of soils, the surface area of a small volume of material quickly becomes large as grain size is reduced. Wetting a fine grained soil, which is known to occur spontaneously, is therefore associated with a measurable release of surface energy. This release of some of the surface energy of the soil samples described above is responsible for the small rise in temperature associated with the passage of the wetting front. After passage of the wetting front the thermal mass of the colder liquid released by the leak results in a drop in temperature which, if measured, allows a leak to be detected which illustrates the potential success of a leakage detection system based on temperature measurement installed in close proximity along a pipeline.

3.8 Investigating temperature changes caused by water leaks (field phase)

A Class 6 110 mm diameter 12 m long pipeline with 3 separate leak locations spaced 2 m apart was used to test the effect of a leak on in situ soil temperature and possible strain development. Temperature changes and pipeline strains changes due to a possible softening of the support conditions are predicted to occur close to the leak location.

Each leak locations has 27 thermistors placed around the pipe with a total of 8 FBGS attached longitudinally to the pipe and 8 FBGS loose within 4 mm polyurethane pipe spaced 1 metre apart partially over the 12 metre pipeline length as illustrated in Figure 3-11. A Datataker DT85 logger was used to monitor 27 thermistors at once, which represents all the thermistors at one complete leak location. A Datataker DT615 was used to continuously monitor one thermistor string at a reference location for the whole experimental test period to record soil temperatures with depth.

The pipeline was allowed a settling in period of two weeks after installation, before commencing initial daily FBGS readings. These readings were taken with a HBM FS22DI BraggMETER, logging all Braggs at 10Hz for a 15 minute period each day. This phase was proceeded by permanently installing the logger in a building in close proximity to the experiment to continuously monitor the Braggs.

Continuously monitoring the Braggs proved more effective than the short duration daily observations, as it indicated the daily temperature variation over time which is necessary for a thorough interpretation of the data. The logging interval for the fibre optic sensors was changed to 1Hz.

The internal pipe pressure was monitored at one minute intervals with an Onset Hoboware U12 logger and a 7 bar pressure transducer during the leak tests. The logging frequency of the thermistors during leak test was 1 reading every 5 seconds or 0.2Hz. The logging frequency during dormant periods, where no leaks were induced, was set to 15 minutes to provide information on the magnitude of the daily temperature fluctuations. The temperature of the water exiting the pipe into a downstream storage tank was logged during the leak tests, as well as the temperature of the water in the pipeline during dormant periods.

During daily temperature fluctuation observations the pipeline was isolated from the water distribution network after and before a leak was initiated. The flow rate at the leak location was measured with a measuring beaker and stopwatch and the flow rate of the water entering the pipeline was determined with a gear type Class C flow meter.

Brief summary of typical measuring regime during leak tests is presented below:

- 1.) Setting-up Onset Hoboware U12 logger with pressure transducer with a 1 minute logging interval. Leave at atmospheric pressure to allow for base or “zero” reading to be determined.
- 2.) Download “dormant” data from DT615 and DT85 loggers which measure resistance (temperature) of thermistors recorded every 1 hour for the DT615 recording in situ soil temperature and 15 minutes for the DT85 recording thermistors at the leak locations.
- 3.) Set new logging frequency to 5 seconds for DT85 at leak location (DT615 remains at 1 hour logging frequency).
- 4.) DT85 logger is allowed to obtain base resistance readings for a few minutes before opening valves.
- 5.) Ensure that all the loggers and channels read ‘acceptable’ values, which are 4 to 7 k Ω for the thermistors, 4 mA for the pressure transducer (at atmospheric pressure) and the Fibre Bragg readings are within the range from 1509 nm to 1570 nm.
- 6.) Initiate leak by opening upstream valve. Set flow rate at leak location by disconnecting leak tube at surface and measuring amount of water with measuring beaker per time period with a stopwatch. Use the gear type flow meter to determine flow volume into the pipeline at the test start.

- 7.) Let leak proceed for long or short duration leak test, depending on predetermined test regime.
- 8.) During the leak test a remote connection to the HBM BraggMETER can be established to ensure that the logger is functioning “normally” and if an error does occur, that the logger can be restarted remotely or other troubleshooting action can be taken.
- 9.) After the leak test is completed, stop the leak by closing valve upstream of pipeline and at the leak location.
- 10.) Read gear-type flow volume. This value can be subtract from initial value to determine the total amount of water that flowed through the pipe.
- 11.) Retrieve data from all the loggers before resetting the logging interval to their dormant rate of 15 minutes for the DT85 logger and 1 hour for the DT615.
- 12.) Observe temperature data continuously and ensure that Bragg data is taken for a few days after the leak was terminated to observe “recovery” trends.

The above mentioned methodology was repeated at all three leak locations.

The first test conducted was a short duration leak test for less than an hour to determine whether all the instruments are functioning as intended. However, during the first test problems were experienced with the fibre optic Bragg sensors. The signal of the fibre optic sensors seemed to be unstable and not representative of the actual physical phenomena, as peak dropout of the first few Bragg sensors were experienced. This was corrected by splicing a new angled FC/APC connector onto the Bragg string and replacing the FC/PC connector, which subsequently resulted in a better signal quality with no peak drop out occurrences.

After the initial fibre optic Bragg problems were resolved and all the sensors gave reasonable outputs, daily leakage tests were conducted at the various leak locations. For the tests the water within the pipeline was stagnant up to the initiation of the leak event, the leak was retained for less than a day. Between the leak occurrences 3 days were given for the pipeline to return to its normal daily temperature fluctuation. During this period all the fibre optic sensors were logged. However, the fibre optic BraggMETER logger did give a ‘timeout’ error during some logging periods. This error is experienced because the host computer cannot connect to the logger for a short time duration. The issue was corrected during later tests by using a reconnection configuration, which allows the host computer to reconnect even if the logger connection is lost for a short duration.

The thermistor data is discussed first in the following section after which the fibre Bragg grating data is summarised. Table 3-1 below indicates the tests carried out to date (test 1- test 4),

tests which have to be evaluated (test 5-test 6) and future dated tests (test 7) not included in this report.

Table 3-1: Tests carried out

Test Nr.	Description
1	Short duration leak test to verify sensors and loggers are functioning
2	Medium duration (>5 hours and <1 days at leak location 3)
3	Medium duration at leak location 2
4	Medium duration at leak location 1
5	Long duration (>2 days) at leak location 1 (data evaluation phase)
6	Pressure vs. strain test with (data evaluation phase)
7	Long duration at leak location 2 (future)

3.8.1 Thermistor data

Two loggers were used to log the resistance values from thermistors placed around the pipe and inside the trench which were converted to temperature values.

3.8.1.1 Leakage test 1

The first longer duration leak test conducted was initiated on 13 September at 16h43 and closed at 05h51 on 14 September. Therefore a total leak time of just over 13 hours was applied. The imposed leakage rate was 0.61 l/min. The corresponding flow rate through the pipe was 3.75 l/min and the internal pipe pressure 36 kPa. The outlet valve from the pipe was opened allowing water to discharge into a tank at atmospheric conditions.

The leak was initiated at leak location 3 (LL3) (see Figure 4-18 below). Thermistor string (TS) 8 was located at LL3 with TS9 0.15 m downstream and TS7 0.15 m upstream of LL3.

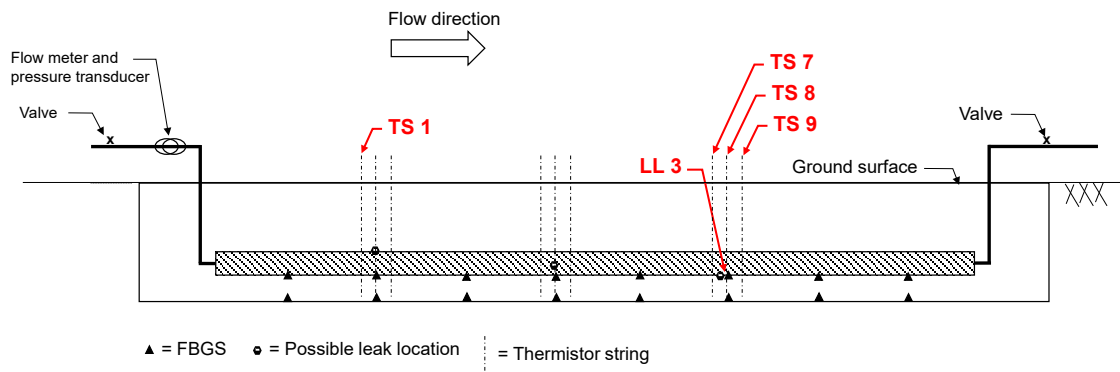


Figure 3-37: Elevation of experimental installation showing location of Leakage test 1

The thermistor data obtained is separated into data obtained in close proximity to the pipe (i.e. thermistors T1-T4, see Figure 4-20) and in the trench corners (thermistors T5-T9).

The water supply from the municipal connection was only opened when the leak was initiated. This was intentional and implies that the water in the pipe had been stagnant prior to commencement of the leak so that the temperature differential between the water in the pipe and the surrounding soil would have been minimal. The ability to detect a leak under such conditions (i.e. when the temperature of the water in the pipe was similar to the soil temperature) implies that a leak will be detected more easily under conditions when the water in the pipe had been circulating as there would have been a larger temperature differential between the water in the pipe and the surrounding soil.

The water temperature during the test is summarised in Figure 3-38. An initial temperature spike can be observed due to warm stagnant water in the distribution network upstream of the test installation, which was flushed through the pipe after which a significant drop can be observed. The temperature spike was not intended to form part of the test sequence but provided an opportunity to examine the effect of such rapid water temperature changes on the temperatures around the pipe.

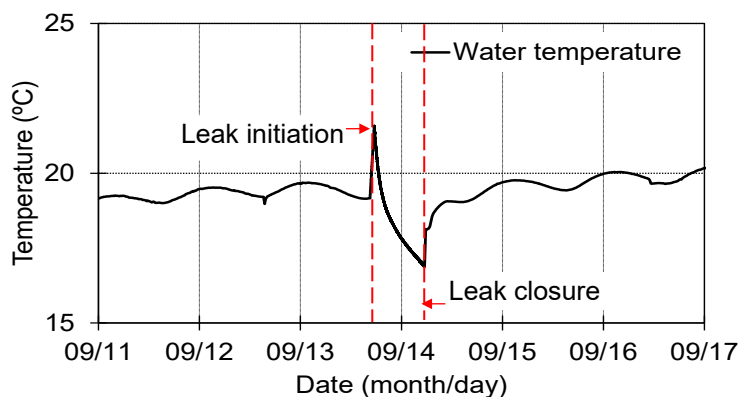


Figure 3-38: Water temperature during the first leak test

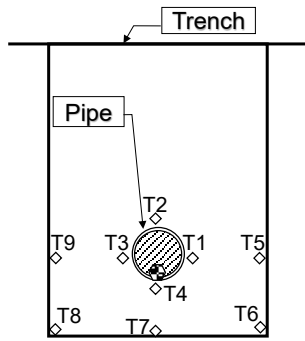
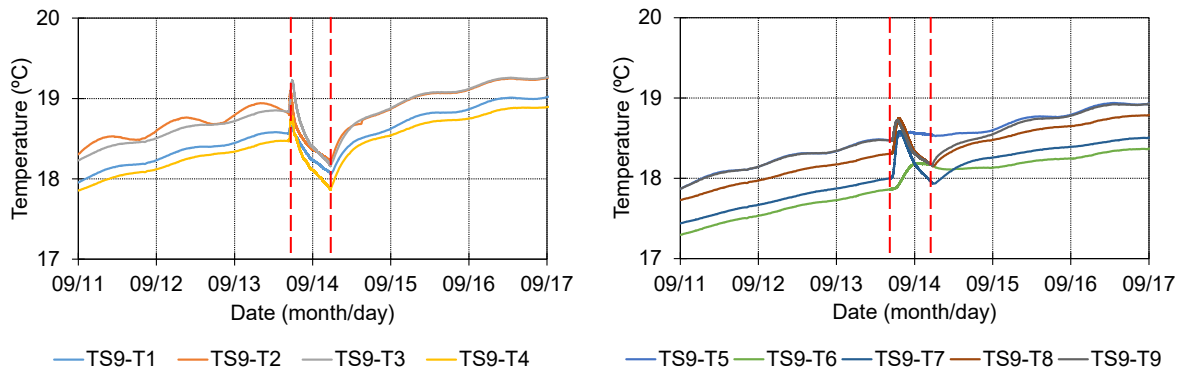


Figure 3-39: Thermistor layout for each thermistor string

The thermistor data for the leak test at LL3 is summarised in Figure 3-40 to Figure 3-43. The left graph in Figure 3-40



, indicates temperature readings from the thermistors around the pipe (thermistors T1 to T4) and the right graph indicates readings from the thermistors in the trench perimeter (corners) (thermistors T5 to T8). Figure 4-20 applied to thermistor string TS8, installed in-line with the leak location LL3. Figures 4-21 and 4-22 present similar data for thermistor strings TS7 and TS9, respectively located 0.15 m downstream and upstream of the leak location. Figure 4-23 present temperatures recorded at thermistor string TS1, located away from the leak location and is included for reference purposes. The left dotted red line on each graph indicates the leak initiation and red line indicates the leak closure. The leak location is at the crown of the pipe.

It is evident that the magnitude of the temperature is greatest at the leak location and smaller upstream and downstream of the LL3 at TS7 (Figure 3-41) and TS9 (Figure 3-42). The reference cross-section TS1 in Figure 3-43 indicates that the thermistors around the pipe note a change in a temperature but the thermistors in the trench corners do not.

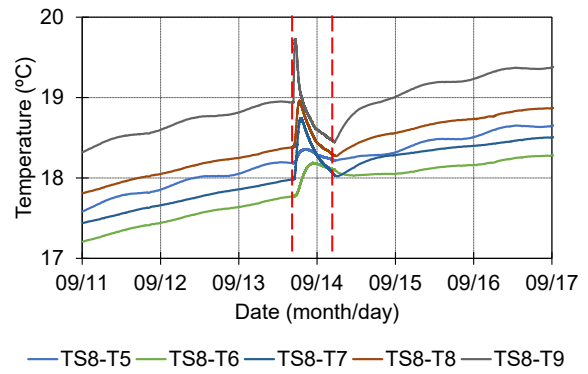
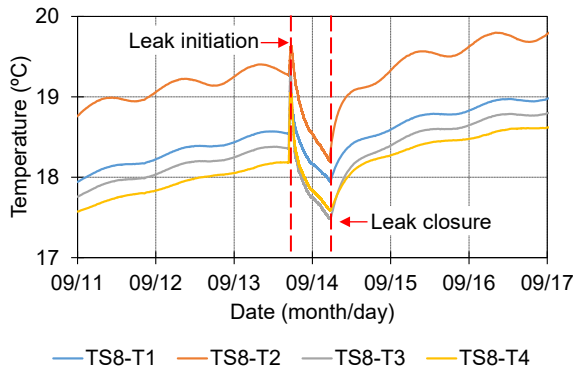


Figure 3-40: Temperature changes at leak location LL3 (TS8)

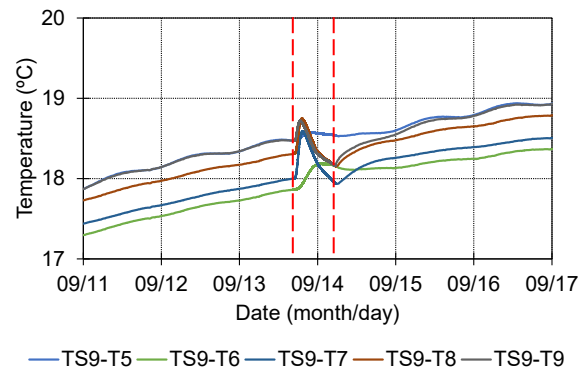
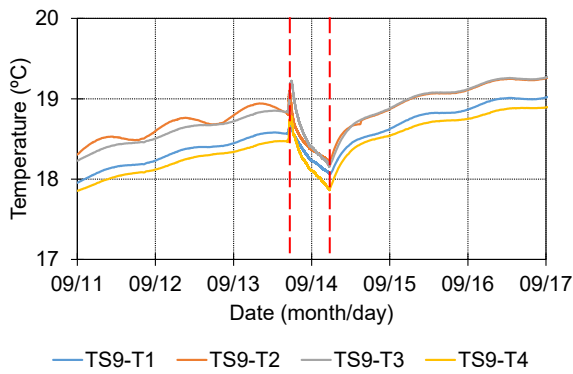


Figure 3-41: Temperature changes 0.15 m upstream of leak location LL3 (TS7)

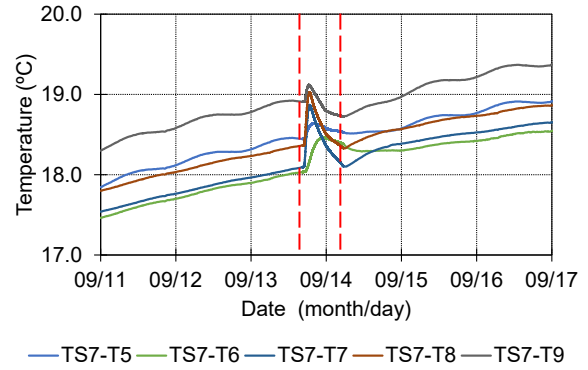
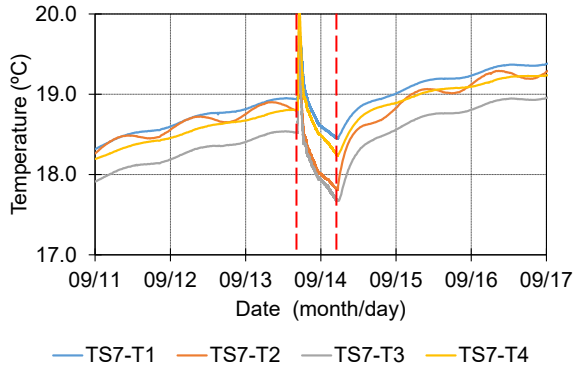


Figure 3-42: Temperature changes 0.15 m downstream of leak location LL3 (TS9)

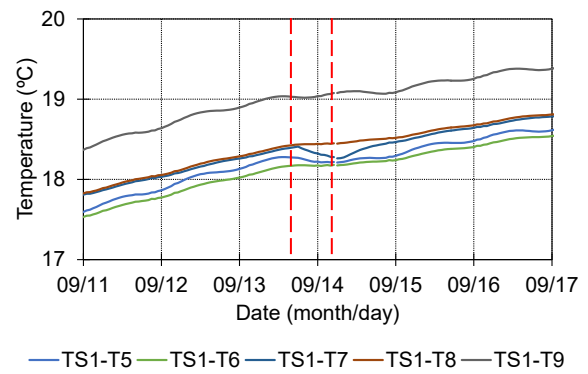
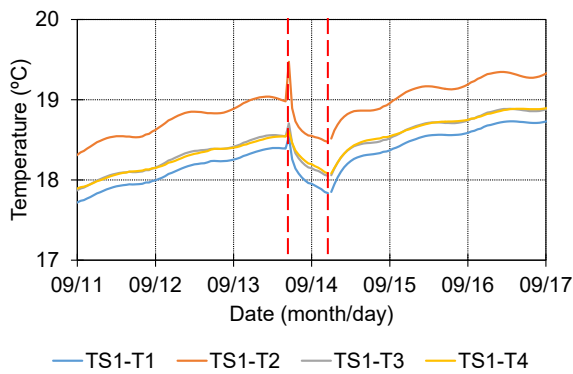


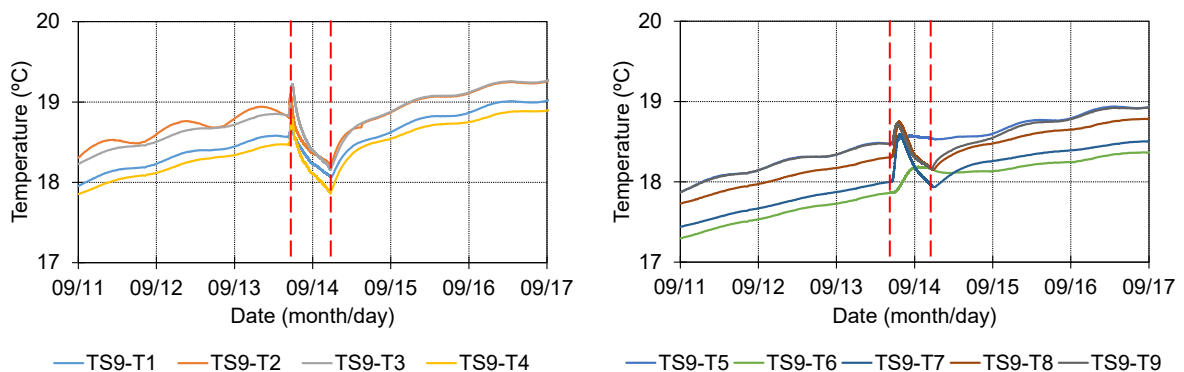
Figure 3-43: Temperature changes at reference string LL3 (TS1) away from the leak location

Temperature distribution around leak location

The data was used to create a two dimensional temperature profile contour plot to visualise leak-induced temperature changes around the leak location. Figure 3-44 indicates a two dimensional (2D) contour plot for thermistor string TS7 (0.15 m upstream), TS8 (at the leak location) and TS9 (0.15 m downstream). It is evident from the visualisation that the temperature behaviour immediately upstream and downstream of the leak were similar and differed somewhat from the situation at the leak location. Before the leak occurred a clear horizontal temperature stratification can be seen (left column, Figure 4-25) compared to a cooling bulb forming around the leak location during the leakage test (right column). In addition to the absolute temperature plot, differential a temperature plot was created indicating the change in temperature before and during the leak event in Figure 3-45.

Discussion

The success of the proposed leakage detection system depends on the ability to detect leakage-induced temperature changes around a pipeline and to distinguish such temperature changes from those resulting from changes in the water temperature circulating through the pipe. The abovementioned test provided an opportunity to compared temperature changes observed due to warmer water circulating through the pipe to compare to temperature changes when warmer water is allowed to leak from the pipe for a short period (13 hours). Comparing the temperature responses measured in direct contact with the pipe (left hand side in



to Figure 3-42), responses at and away from the leak location appear similar. The temperature changes at the leak was however somewhat larger than away from the leak. However, when comparing temperature changes along the perimeter of the pipe trench it appears that insignificant changes occurred where a leak was not present, while at the leak location, significant temperature changes were observed. This suggests that observing temperatures some distance removed from the pipe perimeter may allow leaks to be identified. It is also pointed out that leaks of any significance will not be of short term nature so that they are likely

to cause long term changes in the ground temperature. Comparing temperature records over time with baseline values should therefore allow leaks to be identified with relative ease.

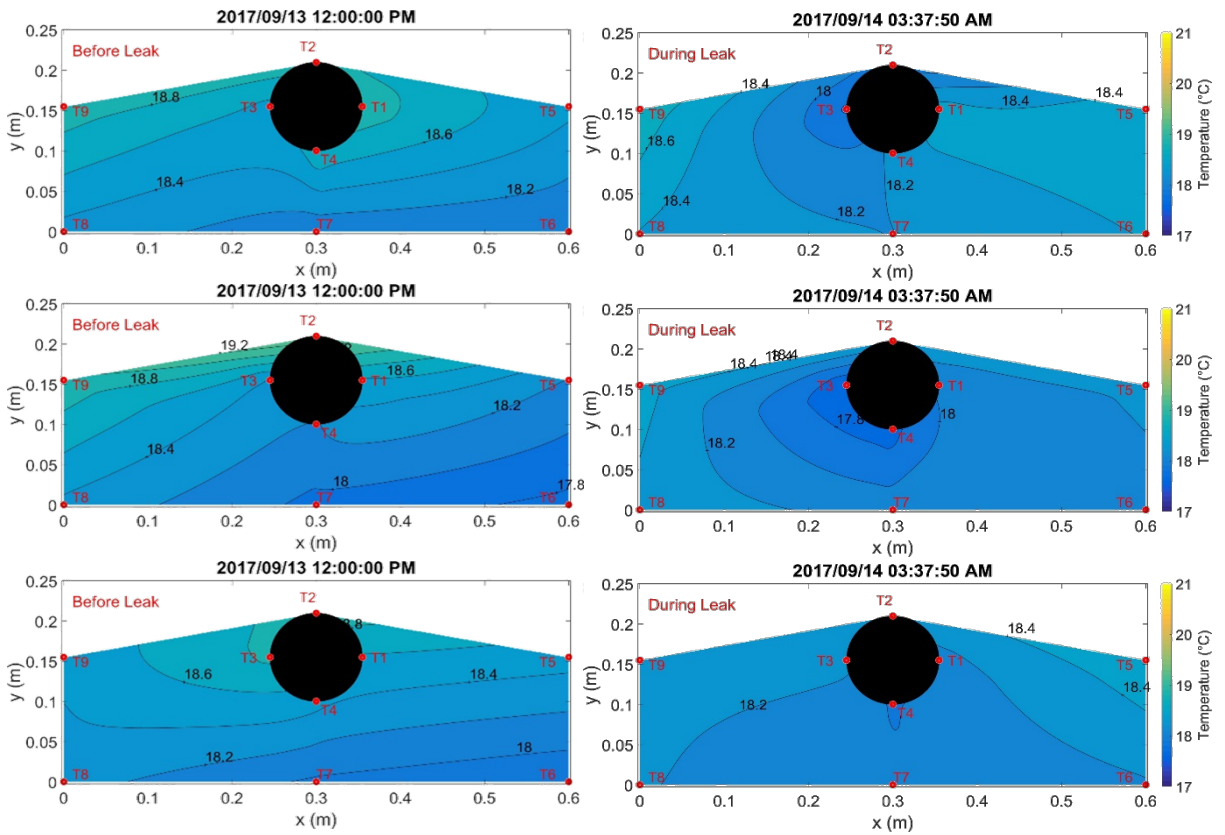


Figure 3-44: Temperature profile around LL3 before (left) and during (right) the leak

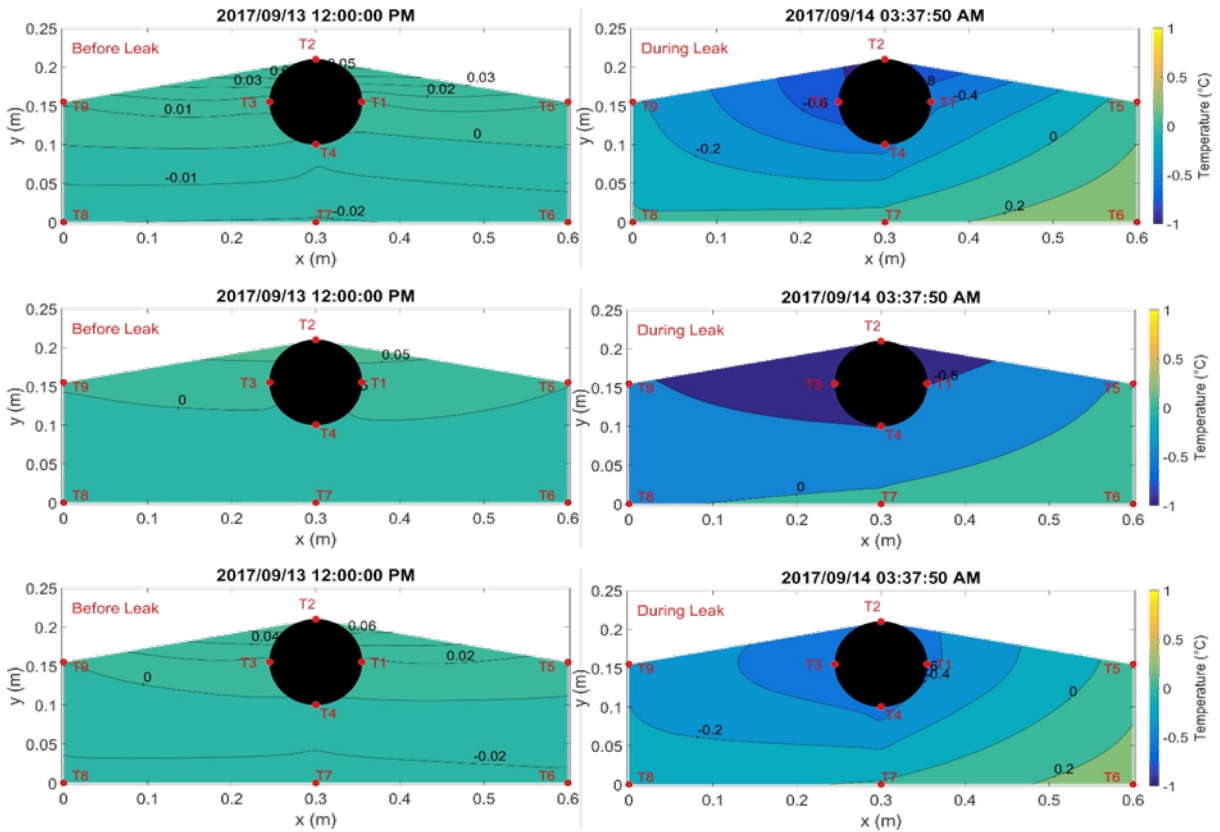


Figure 3-45: Temperature change profile around LL3 before (left) and during (right) the leak

3.8.1.2 Leakage test 2

The second leak test was conducted from 17 September at 08h09 to 16h13. The flow rate entering the pipeline was 4.35 l/min and the leakage rate was 0.83 l/min with an average pressure of 24 kPa during the leak test. A schematic of the second test is shown in Figure 3-46. Thermistor string TS5 is located at the leak locations (LL2), TS4 is 0.15 m upstream of LL2 with TS6 0.15 m downstream. TS1 was again used as a control to indicate the change of temperature around the pipe where no leak occurred.

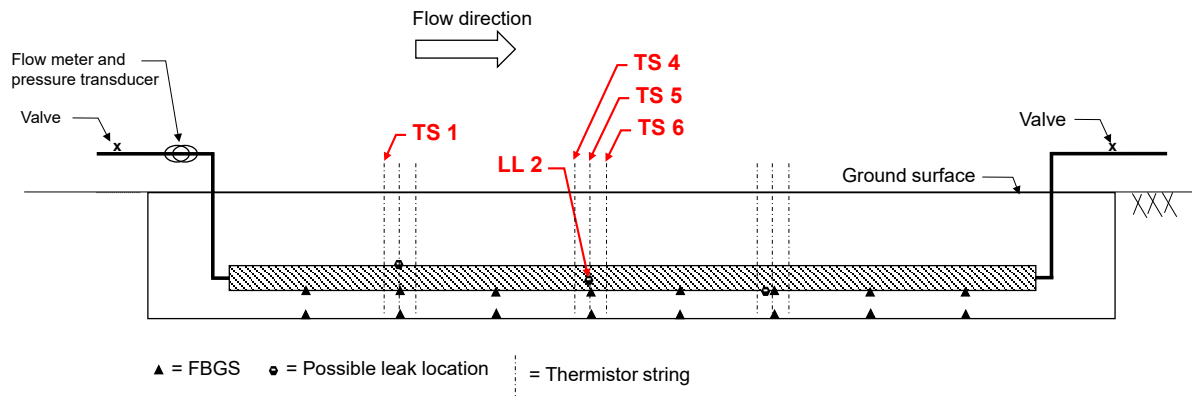


Figure 3-46: Elevation of experimental setup showing location of Leakage test 2

The same methodology used for the presentation of data from Leakage test 1 at LL3 is also used for the second leak test at LL2. The data from the leak location itself (thermistor string TS5) is shown first (Figure 3-48). Thereafter data from 0.15 m upstream at TS4 is shown in Figure 3-49 and finally data from 0.15 m downstream at TS6 is shown in Figure 3-50. Data from the reference string TS1 is shown in Figure 3-51. The water temperature during the leak test is presented in Figure 3-47.

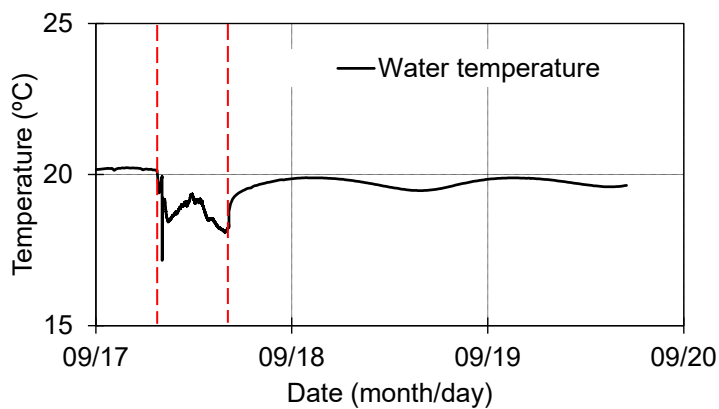


Figure 3-47: Water temperature during the second leak test at LL2

The temperature around the pipe changed immediately at TS 5 upon commencement of the leak while a lag time can be observed at TS4 and TS6. The magnitude of temperature change was small due to the relatively small differential temperature of less than one degree Celsius between the water in the pipe and the soil temperature. The same temperature trend present in the water temperature graph can be observed at all the thermistors, where an initial negative temperature spike was caused by stagnant water upstream of the test section. The water temperature trend observed was directly transferred to the surrounding thermistor strings. The

reference string TS1 did not register a major change in temperature because the thermistors were not in direct contact with the water and the uPVC pipe acts as a weak thermal insulator.

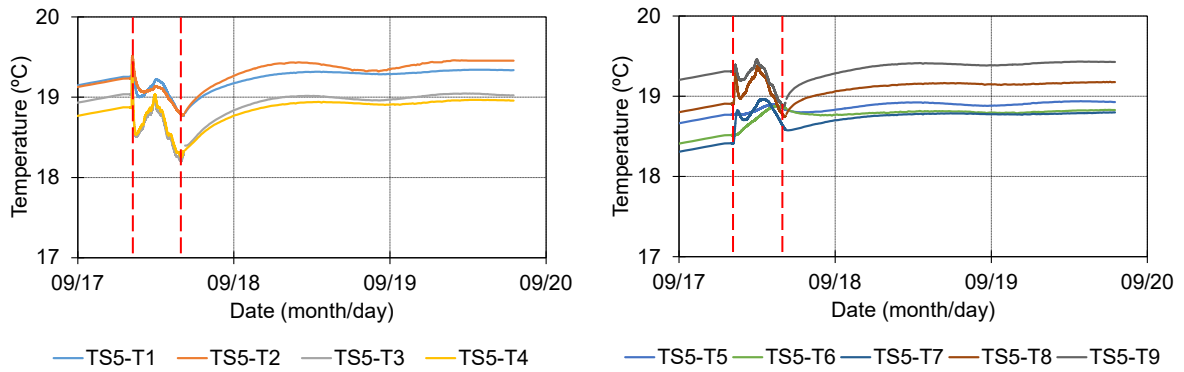


Figure 3-48: Temperature change at leak location LL2 (TS5)

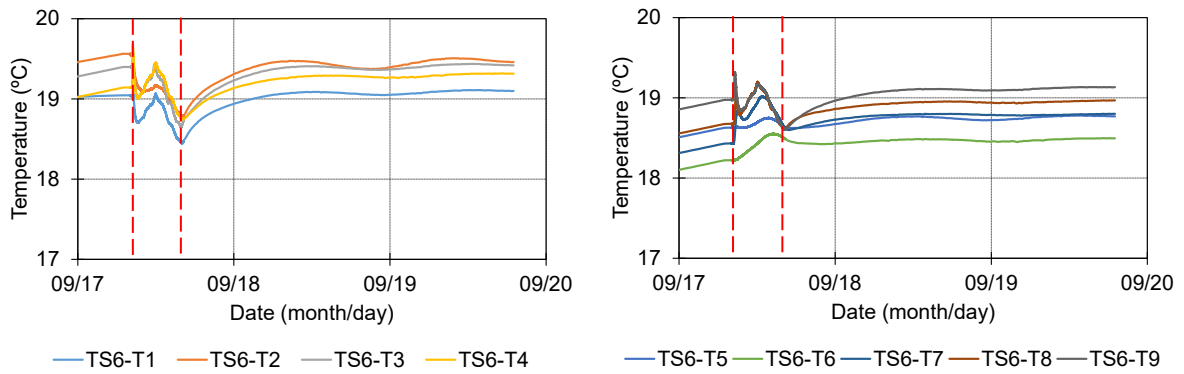


Figure 3-49: Temperature change 0.15 m upstream of leak location LL2 (TS4)

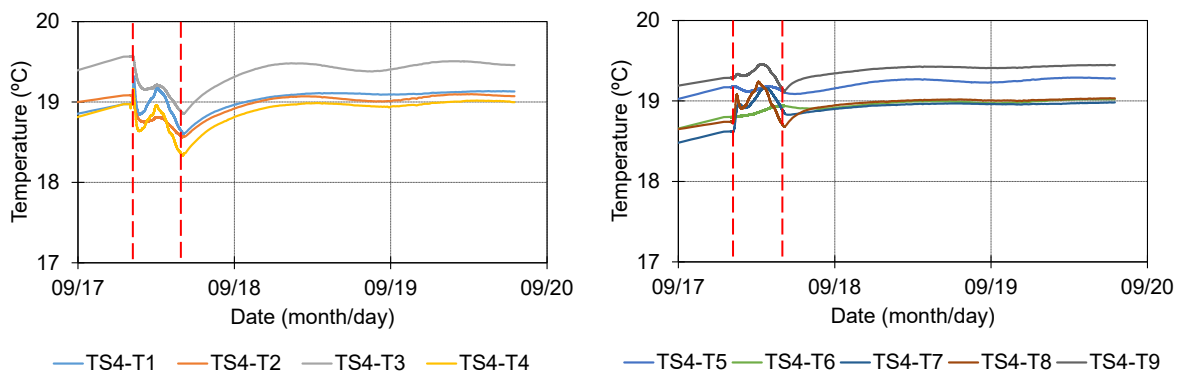


Figure 3-50: Temperature change 0.15 m downstream of leak location LL2 (TS6)

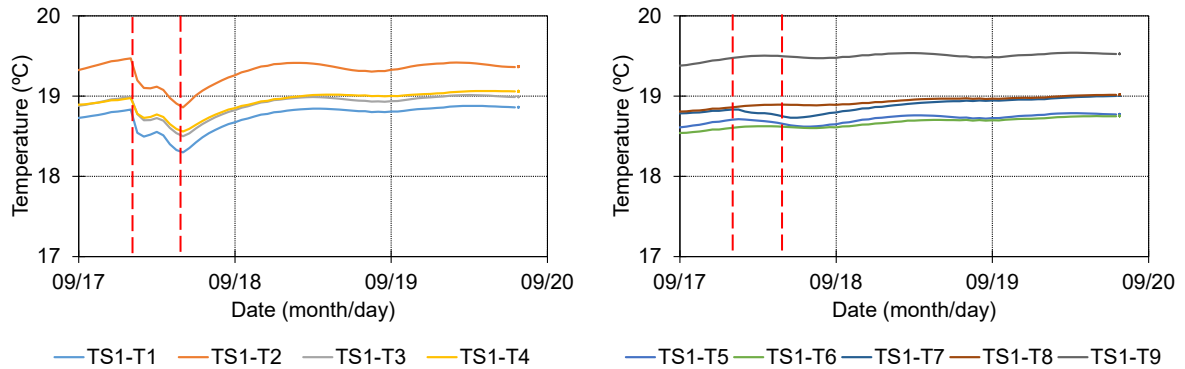


Figure 3-51: Temperature change at reference string LL2 (TS1)

Temperature distribution around leak location

Figure 3-52 presents a 2D contour plot of temperature observed before the leak was induced in the left column and during the leak in the right column. The differential temperature before and during the leak is shown in Figure 3-53. Before the leak was initiated a clear temperature stratification or bands could be seen in the left column and a small discontinuity at the pipe due to changes in thermal properties. It is evident that a leak caused a cooling or heating bulb, depending on the temperature differential, to form around the leak location, which spread over time as can be seen in the right column. The images are shown from top to bottom in the direction of flow, i.e. TS4 is in the first row, TS5 is in the middle (at the leak) and TS6 is downstream of the leak in the last row.

Discussion

During Leakage tests 2 the influx of warm water into the pipe did not occur so that the temperature differential between the water in the pipe and the surrounding soil was smaller. Despite the smaller temperature differential clear temperature changes were observed caused by the leak. As in the case of Leakage test 1 it appears that leakage will be most reliably detected by measuring temperatures some distance from the pipe, i.e. in the corners or invert of the pipe trench. While all thermistor in the string registered leak-induced temperature changes, thermistors located along the invert of the pipe registered somewhat larger temperature changes than those located adjacent to the pipe. This suggests the pipe invert to be the more optimal position for the temperature sensors.

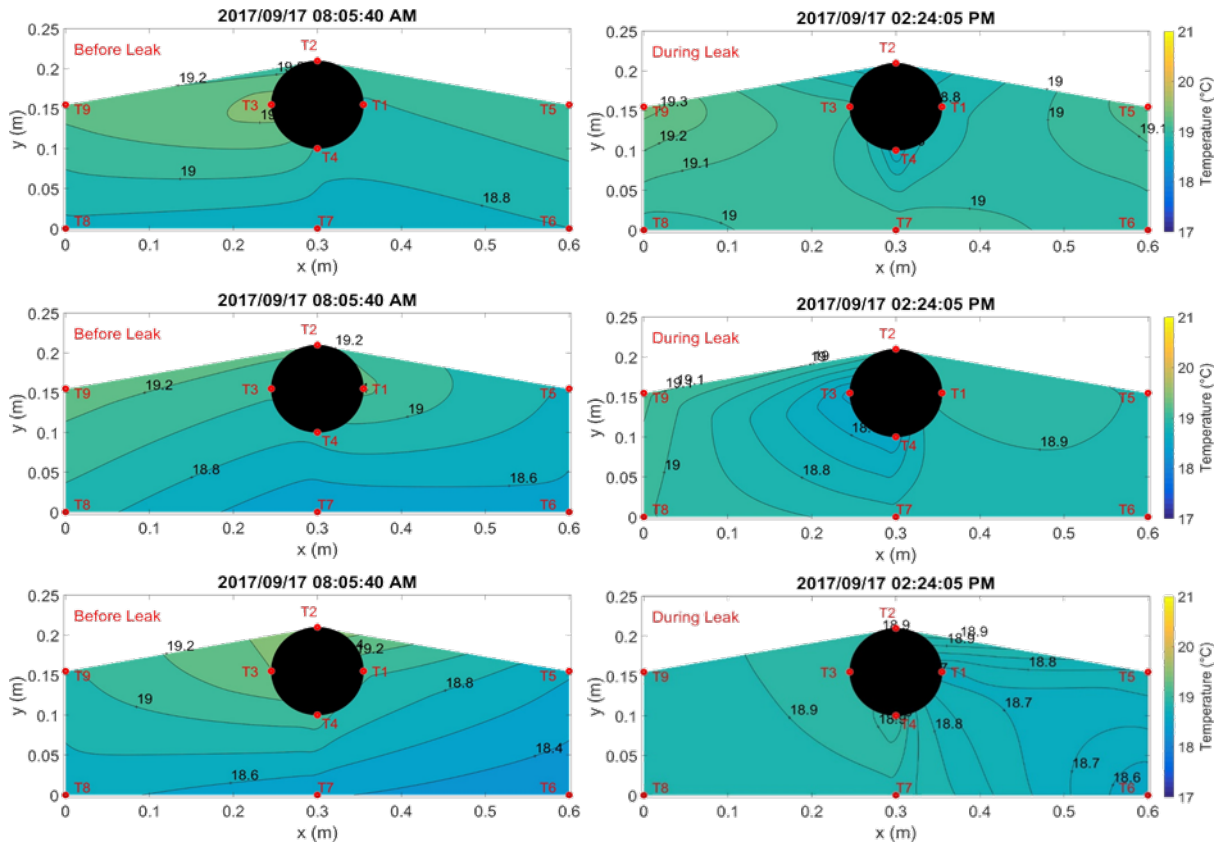


Figure 3-52: Temperature profile around LL2 before (left) and during (right) the leak

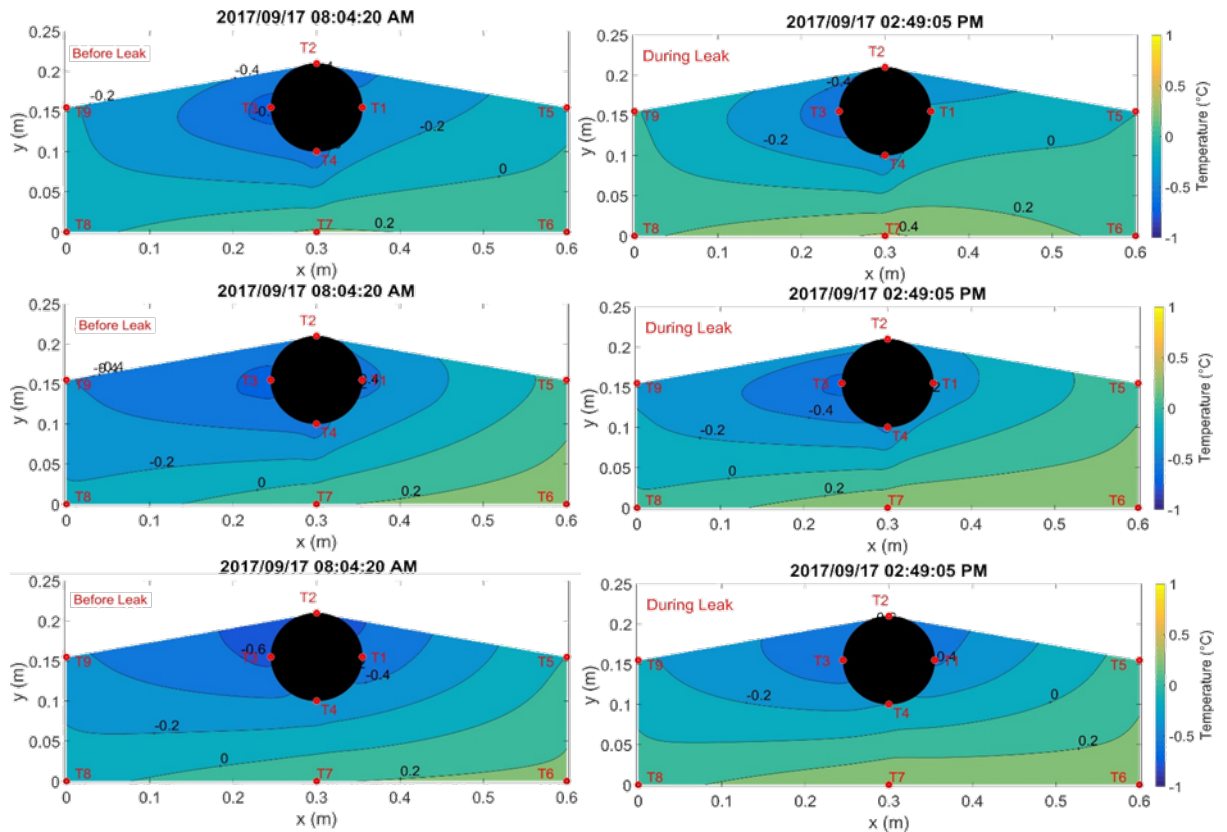


Figure 3-53: Temperature change profile around LL2 before (left) and during (right) the leak

3.8.1.3 Leakage test 3

The third leak test was conducted at leak location (LL1) as shown in Figure 3-54 below. The leak was initiated on 19 September at 19h39 and was closed the following day at 12h46. The average flow rate entering the pipe was 6.7 l/min and the leakage rate was 0.5/4 l min the average pressure during the test was 34 kPa. The reference thermistor string (TS) used for this test was TS4 (2 m downstream of leak location LL1). Thermistor string TS2 was at the leak location, TS1 0.15 m upstream of the leak and TS3 0.15 m downstream. The thermistor layout for each string was the same for this test setup as for the previous tests.

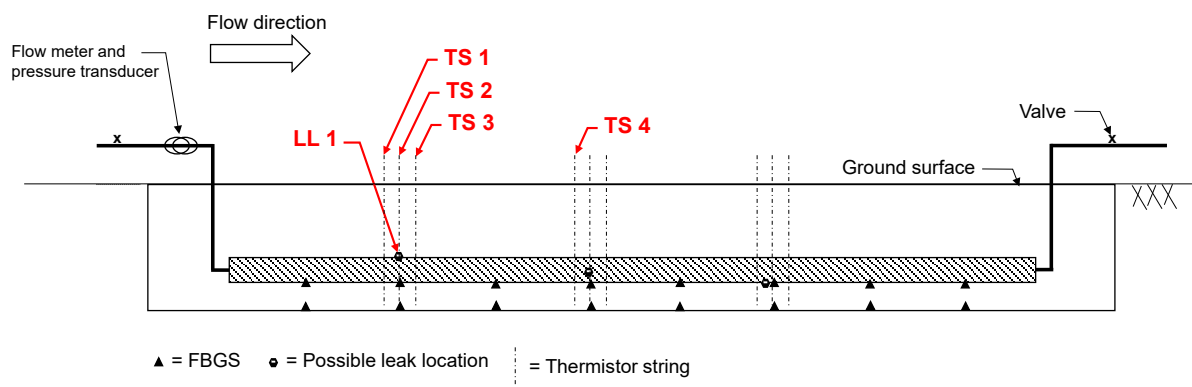


Figure 3-54: Experimental elevation schematic of test 3 at LL1

Stagnant water upstream of the installation had cooled down significantly prior to the test and explains the initial cooling spike in Figure 3-55. The initial spike was followed by a gradual increase in water temperature as 'new' water was flushed through the pipeline.

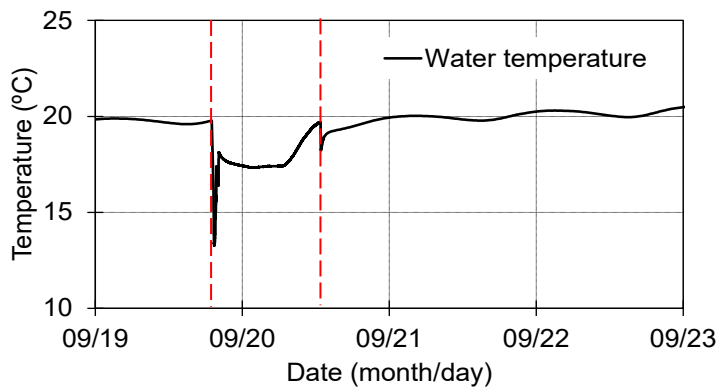


Figure 3-55: Water temperature during the second leak test at LL1

The temperature data is summarised in Figure 3-56 to Figure 3-59. Figure 3-56 indicates temperature changes at the leak location LL1 based on TS2. It is evident that similar

temperatures were measured around the pipe (thermistors T1 to T4 of thermistor string TS2, left figure) and that it reacted rapidly to the change in water temperature caused by the leak. The temperature in the trench corner, however, did not change significantly at all the 'perimeter' thermistors. Only TS2-T9 reacted significantly to the change in water temperature at the leak location (see Figure 3-56). The same trend can be observed at TS1 (Figure 3-57) and TS3 (Figure 3-58). The reference string TS4 (Figure 3-59) behaved similar to the thermistor strings at the leak location. The difference in behaviour in this test is related to the flow of water around the pipe. The leak location is at the top of the pipe. The pipe trench slopes from LL1 towards LL3 which explains why temperature changes were registered at some of the thermistors at LL2.

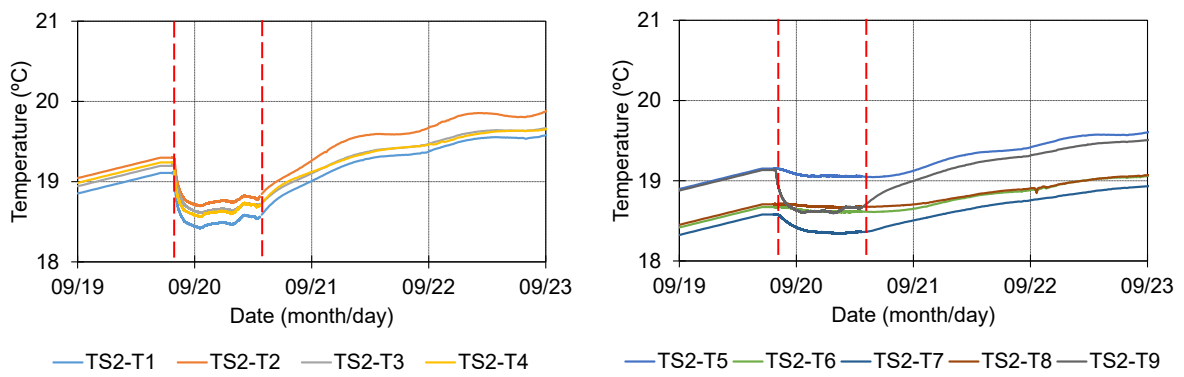


Figure 3-56: Temperature change at leak location LL1 (TS2)

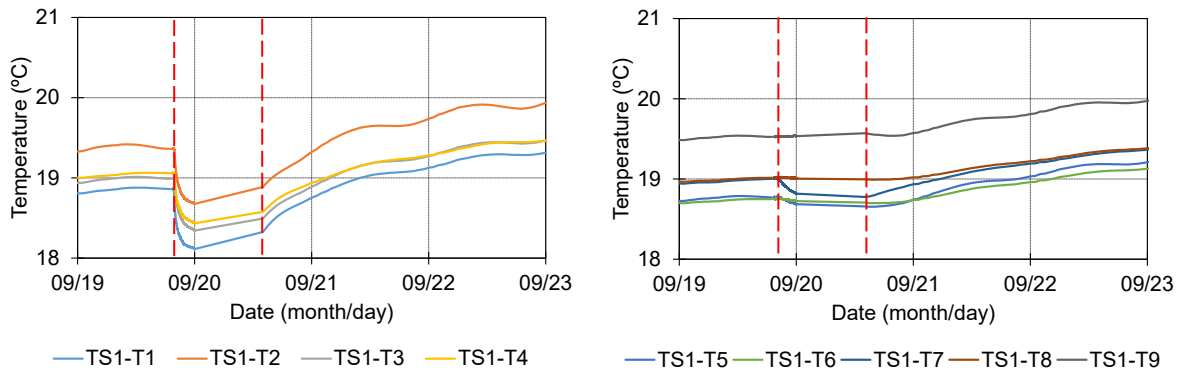


Figure 3-57: Temperature change 0.15 m upstream of leak location LL2 (TS1)

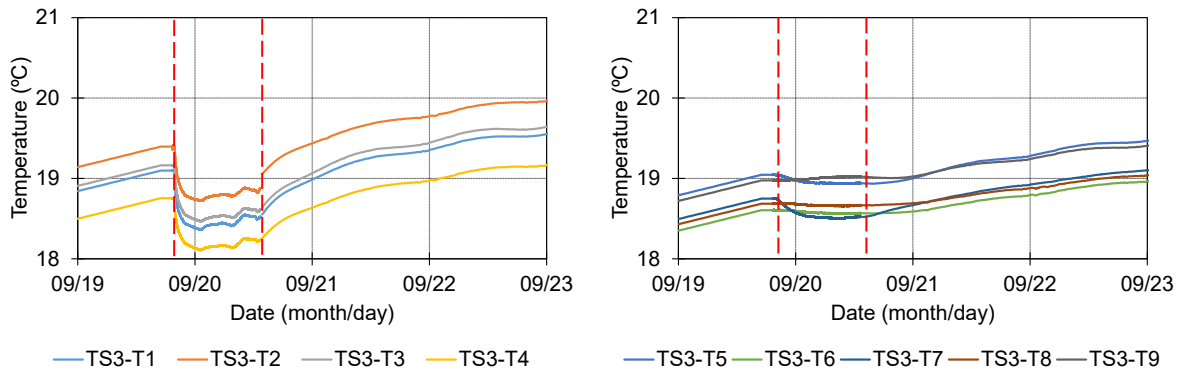


Figure 3-58: Temperature change 0.15 m downstream of leak location LL1 (TS3)

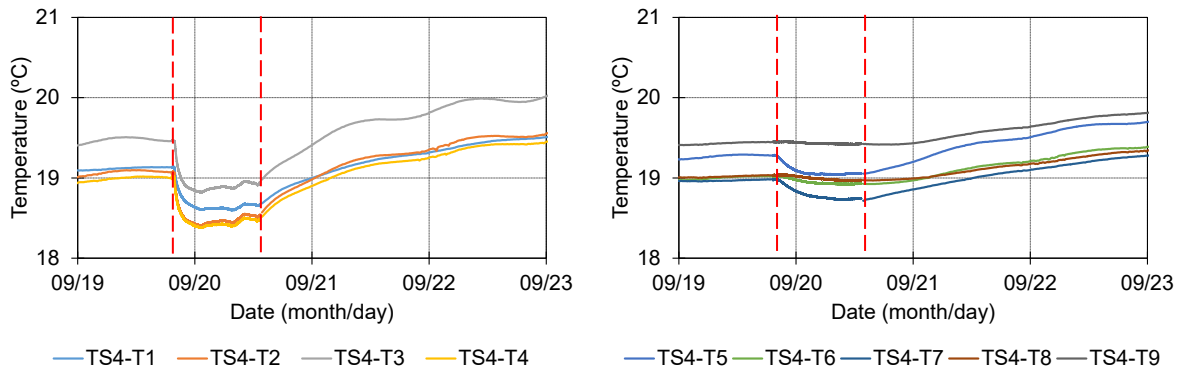


Figure 3-59: Temperature change at reference string LL1 (TS4)

Temperature distribution around leak location

Figure 3-60 presents a 2D contour plot of the temperature data obtained at and around LL1 with TS1 (0.15 m upstream), TS2 (at the leak location) and TS3 (0.15 m downstream). Again a clear temperature stratification can be observed in Figure 3-60 before the leak was initiated (left column) with a temperature discontinuity at the pipe. During the leak test a clear cooling bulb (right column) formed around the LL1 which reached thermistor T8 and T6 which were most distant from the pipe in the trench corner. A temperature differential plot is shown in Figure 3-61, showing the change in temperature before and during the leak event.

Discussion

Results similar to the previous tests were obtained, i.e. indicating that leaks can be detected by measuring temperature changes around the pipe. The effect of sloping pipe trenches may result in water flowing in the direction of the slope so that temperature changes can occur a short distance from the leak location.

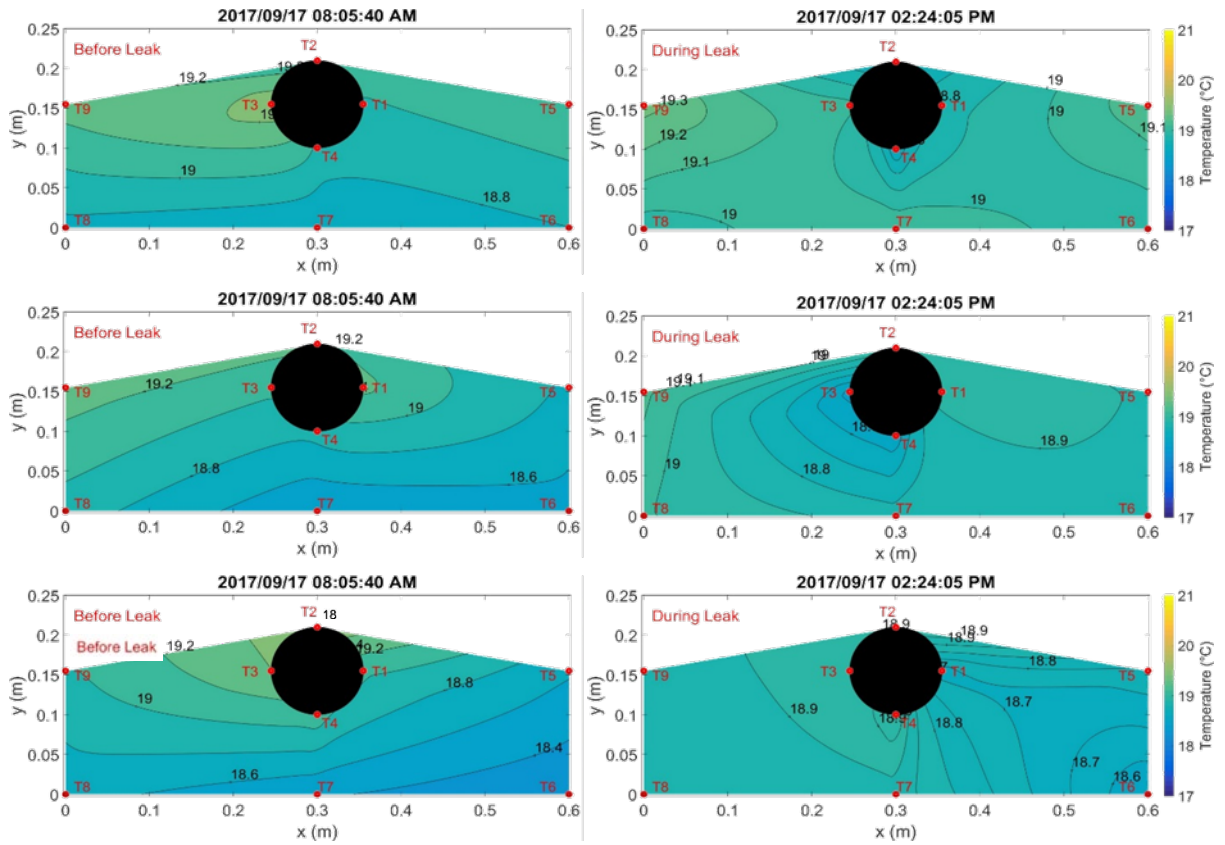


Figure 3-60: Temperature profile around LL1 before (left) and during (right) the leak

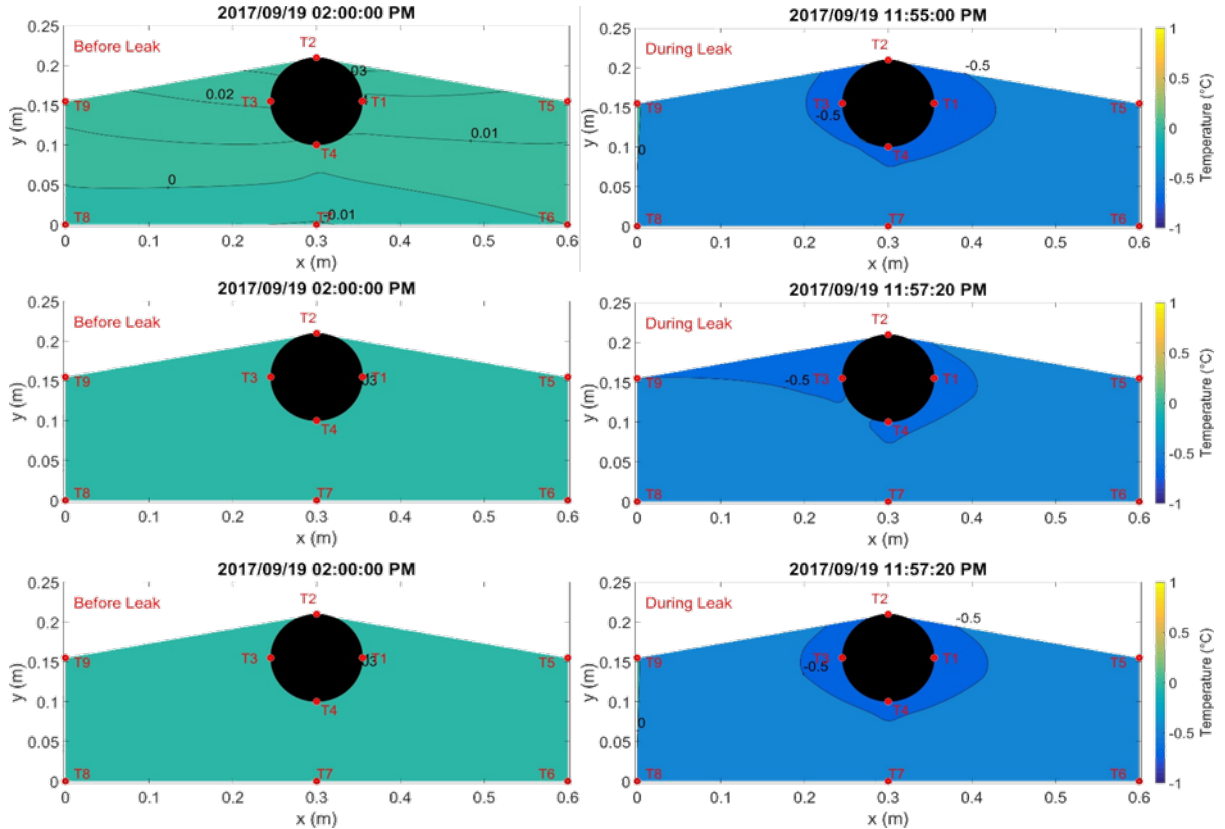


Figure 3-61: Temperature change profile around LL1 before (left) and during (right) the leak

The following section discusses fibre optic Bragg data obtained during the 3 leak tests discussed above.

3.8.2 Fibre Optic Bragg data

The pipeline leakage test installation included a total of 16 discrete fibre optic Bragg sensors, of which 8 were epoxied rigidly to the pipe invert and the remaining 8 were housed loosely in a 4 mm polyurethane tube in the left bottom trench corner. It was initially hypothesized that a wetting front will cause a significant softening of the soil surrounding the leak location, inducing a change in support conditions around the pipe. The intention with the fibre optic sensors in the trench corner isolated from mechanical strains within the 4 mm tube was to only measure thermal strain changes, while effects of softening of the ground around the pipe would be measured by the FBGS attached to pipe. The latter would be sensitive to both mechanical and thermal strains.

An elevation layout schematic of the FBGS layout is shown in Figure 3-62 and a cross section through the leak location is shown in Figure 3-63. The FBGS leak test data were obtained from the same tests producing the thermistor data. The individual test details are therefore not repeated here. The observed FBGS strain changes and temperature compensated strain graphs are presented in this section.

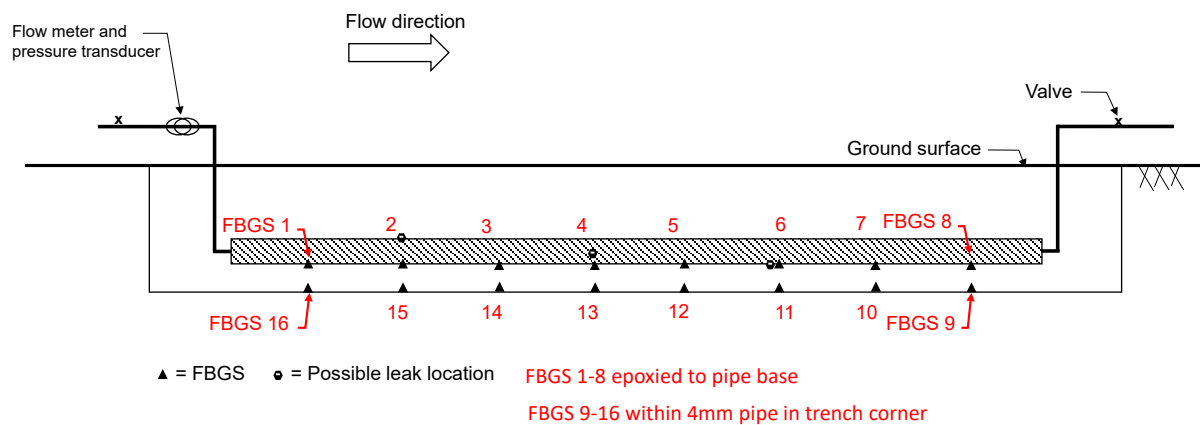


Figure 3-62: Elevation of experimental setup

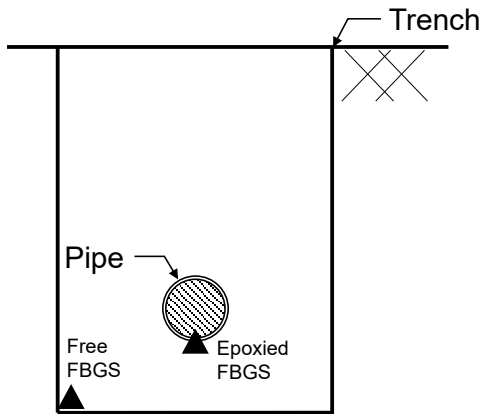


Figure 3-63: Cross section through the leak location showing the FBGS layout relative to the pipe

3.8.2.1 Leakage test 1

An elevation layout schematic of the first leak test is shown in Figure 3-64.

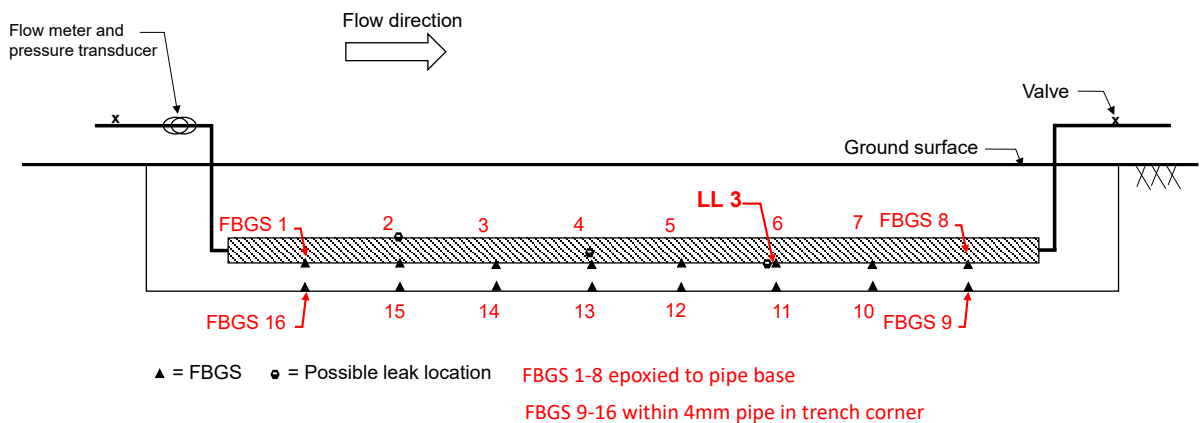


Figure 3-64: Elevation of experimental setup for LL3

Figure 3-65 and Figure 3-66 present the strain changes observed at the base of the pipe (FBGS 1 to 8) and in the trench corner (FBGS 9 to 16) respectively. The base strain readings were taken one day before the test started. The vertical axis therefore represents the change in strain observed during the leak test and not the absolute strain. The first vertical red dotted line indicates the leak initiation and the second dotted line indicates leak closure. Larger strains were observed closer to the leak location compared to further away as shown by the results from FBGS 6 (at leak location LL3), 7 and 8 (downstream of the leak location) in for. It should be noted that the scale of the vertical axes in Figure 3-65 (epoxyed FBGS) to Figure 3-66 (free FBGS) differ. Free FBGS 11, at the leak location, registered the greatest strain of

all the free FBGSs. Strains from the epoxied FBGS are about one order of magnitude larger than those from the free FBGS.

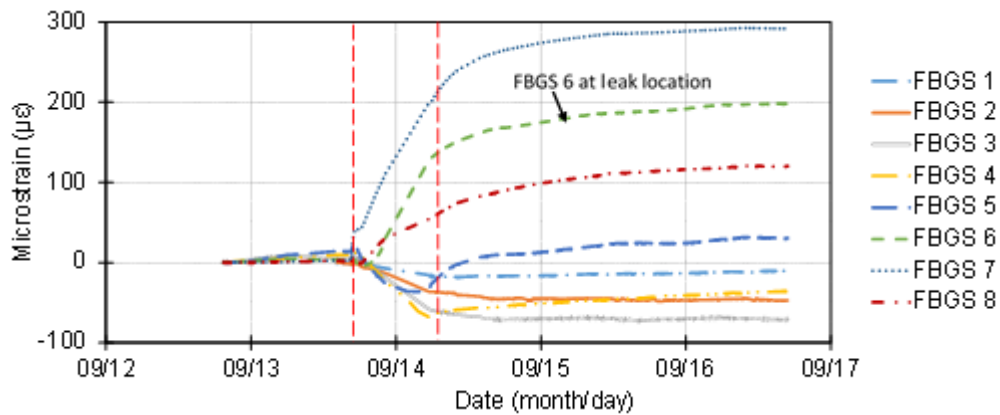


Figure 3-65: Strain changes over time for Leak test 1 from epoxied FBGS

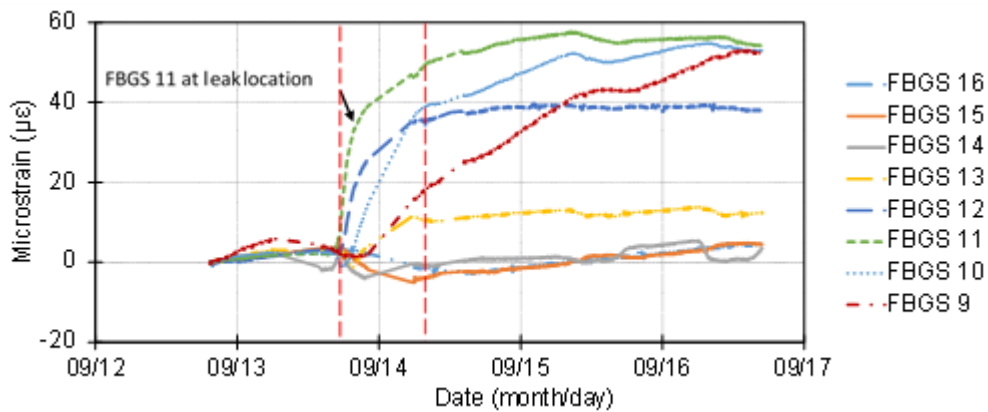


Figure 3-66: Strain changes over time for Leak test 1 from free FBGS

It was of interest to determine the proportions of strains measured on the pipe resulting from thermal and mechanical effect respectively. The total strains observed were therefore adjusted by applying temperature correction. Temperature compensation was only available at the leak locations where thermistor data was available, i.e. at FBGS 6 and 11 in Leak test 1. Figure 3-67 and Figure 3-68 show the compensated and original curves for FBGS 6 and 11. The temperature compensated strain graph is indicated in dark green and the non-temperature compensated graph is indicated in a square dotted light green line. The same vertical scale as used for the previous uncompensated FBGS graphs (Figure 3-65 and Figure 3-66) is used for the graphs below. It is evident that temperature compensation is not critical for this investigation as it did not significantly impact the research results for FBGS 6 and 11 due to the small temperature changes induced by the leak.

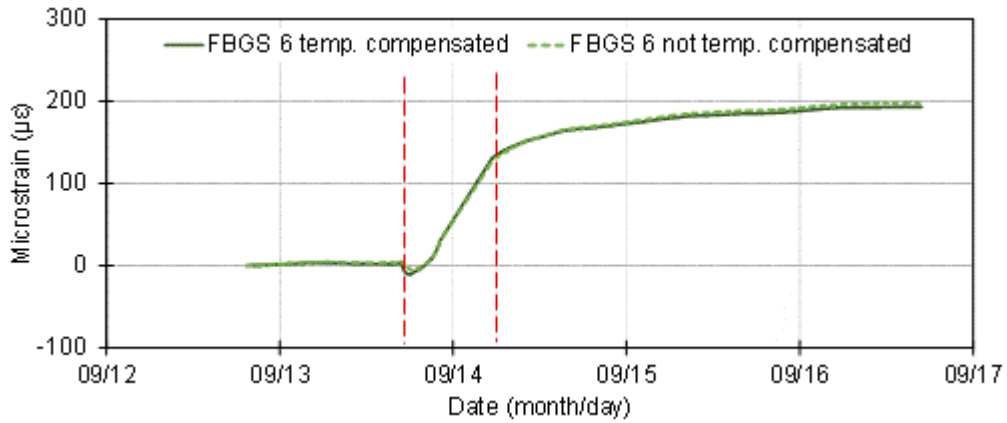


Figure 3-67: Comparison of temperature compensated vs non-compensated strains for epoxied FBGS 6

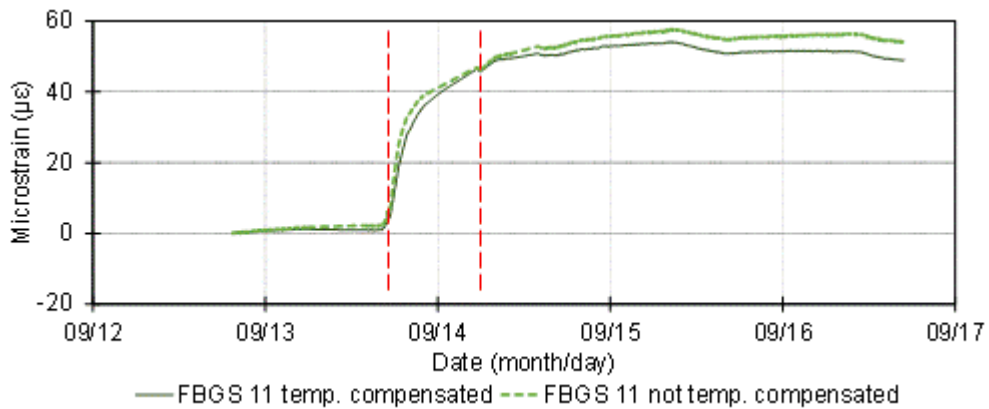


Figure 3-68: Comparison of temperature compensated vs non-compensated strains for free FBGS 11

Discussion

Comparing the strain readings from the free and fixed FBGSs reveal an order of magnitude difference in the strains measured in the case of the epoxied sensors relative to the sensors recording thermal strain only. It appears that wetting of the ground results in softening, causing a change in the support conditions around the pipe manifesting as strain changes which are an order of magnitude larger than those induced by thermal effects only. It therefore appears highly beneficial to attach the fibre optic cable to the pipe as increases the sensitivity of the leakage detection system considerably. However, it is necessary to investigate strain changes resulting from normal pressure fluctuations which occur in a pipe system during normal operation to make sure that these changes can be distinguished from those resulting from a leak.

3.8.2.2 Leak test 2

The second leak test was conducted at LL2, with epoxied FBGS 4 and free FBGS 13 being the closest to the induced leak location. Figure 3-69 below indicates the experimental layout for the second induced leak test.

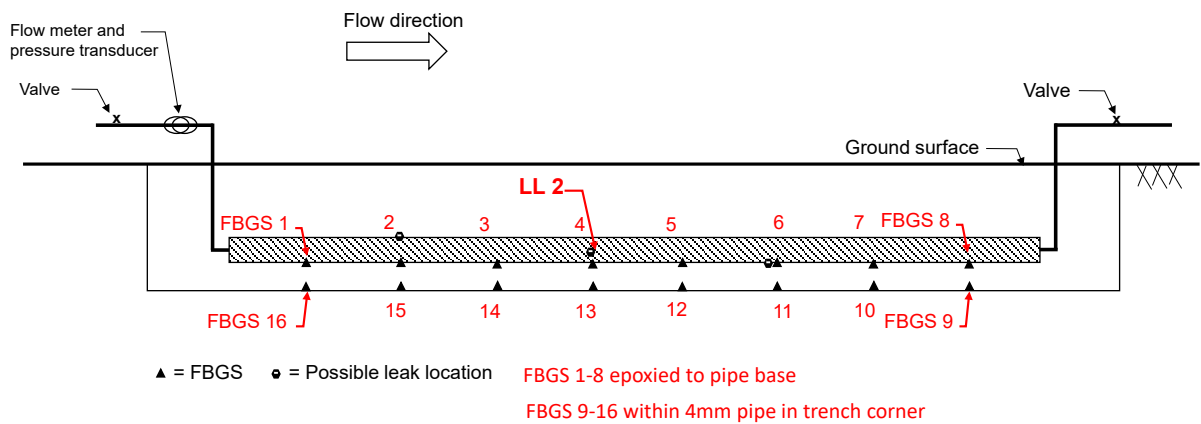


Figure 3-69: Elevation of experimental setup for Leak test 2 LL2

Figure 3-70 and Figure 3-71 indicate changes in strain obtained during the test. Interestingly FBGS 5 located 1 m downstream of the leak location registered the largest strain change of all epoxied FBGS despite it not being the closest to the leak location. FBGS 6, located 2 m downstream also shows a significant strain change. Figure 3-71 indicates that the largest strain change for the free fibre sensors occurred at FBGS 13, which is the immediately adjacent sensor to the leak, located in the trench corner.

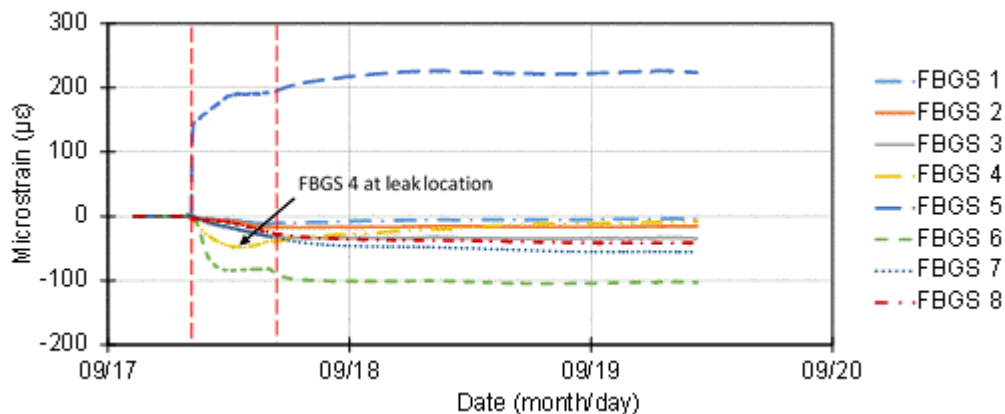


Figure 3-70: Strain changes over time for leak 2 from epoxied FBGS

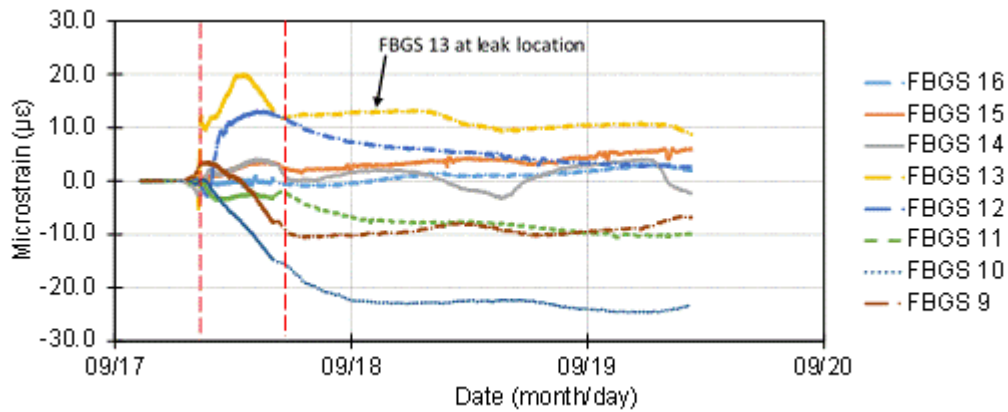


Figure 3-71: Strain changes over time for Leak test 2 from free FBGS

As for Leakage test 1 temperature compensation was done for FBGS 4 and FBGS 13 using data from thermistors TS5-T4 and TS5-T8 respectively. It is evident from Figure 3-72 and Figure 3-73 that no significant changes can be observed between compensated and uncompensated strain values. This means that the thermal strain component is insignificant compared to mechanical strain component due to the small changes in temperature.

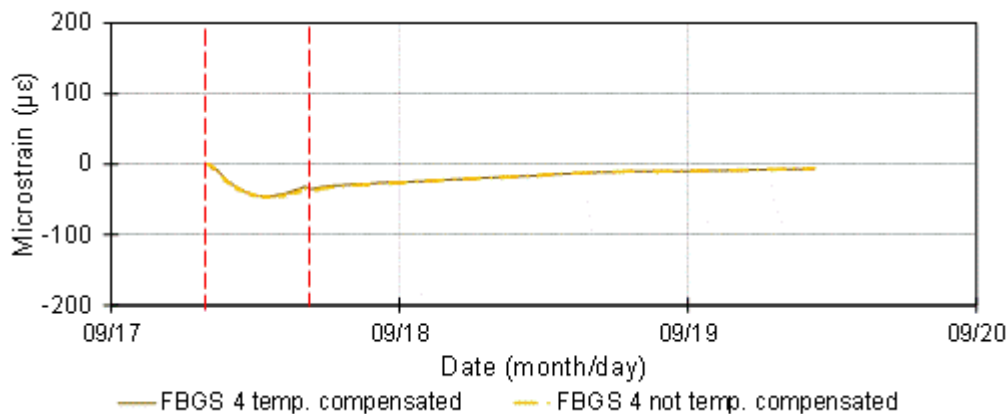


Figure 3-72: Comparison of temperature compensated vs non-compensated strains for epoxyed FBGS 4

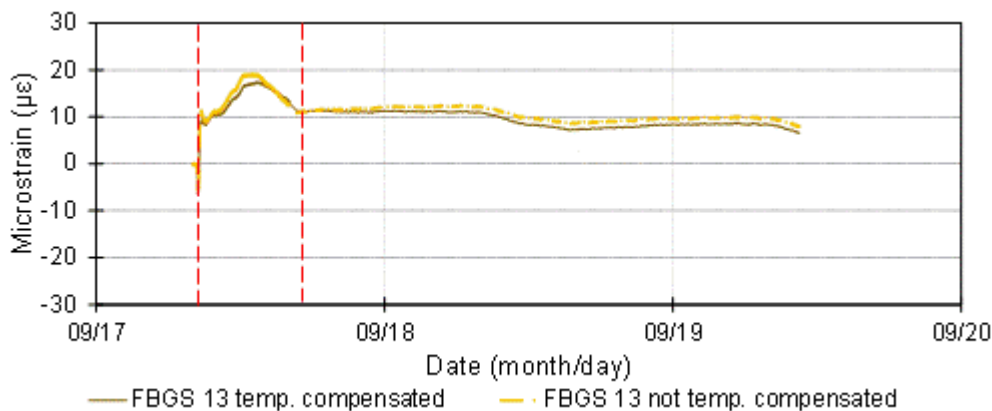


Figure 3-73: Comparison of temperature compensated vs non-compensated strains for free FBGS 13

Discussion

Again, it is shown that clearly measurable strain changes occurred in the pipe and that these could be measured to a very high resolution. Strain changes due to mechanical effects caused by softening of the pipe support were again an order of magnitude larger than temperature-induced strain changes resulting from the leak. An important observation from this test is that the maximum mechanical strain change did not occur immediately opposite the leak location. This can be explained by considering the way in which the pipe deflects in response to a softening of its support upon wetting. It is proposed that non-uniformities in the pipe bedding and an asymmetric spread of leakage water around the leak location can explain the asymmetric strain changes observed. The magnitude of strain changes themselves are not of so much interest, but rather the fact that a strain change occurred.

3.8.2.3 Leakage test 3

The final leak test, test 3, was initiated at LL1 as shown in the schematic in Figure 3-74. FBGS 2 and FBGS 15 are the closest fibre optic sensors to the leak location.

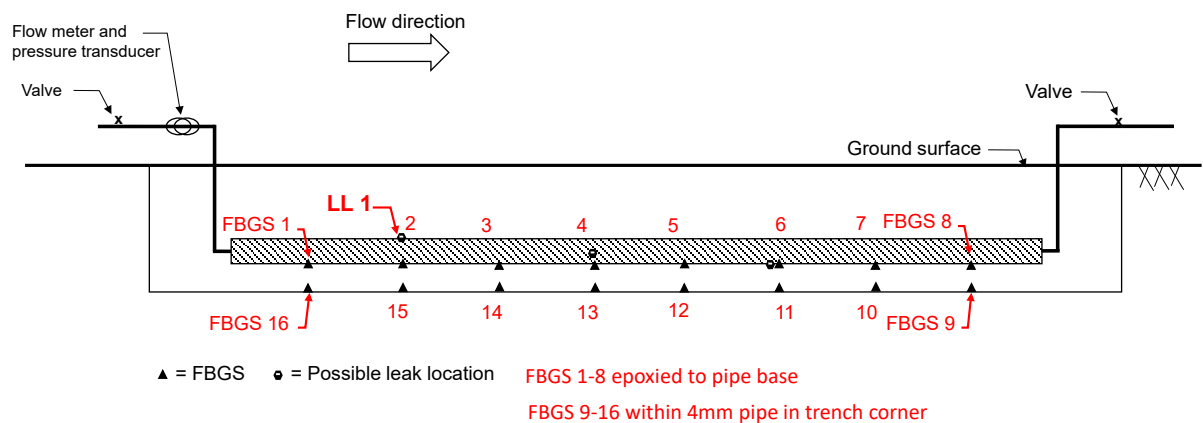


Figure 3-74: Elevation of experimental setup for Leak test 3 LL1

The strain change for the epoxied and free FBGS are shown in Figure 3-75 and Figure 3-76 respectively. It is evident that the previous leakage events had an impact on the subsequent leakage tests: The first test softened the support around the pipe, leading to strains over a greater length of pipe during the subsequent compared to the first. The epoxied FBGS further from the leakage source seem to recover rapidly after the leak was closed. However, at the leak location FBGS 2 and 3 seem to have undergone a more permanent deformation. Results from the free FBGS presented in clearly registered compressive thermal strain changes resulting from the leak. A clear daily temperature variation is also evident on the free

temperature sensitive sensors as temperatures recovered in the soil during the days after the leak.

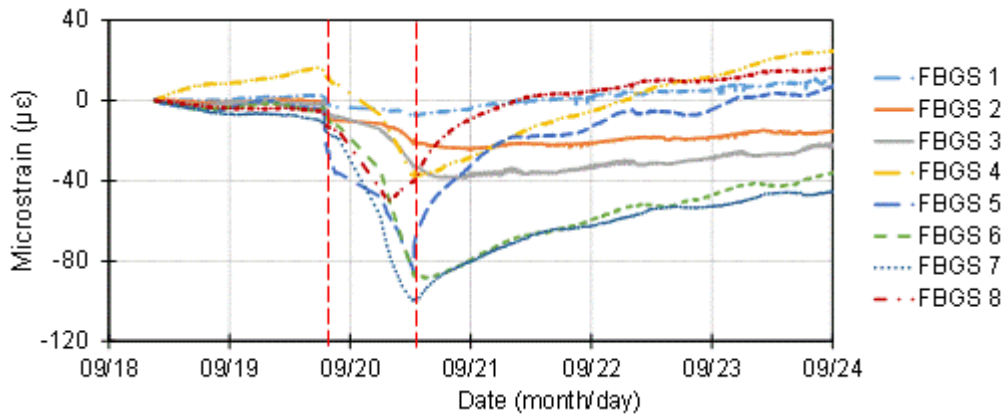


Figure 3-75: Strain changes over time for Leak test 3 from free FBGS

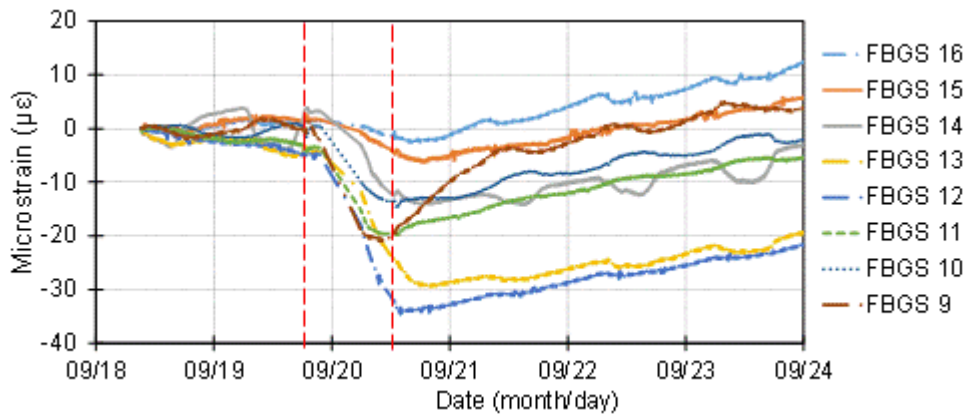


Figure 3-76: Strain changes over time for Leak test 3 from free FBGS

As with the previous leakage tests temperature compensation had a very small influence on the strain changes as shown in Figure 3-77 and Figure 3-78.

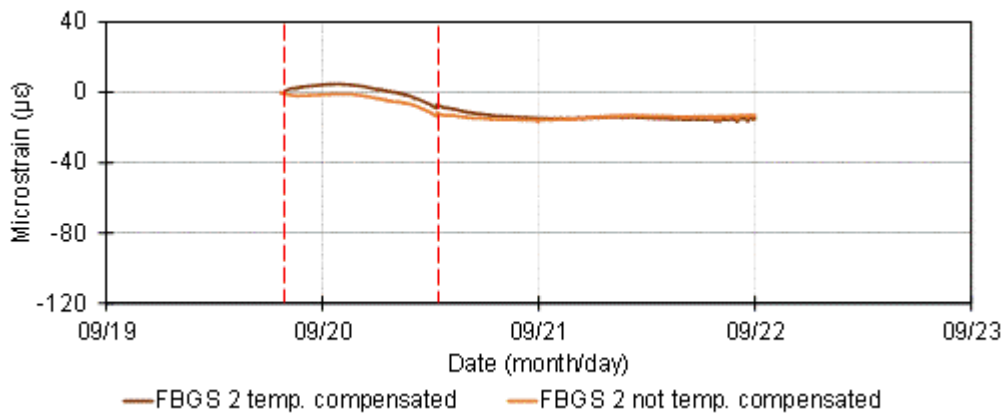


Figure 3-77: Comparison of temperature compensated vs non-compensated strains for epoxied FBGS 2

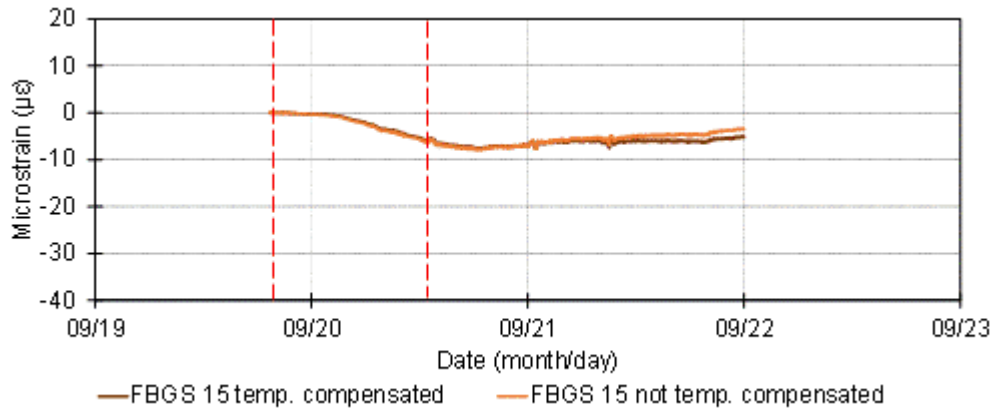


Figure 3-78: Comparison of temperature compensated vs non-compensated strains for free FBGS 15

Discussion

It is evident from the FBGS data that strain values as recorded in the experimental setup are very sensitive to changes in support properties around a pipe. Initially the FBGS isolated from external mechanical strains within the 4 mm tube in the trench corner were envisaged to measure only temperature effects, but the wetting patch did appear to have a significant impact on the support condition around the small conduit, causing some bending to occur as illustrated by the fact that strain reading did not return to their initial values prior to the leak as the temperature of the ground recovered. This illustrates the benefit of also measuring mechanical strain resulting from a leak as it increases the sensitivity of the measurement system. Results to date suggest that a leakage detection system comprising of a fibre optic sensor capable of recording both mechanical and thermal strains would provide a highly sensitive means of leak detection for pipelines or other infrastructure suitable for instrumentation by means of such a sensor.

4 PHYSICAL MODEL STUDY INTO LEAKAGE-INDUCED STRAIN CHANGES

4.1 Introduction

Results from the study obtained to date have shown that measuring pipe strain response, in addition to leak-induced temperature changes, may provide a highly sensitive means of leak detection. A complication exists in that pipe strains are significantly influenced by pressure fluctuations which occur in pipe systems due to changes in demand and operating conditions during the course of every day. This may result in difficulty in identifying leakage-induced strain changes. Results from the strain changes observed on the field installation showed larger axial strains close to a coupling where some room for axial movement exists, while strains away from the joints were subdued due to restraint from the soil. It is likely that a leak will change the support conditions around the pipe, as well as the restraint conditions, thus changing the way in which the pipe will strain due to normal pressure fluctuations. In a well-restrained pipe, axial strains are inhibited and it is likely that in-pipe pressure fluctuation will largely manifest as circumferential (hoop) strains in the pipe. It is hypothesised that a loss in restraint will occur due to a leak softening the supporting soil, permitting large axial strains to develop. These strain responses will be investigated in greater detail to obtain a better understanding of their behaviour to assess whether leakage-induced strain changes can be distinguished from those occurring under normal pipe operating conditions.

A physical model study was carried out to allow pipe strain components from in-pipe pressure fluctuations to be studied separate from those induced by pipe leaks and then to investigate these strain-inducing phenomena together to determine whether leak-induced strains can be distinguished from normally occurring changes.

The physical model developed to investigate the effect of ground strains on pipes is presented in this chapter. The model allows leaks to be imposed and resulting strains monitored on the pipe. It also allows the pipe to be internally pressurised to model strain changes due to pressure fluctuation. In addition, leakage-induced ground strains were monitored using thin strain gauged brass strip placed below the pipeline, simulating a fibre optic cable capable of measuring strain close to the pipe. The model was further designed to be capable of imposing user controllable ground strains in a controlled fashion on a model pipe by means of retracting a trapdoor. It was however not found necessary to use this capability because induced leakages resulted in substantial ground strains so that it was not necessary to study externally imposed strains.

In addition to a description of the experimental setup, this chapter presents information on the properties of the soils used in the model study, pipe instrumentation, model preparation and various sets of equipment forming part of the study.

4.2 Soil properties

The model tests were carry out using two soil types, i.e. a fine dry silica sand and a chert gravel containing slightly clayey silty fine sand taken from the transported overburden overlying the Centurion dolomite south of Pretoria. The first material comprises a purely frictional soil and was tested dry, while the second material is typical of an unsaturated soil containing some moisture, giving it some cohesive strength in addition to frictional strength. For the purposes of this report, the first material is referred to as silica sand and the second material is referred to as chert gravel.

4.2.1 Particle size distribution

Prior to model preparation and the execution of the various model tests in the geotechnical centrifuge, the particle size distribution was determined for both soil types (see Figure 4-1). Particle size distribution is an important aspect that determines the behaviour of soils. The British Soil Classification System classifies soils into groups, named Basic Soil Types, depending on their particle sizes. Soils can be classified per Table 3.1.

Table 4-1: Particle size ranges

Clay	Silt			Sand			Gravel			Cobbles	Boulders
	Fine	Medium	Coarse	Fine	Medium	Coarse	Fine	Medium	Coarse		
Dimension - mm											
< 0.002	0.002 - 0.006	0.006 - 0.02	0.02 - 0.06	0.06 - 0.2	0.2 - 0.6	0.6 - 2	2 - 6	6 - 20	20 - 60	60 - 200	> 200

The particle size distribution of the two soils was measured using the Malvern Instruments Mastersizer 2000 (Hydro 2000MU) apparatus.

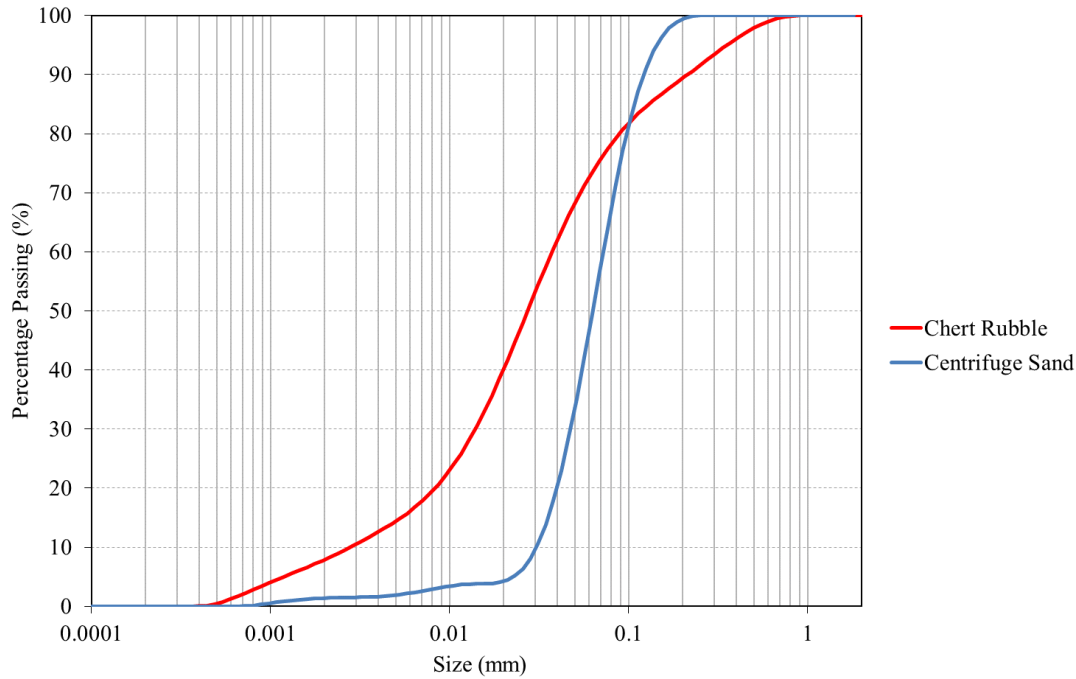


Figure 4-1: Particle size distribution of soils to be used in model studies

From Figure 4-1 it can be seen that the silica sand particles fall primarily within the range of 0.06 mm to 2 mm, indicating that it classifies as a sand according to the British Soil Classification System. Parts also fall within the silt category. On the other hand, the majority of the chert gravel particles fell below the 0.06 mm sieve size, resulting in a silty-clay material. It is important to note that the chert gravel contains approximately 10% clay, where the percentage of clay in the silica sand is close to zero.

4.2.2 Soil stiffness

Figure 4-2 and Figure 4-3 show the stress-strain diagrams for the centrifuge sand and chert rubble, respectively, based on measurements obtained from the oedometer test, where σ is the stress applied to the soil specimen and ϵ , the measured axial strain. The stiffness of the soils was calculated by plotting a linear trendline to the 200% loading curve, and obtaining the gradient of that line. It will be seen that the stiffness of the centrifuge sand was 40.71 MPa, taken as 40 MPa for future calculations, and the stiffness of the chert rubble was 20.03 MPa, taken as 20 MPa.

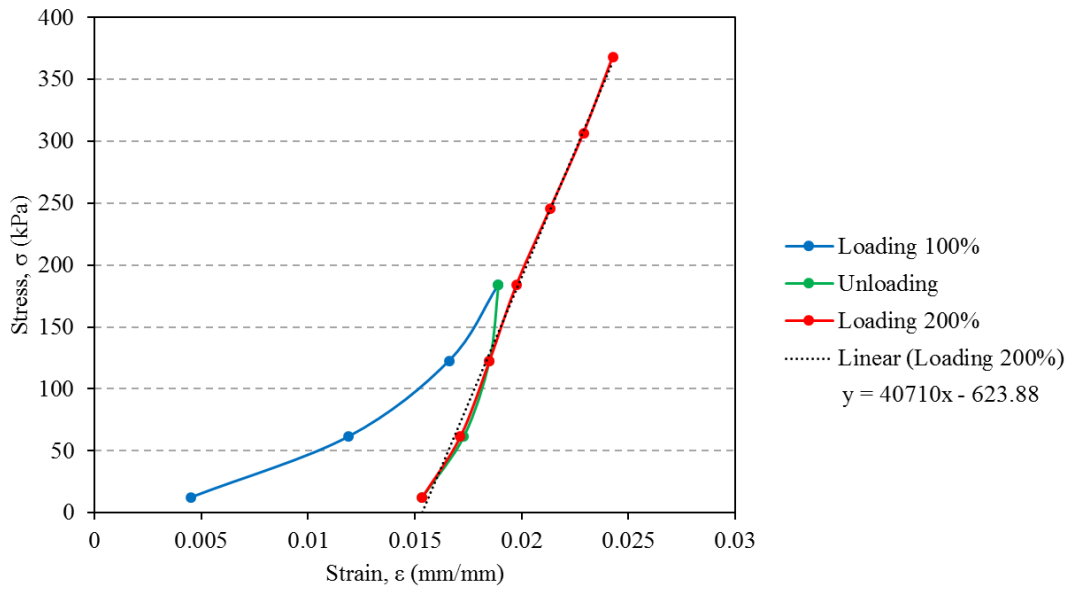


Figure 4-2: Oedometer test result – Silica sand

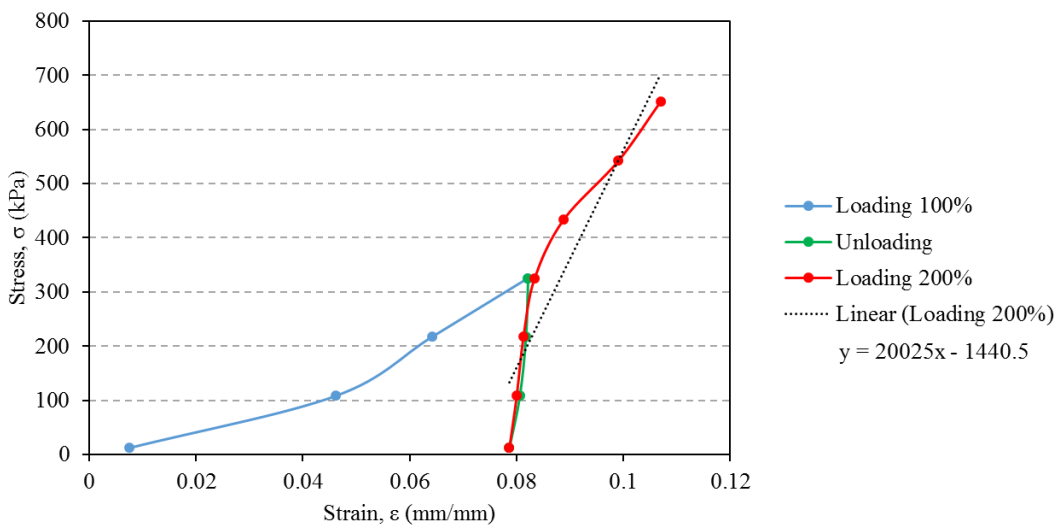


Figure 4-3: Oedometer test result – Chert gravel

4.3 Physical model description

This section contains a description of the experimental set-up and the equipment developed to carry out the proposed model tests. The first part of this section describes the equipment used for modelling and measurements in the centrifuge, followed by a discussion on model preparation and testing procedures to test models.

4.3.1 Geotechnical centrifuge facility

Due to the non-linear stress-strain behaviour of soils, a centrifuge is required to accelerate small-scale soil physical models of geotechnical problems to a high acceleration to produce elevated stresses resulting in realistic strains. Realistic stress-strain behaviour of small-scale soil models cannot be achieved at 1 g (Schofield, 1980). The geotechnical centrifuge of the University of Pretoria was used for this study. The University of Pretoria commissioned a geotechnical centrifuge in 2012 with a capacity of 150 g-ton, which implies that the centrifuge is capable of accelerating a model weighing 1 ton up to 150 g. The centrifuge is shown in Figure 4-4. Selected characteristics and specifications of the centrifuge can be seen in Table 4-2.



Figure 4-4: Geotechnical centrifuge of the University of Pretoria

Table 4-2: Specifications of the geotechnical centrifuge (Jacobsz et al., 2014)

Specification	Description
Model Name and Type	Actidyn C67-4
Capacity	150g-ton
Radius	3 m

4.3.2 Model setup

Figure 3.3 and Figure 4-6 illustrate the model developed to contain the soil and model pipes for testing. The model comprises a frame built from aluminium alloy channel sections that contains a soil volume measuring 500 mm wide by 450 mm high. The thickness of the soil compartment is 80 mm. The front of the sand sample is contained by a 20 mm thick safety glass panel which allows experiments to be observed using a high resolution digital camera. A trapdoor that can be lowered during experiments to impose ground deformation, if required, is located in the base of the frame. The frame can accommodate trapdoor widths of between 50 mm and 100 mm. The centrifuge is equipped with a water supplying the model via a set of hydraulic slip rings, controlled from a panel in the control room. Leakage could be modelled by discharging water at the desired location in close proximity to the pipe. The desired flow rate was set before the test by means of a slow restrictor in the discharge pipe. Supply could be controlled by means of a solenoid valve operated from the control room.

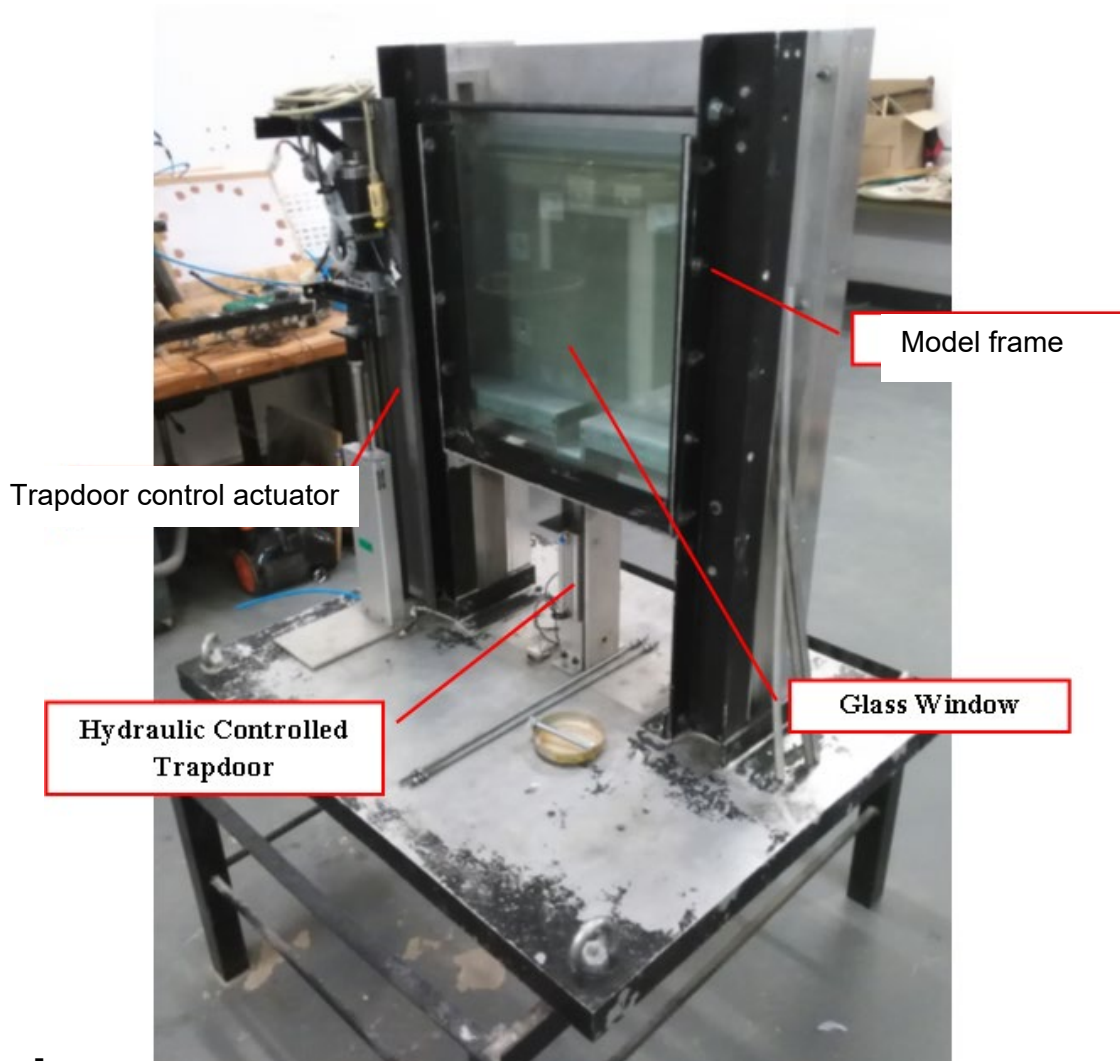


Figure 4-5: Centrifuge strong box

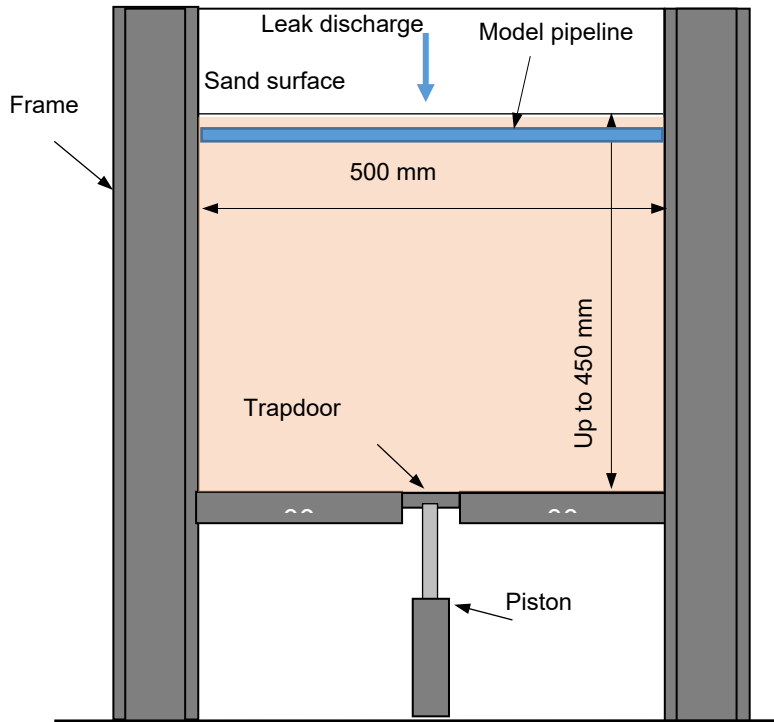


Figure 4-6: Schematic few of the centrifuge model frame

4.3.3 Simulation and additional measuring equipment

Different sets of equipment were used to imposed ground movement and measure the applicable parameters during testing. These parameters included the settlement of soil surface, settlement of the pipeline, as well as trapdoor settlement. Figure 4-7 shows the stepper motor controlled actuator and the trapdoor with supporting piston.

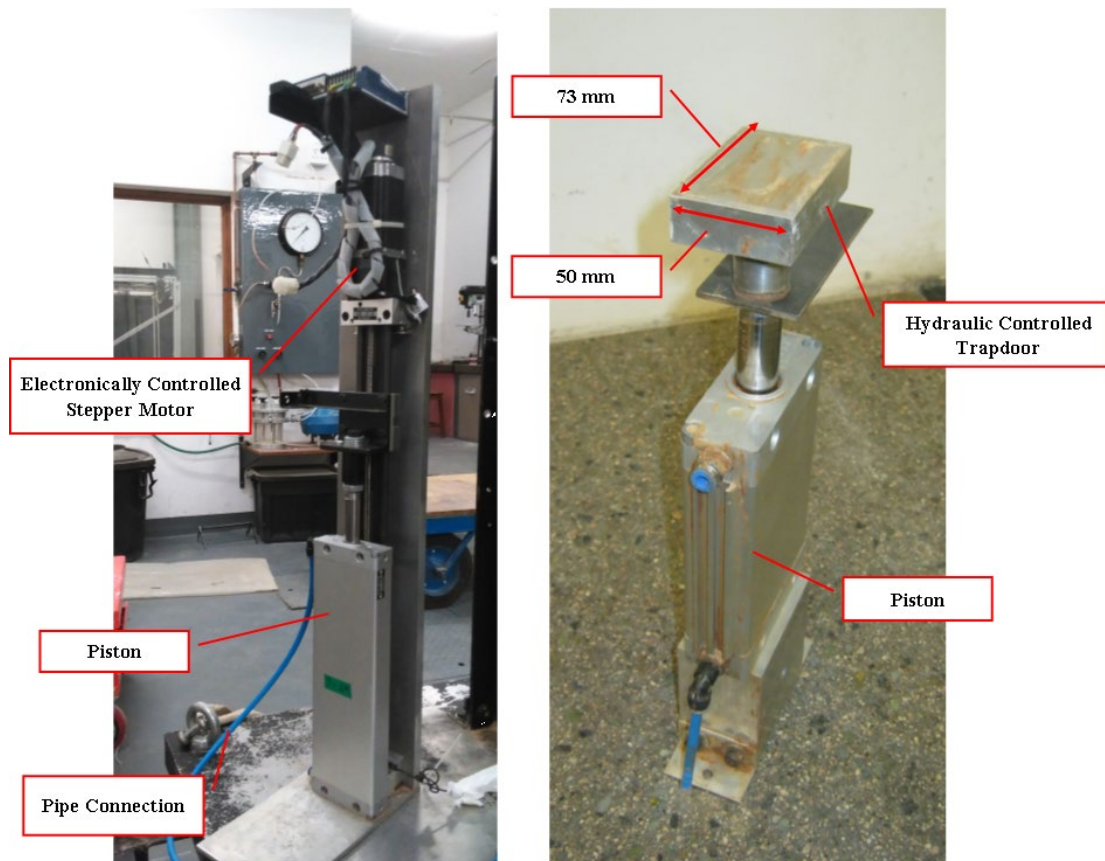


Figure 4-7: Stepper motor and trapdoor

Deflections of the pipeline and settlement of the soil surface were measured using 5 linear variable differential transformers (LVDTs) connected to a bracket and attached to the frame at the top of the soil model. The LVDTs used are from Ametek Solartron (type – M930988AD14-07), had a range of 30 mm and resolution of approximately one micron. The LVDT, fixed into position, can be seen in Figure 4-12, showing a complete model set-up. Trapdoor settlement is measured using an additional LVDT that attaches at the back of the model. This LVDT was manufactured by HBM (model name and type – 164110464) and has a range of 200 mm. DigiDAQ (from the University of Western Australia) and CATMAN software (from HBM) are used to log the deflection (LVDT) and strain data, respectively.

4.3.4 Pipeline instrumentation and properties

Two instrumented model aluminium pipes measuring 500 mm in length were used in this study. The first pipe is referred to as the “stiff pipe” and the second, the “flexible pipe”. The two pipes were machined to have different bending stiffnesses to allow the effect of leakage-induced strains on pipes of different stiffness to be assessed. Dimensional properties of the

pipe can be found in Table 4-3. The Young's modulus of the aluminium tubing was taken as 70GPa.

Table 4-3: Pipe dimensions

Pipe	Outside Diameter (mm)	Inside Diameter (mm)	Wall Thickness (mm)	Area (mm ²)	Second Moment of Inertia (mm ⁴)	Bending Stiffness (N.mm ²)
Stiff pipe	12.72	11.20	0.76	28.57	513.16	35.9x10 ⁹
Flexible pipe	10.61	8.53	1.04	31.23	361.71	25.3x10 ⁹

The stiff pipe was instrumented with a total of eight precision resistance strain gauges (Relevant properties of the precision resistance strain gauges are summarised in Table 4-4.) These strain gauges were connected to form four half-Wheatstone bridges, with the first located at the centre of the pipeline. Strain gauges are spaced 75 mm apart along one half of the pipeline. It was assumed that the pipe would behave symmetrically. The half-bridges were fixed by placing one of the two gauges on the top of the pipe and the other directly underneath, forming a half-bridge beam-type configuration suitable for measuring bending strains. A view of the instrumented model pipe can be seen in Figure 4-8 showing some dimensions. Vertical rods, extending through the sand for measuring of pipe deflection during testing, can also be seen in Figure 4-8.

The second model pipe, with a lower bending stiffness was made to study the effect of different pipe stiffness and was instrumented to measure the longitudinal and circumferential (hoop) strain components separately. The model pipe was instrumented with thirteen precision resistance strain gauges. Ten of these strain gauges were attached in the longitudinal direction (five along the top of the pipe and the other five below those) to measure strain caused by the pipeline deflecting. These pairs of strain gauges (one on top and one directly below it) were also connected to form half Wheatstone bridges to measuring bending strains. The strain gauge bridges were attached 100 mm apart. Three more strain gauges were attached on the circumference of the pipeline next to the three middle half bridges to measure the effect that varying the pressure in the pipeline has on the strains relative to the bending strain. These quarter Wheatstone bridges were connected with completion circuits in order to be logged. Figure 4-8 shows the layout of the three middle sets of strain gauges. A fitting was attached to the model pipe to allow it to be internally pressurised to study the effects of in-pipe pressure fluctuations.

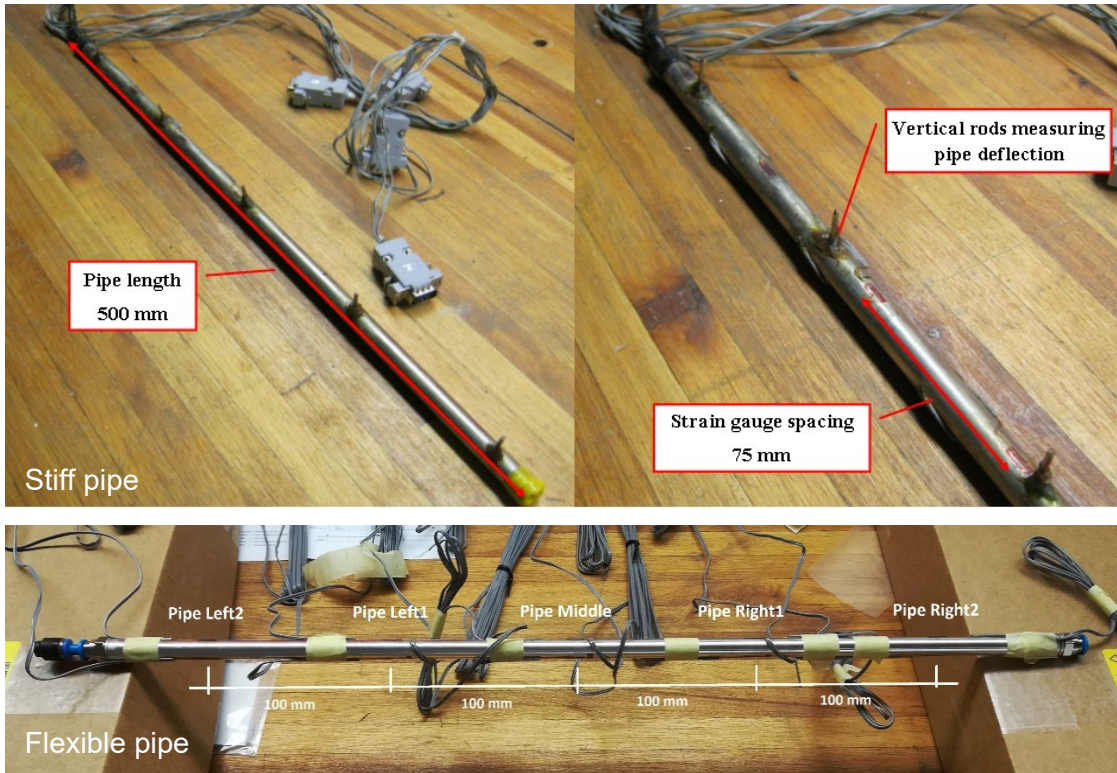


Figure 4-8: The instrumented model pipes

Table 4-4: Strain gauge specifications

Specification	Description
Manufacturer	Tokyo Sokki Kenkyujo Co., Ltd.
Model Name and Type	FLA-5-11-1L
Gauge Factor	$2.13 \pm 1\%$
Gauge Length	5 mm
Gauge Resistance	$120 \pm 0.5 \text{ Ohm}$
Thermal Coefficient	$11 \times 10^{-6}/^{\circ}\text{C}$

4.3.5 Strain gauged brass strip

In order to measure leakage-induced strains in the ground, similar to what would be achieved using a fibre optic cable in the envisaged leakage detection system investigated in this project, a 5 mm wide, 0.1 mm thick brass strip, instrumented with 5 strain gauges was placed just below the flexible model pipeline. This allowed for the measurement of soil strains cause by the leak. These strain gauges were spaced at the same intervals as the gauges on the flexible pipeline. The brass strip is shown.

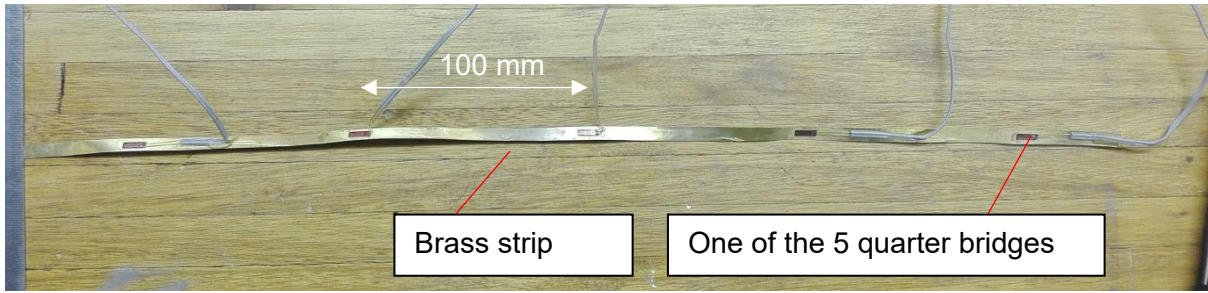


Figure 4-9: Brass strip instrumented with strain gauges to measure leakage-induced ground strains.

4.3.6 Imposing water leaks

To simulate a water leak in the pipeline during the pipe test, water from the main water supply network of the laboratory was discharged onto the surface of the soil above the centre of the pipeline. To control flow, a FESTO flow restrictor was used to reduce the flow of water at 30 g to 0.195 ml/s. Solenoid valve 1 (see Figure 4-10) was used to activate the leak from the control room. In further test, water was leaked onto the soil using the stepper motor controlled piston instead of the water supply network as it proved difficult to control the flow rate of water on the centrifuge during testing using the arrangement shown below.

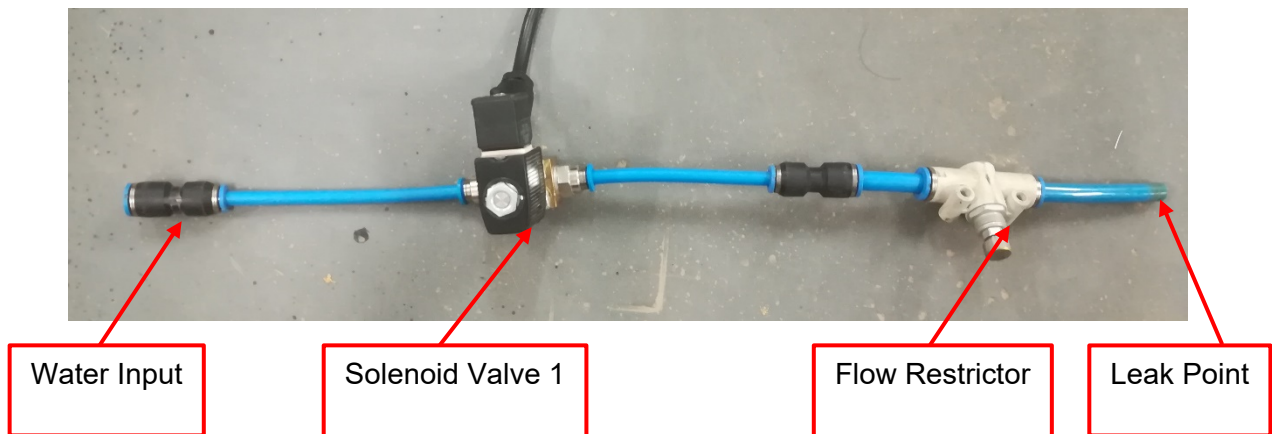


Figure 4-10: Leak mechanism

4.3.7 Scaling laws

Due to the models being at a reduced scale, observations from the model need to be translated to full scale. This is achieved by applying a range of scaling laws which are summarised in Table 4-5.

Table 4-5: Scaling laws applicable to centrifuge testing (Taylor, 1995)

Parameter on Prototype Scale	Scaling Law for Centrifuge Acceleration, N.g
$\sigma, \varepsilon_b, E_p, E_s$	1
D_p, r_0, i, S_{max}	1/N
$E_p A_p$	1/N ²
M	1/N ³
$E_p I_p$	1/N ⁴

Descriptions of the symbols used above can be found under the list of symbol at the beginning of the report.

4.3.8 Model set-up and testing procedure

This section describes the procedure followed to prepare and set-up models for testing. The set-up procedure is somewhat different for the two soil types tested as summarised below.

The study investigated the behaviour of model pipes of two stiffness in two soil types. As mentioned in Chapter 2, the relative rigidity of a pipe-soil system is a function of the stiffness of the soil, the pipe bending stiffness and the cross section dimensions of the pipeline. A pipe may behave rigidly, flexible or in-between. When flexible, the pipe will follow the deflected shape of the soil supporting it and usually have a relative rigidity factor of less than 0.1 (Equation 2-13). A pipeline is considered to be rigid if the movement of the supporting soil has little impact on the deflection of the pipe and the relative rigidity factor is more than 5.

Careful consideration had to be given to establish the required soil densities for the experimental work because density influences the stiffness of the soil and ultimately the relative rigidity of the soil-pipe system. Two different methods were used to obtain the required densities.

During model preparation the silica sand was placed by means of air pluviation using a sand hopper shown in Figure 4-11. The sand hopper, with a hose attached to the outlet, was hoisted by a crane to a height of 300 mm above the surface level of the soil. During model preparation sand particles travelled a distance of 1500 mm (1200 mm inside the hose, with 300 mm freefall) at a constant mass flow rate. The 300 mm freefall distance was selected after a series of trial runs using the silica sand in a smaller container to obtain the height required to achieve a density of approximately 1500 kg/m³. The sand hopper was raised regularly to maintain a constant drop height during model preparation to insure a uniform sand density in models. No

moisture was added to the sand during model preparation using the sand hopper. A model ready for testing can be seen in Figure 4-12



Figure 4-11: Sand hopper used for placing silica sand in models

The chert gravel was placed in the model container by hand. In addition to testing dry silica sand, it was also necessary to test an unsaturated soil to investigate a material with some cohesive strength as this is typical of South African conditions in which pipes are normally laid. Approximately 10% moisture (by mass) was added to the soil prior to compaction. Soil was compacted using a wooden tamper to reach a density of approximately 1600 kg/m^3 . During model preparation the soil was placed in 30 mm thick layers and compacted after placement of each layer.

A brief description of the model preparation and test procedures is presented below.

The silica sand test model preparation:

- The model frame was assembled, ensuring that the trapdoor piston was fixed and fully extended to be flush with the floor of the strong box.
- The procedure for sand pluviation described above was followed.
- The sand was pluviated to a final depth of 400 mm above the model floor level.
- The instrumented pipe was typically placed at a depth of 35 mm from the top of the soil surface (invert level) along the centreline of the model space. As tests were conducted at

30-g corresponding to a full-scale pipe invert level of 1.080 m. A tube was attached to the model pipe to allow the internal pressure in the pipe to be controlled via the centrifuge's hydraulic system.

- After completion of sand pluviation, the sand surface was levelled to ensure a flat surface.
- A tube supplying water to the soil/pipe was placed into position to simulate a water leak.

Figure 4-12 presents a completed model prepared with silica sand, with instrumentation fitted, ready for testing on the centrifuge swing platform.

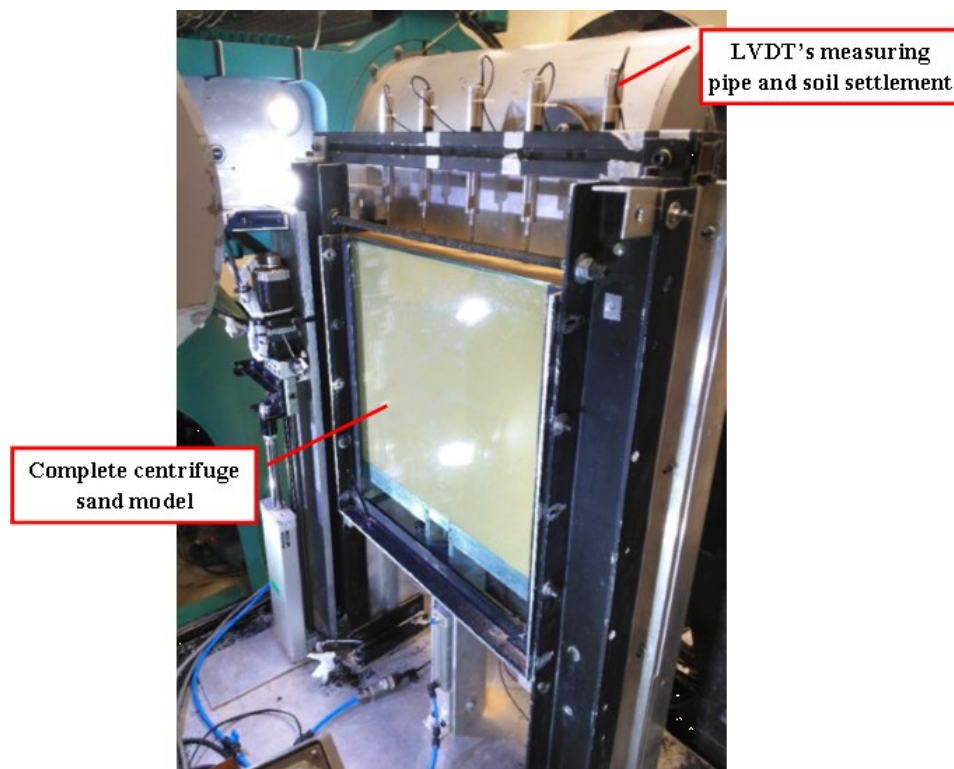


Figure 4-12: Complete model set-up with silica sand

Model preparation with the chert gravel is described below:

- The model frame was assembled, ensuring that the trapdoor piston was fixed and fully extended to be flush with the floor of the strong box.
- The same basic procedure for soil placement and compaction as mentioned above was followed.
- Layers of moistened chert gravel were placed and compacted in layers to a level of 340 mm above the trapdoor level.
- The instrumented pipe was placed at a depth of 22 mm from the top of the soil surface (invert level) along the centreline of the model compartment. A tube was attached to the

model pipe to allow the internal pressure in the pipe to be controlled via the centrifuge's hydraulic system.

- Attention was paid to obtain similar densities for all tests to ensure comparable soil behaviour.
- To discharge water in the model to simulate a leak, a solenoid valve was attached to the centrifuge water supply. A flow restrictor was fitted to the pipe to allow to the leakage rate to be set before testing tot the required rate. Once the required acceleration was reached water could be released to impose a leak and the propagation of the wetting front studied.

Figure 4-13 presents a complete model set-up with the chert gravel with provision for leak simulation incorporated.

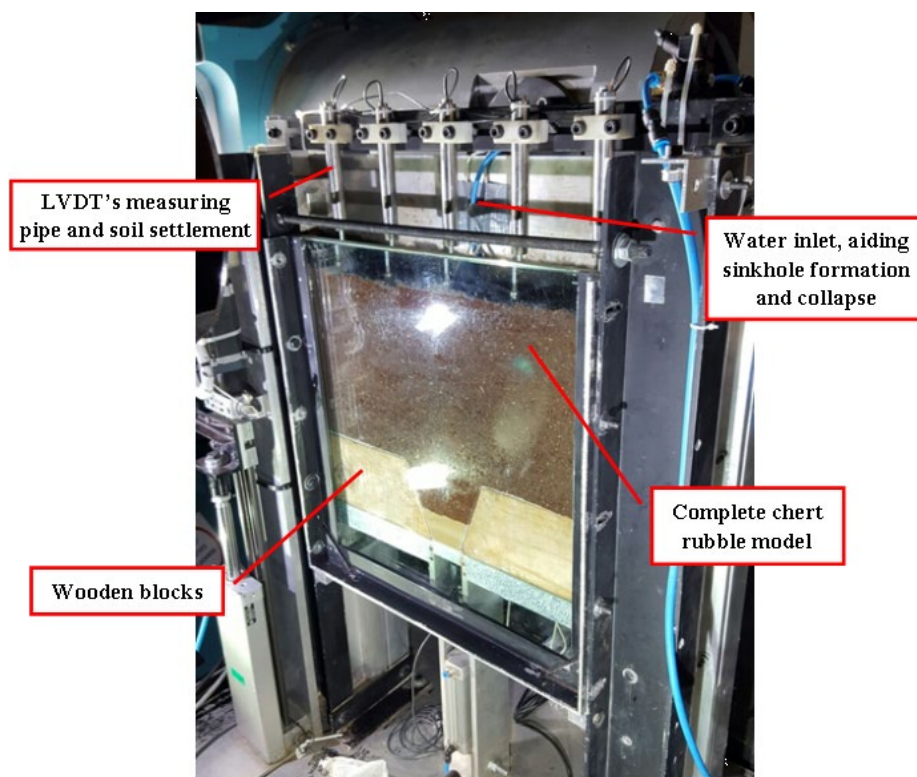


Figure 4-13: Experimental model set-up with chert gravel and provision to leak simulation.

4.3.9 Surface and trapdoor settlement

In all tests LVDTs were attached to a bracket and fixed to the top of the model to record surface and pipe settlement during the experiments. The LVDTs can be seen in Figure 4-12 and Figure 4-13. An additional LVDT was attached to the back of the strong box to measure the settlement of the trapdoor when used. Light weight rods, fixed to the pipe, extended above the soil surface to allow pipe settlement to be monitored by means of LVDTs at the top of the model.

4.3.10 Monitoring soil displacement fields

In addition to surface settlement recorded using LVDTs, Particle Image Velocimetry (PIV) (White et al., 2003) was used to measure the displacement field across the soil mass by means of digital images recorded through the glass front. PIV operates by tracking patches of pixels distributed in a grid across the recorded digital images to provide displacement vectors for each patch. From the displacement field, strain fields were calculated to allow leakage-induced soil deformations to be observed.

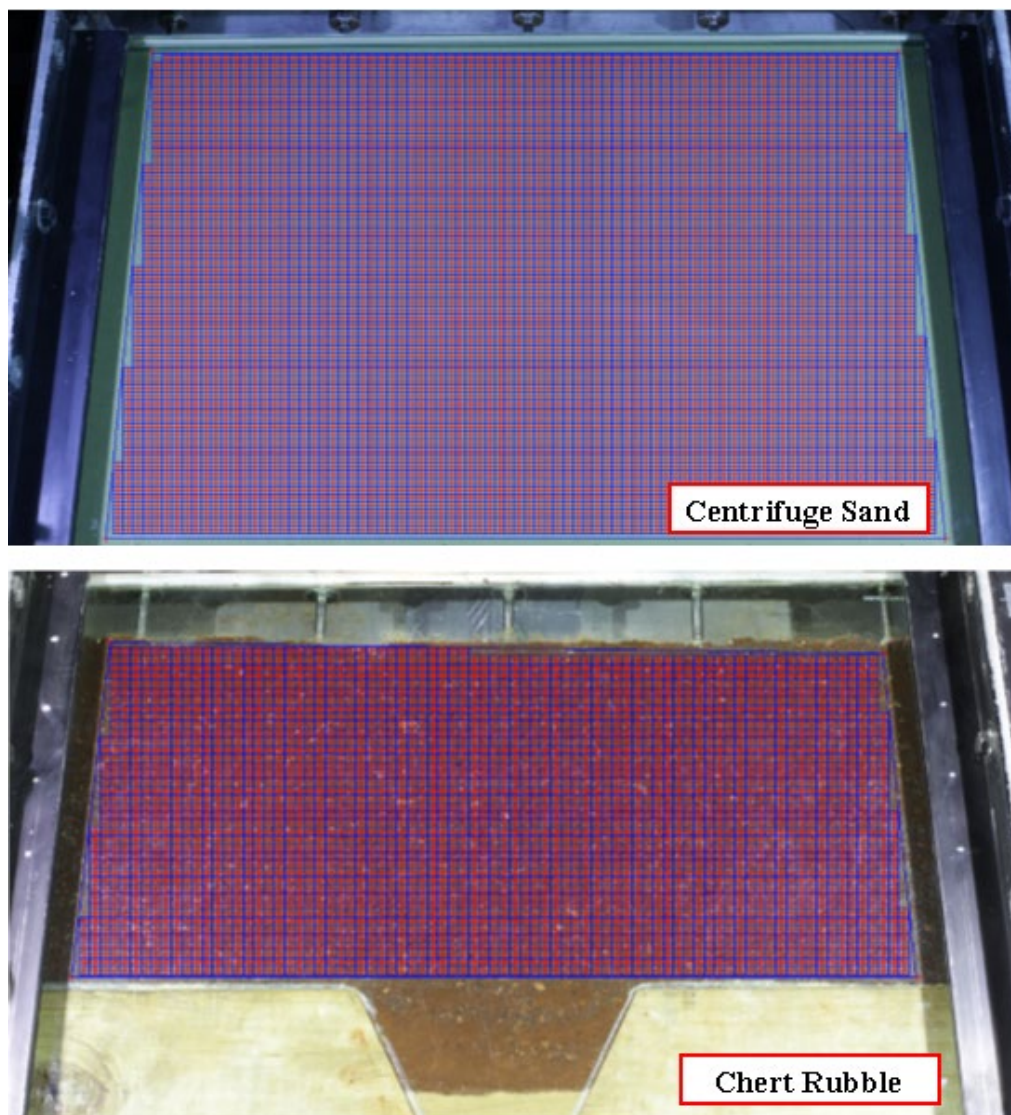


Figure 4-14: PIV representation of patches on initial images

4.3.11 Test sequence

Prior to testing, a model was loaded onto the centrifuge platform and all electronic measuring equipment connected and initialised. For the purposes of this study the centrifuge was accelerated to 30 g as the model scale was 1:30. Once the test acceleration was reached, time lapse photography commenced to record each test. The following aspects were investigated in the tests carried out:

- The effect of in-pipe pressure fluctuation on longitudinal and circumferential pipe strains. In addition to the centrifuge model tests, pressure fluctuation was also investigated in the full scale pipe installation on the University's experimental farm.
- Ground and pipe strains induced by artificially induced leaks.
- The influence of pipe stiffness on the measured strains.

During tests in-pipe pressure fluctuation will be imposed and longitudinal and circumferential pipe strains monitored in addition to soil and pipe settlements.

4.4 Leakage-induced ground strains

It is of interest to study leakage-induced ground strains to gain an understanding of how such strain would impact a pipe buried in the ground. Leakage-induced ground strains were studied using physical models in the geotechnical centrifuge.

4.4.1 Greenfield conditions

The first centrifuge test carried out investigated greenfield leak-induced ground deformation, i.e. ground deformation in the absence of a pipe. This was necessary because the greenfield ground deformation is required to assess the relative stiffness of the combined soil-pipe system based on Equation 2-13. The surface settlement was measured with an array of 5 LVDTs. It was found that Gaussian curves (Equation 2-16) closely matched the observed settlement troughs. Gaussian curves were fitted through the data points as shown in Figure 4-15. Figure 4-16 presents the development of the wetted zone around the induced leak, as well as the associated surface settlement.

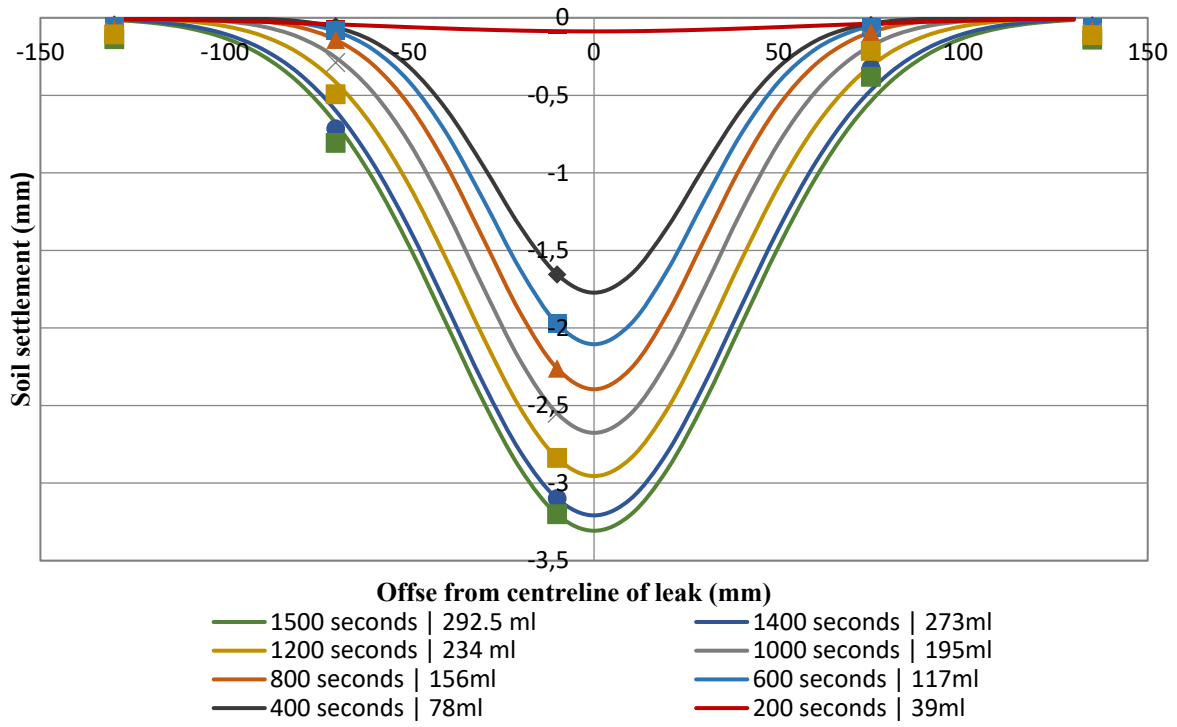
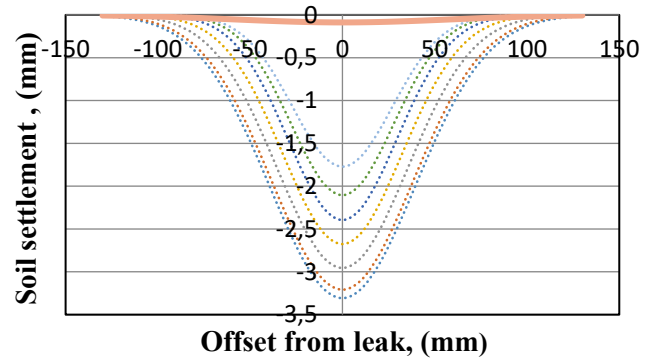
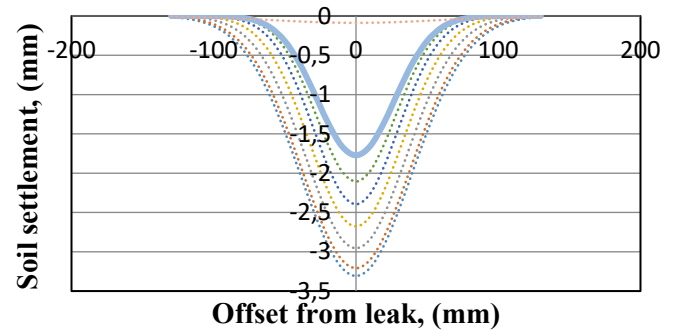


Figure 4-15: Leakage-induced greenfield surface settlement curves

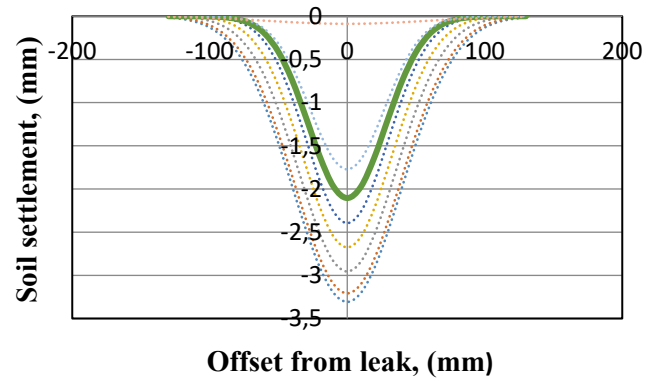
200 seconds, 39 ml, i-value = 57.94 mm



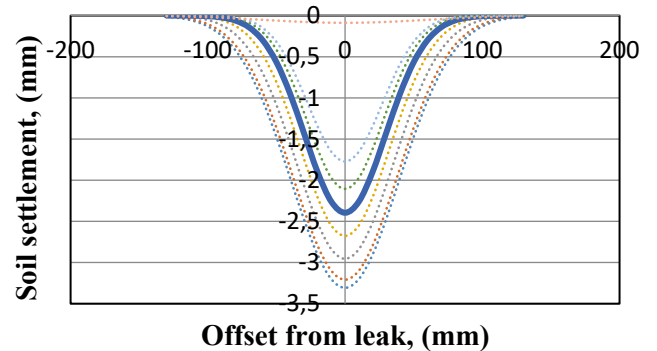
400 seconds, 78 ml, i = 26.98 mm



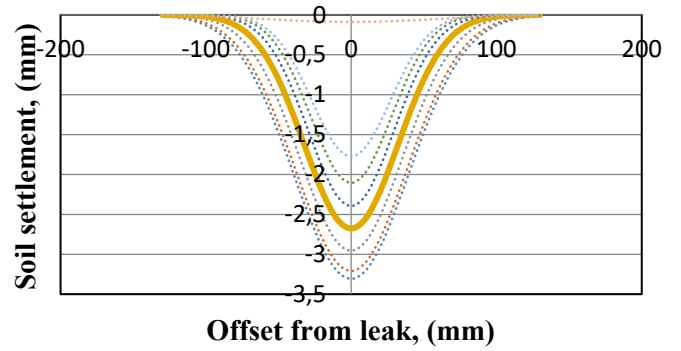
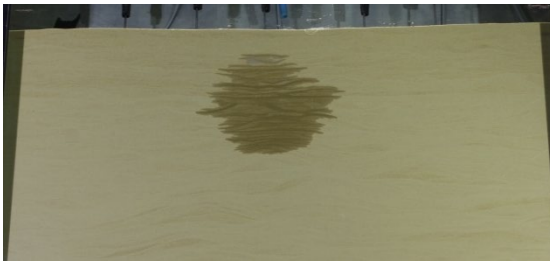
600 seconds, 117 ml, i = 27.73 mm



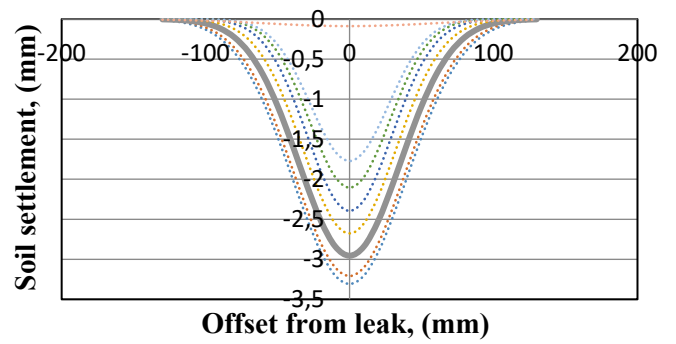
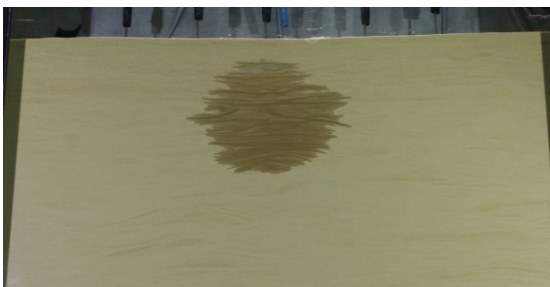
800 seconds, 156 ml, i = 29.44 mm



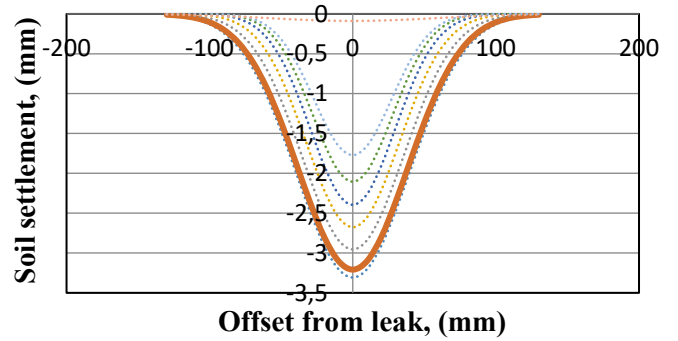
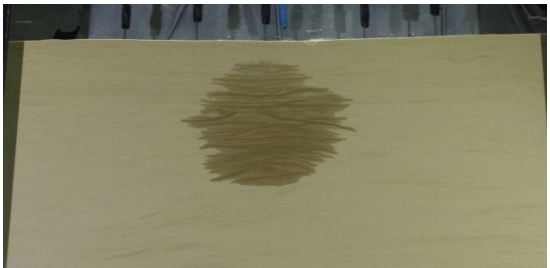
1000 seconds, 195 ml, $i = 32.31$ mm



1200 seconds, 234 ml, $i = 35.33$ mm



1400 seconds, 273 ml, $i = 38.19$ mm



1500 seconds, 293 ml, $i = 39.34$ mm

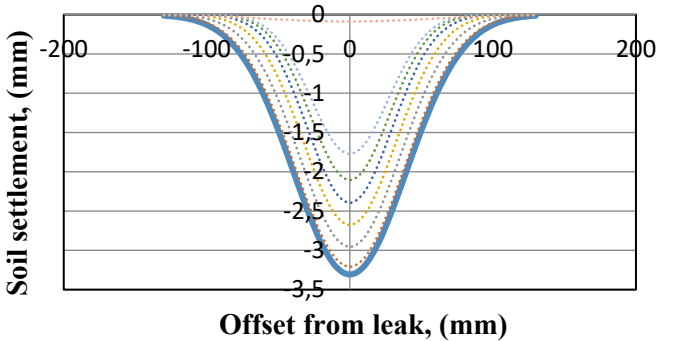


Figure 4-16: Leak progression and associated surface settlement under greenfield conditions

It can be seen that, as water was leaked, a settlement trough rapidly formed at the ground surface. The shape of the settlement trough was confirmed by tracking a row of patches illustrated in Figure 4-17 along the soil surface. The patches were tracked using PIV (White et al., 2003) to generate settlement troughs. The resulting settlement troughs are illustrated in Figure 4-18 and can be seen the closely resemble Gaussian curves. This confirmed that the greenfield leakage-induced settlement trough closely resembled a Gaussian curve.



Figure 4-17: Row of patched tracked using PIV to study shape of leakage-induced surface settlement trough

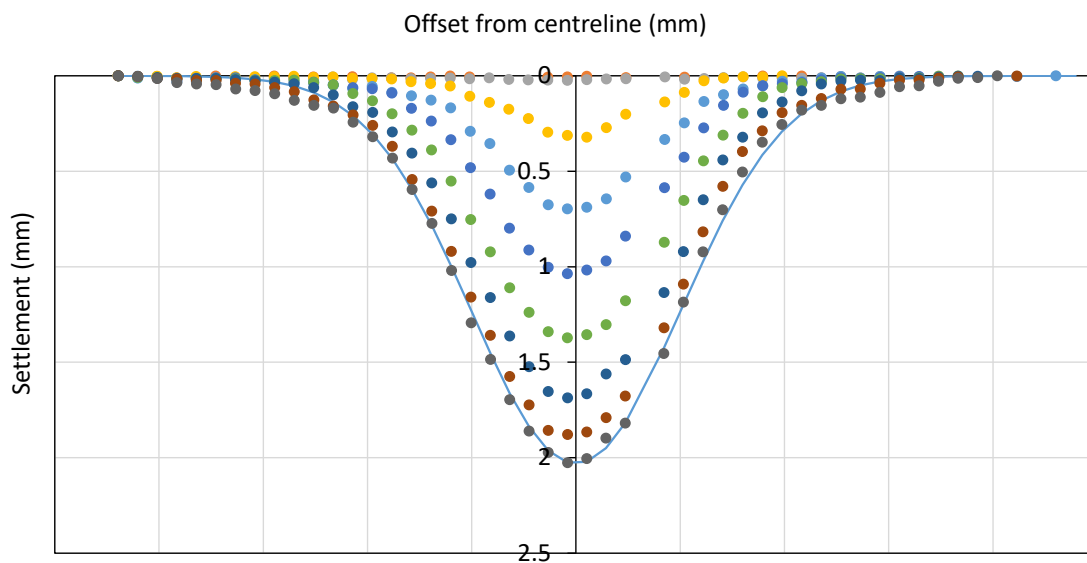


Figure 4-18: Greenfield leakage-induced surface settlement troughs tracked using PIV during leak propagation.

Of particular interest was the offset of the inflection point on the settlement trough from the centreline (i) (i.e. the inflection point is the point where the curvature changes from hogging to sagging) as this controls the relative rigidity of the soil-pipe system (see Equation 2-132-13). Figure 4-19 present the variation in parameter i as a function of the amount of moisture leaked into the soil. It can be seen that after some initial fluctuation, the inflection point soon stabilised and did not change much with further water leakage, showing that the depression in the soil surface was quite localised. Given a scale factor of 1:30, the offset to the inflection point varied from 0.8 m to 1.2 m.

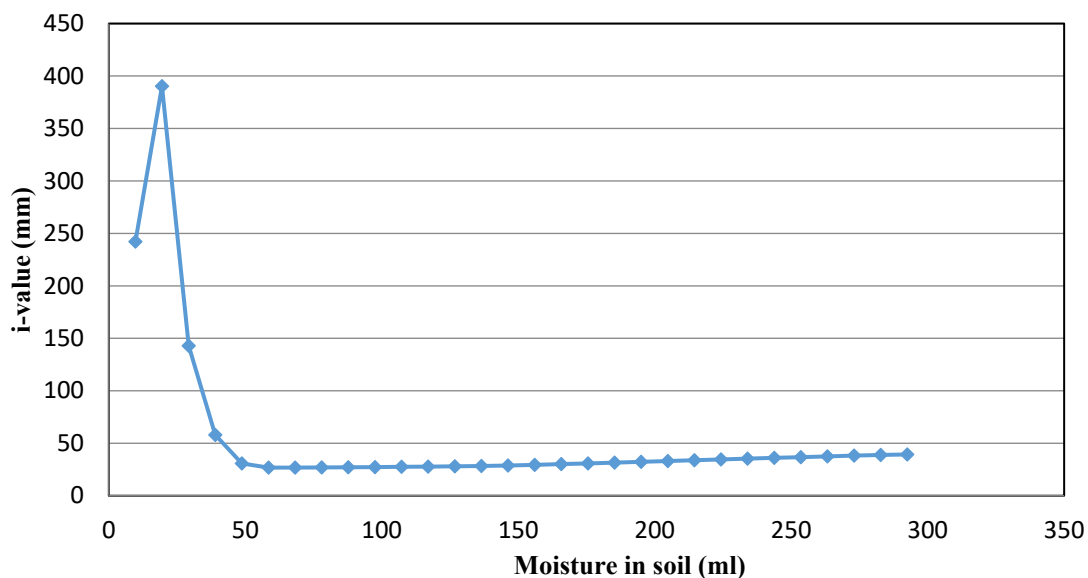


Figure 4-19: Variation in distance to inflection point (i) as a function of the amount of moisture leaked into soil.

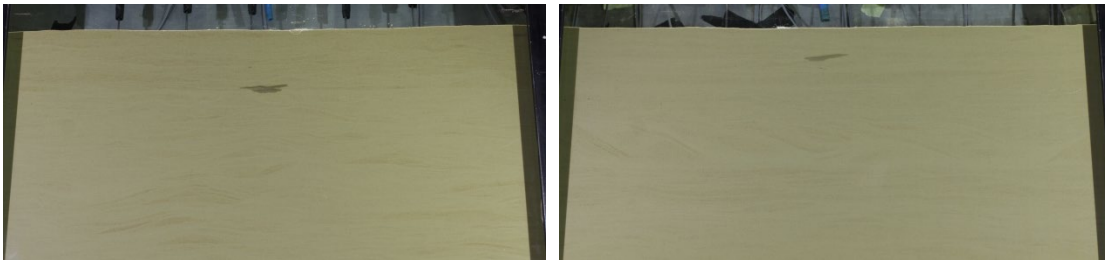
4.4.2 Ground strains in the presence of a pipe

Depending on its stiffness, the presence of a pipe may influence leakage-induced ground strains. The pipe may also affect the way in which a leak will spread in the ground. Figure 4-20 illustrates the spreading of the wetted zone resulting from a leak with and without a pipe in the ground. Although the patches are similar, it can be seen that the pipe did have some influence.

Greenfield test

Pipe-soil test

78 ml of water induced by simulated leak.



156 ml of water induced by simulated leak.



234 ml of water induced by simulated leak.



293 ml of water induced by simulated leak.



Figure 4-20: Comparison of spreading of leakage-induced wetted zones under greenfield conditions (left) and with a pipe in the ground (right).

The deflections from the greenfield test and the test with a pipe present are compared at leaked water volumes of 78 ml, 156 ml, 234 ml and 293 ml in Figure 4-21. These specific

values were decided upon because it corresponds with the values used in Figure 4-15 and Figure 4-16. In both test the deflections were measured at a depth of 50 mm below the surface of the silica sand. The model pipe was installed with its invert depth at 50 mm, 1.5 m at the full scale.

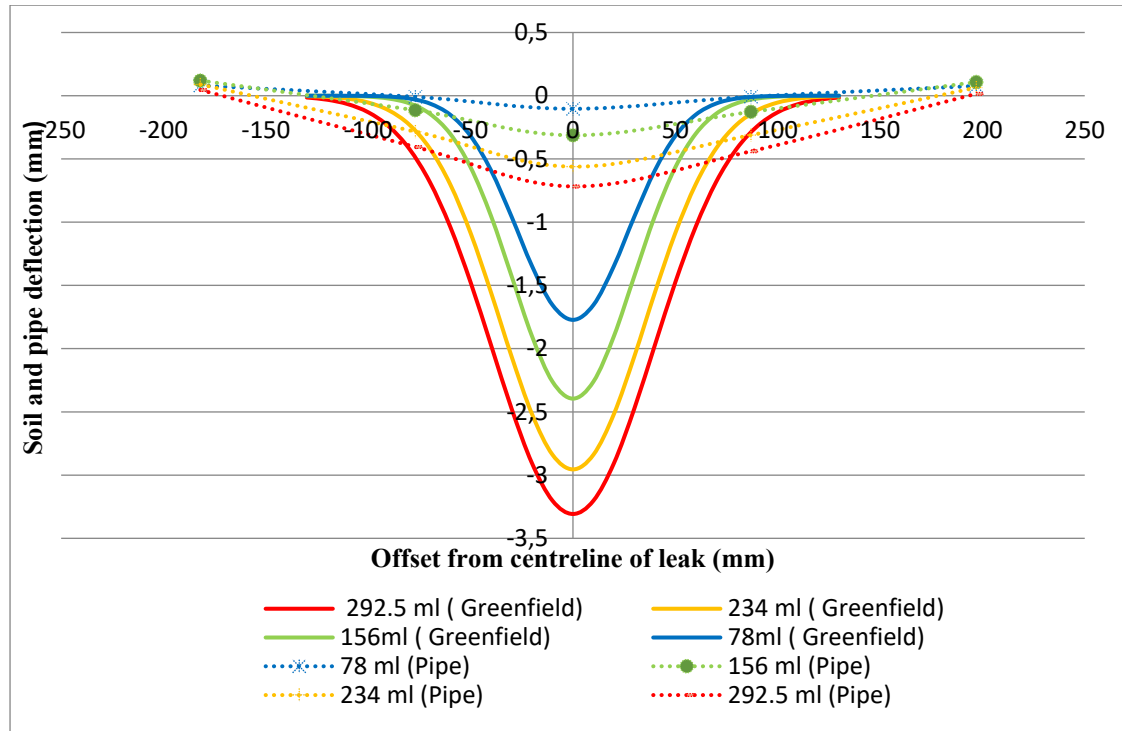


Figure 4-21: Comparison of settlements from greenfield test and with pipe present

Clear differences in pipe settlement and soil settlement are seen in Figure 4-21. The most significant deviation in the amount of settlement that took place between the pipe and soil occurred at the leak location. The pipe clearly had a stiffening effect on the ground and shows that the pipe behaved in a stiff manner in the centrifuge tests.

4.5 Leakage-induced pipe strains

The bending and strain behaviour of a buried pipeline is largely affected by the interaction of the pipe with the surrounding soil. It is thus important to consider these interactions between the pipe and soil and observe the mechanisms governing behaviour. The results are presented for both soil types individually, followed by a summary of the observations for both cases.

The recorded data was plotted at various trapdoor settlements. It should be noted that the trapdoor settlement is expressed as the ratio between the measured downwards movement of the trapdoor and the original distance from the unretracted trapdoor to the pipe invert level.

4.5.1 Pipe-soil interaction – Silica sand

For the centrifuge sand, data obtained from the greenfield and pipe tests were plotted, analysed and compared for 1%, 2%, 5%, 8%, and 10% trapdoor settlements, respectively. Both tests were stopped when 10% trapdoor settlement was reached. The graphs contain the deflection of the soil at pipe invert level with and without the presence of a pipeline underneath the soil surface, and the deflection of the pipe.

The response of the soil due to the existence of a pipeline in the soil structure should be considered, especially considering the response of the soil at pipe invert level, as this is the soil supporting the pipeline. Figure 4-22 indicates the settlement profiles of the silica sand at pipe invert level for the greenfield test and compares it with the soil settlement profiles at the same level in the presence of a pipe. Different profiles were plotted corresponding to different percentages of trapdoor settlement. The presence of the pipeline within the soil structure resulted in a significant reduction in the deflection profile of the soil at the invert level.

The deflection of the soil profile for the greenfield test is more than that observed from the pipe test, with the magnitude of deflection depending on the amount of trapdoor settlement. It can be seen that the presence of the pipeline reduces the soil deflection at the invert level, i.e. less shear strain in the soil below the pipeline. In addition, the presence of the pipe also widens the induced soil settlement trough (larger i value), in comparison to that observed from the greenfield test, also observed by Marshall et al. (2010).

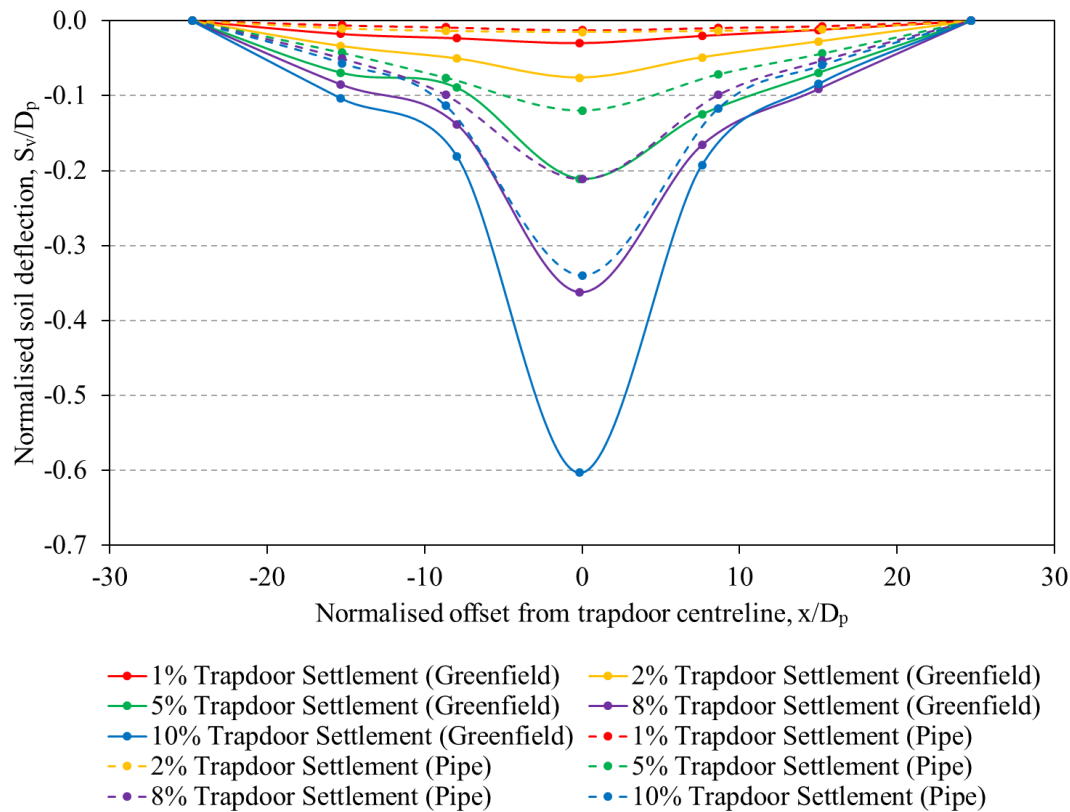


Figure 4-22: Invert level soil deflection – centrifuge sand

The deflection of the pipeline in comparison to the settlement of the soil at pipe invert level should also be considered. Figure 4-23 indicates the settlement profile of the soil at pipe invert level for the greenfield tests and compares it with the deflection of the pipe during the pipe test. The pipe did not follow the greenfield soil profile closely, indicating that the pipe is neither behaving completely flexible nor rigid, which satisfies the original assumption that the pipe can be classified between the flexible and rigid ranges. As mentioned in the literature, due to soil behaviour being nonlinear with respect to stress-strain behaviour, behaviour of a pipeline in soil may vary from location to location. The pipeline approximately followed the greenfield soil profile at pipe invert at small settlement trough depths. However, as the settlement trough depth increased, pipe deflection started to deviate from the greenfield settlement, with deviation increasing towards the centre, indicating that the pipe behaviour became more rigid.

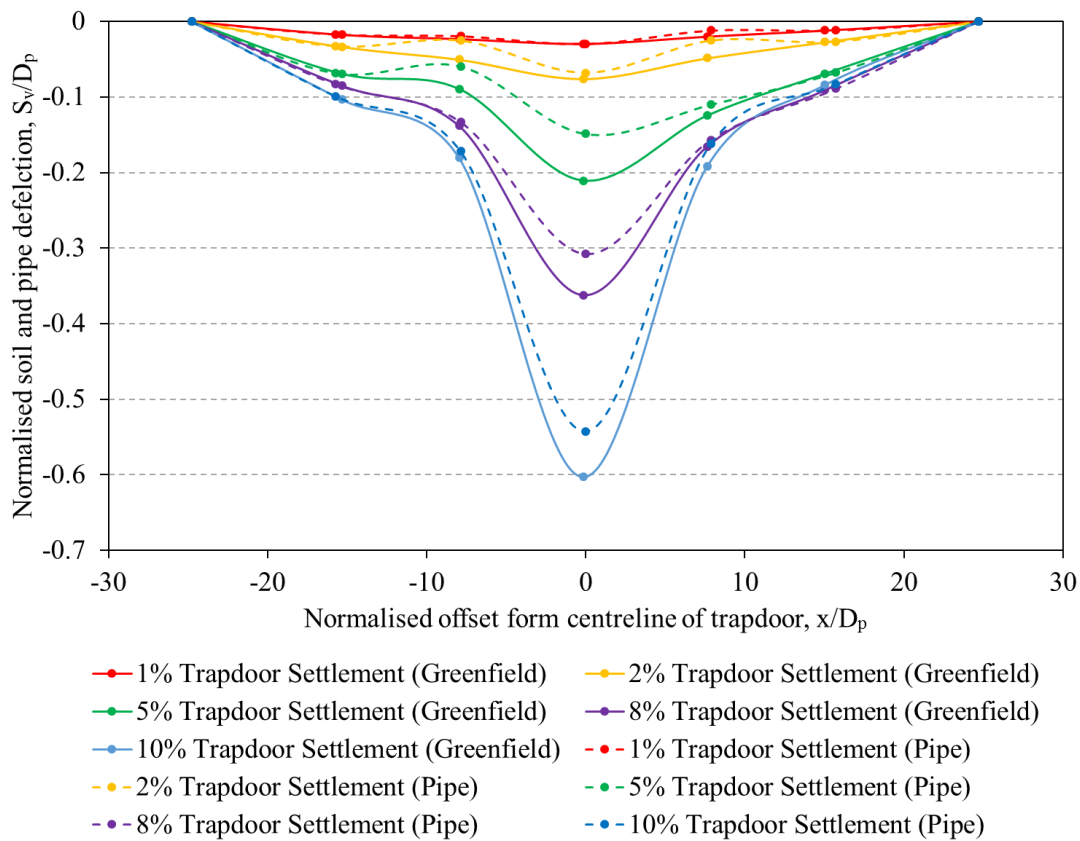


Figure 4-23: Pipe and invert level soil deflection – centrifuge sand

This difference can be seen by plotting the relative pipe-soil settlement. The relative pipe-soil settlement (S_{rel}) is the numerical difference between the deflection of the greenfield subsoil profile at pipe invert level and the deflection of the pipe at that same level (Vorster et al., 2006). The relative pipe-soil settlement was calculated and plotted against the offset from the centreline of the trapdoor in Figure 4-24. This shows that an increase in trapdoor settlement resulted in an increase in the relative pipe-soil settlement, agreeing with the observation of Vorster et al. (2005) that the magnitude of soil movement directly affects the relative pipe-soil settlement.

Negative values indicate that a gap was forming (Vorster et al., 2006) between the pipeline and the underlying soil over the length of the pipe shown, i.e. the vertical contact pressure reduced. The pipe is therefore no longer supported continuously along its length, resulting in the pipe preventing deflection caused by the soil above the pipe.

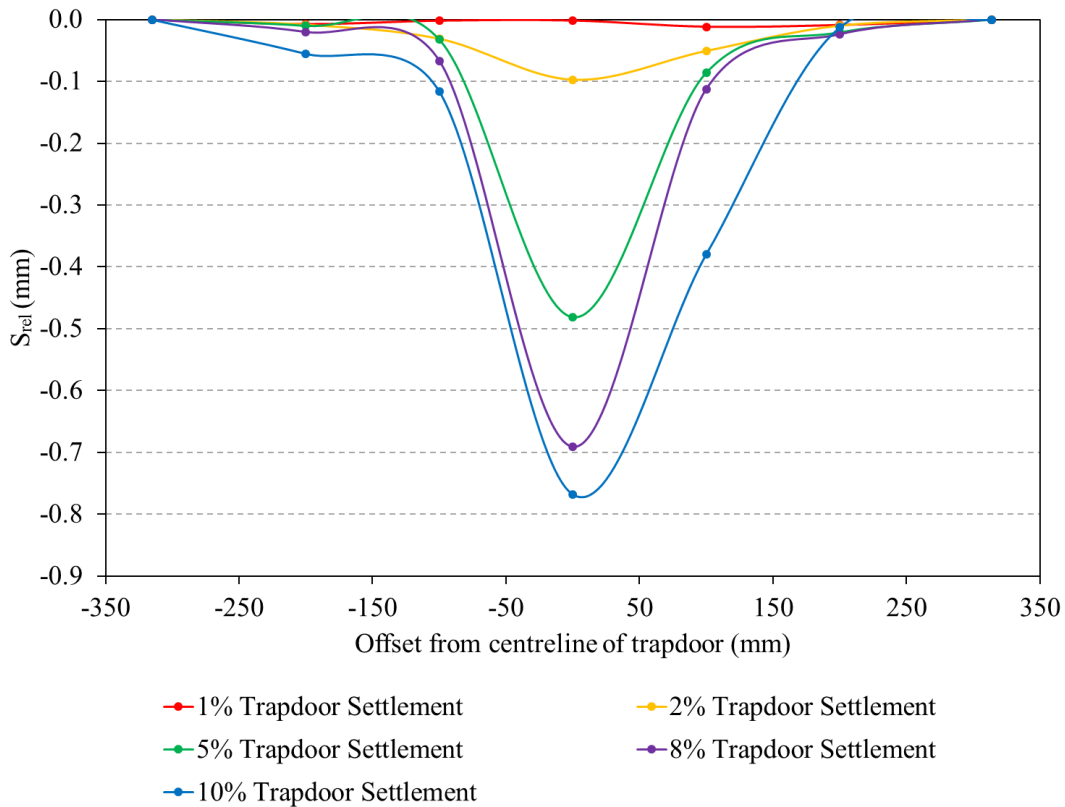


Figure 4-24: Relative pipe-soil settlement – silica sand

4.5.2 Pipe-soil interaction – chert gravel

For the chert gravel, data from the greenfield and pipe tests were analysed for 1%, 10% and 20% trapdoor settlements. Settlement between these values were insignificant due to small amounts of settlements that occurred due to cohesion in the soil. Water was subsequently added to simulate leaks, inducing ground movements, without needing movement to be imposed using the trapdoor.

Figure 4-25 presents the settlement profiles recorded in the chert gravel at pipe invert level for the greenfield test and compares it with the settlement profiles at that same level during the test with a pipe present. The presence of the pipeline within the soil resulted in a significant change in the deflection profile compared to the greenfield. The soil settlement at pipe invert level for the greenfield test was greater than that observed in the pipe test. Due to cohesion between soil particles, settlements of the chert gravel were small at low trapdoor settlements for both the greenfield and tests with a pipe present. The difference between the greenfield and pipe test deflection profiles became more prominent with an increase in trapdoor settlement. Larger settlements occurred after the addition of water modelling a leak.

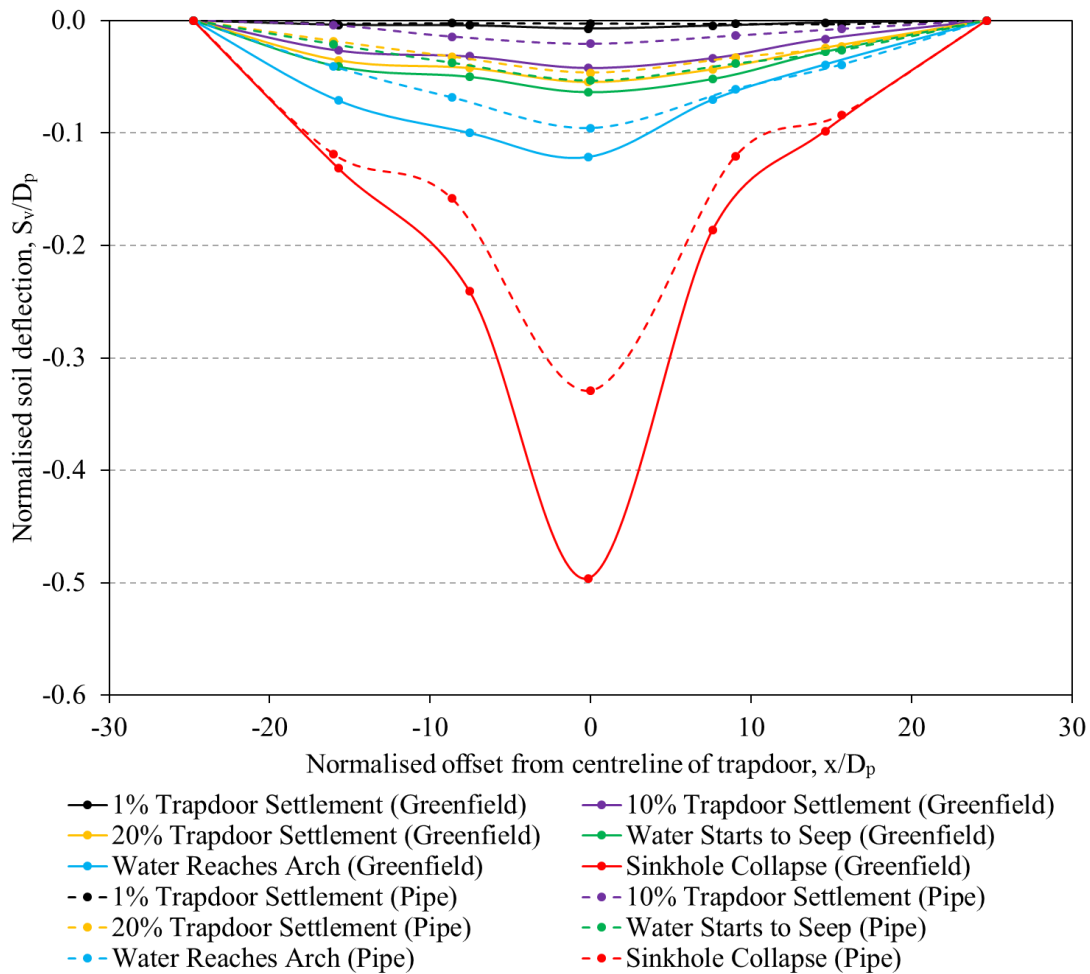


Figure 4-25: Invert level soil deflection – chert gravel

The deflection of the pipeline in comparison with the settlement of the soil at pipe invert level are presented in Figure 4-26. The pipe did not closely follow the greenfield soil profile, indicating that the pipe is neither behaving completely flexibly nor rigid, which satisfies the original assumption that the pipe can be classified between the flexible and rigid ranges. Due to soil behaviour being nonlinear, behaviour of a pipeline in soil may therefore vary from location to location. It can be seen from the graph that the pipeline approximately followed the greenfield soil profile at pipe invert at small trapdoor settlements. However, as the trapdoor settlement increased and as water was added to model a leak, pipe deflection started to deviate from the greenfield soil deflection. Deviation increased towards the centreline of the model. This indicates that the pipe behaviour became more rigid.

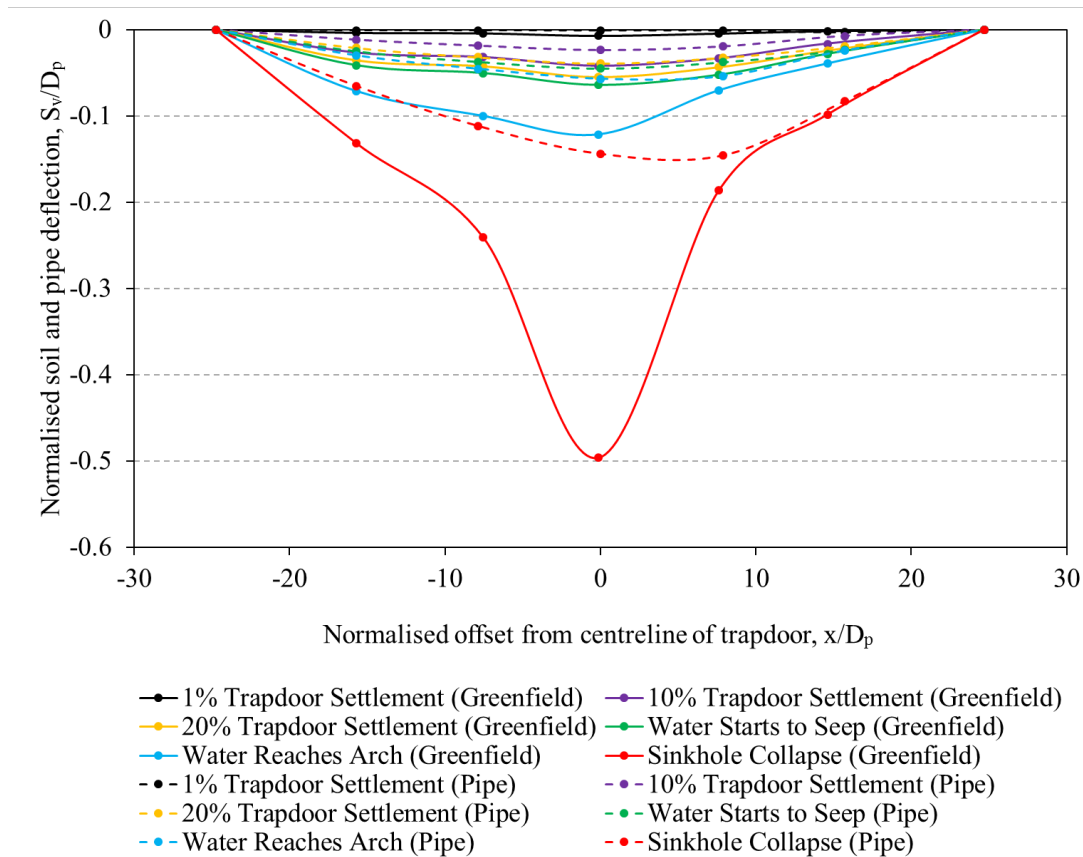


Figure 4-26: Pipe and invert level soil deflection – chert gravel

The difference between soil and pipe settlement is again illustrated by plotting the relative pipe-soil settlement. The relative pipe-soil settlement is plotted against the offset from the model centreline Figure 4-27. An increase in trapdoor settlement results in an increase in the relative pipe-soil settlement agreeing with Vorster et al. (2005) who reported that the magnitude of soil movement directly affects the relative pipe-soil settlement. However, for the chert gravel the relative pipe-soil settlement was not large due to cohesion between soil particles. The difference became greater after the addition of water modelling a leak.

The relative pipe-soil settlement values were negative, indicating that a gap formed (Vorster et al., 2006) between the pipeline and the underlying soil over the length of pipe show in the figure. This again implies that the vertical contact pressure reduced. As in the tests with silica sand, due to soil movement underneath the pipeline and the formation of a gap, the pipe was no longer continuously supported along its length, resulting in the pipe deflecting under the load of soil above the pipe. This induced additional strains and bending moments in the pipeline indicating the presence of a leak. For the chert gravel, the gaps were smaller in comparison to that experienced with the silica sand. This indicates that the type of soil plays a significant role in the behaviour of a pipeline due to ground movement.

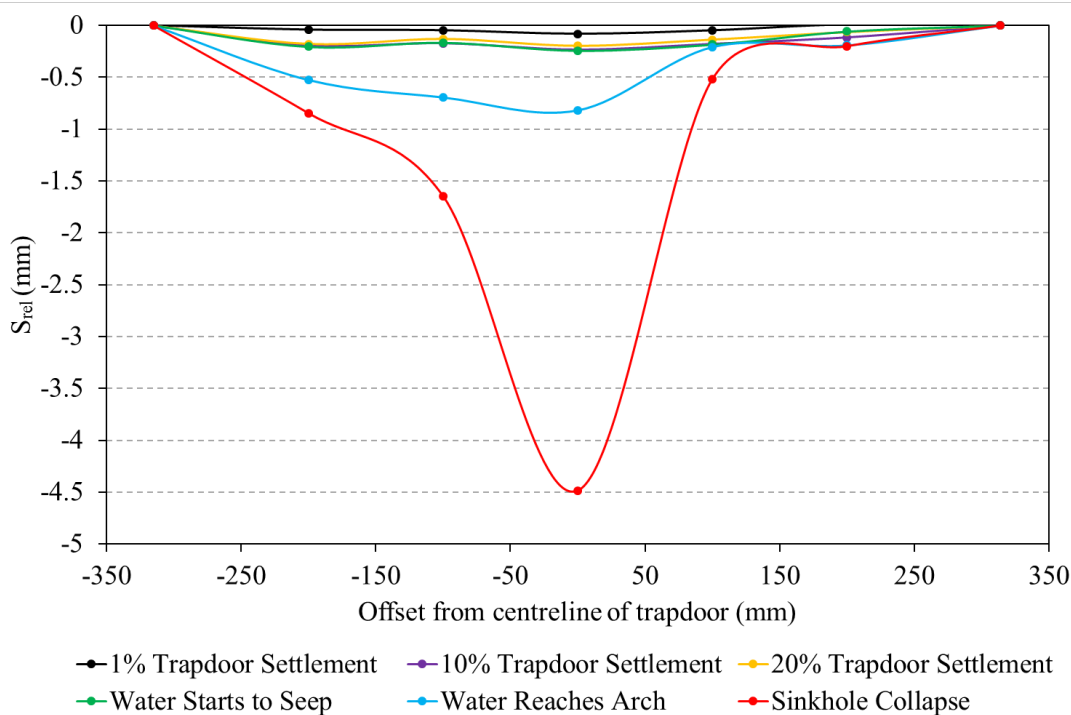


Figure 4-27: Relative pipe-soil settlement – chert gravel

4.6 Pipe strains from in-pipe pressure fluctuation

The pressure in most water distribution networks is not constant over time and fluctuates with time, depending on water use and supply characteristics. Such pressure fluctuations will result in mechanical strain changes in the walls of water distribution pipes. It is important that these strain changes must be distinguishable from changes resulting from a water leak. These strain changes were investigated in the centrifuge model and also in the field installation on the University's experimental farm

4.6.1 Centrifuge study

Figure 4-28 presents hoop strain changed recorded on the instrumented model pipe during the centrifuge test on the flexible pipe. The internal pressure in the pipe was varied as shown by the yellow curve on the secondary vertical axis. It can be seen that as the pipe pressure was increase after the start of the test, the hoop strains increase. After approximately 275 seconds, the leak test commenced as water was discharged to simulate a pipe leak. The point in time when the wetting front reached the pipe is indicated, which was immediately followed by large pipe strains considerably exceeding the strain from in-pipe pressure fluctuation. The strain recorded near the middle of the pipe was also of an opposite sign to that recorded to the left and right. It can be concluded that these strains were the result of

bending of the pipe, with sagging occurring the middle and hogging at the strain gauges away from the middle, matching the Gaussian settlement trough caused by the leak discussed in 4.4.1. The leakage-induced bending strain effects completely overshadowed the contribution from internal pressure fluctuation, with the latter just resulting in small perturbations in the overall strain trends recorded during the pressure fluctuations imposed towards the end of the test.

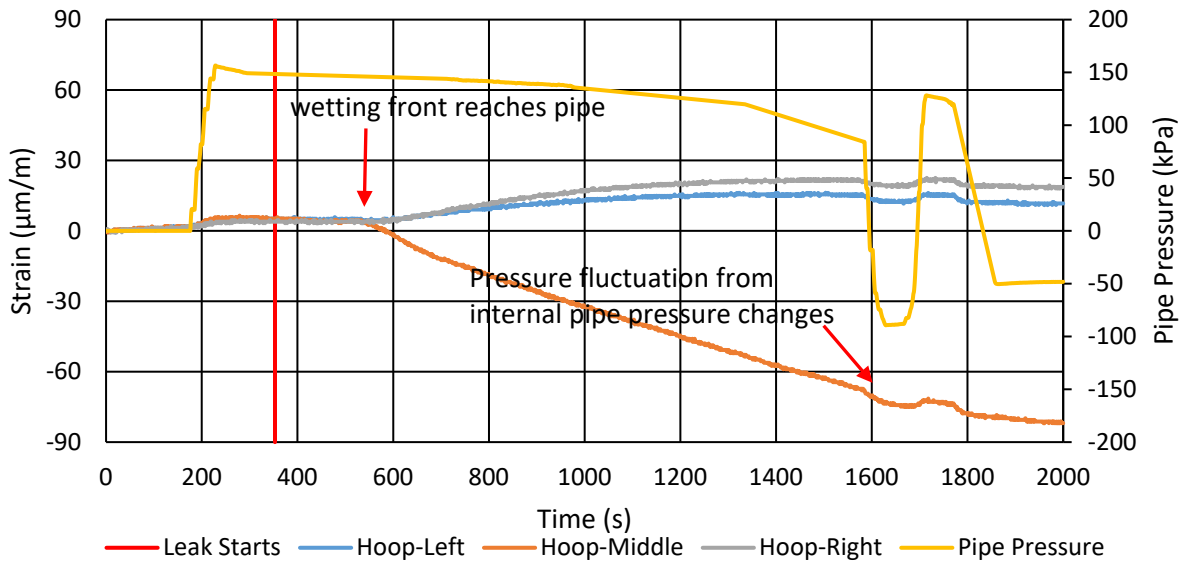


Figure 4-28: Pipe hoop strain during internal pressure fluctuation during a leak test studied in the centrifuge

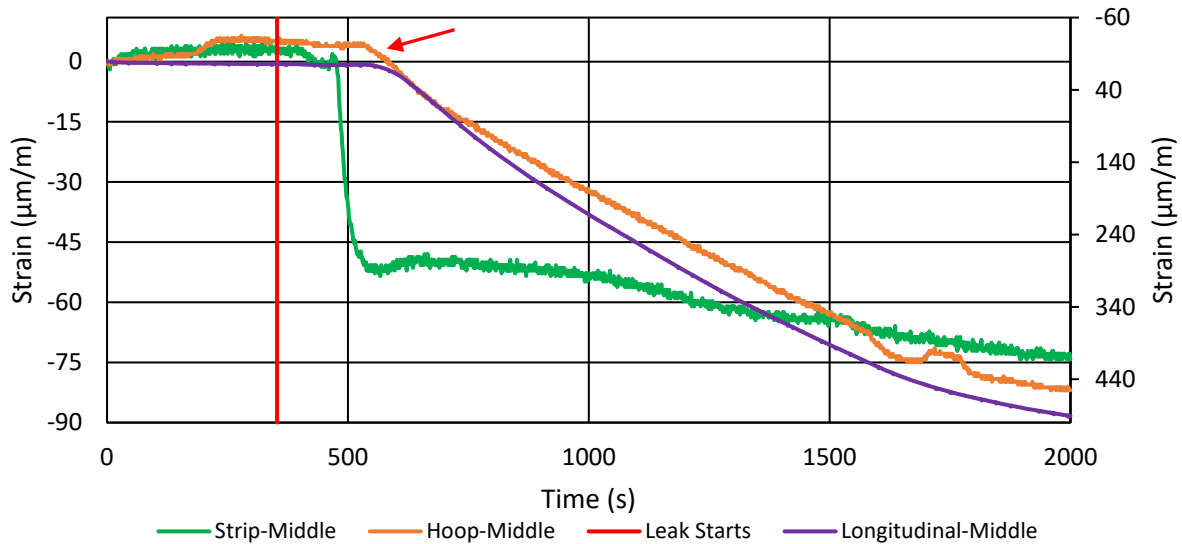


Figure 4-29: Longitudinal and hoop pipe strain during internal pressure fluctuation during a leak test studied in the centrifuge.

Figure 4-29 presents the hoop strain recorded at the middle of the pipe, as well as the longitudinal strain at this location. The green curve presents the strain recorded on the strain gauged brass strip on the secondary vertical axis. The instance of leak initiation is indicated

in red. It can be seen that as soon as the wetting front reach both the brass strip and the pipe, rapid strain change occurred. The strain changes were very much result of bending of the brass strip and the pipe as their magnitude are much than what would be expected from axial strains alone. The data demonstrates that the strain changes imposed by the settlement through resulting from inundation of the soil were substantial and easily measurable in the model. It is however difficult to estimate the likely magnitude of the strain changes as that would be a function of the pipe stiffness, the extent of the leak and the response of the ground to wetting which cannot easily be quantified beforehand. It therefore appears that a leak detection system should focus on the identification of change in strain rather than to look for pipe of ground strain of a certain magnitude to indicate a leak.

4.6.2 Field study

Figure 4-30 presents strain changes measured on the experimental pipe setup in the field during which the internal pipe pressure was incrementally raised and lowered, imposing three pressure cycles. It can be seen that significant strains of several hundred microstrain were generated in parts of the pipe due to the applied pressure cycles. The largest strains occurred near the middle of the 12 m length of pipe where a coupling allowed for a certain amount of freedom, permitting some axial deformation. Strains reduced away from the coupling where the pipe was longitudinally restraint by the surrounding compacted soil. The maximum strains were large and of a similar magnitude to the pipe strains imposed by the leak demonstrated above.

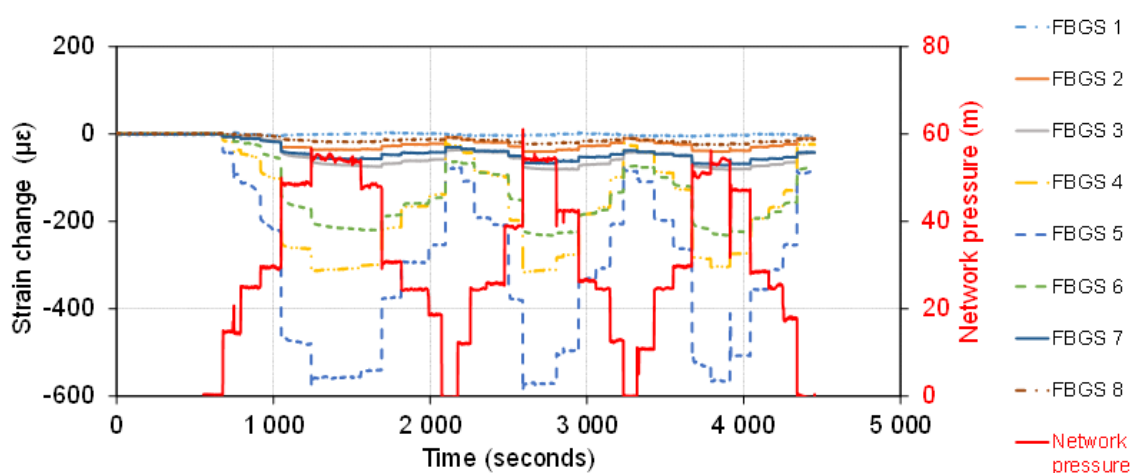


Figure 4-30: Strain changes measured by the epoxied FBGSs during internal pressure fluctuations.

Figure 4-31(a) presents strain changes measured in the ground during the same pressure cycles described above at a location where no water had been leaked before, i.e. where the

ground had not yet been saturated by a leak test. It can be seen that pressure fluctuations resulted in minimal strains being registered, so that the FBGSs were essentially not affected by the pressure cycles.

Figure 4-31(b) presents strain changes from an area that had been affected by a previous leak, i.e. where the soil was saturated or at least partially saturated. Substantially greater strains were measured in response to the pressure fluctuations compared to what was observed in the unsaturated soil (Figure 4-31(a)). Saturation of the soil would have resulted in displacement of much of the soil pore air content by water, resulting in a less compressible medium. Due to the increased volume rigidity of the saturated soil, the pipe pressure cycles manifested more clearly, imposing much larger strains of up to approximately 8 microstrain on the FBGSs.

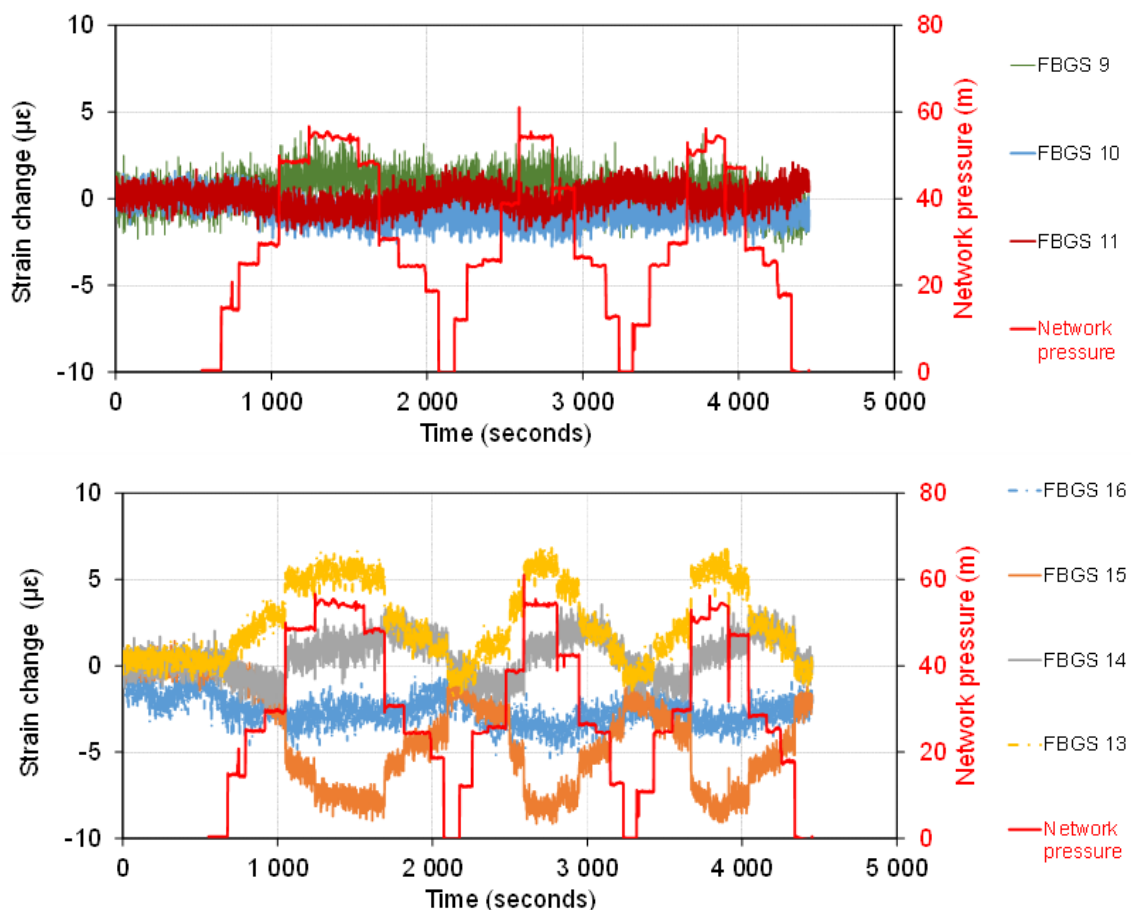


Figure 4-31: Strain changes measured by the free FBGSs in the ground during internal pressure fluctuations in the pipe in (a) unsaturated soil and (b) saturated soil.

It can be concluded that internal pressure fluctuation can result in pipe strain changes amounting to many hundreds of microstrain. Also, the strain changes are not easily predictable as they vary along the length of the pipe depending of the variation in the

confinement of the pipe along its length. The degree of confinement is not easily quantifiable in the field. However, it can be seen that in-pipe pressure variation had minimal influence on ground strains near the pipe, especially in the case of soils which had not previously been saturated. Even in soil which had previously been saturated, the strain changes from in-pipe pressure variation were small, amount to less than 10 microstrain. It therefore appears that leakage-induced strain changes should be monitored in the ground, as ground strains are highly sensitive to water leaks in unsaturated ground as shown by the field and centrifuge test results.

4.7 The effect of pipe stiffness on strain response

Calculations, complimented by model tests, were carried out to assess the length of pipe over which leakage-induced strain influences will be transferred along a pipeline by means of bending. This serves as an indication of the spacial frequency at which pipe behaviour should be monitored to observe leakage-induced strains on pipes of various stiffness.

4.7.1 Relative rigidity of pipe-soil system

One aim of this study was to investigate soil-pipe interaction for relative rigidity values from 0.1 (perfectly flexible) to 5 (perfectly rigid) for the two soil types (silica sand and chert gravel). Vorster et al. (2006) mentioned that the greenfield i -value is not only affected by the depth of pipe invert, but also by an increase in ground movement. The trough width was calculated from the representative greenfield soil profiles, and amounted out to approximately 50 mm for both soil types. The soil stiffness (E_s) of the sand and chert gravels were measured by means of oedometers tests at approximately 40 MPa and 20 MPa respectively.

After consideration of the various parameters mentioned above, the relative rigidity of the pipe-soil system could be calculated, assuming bending only. By applying the formula set up by Klar et al. (2004) the relative rigidity factor for the two soil types were as follow, and can be seen in Table 4-6.

Table 4-6: Relative rigidity of pipe-soil system in model test

Pipe	Soil type	E_s	r_0	i (mm)	R
Stiff	Silica sand	40	6.36	50	1.13
	Chert gravel	20	6.36	50	2.26
Flexible	Silica sand	40	5.30	50	0.96

It should be noted that for both cases, the pipeline falls within the intermediate zone, having approximately the same relative rigidity factor, based on Vorster et al. (2006) predictions, meaning that the pipeline will neither behave flexible, nor will it behave rigid. Despite efforts to fabricate a more flexible pipe, it was not possible to reduce the relative rigidity of the model pipes to less than 0.96.

Subsequently it was decided to calculate the likely ranges of relative rigidity values of commercially available uPVC and steel pipe in the field using Equation 2-13, repeated below:

$$R = \frac{E_p I_p}{E_s \cdot r_0 \cdot i^3}$$

It can be seen that increasing the pipe stiffness will increase the relative rigidity of the pipe-soil stiffness while increasing the soil stiffness, pipe radius and/or width of the leakage-induced settlement trough will reduce the relative rigidity. Figure 4-32 presents zones indicating relative flexibility as a function of pipe radius (r_0) and the leakage-induced trough width parameter i . The width of the zones indicating relative rigidity values of 0.1 and 5 respectively represents the range of wall thicknesses available for pipes of various radii. It can be seen that both for uPVC and steel pipes leakage-induced trough widths need to be very narrow for the pipes to classify as rigid. Pipes are therefore likely to behave in a flexible or semi-flexible manner in response to leakage-induced ground movement because the effects of a prolonged leak is likely to spread, widening the settlement trough. Because of the flexible behaviour, leakage-induced bending strains will not be transmitted far from the point of leakage. This suggests that strain monitoring discrete locations will be less effective because the effect of a leak will result in localised straining of a pipe, illustrating a need for distributed strain monitoring.

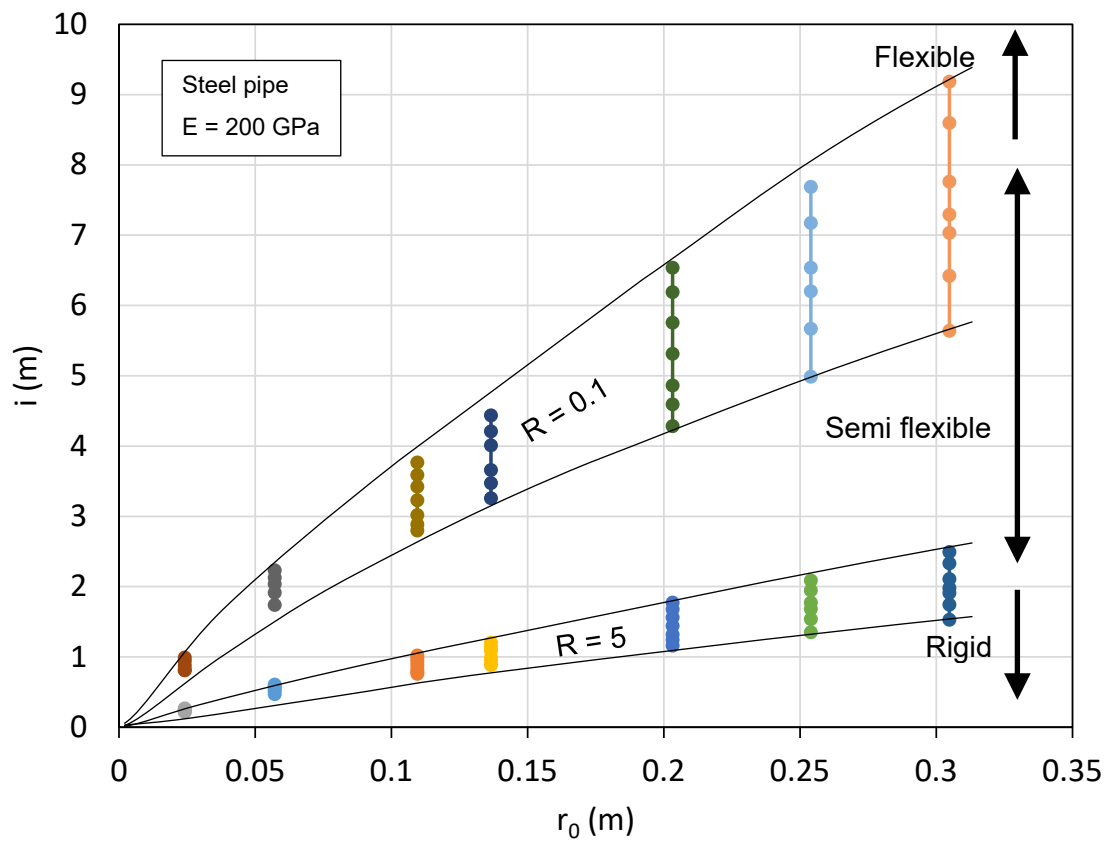
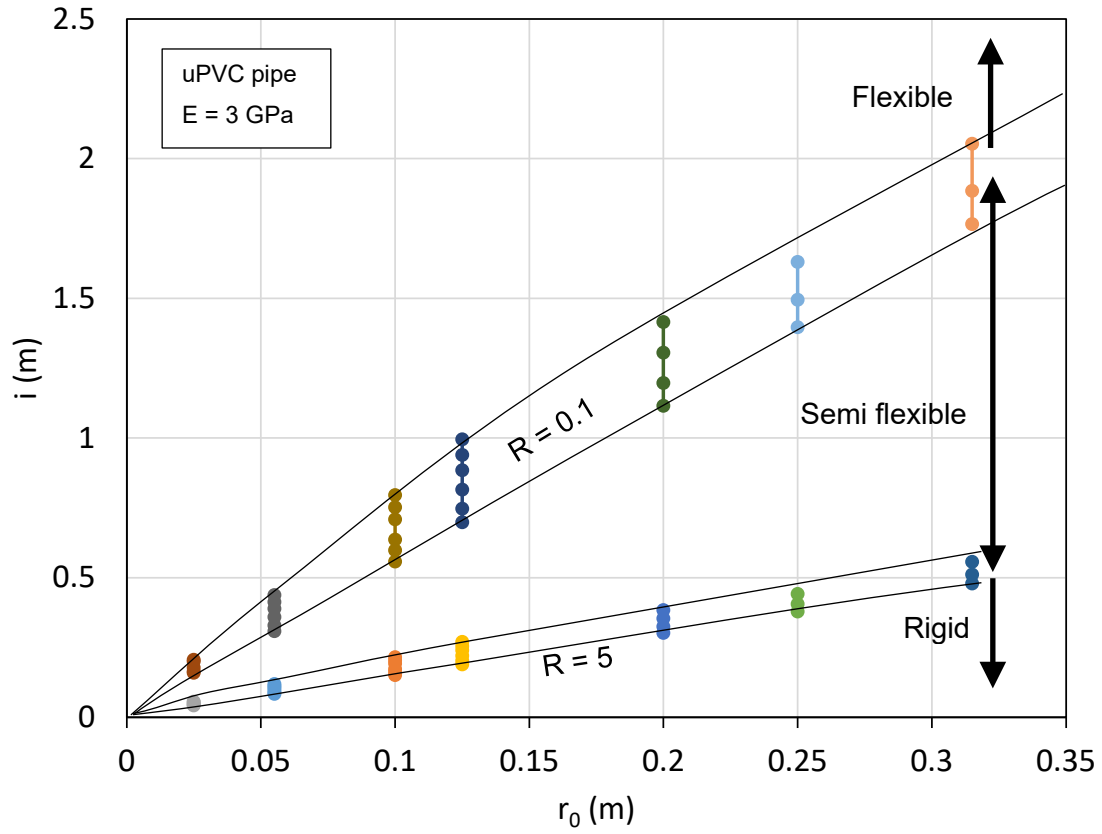


Figure 4-32: Relative flexibility classification of uPVC and steel pipe of different radius and leakage-induced trough width parameter (i)

4.8 Discussion

The introduction of water into unsaturated or dry soils changes the stress regime in the soil by creating or changing pore water suctions in the soil. This results in a change in the effective stress in the soil and therefore induces soil strains and hence measurable deformations. Observing these deformations is the principle on which the proposed leak detection system operates.

At the onset of the centrifuge model study it was planned to assess the relative rigidity of the soil-pipe system and to use this as a guideline for the determination of the spatial interval at which strain should be measured using discrete strain measurement on pipelines. Pipes of two different stiffness values and two different soil types (silica sand and chert gravel) were therefore used to investigate this behaviour over a range of stiffness values. Results from the study showed that relative rigidity of the pipe-soil system is not an important consideration for practical leak detection systems because:

- For practical field leakage detection installations, it is not be practical to use discrete strain measurement as a means of leak detection because the number of strain measurements possible per optic fibre is limited. Only short lengths of pipe can therefore be monitored using discrete monitoring locations. Instead, for useful field installations, distributed strain measurement technology will be required. The performance of such system should be investigated in a follow up study.
- The relative rigidity of a soil-pipe system is highly dependent on the stiffness of the soil around the pipe and this will be significantly influenced by the standard of compaction and the uniformity of backfill and pipe bedding material and these factors cannot be easily quantified in the field. It is therefore not possible to accurately calculate the interval at which discrete strains should be monitored, further illustrating the need for using distributed strain technology.
- The exact value of strain induced by a leak is not of interest, but rather the fact that a sudden strain change had occurred. Due to non-uniformity in system stiffness along the length of a pipe and because of the variable strains that can be imposed by the water leak, exact strain changes cannot be predicted with confidence. Sudden changes in strain should be flagged as a potential water leak and should be investigated.

Leakage-induced soil strains result in ground deformations which induce significant strain changes in pipes buried in the ground. However, internal pressure fluctuations in pipelines also result in significant pipe strains. It is likely to be difficult to distinguish the two types of strain from one another which may trigger false leakage alarms. Based on the information presented here, it is therefore not ideal to rely on pipe strains as a means of leak detection. Also, attaching a sensing cable to a pipe during pipeline construction is undesirable as it complicates the construction process and the cable will be prone to damage.

It was found that strains recorded using a fibre optic cable buried in relative close proximity to the pipe (i.e. in the same pipe trench) were not sensitive to in-pipe pressure fluctuation, while they were highly sensitive to record strains induced by a water leak. It therefore appears that the most practical means of leak detection is the detection of ground strain in close proximity to the pipe. In the installation considered in this study, the sensing fibre optic cable was installed in the pipe trench corner. It is considered likely that a fibre optic cable buried in close proximity, but above the pipe, may also react to leakage-induced ground strains as some ground movement is likely to occur due to a leak. This will enable the leakage detection system to be retrofitted to existing pipes by burying a cable in close proximity to the pipe. It is recommended that such an installation be field tested using distributed strain measurement technology.

5 LONG TERM FIBRE OPTIC STRAIN MEASUREMENT AND LEAK DETECTION

5.1 Introduction

The installation of fibre Bragg gratings (FBGs) on the short length of pipeline installed on the Hillcrest Campus of the University of Pretoria was monitored from January to December 2018 to gain an understanding of natural long term variation in strain recorded on an installed pipe as well as strain recorded on a free-floating fibre optic cable in the ground. This is important because natural strain variation can be expected due temperature fluctuation as well as rainfall. It is necessary that leakage-induced strain changes must be distinguished from natural occurring changes. In addition, a leak was imposed in September 2018 and its influence on the measured strains was studied.

5.2 Strain calculation using Bragg gratings

The change in wavelength recorded by a fibre Bragg grating ($\Delta\lambda$) is given by the following expression:

$$\frac{\Delta\lambda}{\lambda} = (1 - p_e) \cdot \varepsilon + (\alpha_\Lambda + \alpha_n) \cdot \Delta T \quad \text{Equation 5-1}$$

Where λ is the Bragg wave length, p_e the strain-optic coefficient, ε the strain experienced by the optic fibre, α_Λ the change in refractive index of the fibre with temperature and α_n the thermal expansion coefficient of the fibre. For the particular type of fibre used in this study the following parameter values are applicable:

$$p_e = 0.22$$

$$\alpha_\Lambda = 6.5 \times 10^{-6} \mu\varepsilon/^\circ\text{C}$$

$$\alpha_n = 0.5 \mu\varepsilon/^\circ\text{C}$$

Strain from fibre Bragg gratings ε are calculated using the above expression. It is evident from the above that, in order to calculate the correct strain, the variation in temperature at the strain measurement location must be known. However, in order to detect leaks in the context of this study the exact strain values if not of interest, but rather changes in strain. By simply taking the change in wavelength measured by a given FBG and dividing that number its wavelength

a suitable indicator of strain change is obtained differing by a factor from the actual strain change that can be assessed using Equation 5-1.

5.3 Pipe and ground strain variation

Figure 5-1 presents the variation in strain recorded by FBGs epoxied to the 12 m long 100 mm diameter uPVC pipe installed on the Hillcrest campus of the University of Pretoria as described in Chapter 3. Figure 5-2 presents the strain variations recorded on the length optic fibre free floating in the ground parallel to the pipe. The location of the various FBGs are indicated in Figure 5-3. The daily rainfall recorded during the study period by a weather station on the main campus of the University of Pretoria, 1 km from the site, is plotted on the secondary axes.

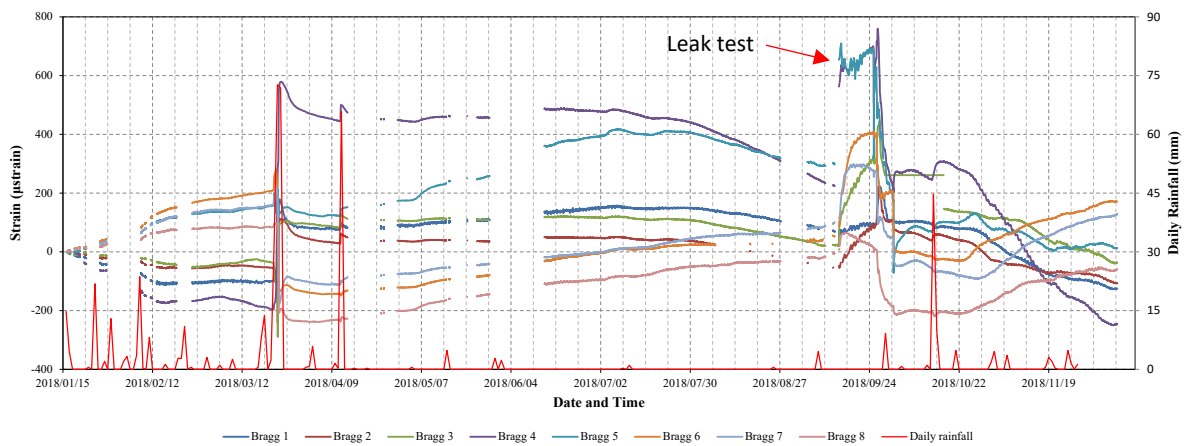


Figure 5-1: Variation in pipe strain during 2018

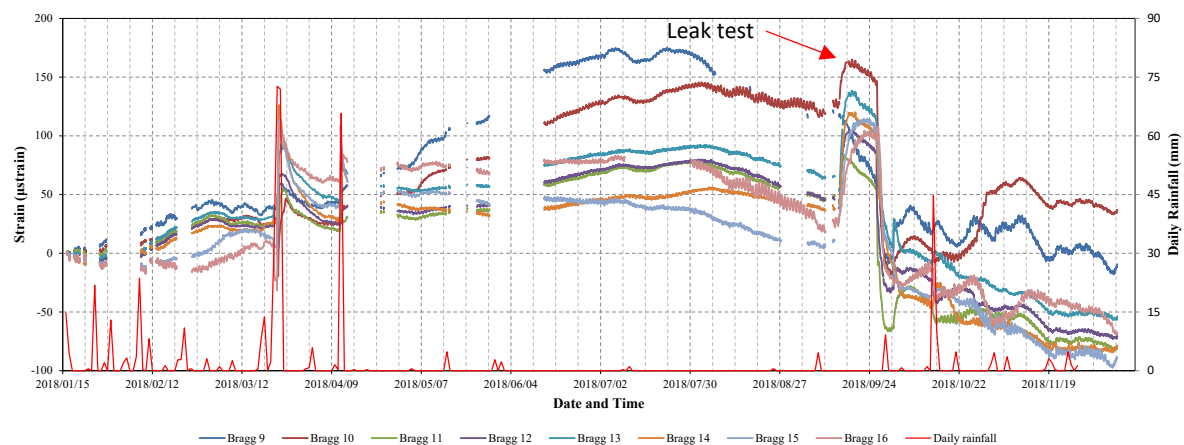


Figure 5-2: Variation in ground strain during 2018

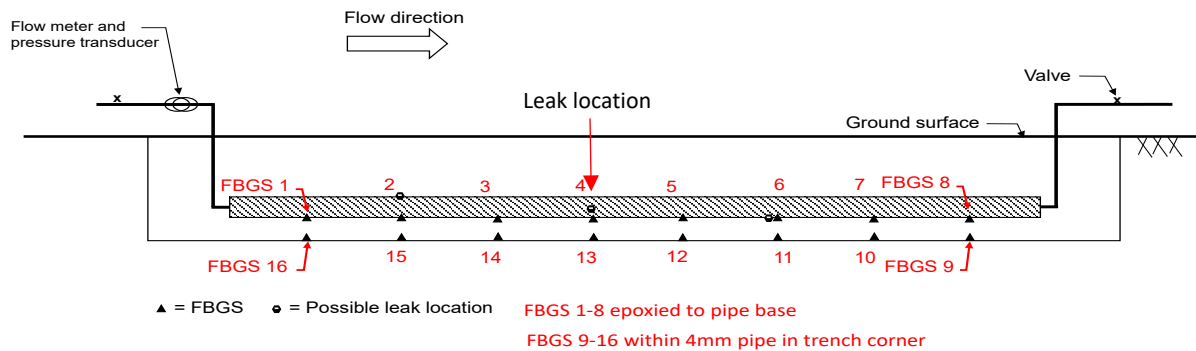


Figure 5-3: FBG location in experimental pipe installation

Examining the variations in strain between the two figures above reveals that the strain changes experienced by the FBGs mounted to the pipe were significantly larger than the strain changes recorded by the free-floating FBGs. These changes are attributed to bending of the pipe due to changing load conditions associated with water infiltration after rainfall, settlement of the ground in the pipe trench and temperature changes. It should be kept in mind that a concerted effort was made to isolate the free floating FBGs by placing the fibre optic cable in a thin tube filled with oil. Despite this, the free floating length of fibre clearly underwent significant strain changes.

During most of the year a relatively smooth variation in strain was observed. However, major rainfall events, exceeding approximately 40 mm in daily rainfall, had a significant effect on both the strain on the pipe, as well as in the ground, while no effect was evident from more minor events. This indicates that the rainfall record has to be consulted when using strain measurements to assess the occurrence of a pipe leak.

The substantial strain deviation recorded at the end of September, shown both figures was the results of a leak test and is considered in more detail below.

5.4 September 2018 leak test

Figure 5-4 below presents the flow rate and internal pipe pressure during a leak test imposed at leak location 2 (see Figure 5-3) from 14 September to 2 October 2018. The leak was initially imposed at a rate of approximately 30 litres per hour, a slow leakage rate. After approximately 12 days, the rate was increased approximately ten-fold to just under 300 l/hour and maintained for 6 more days. The pressure head fluctuation demonstrates daily pressure cycles in response to variations in demand in the network.

Figure 5-5 presents the strain record measured by FBGs epoxied to the pipe over the duration of the leak, with Figure 5-6 presenting the equivalent data recorded by the free-floating optic fibre. It can be seen the strain response was immediate following onset of the leak, with the most rapid change in strain closest to the leak location (FGBs 4 and 5 in Figure 5-5 and FGBs 13 and 14 in Figure 5-6). The measured strain shows some variation due to in-pipe pressure fluctuation, but the effect was substantially smaller than the strains caused by the leak.

The change in strain is shown more clearly in Figure 5-7 and Figure 5-8, presenting strain values zeroed on the day before the onset of the leak test. Comparing Figure 5-7 and Figure 5-8, plotted at the same scale, shows that the magnitude of strain change on the pipe was substantially larger than in the ground. However, despite efforts to isolate the part of the optic fibre in the ground from mechanical strain, it still clearly responded to the leak indicating the potential of using ground strain as a sensitive parameter for indicating a potential leak. Figure 5-9 is a copy of Figure 5-8 but at an increased vertical scale. It can be seen that the strain effect was first detected closest to the leak point, but that the effect soon spread outwards so that it was evident along the entire length of pipe monitored.

The approximately ten-fold increase in the leakage rate on 26 September is evident on the strain records. However, the effect was smaller than what might have been expected given the large strain change associated with the first leak, especially when considering the high leakage rate subsequently imposed. The reason for this is believed to be related to the fact that, by the time that the leakage rate was increased, the soils around the pipe were approaching saturation so that the change in pore water suction, and hence strain change in the soils resulting from the increase in leakage rate, was relatively small. It is interesting to note that the change in strain was in the opposite sense to that resulting from the initial leak. It is believed that this is related to buoyant forces trying to float the pipe after the first stage of the leak tests during which the downward load on the pipe might have increased due to saturation of the surrounding ground. Observed strains continued to change over the duration of the leak test although they tended to stabilise with time. The end of the leak test was also accompanied by a strain change and values tended to gradually stabilise to a new baseline.

In terms of parameters for leak detection, it appears that both pipe and ground strain data can be examined for sudden and substantial slope changes, with the most sensitive responses likely to be detected upon first wetting of the soil after formation of the leak. This means that early leak detection is possible, enabling mitigation measures to be implemented before much water loss or damage had occurred.

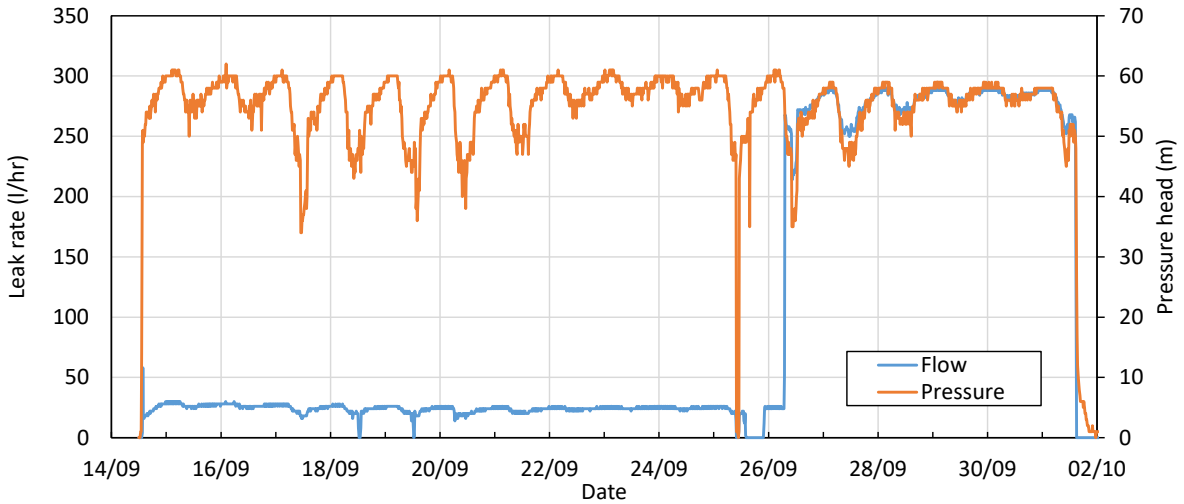


Figure 5-4: Flow rate during the September 2018 leak test

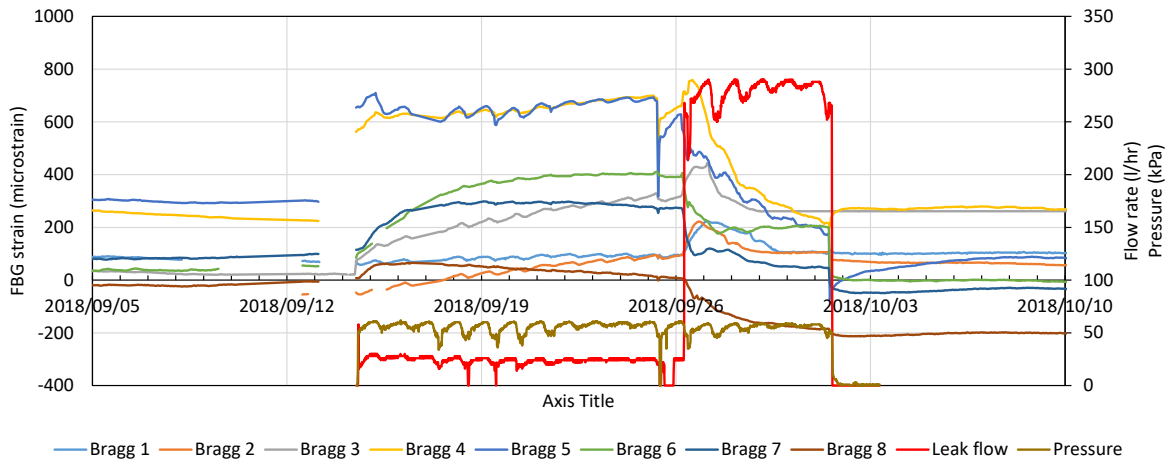


Figure 5-5: Strain readings from FBGs fixed to pipe during the September 2018 leak test

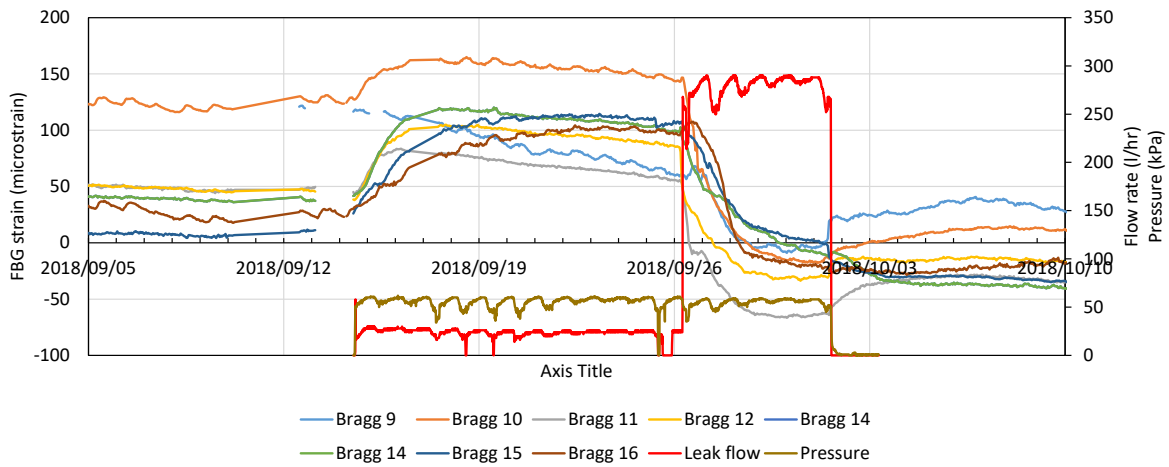


Figure 5-6: Strain readings from free-floating FBGs during the September 2018 leak test

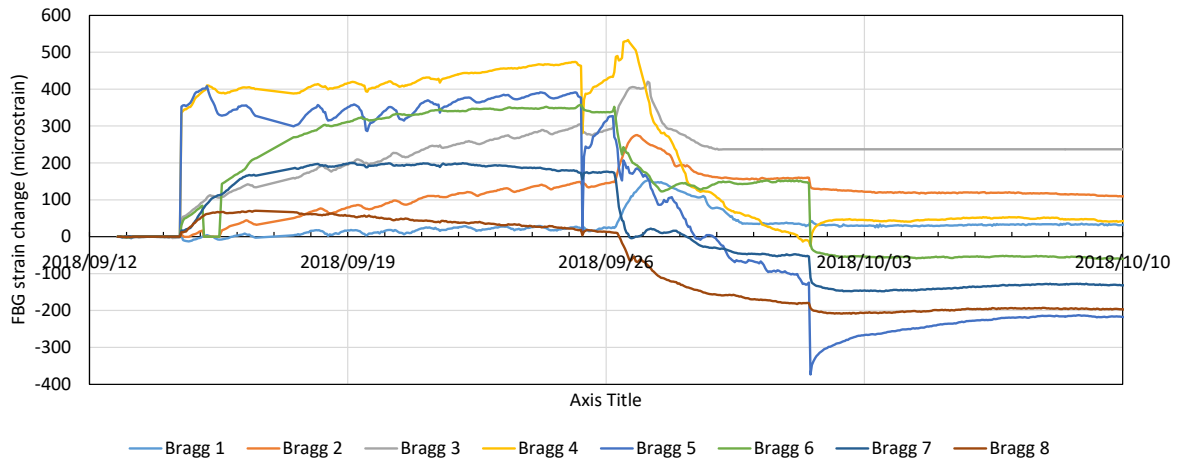


Figure 5-7: Zeroed strain readings from FBGs fixed to pipe during the September 2018 leak test

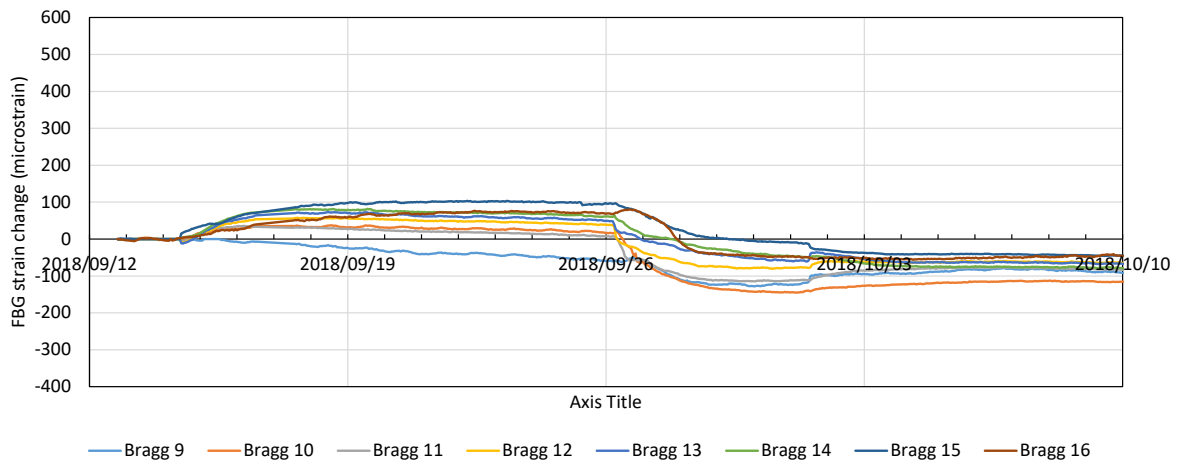


Figure 5-8: Zeroed strain readings from free-floating FBGs during the September 2018 leak test

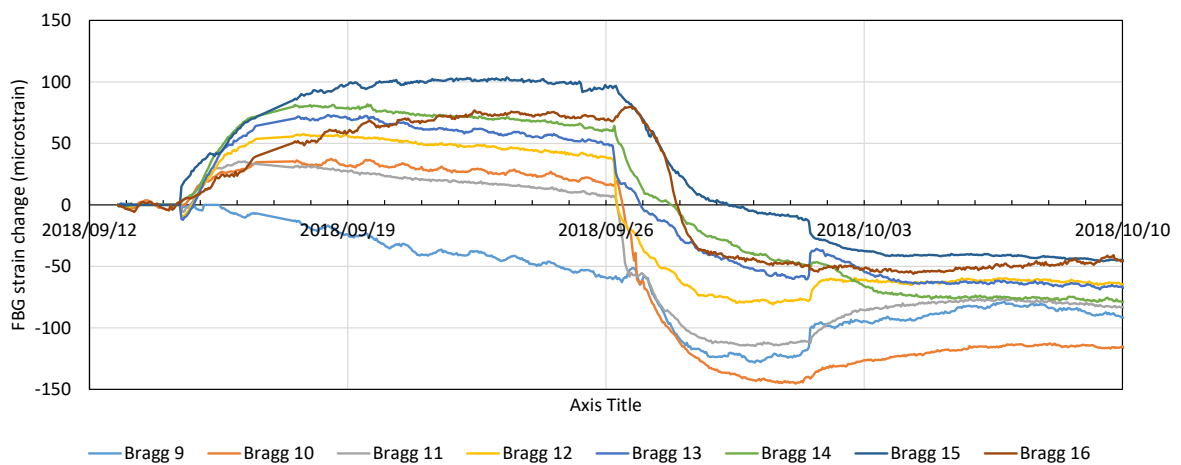


Figure 5-9: Zeroed strain readings from free-floating FBGs during the September 2018 leak test (enlarged scale)

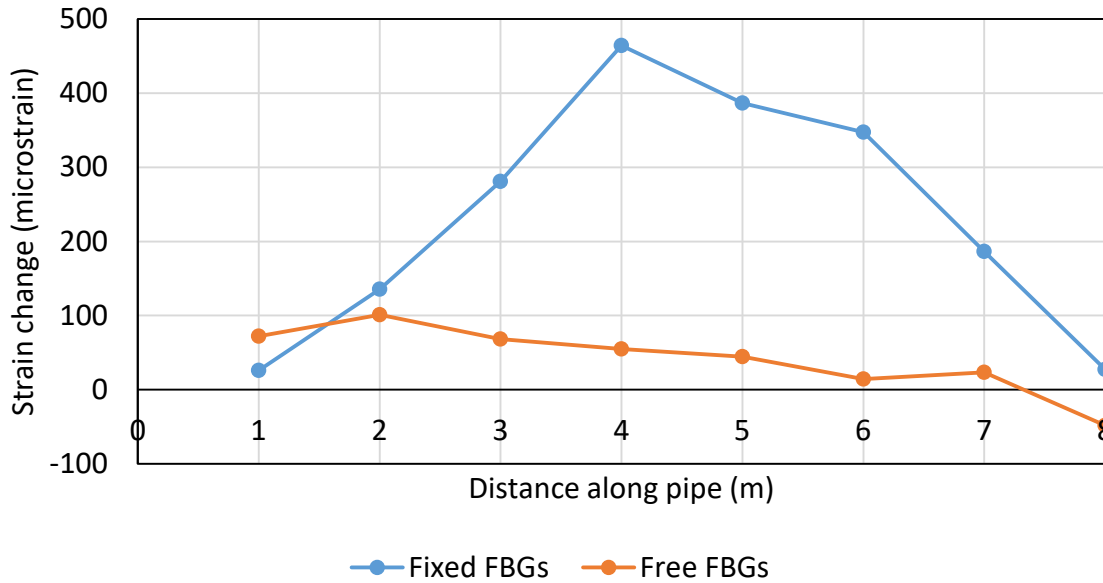


Figure 5-10: Spatial distribution of leakage-induced strain along pipeline.

Figure 5-10 presents the variation of leakage-induced strain changes along the length of the pipeline measured on the pipe and in the ground respectively. It is evident that the maximum leakage-induced pipe strains were mobilised at the leak location and that strain reduced with distance away from the leak. Leakage-induced ground strain seemed to gradually reduce with distance along the length of the pipe and may be related to the slope of the pipe trench with water tending to flow towards the left in Figure 5-10 above.

5.5 Strain changes during significant rainfall events

It was mentioned in Section 5.3 that major rainfall events also affect strain readings recorded by FBGs in the ground and fixed to a pipe. Figure 5-11 presents strain readings recorded by FBGs fixed to the pipe during and after the significant rainfall event of March 2018 illustrated in Figure 5-1. Figure 5-12 presents similar data for the free-floating FBGs. Minor rainfall events did not seem to affect the strain readings. However, significant strain changes were caused by the rainfall which occurred from 21 to 23 March during which 179 mm of rain fell in three days. This resulted in wetting to significant depth. The pipe was installed in July 2017 and this rainfall event was by far the most significant event since installation and probably resulted in the first wetting of the material at the depth of the pipeline. Looking at the locations where strains of different magnitudes were observed it seems, the distribution of strain with distance along the pipe seems to be random.

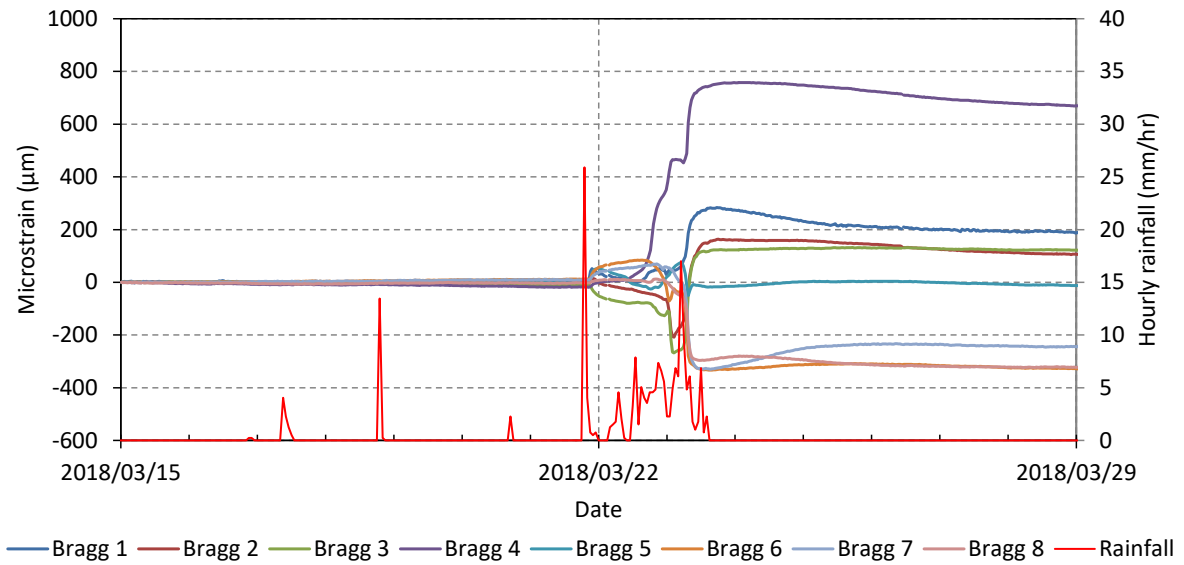


Figure 5-11: Zeroed strain readings from FBGs fixed to pipe during the March 2018 rainfall event

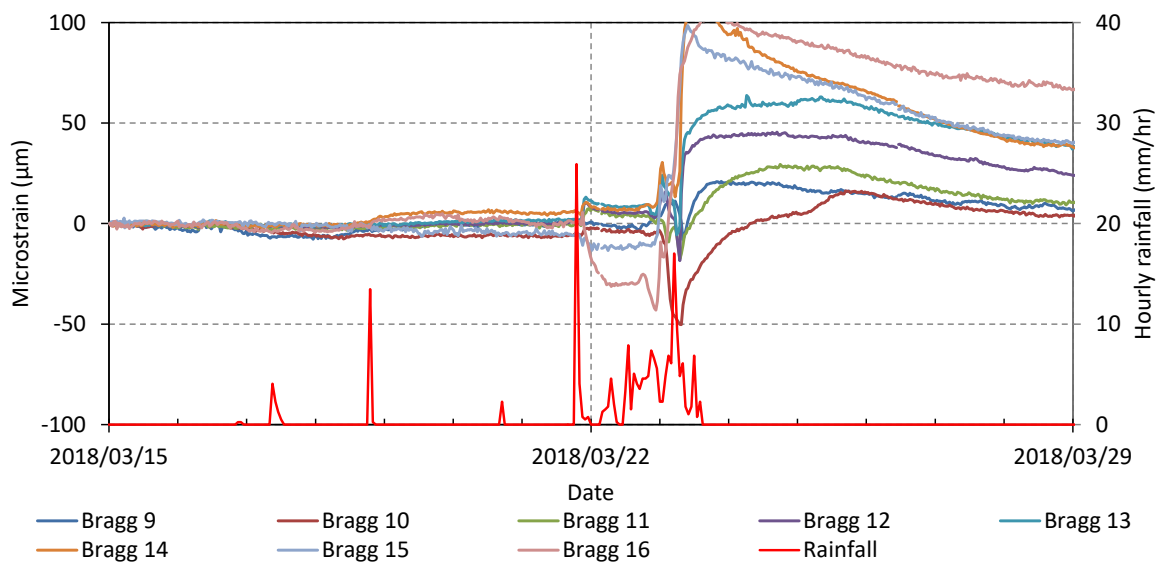


Figure 5-12: Zeroed strain readings from free-floating FBGs during the March 2018 rainfall event

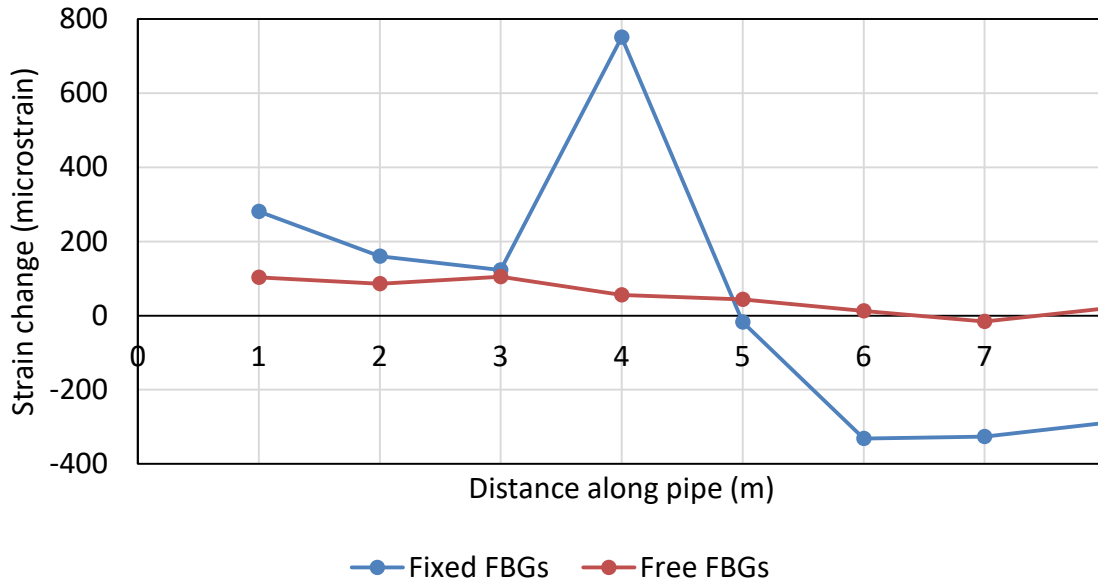


Figure 5-13: Spatial distribution of rainfall induced strain along pipeline.

Figure 5-13 presents the variation of rainfall-induced strain changes along the length of the pipeline measured on the pipe and in the ground respectively. A more random distribution in pipe strain is evident than in the case of leakage-induced strain, indicating that the strain changes are not associated with a specific leak location (although the maximum strain was coincidentally recorded close to the leak location). In terms of the ground strain, strain tended to increase towards the left in Figure 5-13 above as in the case of the leakage-induced strains. Again this is thought to be related to the slope of the pipe trench, encouraging seepage to flow as directed by the slope of the pipe trench.

5.6 Comparison between thermal and mechanical leakage-induced ground strains

At the conception of this project it was hypothesised that leaks could be detected by identifying temperature changes in the ground resulting from water leaking from a pipe. However, it was found that wetting up of the unsaturated soil around the pipe due to a water leak resulted in large strains which may present a more sensitive parameter of leak detection than temperature measurement. This section draws a comparison between leakage-induced thermal vs mechanical strains. At two locations along the length of the experimental pipeline thermistors were installed next to free floating FBGs which allow thermal strains to be independently calculated as explained in Section 5.2 and compared to the FBG-measured strain.

Figure 5-14 and Figure 5-15 present thermal and mechanical strains measured over the duration of the Sept 2018 leak test. The leakage flow rate is shown on the secondary vertical axes. The strain were zeroed at start of the leak test. The thermal strains represent calculated thermal strain measurements that would have been recorded by the FBGs in the absence of mechanical strain. They were calculated from the product of the thermistor-measured change in temperature with the sum of the temperature dependent refractive strain index (α_Λ) and thermal expansion coefficients of the cable (α_n), i.e. $(\alpha_\Lambda + \alpha_n) \cdot \Delta T = 7E-06 \cdot \Delta T$ (see Section 5.2). It is evident from Figure 5-14 and Figure 5-15 that the change in magnitude of the mechanical strain due to the leak were approximately five times larger than the change in calculated thermal strain which demonstrates that in unsaturated ground leakage-induced mechanical strain is a more sensitive parameter for leak detection than thermal strain. Also, the change in mechanical strain is more rapid than for thermal strain, implying that leaks can be detected earlier when using mechanical strain.

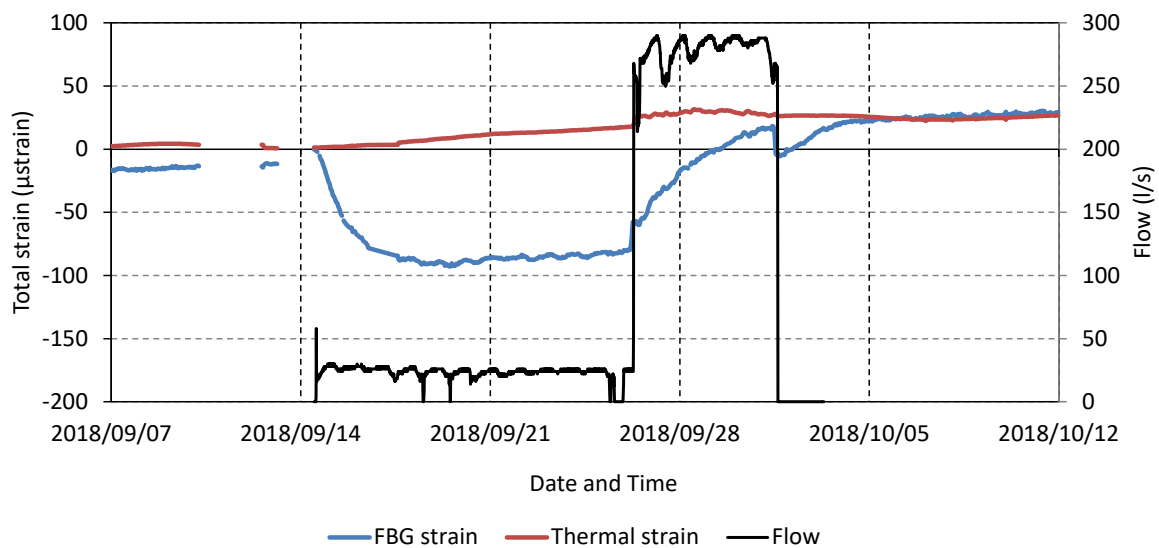


Figure 5-14: Variation in mechanical and thermal leakage-induced strains during the Sept 2018 leak test at FGB 13.

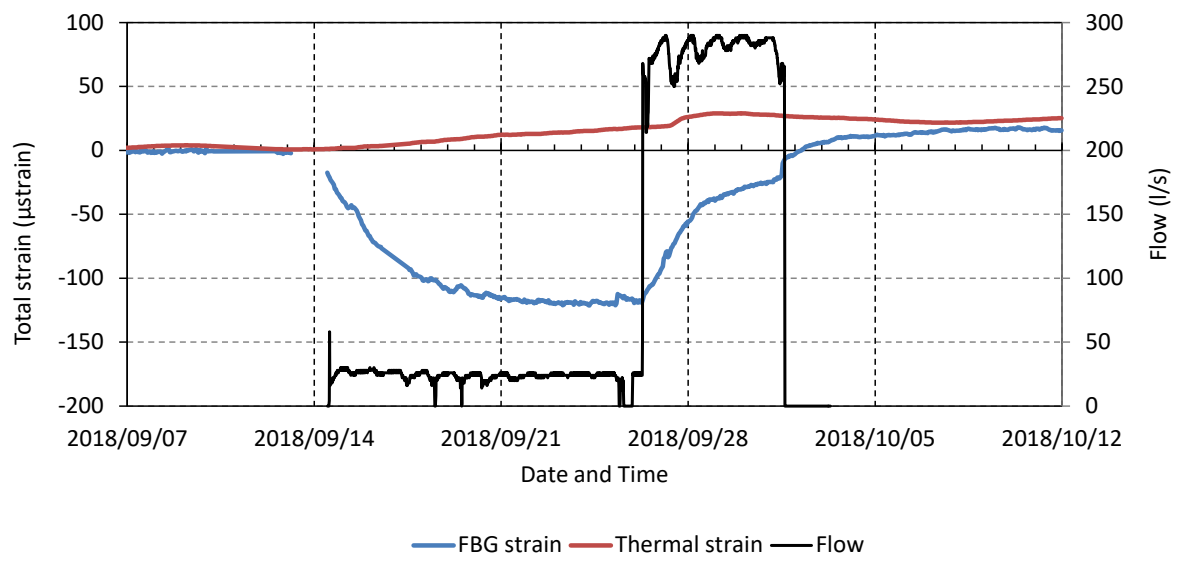


Figure 5-15: Variation in mechanical and thermal leakage-induced strains during the Sept 2018 leak test at FGB 15.

6 CONCLUSIONS

The following conclusions are presented:

A water pipe leak results in a significant ground strains and hence soil movement which can be measured using fibre optic strain measurement. In unsaturated soils the strain effects were found to far exceed the temperature effects and therefore potentially provide a more sensitive means of leak detection if leakage-induced ground strains rather than leak-induced temperature changes can be detected. A literature and patent search was conducted but reports making use of ground strain as a means of leak detection was not found.

A water leak induces significant strains in the leaking pipe due to ground deformation. This exerts additional load on the leaking pipe and changes the pipe support conditions. These strains are easily detected using strain sensors attached to the pipe. However, internal pressure fluctuations also result in significant strain changes so that it may be difficult to distinguish leakage-induced strains, especially since both types of strain are influenced by the degree of confinement of the pipe which will vary along its length due to differences in workmanship during construction and ground properties. Despite this potential difficulty, strain changes from in-pipe pressure fluctuation during a leak test over 18 days showed that leakage-induced stress changes far exceeded those from pressure fluctuation. However, in terms of a practical leak detection system it is preferred to measure leakage-induced ground strains rather than pipe strain due to the difficulty of securely attaching a fibre optic cable to a pipe on a construction site. A potential solution to this problem is discussed under recommendations for further work in Section 7.1.

A water leak induces significant strain and hence deformation in unsaturated ground associated with wetting. These strains can easily be detected using a fibre optic cable detached from the pipe, buried in close proximity to the pipe. A fibre optic sensing cable detached from the pipe is also not prone to pressure fluctuation in the pipe and should therefore not give false alarms. It is therefore proposed that the most practical leakage detection system for newly installed pipes should comprise of a fibre optic cable buried near the pipe in the same pipe trench. This fibre optic cable can then periodically be monitored for strain to detect potential leaks

Field and model testing described in this report showed that the relative rigidity of the combined soil-pipe system, which was initially thought to be important to consider as it would affect the spacing of strain sensors on the leaking pipe, is not a concern. The main reason is

that the envisaged leakage detection system will rely on distributed strain measurement and not measurements at discrete locations as this limits the use of such a system to short pipe lengths.

Due to variation in the relative rigidity (stiffness) of the soil-pipe system along its length due to variation in material properties, pipe bedding support, compaction of backfill and other factors, it is difficult to predict the strain change that is likely to occur in the ground or in the pipe itself due to a leak. This is, however, not a concern as the indicator of a potential leak is a sudden change in strain rather than actual magnitude of the strain measurement.

A fibre optic cable buried in close proximity above a pipe may react to leakage-induced ground strains as some ground movement is likely to occur due to a leak. This may enable a leakage detection system to be retrofitted to existing pipes by burying a cable in close proximity to the pipe. It is recommended that such an installation be field tested using distributed strain measurement technology. A practical constraint of retrofitting is the need to trench to near the pipe to install the fibre optic cable and this is not desirable in the urban environment due to the presence of services in the ground and the associated inconvenience.

The long term behaviour of the proposed leakage detection system over the course of a year has been evaluated to study seasonal changes in pipe and ground strains. It was found that major rainfall events (more than 40 mm per day) which resulted in moisture ingress reaching the fibre optic cable or pipe will also cause substantial and rapid strain changes and these should not be mistaken for leaks. It is therefore necessary to evaluate the identification of a potential leak against the rainfall record to assess whether the strain change might have resulted from heavy rainfall or wetting of the ground by other means. The effect of such rainfall-induced false alarms should also be more wide-spread when compared to a leak, the effect of which will be localised around the leak location.

7 RECOMMENDATIONS FOR FURTHER RESEARCH AND DEVELOPMENT

7.1 Smart pipes

It was shown that detection leakage-induced strain changes in a pipe is a highly sensitive means of leak detection, even more so that detecting leakage-induced ground strain or temperature changes. However, in order to monitor pipe strains it is necessary to firmly attach the sensing fibre optic cable to the pipe. This will probably involve the use of a structural epoxy which will be difficult on an active pipeline construction site as attachment of the cable to the pipe will be hampered by the presence of dirt and water. This is likely to inconvenience the contractor and fixing of a cable to a pipeline is therefore likely to be expensive and potentially unreliable.

A potential solution to this problem is to slightly modify the design pipes and produce pipes manufactured with a special groove to house the cable. This is shown in concept in the figure below. By sizing the groove correctly for a given type of cable, a snug fit can be achieved so that the use of epoxy glues is not required. This modification is probably most relevant to extruded plastic pipes. When installing a new pipeline, the grooves can be lined up along the pipe crown. Once installed the groove can be cleaned with compressed air, if necessary, and the cable can be inserted. Couplings with similar grooves can be designed for joining the pipes, or if sufficiently robust, the fibre optic cable can simply lap over a conventional coupling to the next length of pipe.

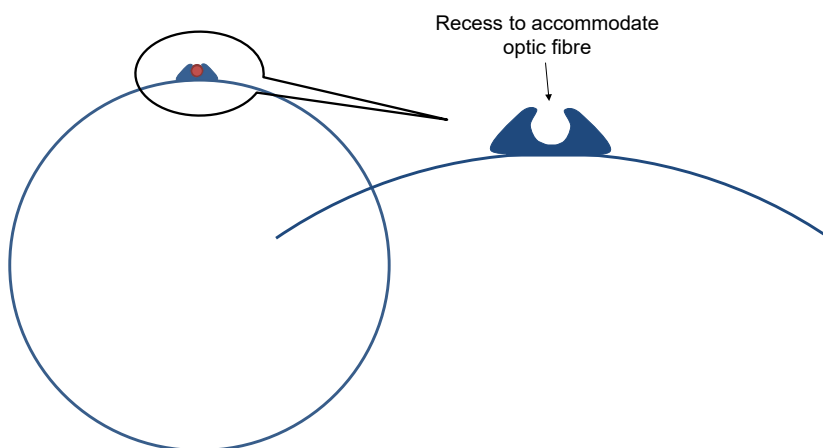


Figure 7-1: Modified pipe design to accommodate a fibre optic cable for pipe strain measurement.

7.2 Distributed strain measurement

All the work described in this report focused on a leakage detection system making use of fibre Bragg gratings (FBGs) to detect pipe and ground strains which may be indicative of water leaks. Current technology allows only approximately 20 FBGs to be monitored along a single length of fibre optic cable. The length of pipe that can therefore be monitored with such a system is limited, as is the spatial resolution of such a system. However, a range of systems are now available to carry out distributed strain measurement to high accuracy and spatial resolution, allowing lengths of optic fibre of 50 km or more to be monitored continuously. It is recommended that a follow-up study be conducted to investigate the use of a distributed strain measurement system to serve as a leak detection system suitable to continuously monitor long lengths of pipeline.

Indications from the laboratory and field installation trials are that the proposed leakage detection system will be successful to detect pipe line leaks. Arrangements should be made to carry out a trial installation of the proposed detection system on a working pipeline to allow the system to be tested under the realistic operating conditions.

Seasonal variations in ground temperature and strain changes on buried fibre optic cables should continue to be studied as leakage-induced temperature and strain changes need to be identifiable despite naturally occurring variation. It is necessary to assess whether this will be possible in the long term.

7.3 Selection of the most suitable fibre optic cable

Optic fibres are of the order of 10 μm in diameter and therefore have to be protected by several protective layers/reinforcement elements when buried in the ground. A wide range of fibre optic cables, ranging in rigidity depending on their robustness, are available on the market. The performance of a range of cables of various degrees of robustness to act as leakage sensors should therefore be investigated. Cable which are too rigid may possibly not respond sensitively enough to indicate a leak.

Fibre optic cable manufacturers advise against the use of metal-armoured cables due to their tendency to conduct lightning resulting in damage to readout units.

8 LIST OF REFERENCES

American Water Works Association (AWWA). 2009. Water Audits and Loss Control Programs – Manual of Water Supply Practices, M36 (3rd Edition). [Online] AWWA. Available from: <http://app.knovel.com/hotlink/toc/id:kpWALCPMW4/water-audits-loss-control/water-audits-loss-control> [Accessed 31 January 2017].

Attewell, P.B., Yeates, J. and Selby, A.R. (1986). Soil movements induced by tunnelling and their effects on pipelines and structures. London: Blackie & Son.

AVX (2017). AVX Product Catalogue. [Online] Available from: <http://www.avx.com/products/thermistors/ntc-disc/> [Accessed 30 March 2017].

Barry-Macaulay, D., Bouazza, A., Singh, R.M. and Ranjith, P.G. (2013). Thermal conductivity of soils and rocks from the Melbourne (Australia) region. *Engineering Geology*, (164), pp.131-38.

Bracegirdle, A., Mair, R.J., Nyren, R.J. and Taylor, R.N. (1996). A methodology for evaluating potential damage to cast iron pipes induced by tunnelling. Proc. Geotechnical Aspects of Underground Construction in Soft Ground. London: Balkema, pp.659-664.

Buttrick, D.B., Van Rooy, J.L. and Ligthelm, R. (1993). Environmental geological aspects of the dolomites of South Africa.

Buttrick, D. and Van Schalkwyk, A. (1998). Hazard and risk assessment for sinkhole formation on dolomite. *Environmental Geology* 36 (1-2), November 1998, Springer-Verlag, pp 170-178.

Conway, M. (2010). *Heat Transfer in a Buried Pipe* (Masters Dissertation, University of Reading).

Du Plessis, J.A. and Hoffman, J.J. (2015). Domestic water meter accuracy. *WIT Transactions on Ecology and the Environment*, 200, pp.197-208.

EPA (2010). Control and mitigation of drinking water losses in distribution systems. Washington: EPA Office of Ground Water and Drinking Water.

Florides, G. and Kalogirou, S. (2007). Ground heat exchangers – A review of systems, models and applications. *Renewable energy*, 32(15), pp.2461-2478.

FBGS (2017). Products – SWM-01 strain sensor. Jena: Germany. Available from: <http://www.fbgs.com/productsadv/be-en/5/detail/item/31/page/1/> [Accessed 20 June 2017]

Frings, J. (2011). Enhanced Pipeline Monitoring with Fibre Optic Sensors. *6th Pipeline Technology Conference 2011, 12 March*, pp1-12.

Gere, James M. and Barry J. Goodno. (2013). *Mechanics of Materials*. 8th ed. Cengage Learning, Stamford.

Gumbo, B., Juizo, D. and Van der Zaag, P. (2003). Information is a prerequisite for water demand management: experiences from four cities in Southern Africa. *Physics and Chemistry of the Earth, Parts A/B/C*, 28(20), pp.827-837.

Henrie, M., Carpenter, P. and Nicholas, R.E. (2016). *Pipeline Leak Detection Handbook*. 2nd edition Cambridge. Gulf Professional Publishing.

Inaudi, D. and Glisic, B. (2010). Long-Range Pipeline Monitoring by Distributed Fibre Optic Sensing. *Journal of Pressure Vessel Technology*, pp 265-74.

Jacobsz, S.W., Kearsley, E.P. & Kock, J.H.L. (2014). The geotechnical centrifuge facility at the University of Pretoria. *Physical Modelling in Geotechnics – Proceedings of the 8th International Conference on Physical Modelling in Geotechnics 2014, ICPMG 2014*, pp. 169-174.

Klar, A. Vorster, T.E.B. Soga, K. and Mair, R.J. (2005). Soil-pipe interaction due to tunnelling: Comparison between Winkler and elastic continuum solutions. *Geotechnique*, Vol 55, No 6, pp 461-466.

Knappett, J. and Craig, R.F. (2012). *Craig's Soil Mechanics*, 8th ed. CRC Press, Abingdon, Oxon.

Kreuzer, M. (2013). *Strain Measurement with Fibre Bragg Grating Sensors*. Darmstadt, Germany: HBM.

Marshall, A.M. Klar, A. and Mair, R. (2010). Tunnelling beneath buried pipes: view of soil strain and its effect on pipeline behavior. *Journal of Geotechnical and Geoenvironmental Engineering*, Vol 136, No 12, pp 1664-1672.

McKenzie, R.S. Siqalaba, Z.N. and Wegelin, W.A. (2012). *The State of Non-Revenue Water in South Africa*. Pretoria: Water Research Commission. (Report no. TT 522/12)

McKenzie, R.S. Lambert, A.O. Kock, J.E. and Mtshweni, W. (2002). *BENCHLEAK – Benchmarking of Leakage for Water Suppliers in South Africa*. Pretoria: SA Water Research Commission. (Report no. TT 159/01)

McKenzie, R.S. and Bhagwan, J.N. (2005). *Leakage Management – Introduction to WRC Tools to Manage Non-Revenue Water*. Pretoria: SA Water Research Commission.

McKenzie, R.S. (2001). *PRESMAC – Pressure Management Program*. Pretoria: SA Water Research Commission. (Report no. TT 152/01)

McKenzie, R.S. (1999). *SANFLOW- Development of a standardised approach to evaluate burst and background losses in water distribution systems in South Africa*. Pretoria: SA Water Research Commission. (Report no. TT 109/99)

McKenzie, R.S. and Lambert, A. E. (2002). *ECONOLEAK – Economic Model for Leakage Management for Water Suppliers in South Africa*. Pretoria: SA Water Research Commission. (Report no. TT 169/02)

Mishra, A. and Soni, A. (2011). *Leakage Detection using Fibre Optics Distributed Temperature Sensing*. 6th Pipeline Technology Conference, Hannover Messe, Germany, pp 1-12.

National Instruments. (2011). *Products – Fibre optic sensing technology*. Texas: USA. Available from: <http://www.ni.com/white-paper/12953/en/> [Accessed 15 March 2017]

Nel, D.T. and Haarhoff, J. (2011). *The failure probability of welded steel pipelines in dolomitic areas*. *Journal of the South African Institution of Civil Engineering*, Vol 53, No 1, April, pp.9-21.

- Oosthuizen, A.C. and Richardson, S. (2011). Sinkholes and subsidence in South Africa. Council of Geoscience. Cape Town. (Report no. 2011-0010)
- Parks, G.A. (1984). Surface and interfacial free energies of quartz. *Journal of Geophysical Research* 89(B6), pp 3997-4008.
- Rajani, B. and Tesfamariam, S. (2004). Uncoupled axial, flexural, and circumferential pipe soil interaction analyses of partially supported jointed water mains. *Canadian geotechnical journal*, 41(6), pp.997-1010.
- Rao, Y.J. (1997). In-fibre Bragg grating sensors. *Measurement science and technology*, 8(4), p.355.
- SABS (1983). SABS 1200 LB: BEDDING (PIPES). Pretoria: South African Bureau of Standards.
- SABS (1989). SABS 1200 DB: EARTHWORKS (PIPE TRENCHES). Pretoria: South African Bureau of Standards.
- SABS (2008). SANS 1200-DP1: Earthworks for buried pipelines and prefabricated culverts. Pretoria: South African Bureau of Standards.
- Schofield, A.N. (1980). Cambridge Geotechnical Centrifuge Operations. *Geotechnique*, 30(3), pp 227-268.
- Schöning, W.L. (1990). Distribution of sinkholes and subsidences in the dolomite areas south of Pretoria. Diss. MSc Dissertation, University of Pretoria, 1990.
- Soga, K., Mohamad, H. and Bennett, P.J. (2008). Distributed Fiber Optics Strain Measurements for Monitoring Geotechnical Structures. 6th International Conference on Case Histories in Geotechnical Engineering. 11-16 August 2008 Arlington. Available from: scholarsmine.mst.edu/cgi/viewcontent.cgi?article=2974&context=icchge [Online].
- Taylor, R.N. (1995). Geotechnical centrifuge technology. Blackie Academic & Professional.
- Utilis Israel Ltd. (2017). Utilis. Israel. Available from: http://utiliscorp.com/#hp_slider [Accessed 4 April 2017].

Van Dijk, M. (2016). Pipeline Course 2016 – Presentation 6 slide 10. 7 July 2016. University of Pretoria. Available from: Pipeline Coursework [CD-OM]. Van Zyl, J.E. 2014a. Introduction to operation and maintenance of water distribution systems. Pretoria: SA Water Research Commission. (Report no. TT600-14)

Van Zyl, J.E. (2014b.) Theoretical modeling of pressure and leakage in water distribution systems. *Procedia Engineering*, 89, pp.273-277.

Van Zyl, J.E. Alsaydalani, M.O.A. Clayton, C.R.I. Bird, T. and Dennis, A. (2013). Soil fluidisation outside leaks in water distribution pipes-preliminary observations. *Proceedings of the Institution of Civil Engineers*, 166(10), p.546.

Vorster, T.E.B. (2005). The Effects of Tunnelling on Buried Pipes. PhD thesis. University of Cambridge.

Vorster, T.E., Klar, A., Soga, K. and Mair, R.J. (2005). Estimating the effects of tunnelling on existing pipelines. *Journal of Geotechnical and Geo-environmental Engineering*, 131(11), pp.1399-1410.

Vorster, T.E.B. Mair, R.J. Soga, K. and Klar, A. (2006). Centrifuge modelling of the effect of tunnelling on buried pipelines: Mechanisms observed. *Geotechnical Aspects of Underground Construction in Soft Ground – Proceedings of the 5th International Conference of TC28 of the ISSMGE*, pp. 327-333.

Wang, C., Olson, M., Doijkhand, N. and Singh, S. (2016, October). A novel DdTS technology based on fiber optics for early leak detection in pipelines. In *Security Technology (ICCST), 2016 IEEE International Carnahan Conference on* (pp. 1-8). IEEE.

Wegelin, W.A. and McKenzie, R.S. (2013). Metropolitan Municipality Non-Revenue/Water Loss Assessment. PEP: National Non-revenue Water Assessment. Department of Water Affairs. South Africa.

Wenzel, R.N. (1936). Resistance of solid surfaces to wetting by water. *Industrial and engineering chemistry* 28(8), pp 988-994.

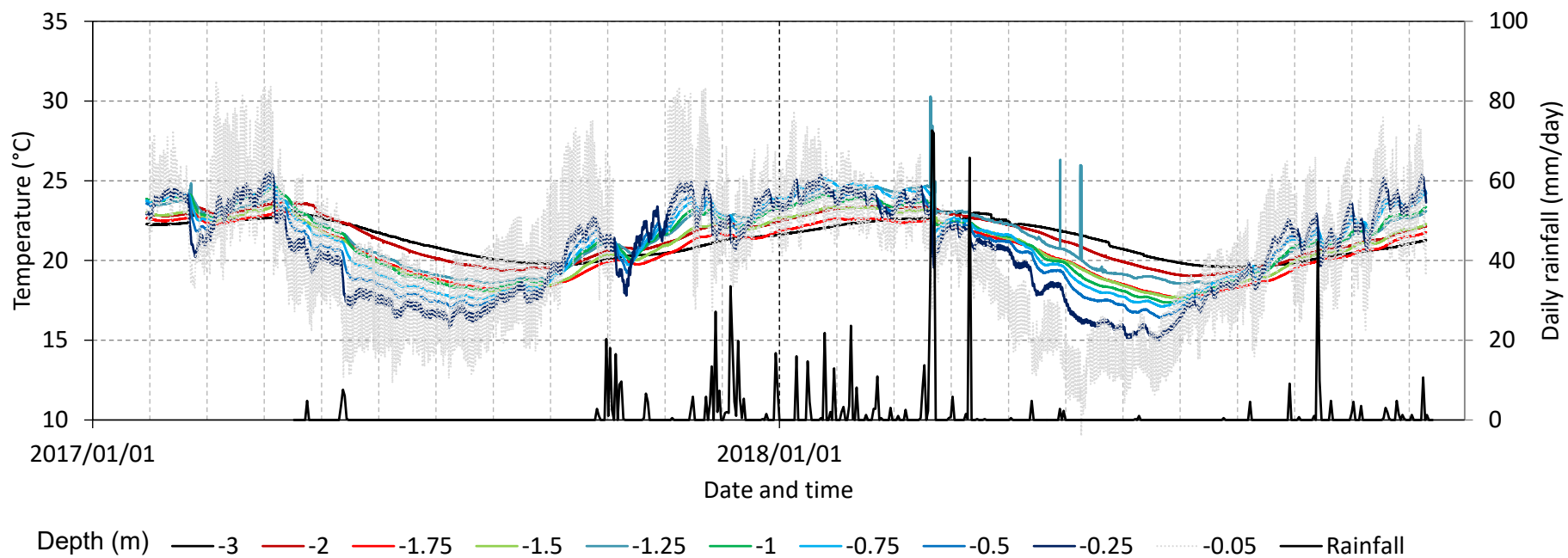
White, D., Take, W. & Bolton, M. (2003). Soil deformation measurement using particle image velocimetry (PIV) and photogrammetry. *Geotechnique*, 53(7): 619-631.

World Health Organization (WHO). 2014. Water safety in distribution systems. World Health Organization.

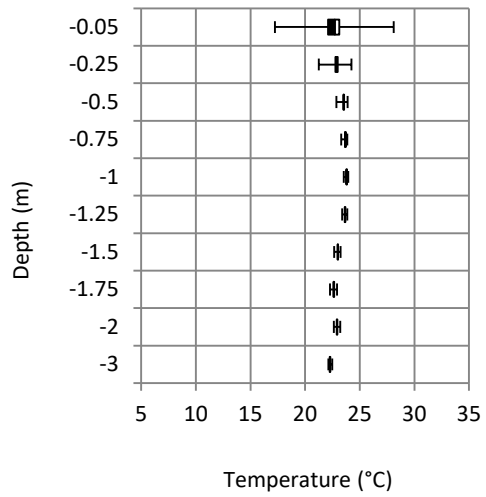
Zou, L. and Landolsi, T. (2014). Pipeline leakage detection using fibre-optic distributed strain and temperature sensors. OZ Optics Ltd., Canada, Ottawa.

APPENDIX A

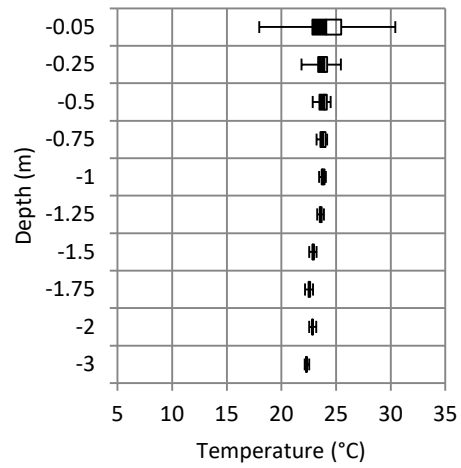
**Temperature fluctuation with depth over study period
Jan 2017 to Dec 2018**



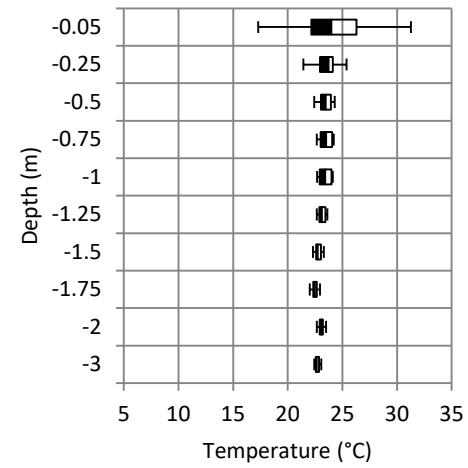
Ground temperature and rainfall variation during the course of the study period.



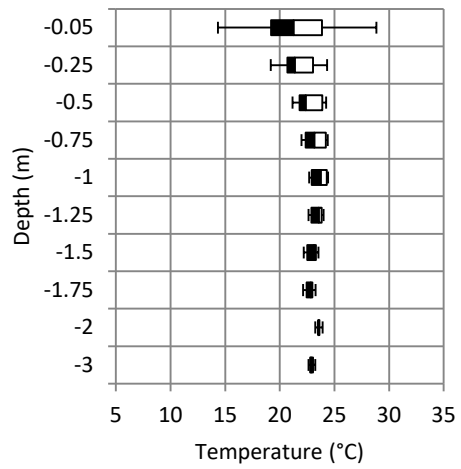
Jan 2017



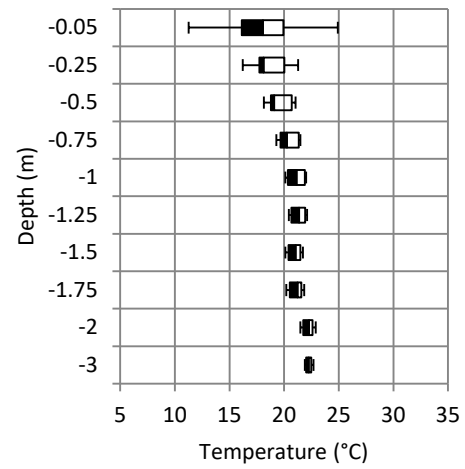
Feb 2017



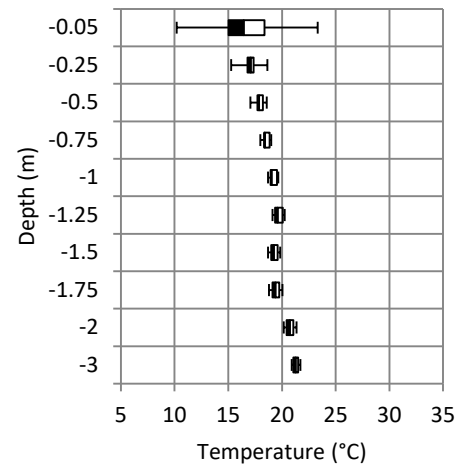
March 2017



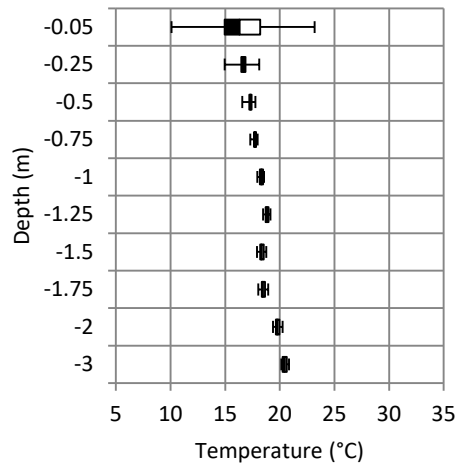
April 2017



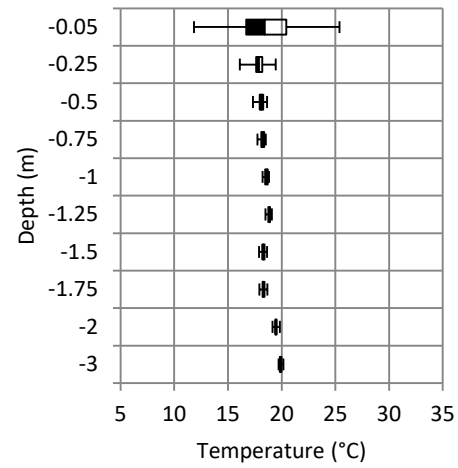
May 2017



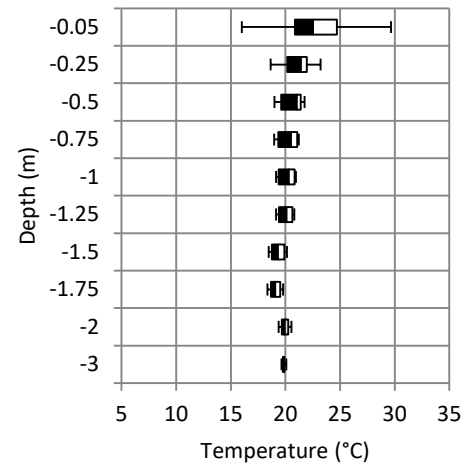
June 2017



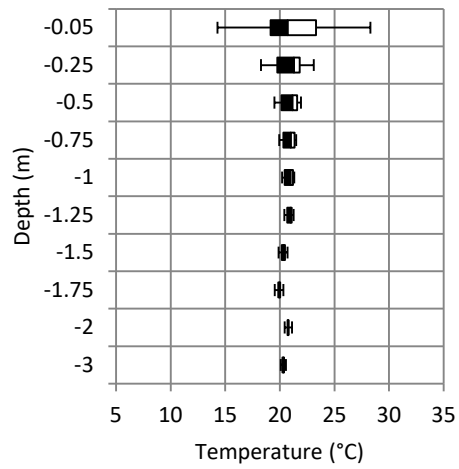
July 2017



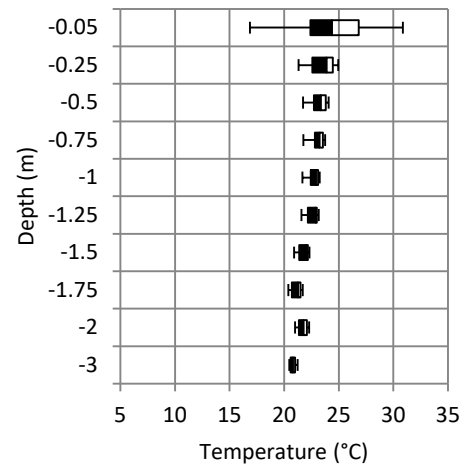
Aug 2017



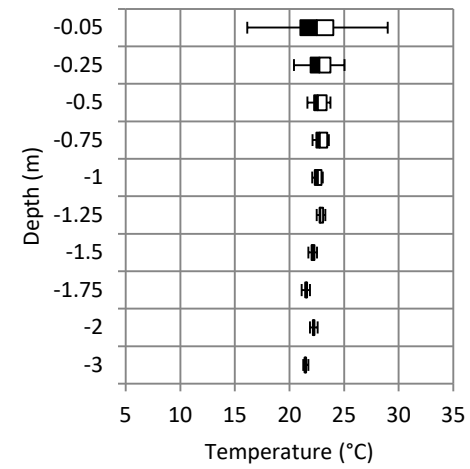
Sept 2017



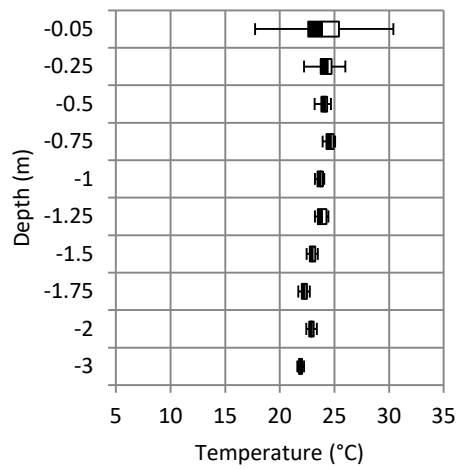
Oct 2017



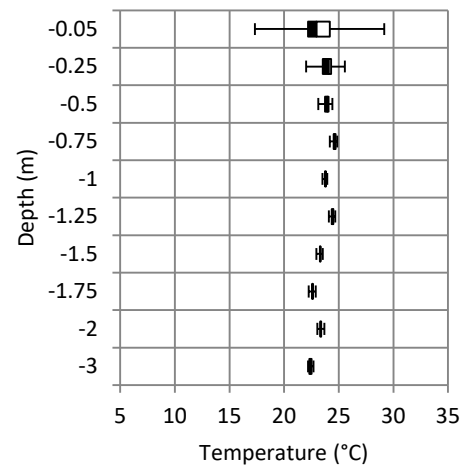
Nov 2017



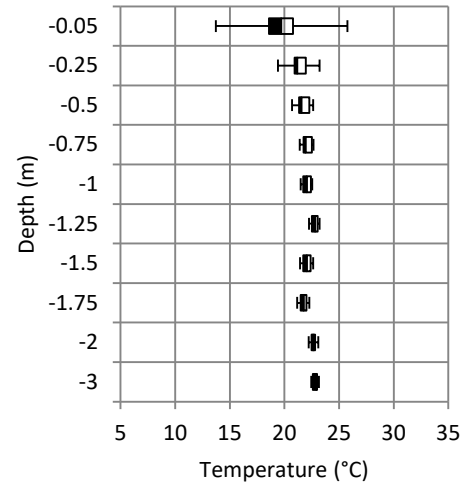
Dec 2017



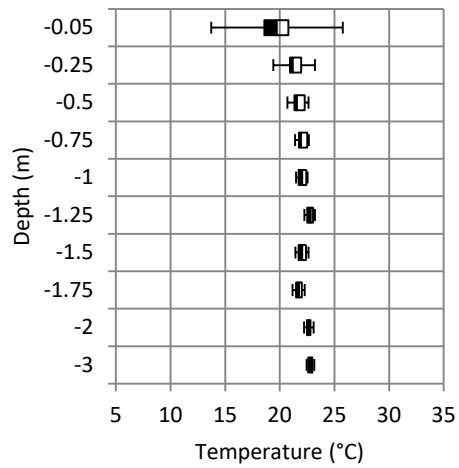
Jan 2018



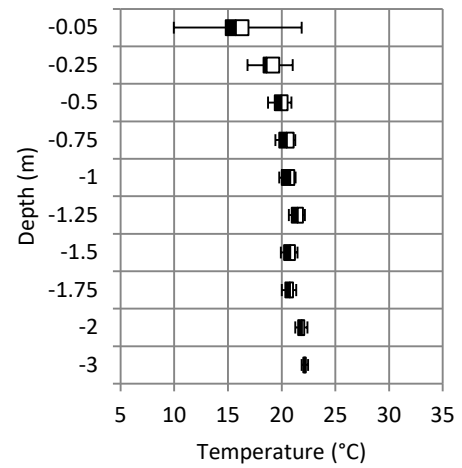
Feb 2018



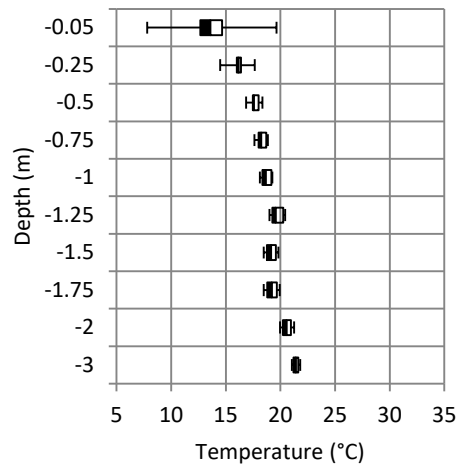
March 2018



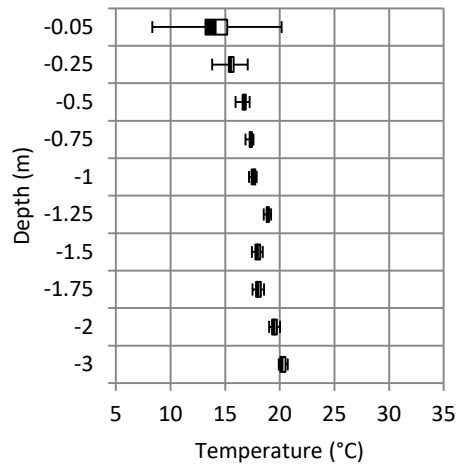
April 2018



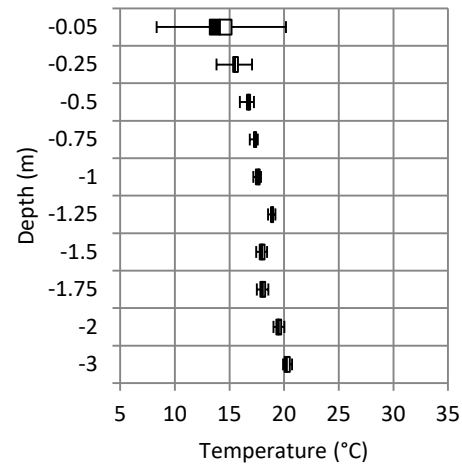
May 2018



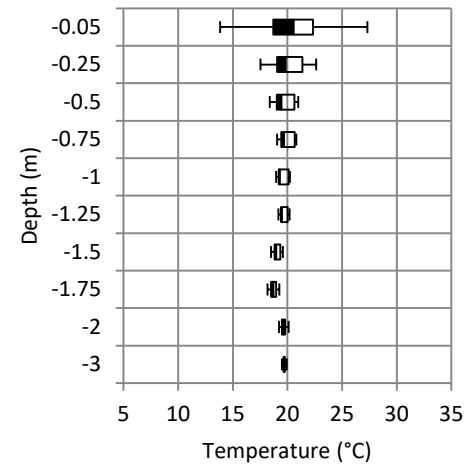
June 2018



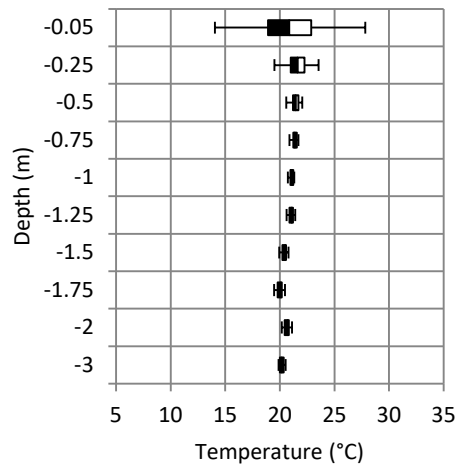
July 2018



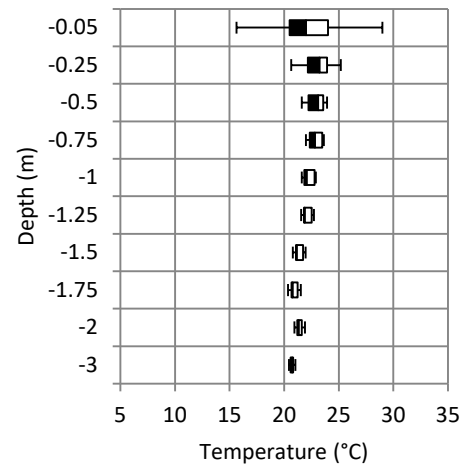
Aug 2018



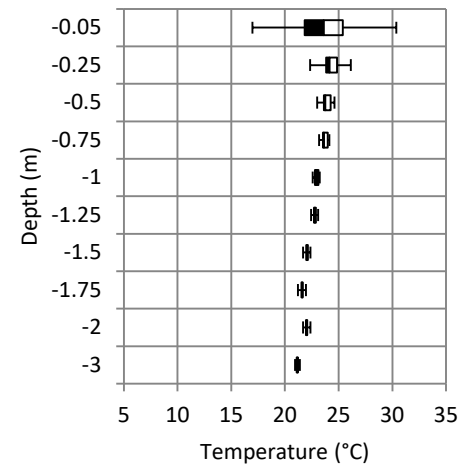
Sept 2018



Oct 2018



Nov 2018



Dec 2018